Phys Eng Sci Med (2022) 45:291–401
https://doi.org/10.1007/s13246-021-01094-z

EPSM 2021 ABSTRACTS

EPSM 2021, Engineering and Physical Sciences in Medicine

O001 Standards of Ethics in AI, where we have come from, why we are so passionate

Prof Liz Kenny AO[1]

[1]Senior Radiation Oncologist, Royal Brisbane and Women's Hospital

The Royal Australian and New Zealand College of Radiologists (RANZCR) led the medical community in Australia and New Zealand in thinking through the impact of Machine Learning (ML) and Artificial Intelligence (AI) in health care.

After analysing global developments in artificial intelligence for over twelve months, particularly those relating to medical imaging, RANZCR identified through 2018 that medical leadership was largely absent from these discussions. RANZCR also observed a notable absence of activity from governments in the Australasian region, which contrasted with a pro-active approach in similar countries in North America and Europe.

Given that AI technologies were reported to be making advances within medical imaging, the clinical radiology and radiation oncology sectors were considered ripe for the adoption of AI. This raised a range of concerns about how to ensure ethical application of AI and how to guide its safe and appropriate use in our two specialties.

RANZCR determined to take a pro-active approach to shape the adoption of AI in clinical radiology and radiation oncology in Australia and New Zealand that would ensure it would be deployed safely into care pathways. RANZCR was aware of the potential for AI to greatly impact patient care in clinical radiology and radiation oncology and had a desire to see AI integrated in a manner that respected the ethics and standards required to deliver safe and quality care to the people of Australia and New Zealand and beyond. This was the principal focus of our endeavour, we concentrated on areas within our remit and influence: to ensure AI would be used ethically in medicine in our jurisdictions; to support quality service provision using AI, and to prepare our trainees and members in transitioning to practise in an AI-rich environment.

O002 Developing a worldwide consortium of intensive care units amidst a global pandemic

Gianluigi Li Bassi[1], MD, PhD

[1]Associate Professor of Clinical Medicine, University of Queensland, Australia

In January 2020, while early warnings of an undefined novel coronavirus causing severe pneumonia were spreading worldwide, three clinical investigators in Brisbane, Australia founded the COVID-19 Critical Care Consortium to rapidly characterise pulmonary dysfunction and ventilatory support for this unknown disease. On March 11 2020, while the WHO Declared COVID-19 a Pandemic and expressed serious concerns about "the alarming levels of global inaction," the Critical Care Consortium became the largest network of intensive care units ever created to collaborate internationally for the characterisation of a novel disease and to find novel solutions to save lives of critically ill patients. The Consortium currently comprises 354 collaborating hospitals, and more than 400 intensive care units across 6 continents. The COVID-19 Critical Care Consortium is currently running a multi-centre short period incidence observational study of COVID-19 patients in participating hospitals and intensive care units. Study aims are to describe clinical features; severity of pulmonary dysfunction; incidence of intensive care unit admission and use of mechanical ventilation and extracorporeal membrane oxygenation and survival of patients with COVID-19. The COVID-19 Critical Care Consortium is endorsed by some of the most distinguished societies of intensive care medicine, such as Extracorporeal Life Support Organization (ELSO) and AsiaPacific Extracorporeal Life Support Organization (APELSO), ECMOnet and all major worldwide organizations including SPRINT-SARI, ISARIC.

O003 Federated Deep Learning in Head and Neck Cancer Overall Survival Prediction

D. Al Mouiee[1,2,3], A. Haidar[1,2,3], P. Chlap[1,2,3], M. Field[1,2,3], L. Holloway[1,2,3,4,5]

[1]Liverpool and Macarthur Cancer Therapy Centres, Liverpool, NSW, Australia; [2]Ingham Institute for Applied Medical Research, Liverpool, NSW, Australia; [3]South Western Sydney Clinical School,

Faculty of Medicine, University of New South Wales, Sydney, NSW, Australia. d.almouiee@unsw.edu.au (Presenting author); a.haidar@unsw.edu.au; phillip.chlap@unsw.edu.au.; matthew.field@unsw.edu.au. [4]Centre for Medical Radiation Physics, University of Wollongong, Wollongong, NSW, Australia; [5]University of Sydney, NSW, Australia. Lois.Holloway@health.nsw.gov.au

Introduction Artificial Intelligence, in particular deep learning (DL), has made much progress in radiation oncology [1]. Its current implementations, however, are limited by its heavy reliance on data-driven approaches, as clinical and medical data are largely distributed across institutions, each governed by complex legal and ethical regulations. As a result, DL generalizability is heavily affected when attempting to solve many medical classification tasks. To overcome such limitations, we propose and evaluate a federated learning (FL) approach to train a DL model over datasets distributed in various data centres.

Method A head and neck cancer dataset was collected from the cancer imaging archive (TCIA) [2]. The central slices, defined as the slices with highest number of tumour pixels in the Computed Tomography (CT) image on the axial plane, were extracted from the CT images. A FL framework was designed and implemented, with three clients representing clinics for training and one for testing, interchangeably. The experiments were repeated ten times, where each client was used in turn for testing and Area Under the Curve (AUC) was measured accordingly. The datasets were kept isolated at their respective clinics, as only model weights were exchanged between the clients and the central server. The proposed approach was compared to a centralised learning (CL) approach where each dataset was trained locally at each client (no data sharing).

Results The mean testing AUC scores for FL were (0.52 ± 0.08) compared to CL (0.53 ± 0.05) (Fig. 1), with a p value (t test) of 0.563.

Conclusion Despite the highly imbalanced distribution of the data, CL did not outperform FL. Techniques to overcome this imbalance such as data augmentation and various sampling of the data will be the next step. Finally, we plan to investigate various federated aggregation methods and optimise its hyper-parameters.

References

1. Huynh, E., Hosny, A., Guthier, C. et al. (2020). Artificial intelligence in radiation oncology. *Nat Rev Clin Oncol* **17,** 771–781. https://doi.org/10.1038/s41571-020-0417-8

2. Vallières, M. et al. (2017). Radiomics strategies for risk assessment of tumour failure in head-and-neck cancer. *Sci Rep* **7,** 10,117. https://doi.org/10.1038/s41598-017-10371-5

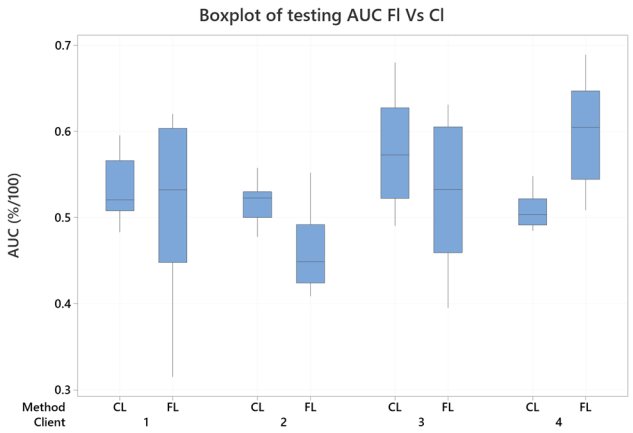

Fig. 1 Boxplot of the testing Area under the Curve (AUC) measured at each client for both Federated Learning (FL) and Centralised Learning (CL)

O004 The impact of dataset quality on autocontouring machine learning models

S. Biggs[1]

[1]Radiotherapy AI, Wagga Wagga, Australia. simon@radiotherapy.ai (Presenting author)

Introduction The recent TG275 report (Ford 2020) presents a failure mode analysis where the 1st, 3rd, and 7th scoring failure modes were all contour related. Recent state-of-the-art machine learning models (Nikolov 2018) might be able to help prevent or detect these. Collecting the data to build these models can be time consuming and subject to privacy concerns. There is however a growing number of datasets available within the creative commons (Clark 2013; Grossberg 2018). This project aims to demonstrate what can be achieved with these open datasets without any curation.

Method An open dataset (Grossberg 2018) from The Cancer Imaging Archive (TCIA) was utilised without curation to build a 3D U-Net based machine learning model. A model was selected utilising a validation subset of the open dataset and then the resulting model was baselined against the curated head and neck dataset produced by DeepMind (Nikolov 2018).

Results The TCIA dataset contained obvious mislabelled contours such as bone being classified as spinal cord and in some cases the brain stem being contoured with circle patches only. See Fig. 1.

When the results of the model were compared to the DeepMind dataset it was able to achieve Dice scores similar to interobserver variance reported within the literature (Loo 2012; Brouwer 2012; Mukesh 2012). See Table 1.

Conclusion A state-of-the-art machine learning model requires a dataset where its label noise doesn't introduce a bias within the model. Nevertheless datasets with label noise that are currently available within the creative commons are still capable of creating models that achieve dice scores comparable to interobserver variance.

References

Ford, E., Conroy, L., Dong, L., de Los Santos, L. F., Greener, A., Gwe-Ya Kim, G., … & Wells, M. (2020). Strategies for effective physics plan and chart review in radiation therapy: report of AAPM Task Group 275. Medical physics, 47(6), e236-e272. https://doi.org/10.1002/mp.14030

Clark, K., Vendt, B., Smith, K., Freymann, J., Kirby, J., Koppel, P., … & Prior, F. (2013). The Cancer Imaging Archive (TCIA): maintaining and operating a public information repository. Journal

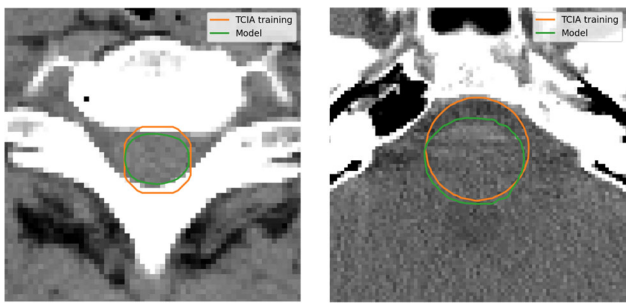

Fig. 1 Examples of the label noise within the utilised TCIA dataset

Table 1 The 3D volumetric dice scores of the model created with the utilised TCIA dataset when compared to the DeepMind dataset

DeepMind Patient ID	Right Parotid	Left Parotid	Brainstem	Spinal Cord
0522c0014	0.66	0.72	0.81	0.86
0522c0519	0.84	0.79	0.70	0.85
0522c0576	0.84	0.82	0.79	0.63
0522c0727a	0.73	0.75	0.87	0.68
0522c0727b	0.86	0.87	0.83	0.69
TCGA-CV-5977	0.71	0.73	0.80	0.82
TCGA-CV-5978	0.76	0.77	0.85	0.85

of digital imaging, 26(6), 1045–1057. https://doi.org/10.1007/s10278-013-9622-7
Nikolov, S., Blackwell, S., Mendes, R., De Fauw, J., Meyer, C., Hughes, C., … & Ronneberger, O. (2018). Deep learning to achieve clinically applicable segmentation of head and neck anatomy for radiotherapy. arXiv preprint https://arxiv.org/abs/1809.04430
Grossberg, A. J., Mohamed, A. S., Elhalawani, H., Bennett, W. C., Smith, K. E., Nolan, T. S., … & Fuller, C. D. (2018). Imaging and clinical data archive for head and neck squamous cell carcinoma patients treated with radiotherapy. Scientific data, 5(1), 1–10. https://doi.org/10.1038/sdata.2018.173
Loo, S. W., Martin, W. M. C., Smith, P., Cherian, S., & Roques, T. W. (2012). Interobserver variation in parotid gland delineation: a study of its impact on intensity-modulated radiotherapy solutions with a systematic review of the literature. The British journal of radiology, 85(1016), 1070–1077. https://doi.org/10.1259/bjr/32038456
Brouwer, C. L., Steenbakkers, R. J., van den Heuvel, E., Duppen, J. C., Navran, A., Bijl, H. P., … & van't Veld, A. A. (2012). 3D variation in delineation of head and neck organs at risk. Radiation Oncology, 7(1), 1–10. https://doi.org/10.1186/1748-717X-7-32
Mukesh, M., Benson, R., Jena, R., Hoole, A., Roques, T., Scrase, C., … & Jefferies, S. (2012). Interobserver variation in clinical target volume and organs at risk segmentation in post-parotidectomy radiotherapy: can segmentation protocols help?. The British journal of radiology, 85(1016), e530-e536. https://doi.org/10.1007/s11060-008-9631-4

O005 Automatic marker segmentation in kilovoltage images using a deep learning framework

D. Chrystall[1], M. Gargett[1], M. Mueller[2], A. Briggs[1], Adam Mylonas[2], P. Keall[2], D. T. Nguyen[1,2], J. Booth[1,3]

[1]Northern Sydney Cancer Centre, Royal North Shore Hospital, Australia. Danielle.Chrystall@health.nsw.gov.au (Presenting author); Maegan.Gargett@health.nsw.gov.au. [2]ACRF Image X Institute, University of Sydney, Australia. Marco.Mueller@sydney.edu.au.; Adam.Briggs@health.nsw.gov.au.; Adam.Mylonas@sydney.edu.au.; Paul.Keall@sydney.edu.au.; DoanTrang.Nguyen@uts.edu.au. [3]Institute of Medical Physics, University of Sydney, Australia. Jeremy.Booth@health.nsw.gov.au

Introduction Accurate fiducial marker detection is important when tracking tumour motion during radiotherapy. A deep learning framework, using convolution neural network (CNN) models, has previously been developed for the automatic detection of fiducial markers in kilovoltage images [1]. This method requires no prior knowledge of patient specific marker properties or an additional learning period. As a step toward clinical use, we evaluated the accuracy of this method in an experimental setting using an anthropomorphic lung phantom.

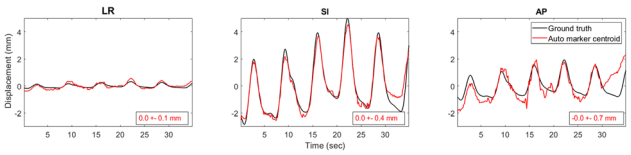

Fig. 1 Comparison between the ground truth tumour motion traces (black) and automatic marker tracking centroid (red) in left–right (LR), superior-inferior (SI) and anterior–posterior (AP) directions for the typical lung motion trace. The accuracy and precision is given in each direction

Method Three fiducial markers were implanted in a 3D-printed, anatomically accurate thorax phantom, and placed on a programmable motion platform (HexaMotion, ScandiDos). Five patient-measured motion traces were applied as ground truth. Kilovoltage image projections were acquired during MV beam on to simulate treatment conditions. The fiducial markers were automatically segmented with a CNN-based tracking method, which was pre-trained using lung cancer patient images. The marker centroid position was normalised to the average of the motion trace in each direction. The centroid geometric accuracy (mean difference) and precision (1 standard deviation) were measured.

Results The accuracy and precision of the automatic marker segmentation was (0.0 ± 1.2) mm, (0.0 ± 0.5) mm and (− 0.1 ± 0.6) mm in the LR, SI and AP directions, respectively, when averaged over all motion traces. The average [5th, 95th] percentile accuracy values were [− 1.2, 2.0] mm, [− 0.8, 0.7] mm and [− 0.9, 0.6] mm in LR, SI and AP respectively. Figure 1 compares the automatic marker tracking centroid to the programmed tumour motion for the Typical Lung trace.

Conclusion The in-phantom application of a deep learning-based automatic marker tracking method showed average geometric accuracy and precision of less than 0.4 mm and 1.5 mm in all directions, respectively. Should this method show similar accuracy for clinical lung patient images it could be implemented for real-time image guided radiation therapy on standard radiation therapy systems.

Reference

1. Mylonas, A., et al., *A deep learning framework for automatic detection of arbitrarily shaped fiducial markers in intrafraction fluoroscopic images*. Med Phys, 2019. **46**(5): p. 2286–2297.

O006 Using deep learning algorithms to automate the segmentation of brain metastases

A. Mehta[1], P. Ramachandran[1], V. Seshadri[1], B. Perrett[1], M. Pinkham[1].

Radiation Oncology, Princess Alexandra Hospital, Ipswich Road, Australia. Akash.Mehta@health.qld.gov.au (Presenting Author); Prabhakar.Ramachandran@health.qld.gov.au.; Venkatakrishnan.Seshadri@health.qld.gov.au.; Ben.Perrett@health.qld.gov.au.; Mark.Pinkham@health.qld.gov.au

Introduction In this preliminary study, we aimed to employ deep learning algorithms to automatically contour brain metastases on MR scans used for Leksell Gamma Knife treatment planning. [1]. The proposed model is expected to assist in improving target delineation of multiple lesions.
Methods U-Net [2], a modified form of a Convolutional Neural Network (CNN), was used to generate a model to automatically segment brain metastases. A total of 30 patients, who have already received Gamma Knife radiotherapy, were selected for this study. MR images without contours were inputted into the algorithm during the training phase, with corresponding contours for comparison to the output. The leave-one-out cross-validation method was employed to train the model, which ensured each patient dataset was tested exactly once and n-1 patient datasets were used to train the model. Output consisted of two-dimensional contours representing brain metastases. The auto segmented contours were compared against their ground truth datasets (contours generated by clinicians) using Dice Similarity Coefficient and Hausdorff Distance.
Results Dice similarity coefficient for all test cases was found to be more than 80% whereas, the Hausdorff distance between generated and actual contour image slices was around 3 mm.
Conclusion The model displayed promising results, indicating that such techniques can be deployed clinically to produce Gamma Knife plans in a relatively shorter time. However, further improvements in the dice similarity coefficient require a larger number of datasets. This task is currently underway at PAH. Ideally, this will result in a tool which will generate contours that can be rapidly reviewed and modified by clinicians prior to treatment, to facilitate volumetric analyses of response after therapy or in various research settings.
References

1. Halasz, L. M., & Rockhill, J. K. (2013). Stereotactic radiosurgery and stereotactic radiotherapy for brain metastases. Surgical neurology international, 4(Suppl 4), S185–S191. https://doi.org/10.4103/2152-7806.111295
2. Ronneberger, O., Fischer, P. and Brox, T. (2015). U-Net: Convolutional Networks for Biomedical Image Segmentation. https://arxiv.org/pdf/1505.04597.pdf

O007 Simultaneous segmentation of tumour, organ-at-risk and diaphragm in thoracic kV-projections using machine learning

M. Mueller[1,2], A. Mylonas[1], P Keall[1], J Booth[3], D. T. Nguyen[1,2,3]

[1]ACRF Image X Institute, University of Sydney, Australia; [2]The University of Technology Sydney, Australia.
marco.mueller@sydney.edu.au (Presenting author); Adam.mylonas@sydney.edu.au; Paul.keall@sydney.edu.au;
[3]Northern Sydney Cancer Centre, Australia.
Jeremy.Booth@health.nsw.gov.au; DoanTrang.Nguyen@uts.edu.au

Introduction A fundamental problem of radiotherapy is the trade-off between the radiation dose delivered to tumour and the side effects caused by dose applied to the surrounding healthy tissue. To increase the efficacy and safety of lung SABR we enable simultaneous localisation of multiple relevant structures during treatment delivery with the proposed method Multi-Target-Segmentation (MTS).
Method MTS used a convolutional-neural-network to simultaneously segment the tumour, the heart, and the diaphragm in kV-projections throughout a rotational lung SABR treatment on a standard-equipped conventional linear accelerator. A patient-specific training dataset consisted of 36,000 digitally-reconstructed-radiographs, created by forward-projecting each of ten planning 4D-CT phases and segmented target volumes equidistantly over a full imaging rotation. The labels of multiple structures were stacked as separate image channels. Data was augmented by randomly cropping the field-of-view within ± 3 mm during training. MTS was trained individually for three lung SABR patients and applied to kV-projections from three treatment fractions per patient. The gantry rotated during image acquisition and patients were breathing freely. The geometric accuracy of MTS was determined as the mean difference between the centroids of the segmented structures and their respective manually-created ground-truth.
Results Fig. 1 shows a segmentation example and quantitative results are presented in Table 1. MTS had a mean tumour localization accuracy of 0.4 ± 2.6 mm and 1.3 ± 1.7 mm in the lateral/ anterior–posterior and superior-inferior directions, respectively. The mean localization accuracy was 1.6 ± 1.0 mm and 1.6 ± 1.2 mm for the

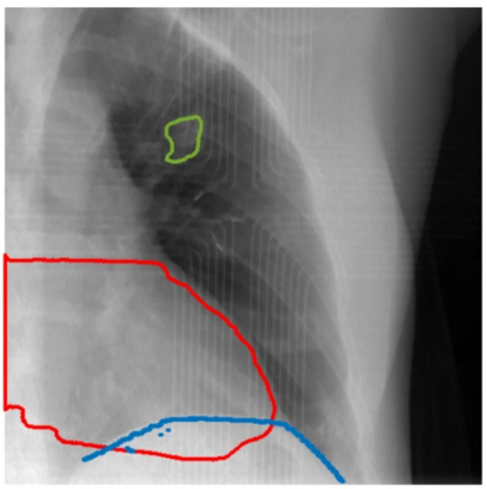

Fig. 1 Segmented tumour (green), heart (red) and diaphragm (blue) in a kV-projection of patient 3

Table 1 Quantitative results for the simultaneous segmentation of the tumour, the heart and the diaphragm in kV-projections for three lung SABR patients. Data is shown as mean tracking error ± standard deviation

Patient Index	Accuracy lateral (mm)			Accuracy superior (mm)		
	Tumour	Heart	Diaphragm	Tumour	Heart	Diaphragm
1	1.2 ± 1.4	2.0 ± 1.4	− 0.1 ± 0.4	1.1 ± 1.0	1.2 ± 0.9	− 2.7 ± 2.3
2	− 0.3 ± 1.7	0.8 ± 0.6	0.0 ± 0.5	2.5 ± 1.0	2.0 ± 1.5	− 1.7 ± 1.3
3	0.1 ± 3.9	2.0 ± 1.3	0.1 ± 0.4	0.3 ± 3.3	1.7 ± 1.2	− 1.7 ± 1.3
Mean	0.4 ± 2.6	1.6 ± 1.0	0.0 ± 0.4	1.3 ± 1.7	1.6 ± 1.2	− 2.1 ± 1.6

heart and 0.0 ± 0.4 mm and − 2.1 ± 1.6 mm for the diaphragm in the lateral/anterior–posterior and superior-inferior directions, respectively.
Conclusion Simultaneous localisation of multiple thoracic structures without fiducials during treatment is feasible and can achieve clinically relevant accuracy for clinical deployment. MTS may widen the therapeutic index of SBRT by minimizing thoracic toxicity for targets in close proximity of critical OARs.

O008 CT number to physical density calibrations: nominally wrong?

Dan Goodwin[1], Abby Rajasekar[1], Ruth Smith[1], Michelle Yap[1]

[1]Te Pūriri o Te Ora—Cancer & Blood Services, Auckland District Health Board, NZ. dgoodwin@adhb.govt.nz (Presenting author); ARajasekar@adhb.govt.nz; RuthSmith@adhb.govt.nz; MYap@adhb.govt.nz

Introduction The relationship between CT number and physical density is typically determined by imaging commercially available CT calibration phantoms consisting of tissue-equivalent inserts. The aim of this work was to evaluate the dosimetric impact of using manufacturer provided nominal versus measured density values for CT-density calibration tables.
Method The physical density of RMI 465 phantom (Gammex Inc. Middleton, WI, USA) inserts was measured and compared with nominal values. The phantom was imaged to produce two CT-density calibration tables; one using nominal the other using measured densities. The dosimetric impact of the different tables for photon beams was evaluated in Pinnacle (V9.10 collapsed cone convolution algorithm, Philips Radiation Oncology Systems, Fitchburg, WI, USA). Measurements were compared with TPS calculations for a heterogeneous slab phantom constructed of water and lung-equivalent material. A representative cohort of clinical patient treatment plans was re-calculated using both calibration tables and compared.
Results Measured and nominal physical density agreed to within measurement uncertainty limits for all inserts except LN-300 Lung where a difference of −17% was found (0.249 ± 0.007 g/cc measured versus 0.300 g/cc nominal). Agreement between measured and calculated dose downstream of lung equivalent material was better for the measured CT-density table; 1.0% and 1.8% for 5 cm and 14 cm respectively. Local dose differences of over 5% were found for lung SABR plans resulting in up to 4.0% reduction in planning target volume D95 dose using the measured density CT-density table. Negligible dosimetric difference was found outside of lung and low density regions.
Conclusion A significant difference between measured and nominal density was found for a commercial CT-density calibration phantom insert. The agreement between TPS calculated and measured dose was found to be better when measured rather than nominal density was used in the CT-density calibration table. The difference in density causes non-negligible differences in clinical dose distributions.

O009 The use of artificial intelligence for radiation dose management in CT imaging

Cynthia H. McCollough[1], PhD, DABR, FAAPM, FACR, FAIMBE

[1]*Brooks-Hollern Professor* and Professor of Medical Physics and Biomedical Engineering, CT Clinical Innovation Center, Department of Radiology, Mayo Clinic, 200 First Street SW, Rochester, MN, USA. e-mail: mccollough.cynthia@mayo.edu

Since the introduction of CT in 1971, a wide range of dose management and optimization approaches have been implemented on commercial CT systems. Now, artificial intelligence (AI) holds the promise of enabling further reductions in patient doses from CT. Machine learning (ML), a subset of AI, can be used to determine patterns in large data sets that can be used for tasks ranging from exam selection to interpretation. Reconstructed images can be independently evaluated with AI tools to assist in interpretation triage, bringing a case to the top of the reading queue if serious disease is suspect by the AI algorithm. Automation of data acquisition processes, including patient positioning and selection of scan acquisition parameters, can improve the quality, consistency, and efficiency of a CT practice, minimizing the impact of the performing CT technologist or the supervising radiologist. Subsequent to data collection, optimization of image reconstruction parameters, advanced reconstruction methods, and image denoising can be used to improve several aspects of image quality, although they are most often used to reduce image noise and hence enable the use of lower doses for data acquisition. Further, AI methods can be used to automatically segment organs or tissues, detect and characterize pathology, increase diagnostic performance (e.g., sensitivity, specificity, accuracy) and enable new clinical applications, ultimately increasing the benefit to the patient from medically justified CT examinations. This presentation will provide a brief introduction to AI and describe several commercial and investigational applications of AI to CT imaging. These AI-based techniques not only have the potential to reduce radiation dose while achieving the same level of image quality, but also can reduce the likelihood of errors in the performance and interpretation of medically justified CT examinations.

O010 A quantitative approach to the monitoring and improvement of patient outcomes in cardiac services

Dr Ian Smith[1]

[1]St Andrew's War Memorial Hospital

Background Graphical Statistical Process Control (SPC) tools have been shown to promptly identify significant variations in clinical outcomes in a range of health care settings. This presentation explores the application of these techniques to qualitatively inform the routine morbidity and mortality (M&M) review process across cardiac services at a single site.
Methods Baseline clinical and procedural data relating to cardiology (diagnostic, interventional and electrophysiology) and cardiac surgical procedures, performed at St Andrew's War Memorial Hospital (SAWMH) were retrospectively evaluated. A range of performance measures, appropriate to the subspecialties involved were identified. Benchmarks of excellence and Risk Adjustments were developed and applied using a range of Statistical Process Control techniques such as Exponentially Weighted Moving Average (EWMA) charts and Funnel Plots. Analysis based on routinely updated charts were discussed at the hospital's routine cardiac surgery and cardiology M&M meetings and annual service wide clinical audit.
Results Discrete and aggregated measures covering patient outcomes (procedural success, mortality and major morbidities) and process of care markers (length of stay, readmission, radiation use) have proved to be usable measures for monitoring outcomes. Monitoring trends in minor morbidities provides a valuable warning of impending changes in significant events. Instances of variation in performance have been examined and could be related to differences in individual operator performance via individual operator charts.

Conclusion SPC tools facilitate near "real-time" performance monitoring allowing early detection and intervention in altered performance. Careful interpretation of charts for group and individual operators has proven helpful in detecting and differentiating systemic versus individual variation.

O011 Status of the ARPANSA Diagnostic Reference Level Program

P. D. Thomas[1], M. Sanagou[1], T. E. Beveridge[1], K. L. Lee[1]

[1]Medical Imaging Section, ARPANSA.
peter.thomas@arpansa.gov.au (Presenting author);
masoumeh.sanagou@arpansa.gov.au;
toby.beveridge@arpansa.gov.au; kam.lee@arpansa.gov.au

Introduction ARPANSA's Diagnostic Reference Level (DRL) program supports optimisation of medical exposures by providing guidance on typical dose for common imaging procedures. Routine comparison against DRLs is included in regulatory requirements such as the Medical Exposure Code [1] and the Commonwealth Diagnostic Imaging Accreditation Scheme [2].
Method ARPANSA's National Diagnostic Reference Level Service (NDRLS) collects CT survey data through a web portal. Data on image-guided interventional procedures (IGIP) is collected using spreadsheet templates. Median dose metrics from each survey are reported as facility reference levels (FRLs). Surveys include data for up to 20 patients in CT and 30 patients for IGIP. National DRLs are based on the third quartiles of the FRL distributions.
Results In 2020, 5078 CT surveys from 722 scanners were completed. Third quartiles of the FRL distributions are shown in Table 1 and compared with the national DRLs [3]. For several scan categories the third quartile for 2020 is $> 10\%$ below the national DRL, suggesting a general review of the CT DRLs may be warranted.
Forty-six (46) surveys were submitted for image-guided procedures. Of these, 22 were for coronary angiography and the third quartiles of the FRL distributions were consistent with the national DRLs [4]. Data for other procedures were quite sparse and more submissions are needed to establish national DRLs.

Table 1 Third quartiles of the 2020 CT FRL distributions for adult patients and comparison with the national DRLs, categorised by scan region

Scan Region	Surveys	$CTDI_{vol}$ (mGy)		DLP (mGy.cm)	
		3rd Quartile (2020)	DRL	3rd Quartile (2020)	DRL
Head	729	47.4	52	835	880
Cervical Spine	597	19.7	21	407	470
Soft-Tissue Neck	530	14.5	15	420	450
Chest	682	8.6	10	344	390
Chest-Abdo-Pelvis	621	10.3	11	842	940
Abdo-Pelvis	693	10.8	13	532	600
Kidney-Ureter-Bladder	521	9.2	10	438	460
Lumbar Spine	672	21.9	26	607	670

A new survey is in development for nuclear medicine, covering both radiopharmaceutical administered activity and metrics for associated CT scans. A liaison panel has advised on survey spreadsheets and a pilot has commenced. The full survey will be conducted towards the end of 2021. Updated DRLs for nuclear medicine and positron emission tomography are expected in 2022.
Conclusion Australia's DRL program is well established. Current data for adult CT suggests a review is warranted. More data is needed for image-guided procedures. A new survey for nuclear medicine procedures is underway.
References

1. Australian Radiation Protection and Nuclear Safety Agency (2019). Code for Radiation Protection in Medical Exposure. ARPANSA. https://www.arpansa.gov.au/regulation-and-licensing/regulatory-publications/radiation-protection-series/codes-and-standards/rpsc-5 Accessed 5 June 2021.
2. Australian Government Department of Health (2015). DIAS Practice Accreditation Standards (from 1 January 2016). Department of Health. https://www1.health.gov.au/internet/main/publishing.nsf/Content/di-DIAS-Prac-Accred-Standards-1-January-2016 Accessed 5 June 2021.
3. Australian Radiation Protection and Nuclear Safety Agency (2021). Current Australian national diagnostic reference levels for multi detector computed tomography. ARPANSA. https://www.arpansa.gov.au/research-and-expertise/surveys/national-diagnostic-reference-level-service/current-australian-drls/mdct Accessed 5 June 2021.
4. Australian Radiation Protection and Nuclear Safety Agency (2021). Current Australian national diagnostic reference levels for image guided and interventional procedures. ARPANSA. https://www.arpansa.gov.au/research-and-expertise/surveys/national-diagnostic-reference-level-service/current-australian-drls/igip Accessed 5 June 2021.

O012 A Pilot Study of Prone Position Neoadjuvant Breast Radiotherapy to Reduce Skin Toxicity (PIONEER) – Medical Physics aspects

D. Basaula[1], R. Bailey[1], A. Yeo[1], T. Kron[1], K Byrne[1], F. Hegi-Johnson[1]

[1]Peter MacCallum Cancer Centre, Melbourne, Australia;
deepak.basaula@petermac.org (Presenting author);
Rachel.bailey@petermac.org; adam.yeo@petermac.org;
tomas.kron@petermac.org; keelan.byrne@petermac.org;
Fiona.Hegi-Johnson@petermac.org

Introduction Although prone breast radiotherapy has been used clinically for many years, the technique continues to evolve with recent international reports demonstrating benefits even for smaller breast patients in randomized clinical trial [1] and extending the technique to patients receiving locoregional nodal radiotherapy [2]. In PIONEER, we will treat patients undergoing neoadjuvant radiotherapy to their breast and locoregional nodes. To our knowledge, this is the first clinical implementation of whole breast and locoregional nodal radiotherapy in the prone position within Australia. This study reports the medical physics aspects of the trial implementation.
Method A prone Breast board was acquired and commissioned for the trial. Commissioning included integrity and compatibility checks as well as transmission measurements (Fig. 1A). Additionally, an IGRT protocol based on Cone Beam CT was developed to accommodate prone positioning with the new immobilisation system. As part of end-to-end testing, an anthropomorphic phantom (Fig. 1B)

was scanned and planned in eclipse planning system (Fig. 1C). Three plans were created with 6/10 and 6/18MV beam combination for 3D conformal and 6/10MV combination for Hybrid IMRT technique. Thermoluminescent Dosimeters (TLDs) were used to evaluate the dosimetry.

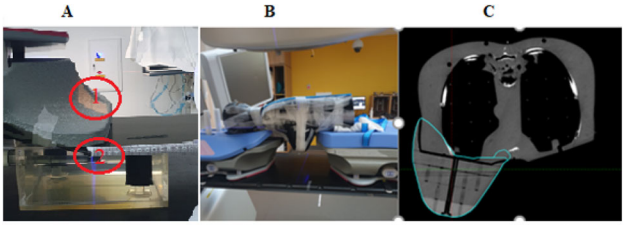

Figure 1: ***A)*** *Setup used for transmission measurement with red circle 1 indicating the measurement region of interest through prone Breastboard and circle 2 indicating chamber position (CAX, 5 cm depth and 100 cm SSD),* ***B)*** *image of Anthropomorphic phantom setup on the treatment unit for end to end testing, and* ***C)*** *Axial CT slice showing PTV volume with blue lines.*

Results The transmission measurement results are shown in Table 1. IGRT protocols have been validated to capture required volume-of-interest. CBCT with centre couch to avoid collision is found to be beneficial for image guidance however multiple scan is required to stitch together for entire volume-of-interest. The overall end-to-end dosimetry results showed that the planned and measured dose are within ± 3% inside the target however measured doses are higher upto 8.5% compared to planned dose on the skin.

Table 1: Typical transmission measurement results for range of field sizes

Field Size (cm × cm)	Beam energy		
	6 MV	10 MV	18 MV
5×5	0.97	0.98	0.99
10×10	0.97	0.98	0.99
25×25	0.98	0.98	0.99

Conclusion In order to introduce the prone breast technique, we performed range of commissioning tests and developed a prone treatment protocol to be feasible in the clinic through end-to-end testing.

Acknowledgements We would like to acknowledge the Victorian Comprehensive Cancer Centre whose Investigator Initiated Trial Support Programme has funded this trial.

References

1. Chung Y, Yu JI, Park W, Choi DH. Korean first prospective phase II study, feasibility of prone position in postoperative whole breast radiotherapy: a Dosimetric comparison. Cancer Res Treat. 2019. https://doi.org/10.4143/crt.2018.423
2. Shin SM, No HS, Vega RM, Fenton-Kerimian M, Maisonet O, Hitchen C, et al. Breast, chest wall, and nodal irradiation with prone set-up: results of a hypofractionated trial with a median follow-up of 35 months. Pract Radiat Oncol. 2015

O013 Online adaptive radiotherapy for simulation-free palliative radiotherapy accounts for rapid patient progression and anatomical changes

A. Kejda[1], S. Roderick[1], S. Wong[1], I. Fent[1], K. Grimshaw[1], A. Quinn[1], J. Booth[1,2], T. Schuler[1,3], S. Bergamin[1,4], T. Eade[1,4]

[1]Northern Sydney Cancer Centre, St Leonards, NSW. Alannah.Kejda@health.nsw.gov.au (Presenting author); Stephanie.Roderick@health.nsw.gov.au; Shelley.Wong@health.nsw.gov.au; Isabelle.Fent@health.nsw.gov.au; Kylie.Grimberg@health.nsw.gov.au; Alexandra.Quinn@health.nsw.gov.au; [2]University of Sydney, Sydney, Australia. Jeremy.Booth@health.nsw.gov.au; [3]Australian Institute of Health Innovation, Macquarie University, Sydney, Australia. Thilo.Schuler@health.nsw.gov.au; [4]Northern Sydney Clinical School, University of Sydney, Sydney, Australia. Sarah.Bergamin@health.nsw.gov.au; Thomas.Eade@health.nsw.gov.au

Introduction Approximately 30% of radiotherapy patients are of palliative intent. Replacing the planning CT with diagnostic CT datasets is feasible for palliative IMRT; reducing the time burden of multiple appointments without impacting quality [1]. Many palliative patients progress quickly and present unanticipated anatomical changes. This study evaluated the use of Varian Ethos online adaptive system to account for these changes.

Method Feasibility of online adaption was tested by simulating adaptive treatment of ten palliative abdominopelvic patients (27 fractions) in a test environment. Patients were 'treated' twice to evaluate two test arms; (1) reference and (2) AI-only. Arm 1 required clinician edits of AI-contours prior to adaptive plan generation, no contours were edited in arm 2. Within each arm, adaptive plans were compared to non-adapted (scheduled) plans using plan metrics PTV D95%, and 100% conformity index. Arm 1 and 2 contours were compared using Dice Similarity Coefficient (DSC).

Results All adaptive plans passed the primary constraint PTV D95% > 95%, while five scheduled fractions failed. Mean PTV D95% for adaptive and scheduled fractions were 104.0 ± 9.9% and 102.4 ± 12.0% (k = 2) respectively, with no statistically significant difference found between the two (t-test P = 0.29). Mean conformity indices measured 0.97 ± 0.14 and 0.85 ± 0.47 (k = 2) for adaptive and scheduled plans, respectively, and were statistically different (t-test P = 0.017). DSCs for CTV, kidneys, liver, small bowel and stomach were 0.90 ± 0.09, 0.930 ± 0.05, 0.98 ± 0.02, 0.928 ± 0.04 and 0.70 ± 0.11, respectively, indicating accurate AI segmentation of all contours except the stomach.

Conclusion Ethos online adaption was shown to account for inter-fraction patient variation by demonstrating conformal target coverage compared to scheduled plans, and good agreement between AI and clinician contours. The adaptive simulation free palliative pathway has the potential to remove referral barriers and expand service, while delivering high quality radiotherapy. Selection criteria and rapid decision-making workflows were established identifying patients suitable for adaption. To date, five patients have been treated clinically.

Reference

1. Thilo Schuler, Michael Back, George Hruby, Susan Carroll, Dasantha Jayamanne, Andrew Kneebone, Mark Stevens, Gillian Lamoury, Marita Morgia, Shelley Wong, Kylie Grimberg, Stephanie Roderick, Jeremy Booth, Thomas Eade, Introducing Computed Tomography Simulation–Free and Electronic Patient-Reported Outcomes–Monitored Palliative Radiation Therapy into Routine Care: Clinical Outcomes and Implementation Experience, Advances in Radiation Oncology, Volume 6, Issue 2, 2021, 100,632, ISSN 2452–1094

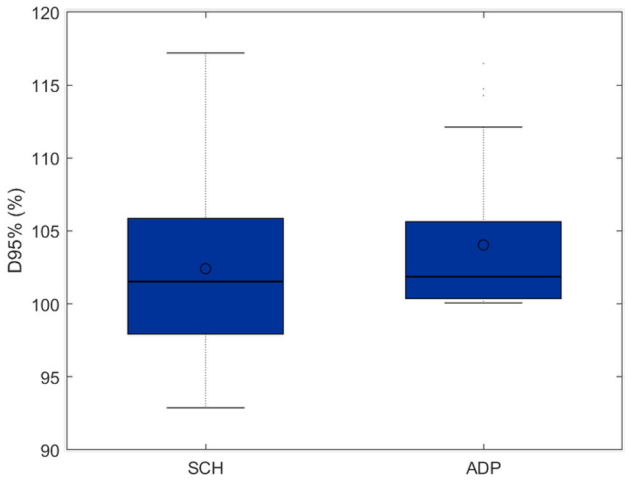

Figure 1. D95% PTV coverage

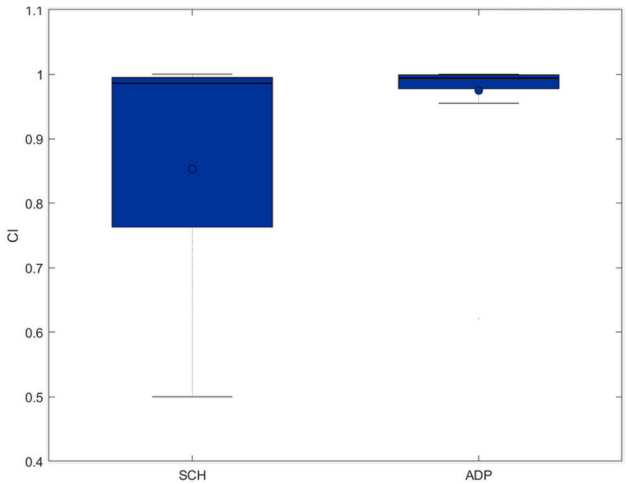

Figure 2. 100% Conformity index

O014 A Framework for Developing Multicentre Knowledge Based Planning Models for State-wide Use

C. Lawford[1], R. Lawrence[1], D. Ball[1], V. Panettieri[2], P. Griffin[3], C. Hornby[4]

[1]Peter MacCallum Cancer Centre, Parkville, Australia; Catherine.Lawford@petermac.org (Presenting author); Rhonda.Lawrence@petermac.org; Peter MacCallum Cancer Centre, Parkville, Australia. David.Ball@petermac.org; [2]Alfred Health Radiation Oncology, Melbourne, Australia. V.Panettieri@alfred.org.au; [3]William Buckland Radiotherapy Gippsland, Traralgon, Australia. P.Griffin@alfred.org.au; [4]Department of Health, Victoria, Australia. Colin.Hornby@health.vic.gov.au

Introduction The Victorian Public Sector RapidPlan Group (VPSRG) collaboratively develops Knowledge Based Planning (KBP) models to support consistent state-wide practice [1]. VPSRG includes nine sites from four radiotherapy providers. We will describe the framework for model development, using radical radiotherapy for lung cancer as an example.

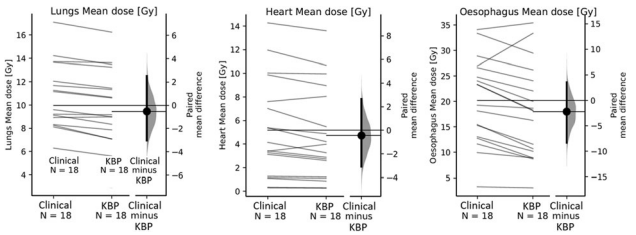

Fig. 1 Estimation plots for OAR mean doses, for clinical plans compared with KBP plans

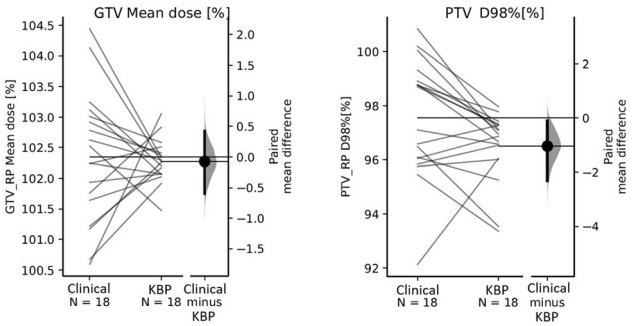

Fig. 2 Estimation plots for target coverage metrics for clinical plans compared with KBP plans

Method Standardised dosimetry objectives, contouring nomenclature (using AAPM TG263 [2]) and guidelines and model scope were developed with input from Radiation Oncologists (RO's) at each site. 137 anonymised patient DICOMRT datasets were submitted through the secure Victorian Patient Document Exchange platform from all four providers. The lead site built, trained and validated the model in Eclipse v15.5. Validation was performed on 18 patients by comparing the approved clinical VMAT plan with the KBP plan, using the Eclipse scripting interface combined with Python for extracting and evaluating plan metrics using Bootstrap estimation plots [3]. A RO performed a blinded comparison of the plans for each patient. A nominated support site independently reviewed the model, which was then distributed to all sites for internal validation and implementation.

Results All organ at risk dose (OAR) metrics were (on average) equal to or lower than the clinical plans (Fig. 1). The KBP model improved consistency in target coverage metrics across the validation set (Fig. 2). The RO preferred 7 KBP plans, 8 clinical plans and had no preference for 3 patients.

Conclusion Using the VPSRG model development framework, a KBP model for radical radiotherapy for lung cancer was developed and shown to produce plans of equivalent quality to plans created using traditional optimisation. Results indicate that the model will improve consistency in radiotherapy treatment planning across the state.

References

1. Panettieri V, et al. (2019) Development of a multicentre automated model to reduce planning variability in radiotherapy of prostate cancer. Phys Imaging Radiat Oncol 11:34–40. https://doi.org/10.1016/j.phro.2019.07.005
2. Mayo CS, et al. (2018) American Association of Physicists in Medicine Task Group 263: Standardizing Nomenclatures in Radiation Oncology. Int J Radiat Oncol Biol Phys. Mar 15;100(4):1057–1066. https://doi.org/10.1016/j.ijrobp.2017.12.013

3. Ho J, Tumkaya T, Aryal S, Choi H, Claridge-Chang A (2019) Moving beyond P values: data analysis with estimation graphics. Nat Methods 16(7):565–566. https://doi.org/10.1038/s41592-019-0470-3

O015 Curvature correction factor for independent dose verification of Eclipse Monte Carlo electron dose calculation

T. Mahmood[1], L. Slama[1], B. McKernan[1]

[1]Department of Radiation Oncology, Sir Charles Gairdner Hospital, Nedlands, WA, Australia. Talat.Mahmood@health.wa.gov.au (Presenting author); Luke.Slama@health.wa.gov.au; Brendan.Mckernan@health.wa.gov.au

Introduction Eclipse treatment planning system (TPS) uses Monte Carlo (MC) dose calculation algorithm to calculate the Monitor Units (MU). Electron MC algorithm is very sensitive to the beam incidence angle and body curvature. In our department, RadCalc 6.4 was used to perform independent dose calculations for electrons treatment plans. Plans calculated with MC algorithms can have up to 10% difference to RadCalc where there is significant curvature of body contour. The aim of this project is to measure and apply correction factors for the patient body contour in the clinical setting.
Method Spherical and cylindrical phantoms were made of water equivalent material of varying diameters with a thickness equal to the D_{max} of the corresponding energies. The bolus was placed on a solid water phantom and measurements were carried out using NACP chamber at D_{max}. The contour factor was defined as the ratio of the chamber reading with the bolus to that with solid water at the same depth. These curvature factors were measured for three electron energies (6 MeV, 9 MeV and 12 MeV) and compared to calculations made in the TPS. These factors are applied to both RadCalc calculations and an in-house spreadsheet for 10 patient cases to compare to Eclipse MU calculation. Varian's Eclipse API scripting is used to assist in calculating the patient curvature and estimating the equivalent square field size for the independent MU calculations.
Results The differences between the measured and TPS data was 0.66 ± 1.90% (1 standard deviation) with a maximum and minimum difference of 4.2% and -4.6% respectively.

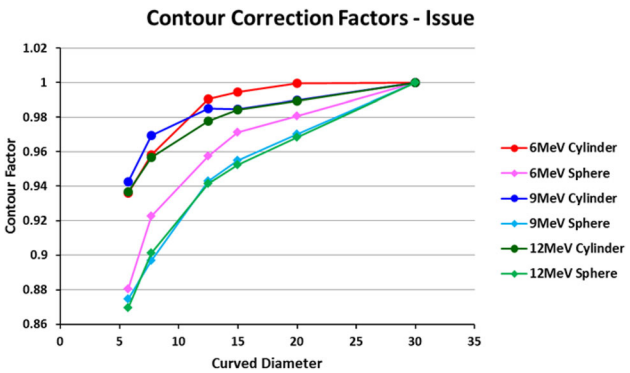

Conclusion The Eclipse TPS accurately calculates the dose for curved surfaces. When applying measured contour factors to the independent spreadsheet and RadCalc calculations, the results become more consistent with Eclipse MU calculations. An in-house excel spreadsheet was implemented in the department to calculate the MU using the measured contour factors.

O016 Hippocampal avoidance in whole-brain radiotherapy using an O-ring gantry radiotherapy system: A planning study

O. M. O[1], T. Cornwell[1], A. Amini[2], S. Sampath[2], S. M. Shirvani[1]

[1]RefleXion Medical, Hayward, CA, USA. ooderinde@reflexion.com (Presenting author); tcornwell@reflexion.com; [2]Department of Radiation Oncology, City of Hope, Duarte, CA, USA. aamini@coh.org; ssampath@coh.org; sean@reflexion.com

Introduction The RefleXion™ O-ring gantry system is a hybrid imaging-therapy system that combines PET/CT imaging with radiotherapy delivery. Its fan-beam kVCT imaging and therapy subsystems are used to deliver IMRT, SRS, and SBRT plans, and eventually, its PET imaging system will be used to deliver BgRT plans. This study evaluated the feasibility and performance of IMRT scenario: Hippocampal avoidance whole-brain radiotherapy (HA-WBRT).
Method Two patients were planned for HA-WBRT on the RefleXion treatment planning system. The whole brain, hippocampus, and hippocampus avoidance regions (volumetric expansion of 5 mm) were contoured. WBRT treatment plans were generated in IMRT mode, in accordance with RTOG 0933 prescription criteria (i.e., deliver 30 Gy in 10 fractions with a 9 Gy maximum dose to the hippocampus structure). Each patient plan was designed with 1 and 2 cm field width (FW), and the HA-WBRT plans for the different FWs were compared to each other.
Results All the HA-WBRT plans met the RTOG 0933 prescription criteria. The 1 cm FW plans significantly improved the lens sparing by 7.27% ± 1.99% compared to the 2 cm FW plans. However, there was an insignificant difference between the hippocampus sparing dose of 1 and 2 cm FW plans (P_{1cm} = 7.15 Gy ± 0.07, P_{2cm} = 7.15 Gy ± 0.07). The average treatment delivery time for 1 cm and 2 cm FW plans was 13.29 min ± 1.11 min and 9.24 min ± 1.29 min, respectively. In addition, the homogeneity index was within 1.5 – 1.7 and PTV D2 being > 37.5 Gy for all the plans generated with 1 and 2 cm FW.
Conclusion This study demonstrates that the RefleXion X1 can be utilized to deliver whole-brain radiotherapy with excellent hippocampus avoidance, while meeting other dosimetric constraints and achieving a homogenous dose distribution to the normal brain.

O017 Evaluation of the DIRs underpinning a commercial online adaptive radiotherapy system

A. Quinn[1], J. Kipritidis[1], J. Booth[1]

[1]Northern Sydney Cancer Centre, NSW, Australia. Alexandra.quinn@health.nsw.gov.au (Presenting author); John.kipritidis@health.nsw.gov.au; Jeremy.booth@health.nsw.gov.au

Introduction Deformable image registration (DIR) underpins the Varian Ethos CBCT-guided online adaptive system. However, tools to evaluate the DIRs at point-of-care as well as retrospectively are limited or non-existent, which can lead to treatment decisions based on inaccurate information. This work evaluated the sCTs used at treatment, and dose accumulation DIRs used for inter-fraction decisions.
Method Data from HN and rectum patients treated with online adaption were retrospectively analysed. For each fraction, the dicom-RT series containing the registered CBCT-sCT image pair, and dose accumulation deformation vector field (DVF) was exported. Qualitative assessment of each CBCT-sCT image pair involved an image

blend and application of a ranking system per TG132 recommendations. Quantitatively, the sCT and CBCT voxels were converted to mass density (MD) and the 3D Gamma pass rate (criteria ΔMD = 3%, DTA = 4 mm) evaluated. The target registration error (TRE) was assessed by using the Scale Invariant Feature Transform (SIFT) algorithm to identify, and calculate 3D displacements, between matching sCT-CBCT landmarks. Each dose accumulation DVF was converted to a Jacobian determinant image and the fraction of negative Jacobian voxels reported. Paired CBCT-Jacobian image overlays were inspected to identify regions for further investigation.
Results Overall, the visual alignment of anatomic structures between sCT and CBCT matched within 2 voxels (4 mm) and was scored 'Useable with risk of deformity'. Local deviations were noted in the bladder and around gas for rectum fractions, and airways for HN fractions. Quantitatively, a tighter range of MD gamma pass rates were calculated for rectum (58–67%) as compared to HN (53–74%). The median (STD) TRE was 2-3 mm (3-6 mm). Negative Jacobian values were calculated in at least 1 fraction for rectum patients.
Conclusion Visual inspection of CBCT-sCT image pairs identified discrepancies not apparent within the clinical system. Non-physical deformations highlighted in the underlying dose accumulation DIRs indicate that care is required when interpreting accumulated dose.

O018 The 3 main ways AI is transforming nuclear medicine and molecular imaging

Irène Buvat[1]

[1]Research Director, CNRS, Institut Curie

Artificial intelligence (AI) is currently invading the medical imaging field, including nuclear medicine and molecular imaging. In this talk, we will very briefly recall the principle of AI and explain how AI is expected to profoundly impact image generation, image analysis and medical decision support, and even possibly our understanding of the molecular features reflected by PET or SPECT images. The different concepts will be illustrated by examples from the recent literature. The challenges associated with this AI (r)evolution will also be discussed.

O019 Age-specific GFR normal reference range to use with two sample slope-intercept method and Jodal Brochner-Mortensen correction

S. Gautam[1]

[1]Hunter New England Imaging, John Hunter Hospital, New Lambton Heights, NSW, Australia. sijan.gautam@health.nsw.gov.au

Introduction Glomerular filtration rate calculated using radiopharmaceuticals vary with age, the calculation method, and the correction factor for slope-intercept overestimation. Hence, any normal reference range accompanying the results should be suitably modified and adapted to fit those parameters.
Method A retrospective analysis of the routine GFR calculation and clinical reports generated locally from 2006 to 2020 was performed. GFR was calculated with ^{99m}Tc-DTPA plasma clearance using a two-point slope intercept method with Jodal Brochner-Mortenson (JBM) correction. Age-specific normal range equations were developed from subjects who did not have known conditions that impaired kidney function. Previously published normal reference ranges were modified with appropriate correction reversal and compared with the locally developed reference ranges.
Results Age-specific normal GFR reference ranges for ^{99m}Tc-DTPA with slope-intercept method and JBM correction were developed. Normal reference range (Mean ± 2SD) for Normalised GFR (ml min^{-1} $(1.73m^2)^{-1}$) within 95% confidence limits suitable for use with JBM correction are shown in Table 1.

Table 1 A table of normal reference range for Normalised GFR (ml min^{-1} $(1.73m^2)^{-1}$) within 95% confidence limits suitable for use with the proposed method for all age groups.

Age (years) 'y'		Mean (ml min^{-1} $(1.73m^2)^{-1}$)	SD	Mean ± 2SD
Children	< 0.1	51.1	9.6	31.9 - 70.3
	0.10 - 0.30	59.3	15.0	29.2 - 89.4
	0.30 - 0.66	68.1	14.5	39.0 - 97.2
	0.66 - 1.00	77.0	17.9	41.2 - 112.8
	1.00 - 1.50	84.4	18.3	47.8 - 121.0
	1.50 - 2.00	87.1	18.6	50.0 - 124.2
	2.00 - 18.00	100.6	17.6	65.5 - 135.7
Adults	> 18.00	$102.9 – 0.00629 \times (Age)^2$	9.7	Mean ± 19.4

Conclusion When GFR results are accompanied by normal reference ranges that are appropriately tailored to the test conditions and the subject's age, it increases consistency in the radionuclide GFR reporting among nuclear medicine physicians and demonstrates reliability of radionuclide GFR to the referring doctors.
Acknowledgements I would like to acknowledge Nick Hill for his guidance and feedback.
References

1. Jodal L, Brochner-Mortensen J (2009) Reassessment of a classical single injection 51 Cr-EDTA clearance method for determination of renal function in children and adults. Part I: Analytically correct relationship between total and one-pool clearance. Scand J Clin Lab Invest 693:305–313
2. Piepsz A, Tondeur M, Ham H (2006) Revisiting normal (51) Cr-ethylenediaminetetraacetic acid clearance values in children. Eur J Nucl Med Mol Imaging 33:1477–1482

O020 Automated analysis of total tumour burden on Ga-68 PSMA PET/CT using convolutional neural network and novel watershed filtering

Lachlan McIntosh[1,2], **James Buteau**[1], **Price Jackson**[1], **Justin Ferdinandus**[3], **Nicholas Hardcastle**[1,4,5], **Rick Franich**[1,2], **Michael Hofman**[1,4]

[1]Peter MacCallum Cancer Centre, Melbourne, Australia; [2]RMIT University, Melbourne, Australia; [3]University Hospital Essen, Essen, Germany; [4]University of Melbourne, Melbourne, Australia; [5]University of Wollongong, NSW, Australia

Introduction Quantitative parameters derived from total tumour burden (TTB) segmentation on 68 Ga prostate-specific-membrane-antigen (PSMA) PET/CT are prognostic indicators for patients with metastatic castration-resistant prostate cancer [1]. Standardised reporting guidelines for PSMA-PET have recently been published, however, work remains to improve accuracy and time required for TTB. We aimed to develop a fully automated algorithm to delineate TTB on PSMA PET/CT by implementing convolutional neural network (CNN) followed by a purpose-designed watershed technique to discriminate between physiological and non-physiological uptake. We compared our results to manually defined TTB contours from trained nuclear medicine physicians on 50 unseen cases from a clinical trial.
Materials and Methods 48 (31 metastatic, 17 normal) PSMA PET/CT images were used to train CNN to detect physiological uptake

with standard uptake value (SUV) > 3 using fused PET and CT images concatenated as input. Model training was implemented using physiological contours that were generated by subtracting clinician-defined TTB from a whole-body SUV > 3 map on fused PET/CT dataset. To improve segmentation accuracy near tissue boundaries, final classification was performed using watershed technique according to local maxima location designated as either malignant or physiological by CNN. Fifty unseen PSMA PET/CT images were used to compare dice score coefficient, PSMAvol, PSMAmean (SUV), and PSMAmax (SUV) metrics derived from the combined model against manually defined clinician contours. Dice score coefficient was used to compare contours, and Bland–Altman mean difference and Pearson's correlation to compare quantitative parameters.

Results In the fifty patient validation cohort, the trained model and watershed filtering achieved a median dice score coefficient of 0.93 (0.30–0.99). PSMAmean, PSMAmax and PSMAvol calculated from manual contour and automated method agreed with a mean difference (Bland–Altman) of 0.2 SUV, 1.6 SUV and 153 mL, and Pearson's correlation of 0.98, 0.97, and 0.93 respectively. Two cases had a dice score of 0.30, both attributed to metastatic disease in the liver.

Conclusion We developed a fully automated algorithm to delineate TTB on PSMA PET/CT using CNN and novel watershed filtering. Performance against unseen data was comparable to that of a trained nuclear medicine physician. Implementation may enable routine reporting of whole body quantitative parameters with potential to improve standardisation or reporting, assessment of suitability for LuPSMA therapy and response assessment.

Reference

1. Ferdinandus, J., Violet, J., Sandhu, S., Hicks, R. J., Kumar, A. S. R., Iravani, A., … & Hofman, M. S. (2020). Prognostic biomarkers in men with metastatic castration-resistant prostate cancer receiving [177Lu]-PSMA-617. European journal of nuclear medicine and molecular imaging, 47(10), 2322–2327.

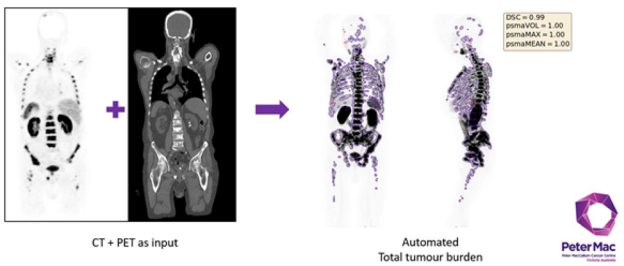

O021 Towards filmless quality assurance of stereotactic body radiation therapy in the axial plane

G. Biasi[1], N. Hardcastle[2], J. Poder[3], I. Filipev[1], L. Pudsey[1], M. Petasecca[1], A. Rosenfeld[1], T. Kron[2]

[1]Centre for Medical Radiation Physics, University of Wollongong, NSW, Australia; [2]Peter MacCallum Cancer Centre, Melbourne, VIC, Australia. gbiasi@uow.edu.au; [3]St George Cancer Care Centre, St George Hospital, Kogarah, NSW, Australia

Introduction Hypo-fractionated high-dose-per-fraction regimens such as stereotactic body radiation therapy (SBRT) are used for an increasing number of cancer patients [1]. SBRT for vertebral metastases [2] and for prostate cancer are particularly challenging scenarios because the target wraps around an organ at risk. Sub-mm dosimetry in the axial plane is often required to verify the steep dose gradients between the target and organs at risk are being delivered accurately

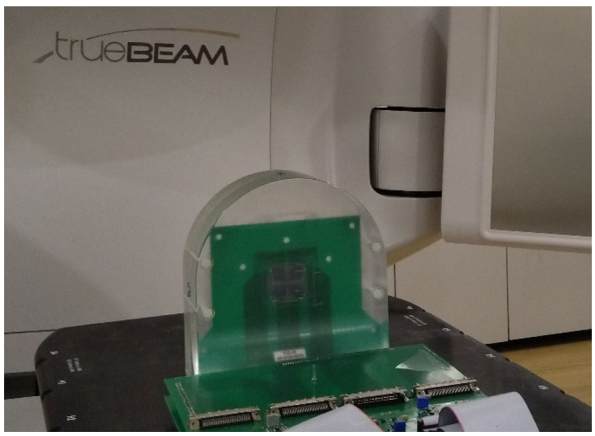

Fig. 3 The Octa, and its Perspex custom-made phantom for dosimetry in the axial plane. The Octa, shown at the centre of the picture, has 4 linear arrays of diodes (vertical, horizontal, 2 diagonals), with a 0.3 mm spacing between diodes. The detector (3.8 × 3.8 mm^2) is soldered on a thin and flexible printed-circuit board (PCB, green colour in the figure)

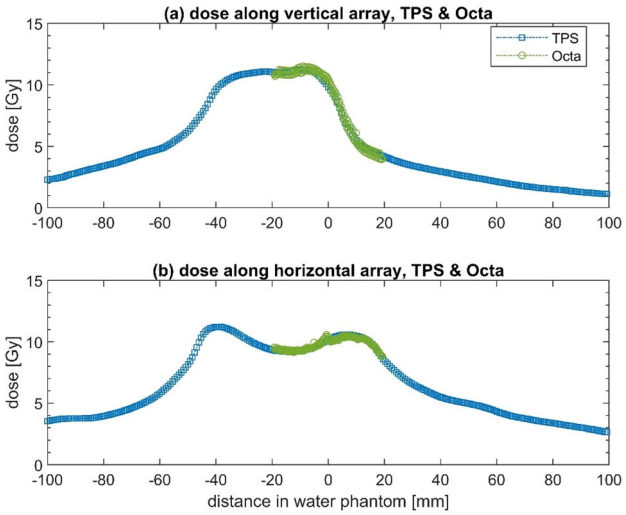

Fig. 4 SBRT VMAT prostate plan case-study: dose calculated with the treatment planning system and measurements with the Octa, along the vertical and horizontal arrays

[3]. At present, this can only be achieved with film dosimetry. Here, we aimed to demonstrate it can also be achieved using a 2D array of silicon diodes, the Octa [4].

Method For this purpose, we fabricated a Perspex phantom, custom-made for the Octa (Fig. 3). The Octa (3.8 × 3.8 mm^2) has 4 linear arrays, with a total of 512 diodes, spaced by 0.3 mm. In this feasibility study we assessed an SBRT prostate plan. The plan was delivered with a TrueBeam linac, and measurements with the Octa were compared with calculations from the treatment planning system (Eclipse v15.6). Measurements were corrected for angular dependence of the detector [5].

Results Comparing measurements and calculations on a point-per-point basis (Fig. 4), there was an overall agreement to within 0.5%, on average. However, 35 diodes in the array (which has 512 diodes in total) were in significant disagreement with calculations, up to more than 4%.

Conclusion In this feasibility study we demonstrated it is possible to achieve filmless dosimetry of a prostate SABR treatment plan in the

axial plane, with a spatial resolution suitable for SBRT. However, (1) further ongoing investigation is required to assess the origin of the disagreement between calculations and measurements, (2) benchmarking with film dosimetry, (3) using an appropriate range of SBRT plans for vertebral metastases and prostate cancer.

Acknowledgements Gross Foundation.

References

1. Grimm J, Marks L B, Jackson A, Kavanagh B D, Xue J and Yorke E (2021) High Dose per Fraction, Hypofractionated Treatment Effects in the Clinic (HyTEC): An Overview *Int. J. Radiat. Oncol. Biol. Phys.* 110 1–10
2. Sahgal A, Myrehaug S D, Siva S, Masucci G L, Maralani P J, Brundage M, Butler J, Chow E, Fehlings M G, Foote M, Gabos Z, Greenspoon J, Kerba M, Lee Y, Liu M, Liu S K, Thibault I, Wong R K, Hum M, Ding K and Parulekar W R (2021) Stereotactic body radiotherapy versus conventional external beam radiotherapy in patients with painful spinal metastases: an open-label, multicentre, randomised, controlled, phase 2/3 trial *Lancet Oncol.* 2045 1–11
3. Kron T, Ungureanu E, Antony R, Hardcastle N, Clements N, Ukath J, Fox C, Lonski P, Wanigaratne D and Haworth A (2017) Patient specific quality control for Stereotactic Ablative Body Radiotherapy (SABR): it takes more than one phantom *J. Phys. Conf. Ser.* 777 012,017
4. Biasi G, Petasecca M, Guatelli S, Hardcastle N, Carolan M, Perevertaylo V, Kron T and Rosenfeld A B (2018) A novel high-resolution 2D silicon array detector for small field dosimetry with FFF photon beams *Phys. Medica* 45 117–26
5. Biasi G, Hardcastle N, Petasecca M, Guatelli S, Perevertaylo V, Kron T and Rosenfeld A B (2019) On the Instantaneous Dose Rate and Angular Dependence of Monolithic Silicon Array Detectors *IEEE Trans. Nucl. Sci.* 66 519–27

O022 To investigate the validity of the geometric accuracy of intracranial stereotactic radiosurgery treatments using Gamma Knife Icon

Atousa Montaseri[1], Elena Ungureanu[1], Adam Yeo[1], Tomas Kron[1]

[1]Physical Sciences, Peter MacCallum Cancer Centre. Atousa.Montaseri@petermac.org; Elena.Ungureanu@petermac.org (Presenting author); Atousa.Montaseri@petermac.org; Tomas.Kron@petermac.org

Introduction Gamma Knife Icon is equipped with cone beam CT (CBCT) and high definition infra-red motion management (HDMM) system, allowing for non-invasive mask and frame-based intra-cranial stereotactic radiosurgery (SRS). Historically, no margin to the gross tumour volume (GTV) is used in Gamma Knife (GK) SRS treatments due to robust fixation method. This study retrospectively investigates the validity of the geometric accuracy of GK treatments.

Methods In the frame-based technique, pre-treatment CBCT is used to verify the patient position at the beginning of the treatment. Shifts are calculated from the registration of the CBCT with the planning images. The resultant dose distribution is assessed by the clinician in order to decide whether to proceed with the current plan or replan based on the new position. For the mask treatments, stereotactic reference is defined on the planning CBCT. Additional CBCTs are acquired at the beginning of each treatment fraction in order to adapt the treatment plan to the new treatment position. Intra-fraction motion is monitored by HDMM system using a nose-tip reflective marker. If motion exceeds the set tolerance, treatment is gated or paused. Additional treatment adaptation is necessary for paused treatments.

An analysis of the patient position shift data was performed after four months into the GK SRS program.

Results Pre-treatment CBCTs of 18 patients treated with frame, revealed median 0.70°, 0.02° and -0.01° rotations and -0.06, 0.01, 0.20 mm translations. One case required a replan due to a significant shift in the patient position.

Median rotations and translations for mask treatments were 0.32°, -0.22° and 0.22° and 0.08, -0.00 and 0.34 mm respectively.

Conclusion Frame-based GK treatments are robust, however small persistent rotations need further investigation.

The relationship between the nose-tip marker intra-fraction motion and target displacement is being analysed in order to validate our local motion management protocol.

References

1. G Wright, J Schasfoort, N Harrold, P Hatfield, P Bownes (2019) Intra-fraction motion gating during frameless Gamma Knife Icon therapy: The relationship between cone beam CT assessed intracranial anatomy displacement and infrared-tracked nose marker displacement. J Radiosurg SBRT 6(1), 67–76
2. M Peach, D Trifiletti, S Dutta, J Larner, D Schlesinger, et al. (2018) Spatial shifts in frame-based Gamma Knife radiosurgery: A case for cone beam CT imaging as quality assurance using Gamma Knife Icon J Radiosurg SBRT 5(4), 315–322
3. M Zeverino, M Jaccard, D Patin, N Ryckx, M Marguet, et al. (20,017) Commissioning of the Leksell Gamma Knife Icon Med. Phys. 44 (2), 355–363
4. I AlDahlawi, D Prasad, M B Podgorsak (2017) Evaluation of stability of sterotactic space defined by cone-beam CT for the Leksell Gamma Knife Icon. J Appl Clin Med Phys 18 (3), 67–72
5. B Maraghechi, T Kim, T Mitchel, S M Goddu, J Dise, et.al. (2021) Filmless quality assurance of a Leksell Gamma Knife Icon. J Appl Clin Med Phys 22 (1), 59–67
6. W N Duggar, B Morris, A Fatemi, J Bonds, R He, et.al (2019) Gamma Knife Icon CBCT offers improved localization workflow for frame-based treatment. J Appl Clin Med Phys 20 (11), 95–103
7. G Wright, N Harrold, P Hatfield, P Bownes (2017) Validity of the use of nose tip motion as a surrogate for the intracranial motion in mask-fixated frameless Gamma Knife Icon therapy. J Radiosurg SBRT 4(4), 289–301
8. A Fatemi, S Taghizadeh, C Yang, M Kanakamedala, B Morris, S Vijaayakumar (2017) Machine-specific magnetic resonance imaging quality control procedures for stereotactic radiosurgery treatment planning. Cureus 9(12): e1957

O023 The dosimetric impact of arc number in SRS for single brain mets

H. Davis[1], A Taychasiraprapagul[1], Dane Pope[1], David Odgers[1], Elizabeth Claridge Mackonis[1], Helen Lo[1], J. E. Morales (Presenting author)[1,2]

[1]Department of Radiation Oncology, Chris O'Brien Lifehouse, Sydney, Australia; [2]Queensland University of Technology, Brisbane, Australia

Introduction Brainlab Elements (Brainlab) has been utilized to treat single metastatic brain tumours. Our department employs five dynamic arcs to ensure optimal dose coverage to the PTV, and minimal dose to surrounding OARs. This study investigated the impact of reducing the number of arcs by comparing Conformity Index (CI) variation in the PTV as well as the volume of normal brain tissue being exposed to 5 Gy (V_{5Gy}).

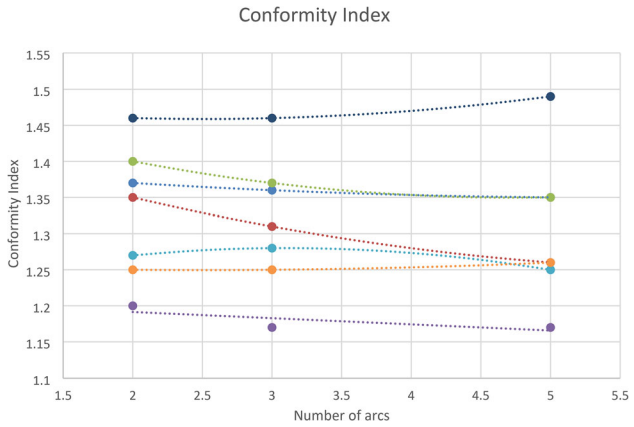

Fig. 1 Conformity Index as a function of number of arcs

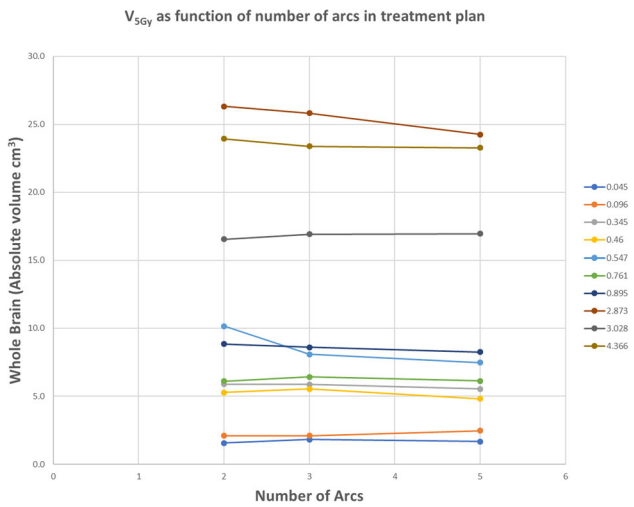

Fig. 2 V_{5Gy} as a function of arcs

Method Previous treatment plans which used 5 dynamic arcs were recalculated in Brainlab Multiple Brain Mets (V1.5) using 2 and 3 arcs. All plans were created for a 6X-SRS beam on a Novalis Trilogy linear accelerator. For each plan, conformity index for the PTV and V_{5Gy} were recorded for the different number of arcs.
Results Fig. 1 shows the variation of CI as a function of number of arcs. The CI values ranged from 1.5 to 1.17. The largest variation in CI for a PTV varied by 0.2 which is considered relatively minor for these treatments. Figure 2 shows the results for the V_{5Gy} as function of number of arcs. It is readily seen that the variation in V_{5Gy} is between 26 to 4 cm^3. This variation is dependent on patient anatomy and the size of normal brain volume.
Conclusion This study shows that the change in CI is minimal when a 2 or 3 arc plan is used to treat a single brain met. The reduction of the number of arcs could reduce treatment time without compromising plan quality.

O024 Comparison of Gold and Polymark™ fiducial markers for liver SABR planning and image-guided radiotherapy

E. L. Seymour[1], S. Tang[1], M. Gibbons[1], R. Cone[1], B. J. Zwan[1]

[1]Central Coast Cancer Centre. erin.seymour@health.nsw.gov.au (Presenting author); simon.tang@health.nsw.gov.au; mitchell.gibbons@health.nsw.gov.au; rebecca.cone@health.nsw.gov.au; benjamin.zwan@health.nsw.gov.au

Introduction The use of fiducial markers in close proximity to the tumour for liver stereotactic ablative radiotherapy (SABR) has been shown to increase dosimetric delivery accuracy [1, 2]. Phantom studies have identified that polymer-based markers produce less artefacts than gold fiducials for CT and CBCT imaging and are visible on MRI and kV planar images, potentially making them more suitable for image guided radiotherapy [3–5]. To date, no liver-specific clinical evaluation of Polymark™ fiducials has been performed.
Method *Phase 1* The feasibility of using Polymark™ fiducial markers was determined by qualitative comparison with gold fiducial markers. Each set of markers was positioned in the abdominal region of an anthropomorphic phantom which was imaged using CT, CBCT and kV triggered imaging. Each image dataset was assessed in terms of marker visibility and artefact production.
Phase 2 MRI, CT, CBCT and kV triggered images were acquired for a patient inserted with Polymark™ fiducials. The acquired images were qualitatively compared to images previously acquired containing gold fiducials.
Results Three Radiation Oncologists and five Radiation Therapists completed a questionnaire to rate the two markers which were visible on all imaging modalities as shown in Fig. 1. Gold fiducials produced extensive artefacts which impacted both target delineation and image matching when positioned close to the tumour volume. As a result, all Radiation Oncologists and Therapists rated the Polymark™ fiducials more favourably. Polymark™ fiducials have consequently been adopted as standard clinical practice for liver SABR.
Conclusion Polymark™ fiducials were deemed advantageous over gold for liver SABR as they resulted in less artefacts, allowing for closer placement to the primary tumour without compromising uncertainty in GTV delineation. The closer proximity improves tumour location surrogacy, thus improving the dosimetric accuracy of Liver SABR.

References

1. Seppenwoolde Y, Wunderink W, Wunderink-van Veen SR et al. (2011) Treatment precision of image-guided liver SBRT using implanted fiducial markers depends on marker-tumour distance. Phys. Med. Biol. 56: 5445–5468. https://doi.org/10.1088/0031-9155/56/17/001
2. Robin TP, Jones BL, Goodman KA (2017) Fiducial markers are necessary for accurate delivery of liver SBRT. Int. J. Radiat. Oncol. Biol. Phys. 99(2) S222. https://doi.org/10.1016/j.ijrobp.2017.06.546

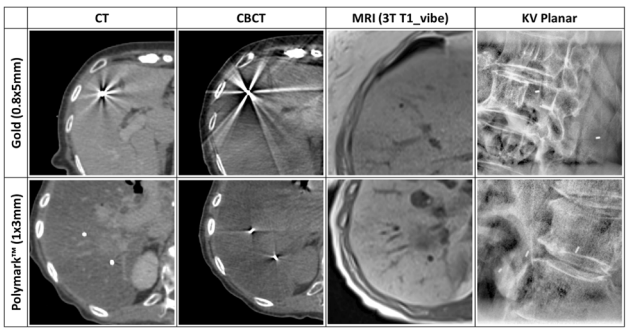

Fig. 5 Comparison between gold and Polymark ™ fiducial markers

3. Chan MF, Cohan GN, Deasy JO (2015) Qualitative evaluation of fiducial markers for radiotherapy imaging. Technol. Cancer. Res. T. 14: 298–304. https://doi.org/10.1177/1533034614547447
4. Osman SOS, Russell E, King RB et al. (2019) Fiducial marker visibility and artefacts in prostate cancer radiotherapy multi-modality imaging. Radiat. Oncol. 14: 237. https://doi.org/10.1186/s13014-019-1447-1
5. Handsfield LL, Yue NJ, Zhou J et al. (2012) Determination of optimal fiducial marker across image-guided radiation therapy (IGRT) modalities: visibility and artifact analysis of gold, carbon, and polymer fiducial markers. J Appl Clin Med Phys. 13(5):3976. https://doi.org/10.1120/jacmp.v13i5.3976

O025 Custom phantom for daily stereotactic isocentre co-incidence of the XVI & ExacTrac imaging systems to a 6MV beam including shift accuracy of the HexaPOD 6DOF couch

Luke K Webb[1] (Presenting author), Christopher Noble[1], Prabhakar Ramachandran[1]

[1]Radiation Oncology Princess Alexandra Ipswich Road, Brisbane, QLD, Australia; Luke.Webb@health.qld.gov.au; Christopher.Noble@health.qld.gov.au; Prabhakar.Ramachandran@health.qld.gov.au

Introduction Daily verification of imaging and treatment isocentre coincidence can be a time-consuming process. Total run-up time on stereotactic machines consists of 1-h RT machine warm-up & safety checks (non-stereo imaging tolerances) + 0.5-h for physics isocentre QA. The goal of this project was to design a suitable phantom that would enable verification of both the XVI (Elekta) and Exactrac (Brainlab) imaging isocentres to the 6MV treatment beam, whilst also covering the required daily imaging safety checks & couch QA to a stereotactic tolerance and hence remove duplication in the morning run-up process.

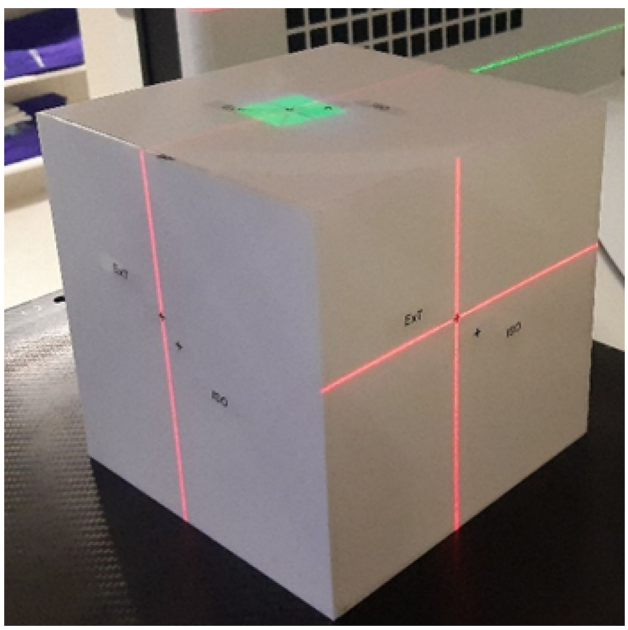

Figure 6 Custom phantom setup to the initial ExacTrac start position

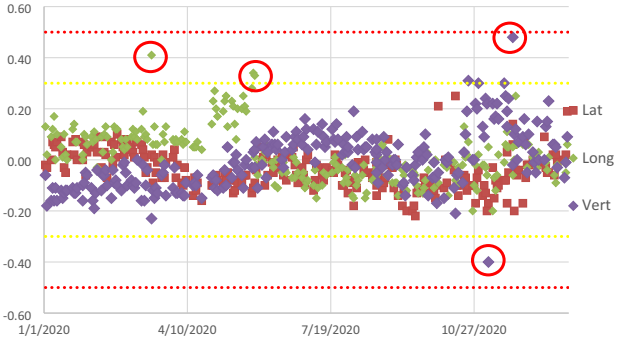

Fig. 7 Exactrac-MV isocentre co-incidence

Method A 16 × 16x16 cm box was made from 3 mm thick Perspex. A 7 mm ball bearing was placed at the isocentre, while 5 × 3 mm ball bearings and 6 × 2.5 cm diameter plastic tubes with a 1 cm diameter central hollow section were placed randomly around the isocentre. The phantom was CT simulated on a Philips Brilliance, with sharpness filters applied to ensure accurate geometrical representation of the ball bearings. The Exactrac fusion settings were based on the ball bearing positions, while XVI fusion was based on the grey value of the plastic rods. To remove user dependence on setup, the workflow ustilises the ExacTrac system for initial positioning. Couch shifts to the isocentre are then acquired and performed using XVI and HexaPOD systems. Verification of the couch shift and isocentre co-incidence of each system is perfomred using a modified Elekta flex-map field ($4cm^2$) with simultaneous intrafraction imaging and the Exactrac inbuilt winston-lutz process.
Results The time required to perform a morning run-up was reduced from 1.5 h to 1 h while still maintaining the required stereotactic QA tolerance. Figure 2 below shows the Exactrac-MV isocentre co-incidence with values outside action level highlighted, with each being corrected before treatment proceeded.
Conclusion An inhouse designed phantom was able to improve efficiency on a daily basis while maintaining stereotactic tolerances required for safe treatment.

O026 Implication of using Mobius 3D as a redundancy check for Acuros XB

Rachitha Antony[1], Elena Ungureanu[1], Jenny Lydon[1]

[1]Peter MacCallum Cancer Centre Melbourne Victoria; Rachitha.Antony@petermac.org (Presenting author); Elena.Ungureanu@petermac.org; Jenny.Lydon@petermac.org

Introduction At Peter MacCallum Cancer Centre we use Mobius V2.1.2 as the secondary dose calculation verification system for all modulated treatments. We aim to reduce the current gamma criteria 3%3 mm to the AAPM TG 218 recommended standards and thereby identify the regions of failure to avoid instance of missing the errors.
Method 35 VMAT and 30 IMRT plans were incorporated for the study. All the plans were generated in EclipseV15.6 and calculated with Acuros XB algorithm. Plans were recalculated with 3%2 mm in Mobius at a threshold of 10%. The default gamma in M3D is 5%3 mm.
Results 33 VMAT plans achieved overall gamma passing rate greater than 95%. For IMRT, 7 plans fell below 95% and 3 plans fell below 90%.The plans with passing rate below clinical tolerance belonged to the skin, lung and head & neck tumour stream.

Conclusion Preliminary study shows that there is no impact on number of VMAT plans passing if we reduce M3D gamma criteria to 3%2 mm.However we noticed a 7% increase in IMRT plan failure. This is due to the complexity in the plan and the known limitations of Mobius in surface, interface and high energy modelling and the difference in Eclipse and Mobius algorithm.M3D calculates energy deposition in dose to water and Eclipse use dose to medium. M3D is a calculation based system with set-up errors not taken into consideration as in measurement. Requirement for tighter tolerance to identify the dose errors have been advised in ref [3].Reducing the tolerance to AAPM recommended values will result in small number of failing plans. However this is appropriate in order to identify errors that cannot be explained by Mobius limitations.

References

1. Report No. 218—Tolerance Limits and Methodologies for IMRT Measurement-Based Verification QA: Recommendations of AAPM Task Group No. 218 (2018) https://doi.org/10.1002/mp.12810
2. Jonas D. Fontenot "Evaluation of a novel secondary check tool for intensity modulated radiotherapy treatment planning". J Appl Clin Med Phys. 2014 Sep; 15(5): 207–215 https://doi.org/10.1120/jacmp.v15i5.4990
3. Benjamin E.Nelms "Per-beam, planar IMRT QA passing rates do not predict clinically relevant patient dose errors". https://doi.org/10.1118/1.3544657

O027 Beyond the passing rate, using gamma statistics for improved analysis

Jessica Lye[1], Leah McDermott[1], Maddison Shaw[2], Benjamin Harris[1], Hema Vaithianathan[1], Reza Alinaghi[1], Nikki Shelton[1], Kym Rykers[1]

[1]Olivia Newton John Cancer Research and Wellness Centre, Austin Health, Melbourne; jessica.lye@austin.org.au (Presenting author). Leah.McDermott@austin.org.au; [2]Australian Clinical Dosimetry Service, ARPANSA, Melbourne. Maddison.shaw@arpansa.gov.au; Benjamin.harris@austin.org.au; Hema.vaithianathan@austin.org.au; reza.alinaghizadeh@austin.org.au; Nikki.shelton@austin.org.au; Kym.rykers@austin.org.au

Introduction The gamma evaluation is the most widely used metric for comparing measured and calculated IMRT/VMAT plans. Gamma combines dose difference and distance-to-agreement in one index per voxel, based on set criteria [1]. Although the passing rate provides an overall assessment, it has limitations for trend analysis as it can easily saturate, or rapidly decline beyond the dose limit. Other metrics that can be extracted are the mean, median, and maximum value of the gamma values (software dependent). The mean gamma index scales with agreement, and is more useful for comparison with other plan parameters [2]. The purpose was to improve comparison tools for plan QA data.

Method From the ONJ centre, γ_{mean} was evaluated for VMAT stereotactic plans, for six anatomical sites, measured with the PTW 4D Octavius-SRS1000 array. 3D dose distributions were compared with plans using Verisoft v7.2 (PTW). ACDS audit plans for the TG-119 C-Shape were also evaluated using γ_{mean} results of 2D dose distributions, planned with three algorithms and measured with PTW Octavius1500 2D array, at departments across Australia.

Results The passing rate for all plans was > 98%. Considering complexity, γ_{mean} was positively correlated with MU/cGy (Fig. 8). Figure 9(a) (all sites analysed with the same gamma index) indicates the higher γ_{mean} for more complex spinecases. The brain outlier was attributed to a complex lesion shape at the base of skull. Figure 9(b) maps audit results from the last year. For one case (homogenous phantom), Eclipse AXB γ_{mean} was higher than for AAA. MC results covered a similar range as AAA and AXB.

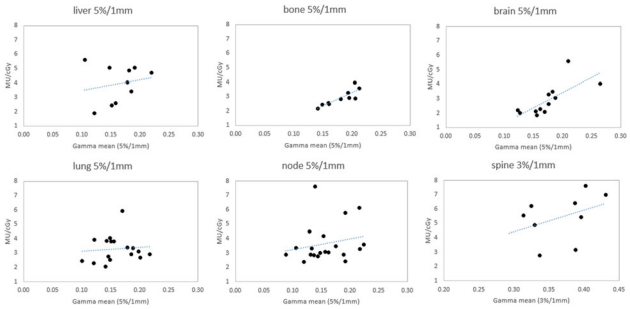

Fig. 8 Mean 3D gamma indices versus complexity, MU/cGy, per plan and anatomical site. Gamma criteria were 5% (3% for spine) and a 10% threshold

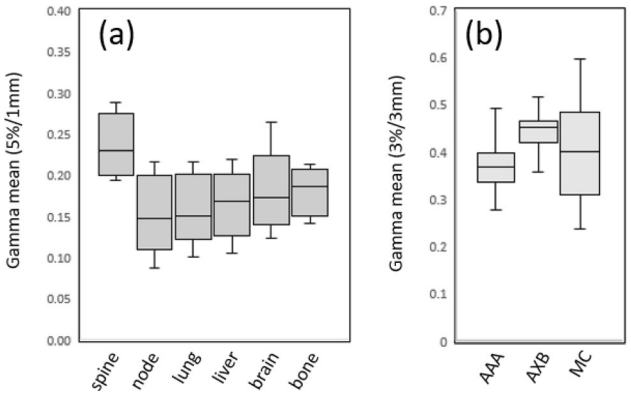

Fig. 9 **a** Mean 3D gamma index summarised for 6 sites from ONJ (using 5%/1 mm, 10% threshold for all sites). **b** Mean 2D gamma index from ACDS audit results for three algorithms (3%, 3 m, 10% threshold.)

Conclusion Mean and maximum gamma can provide insights passing rates cannot, for both clinical QA comparing many patient plans of varying complexity from a single department, or dosimetry audits comparing the same plan type with algorithms/equipment across the country.

References

1. Low DA, Harms WB, Mutic S, Purdy JA. A technique for the quantitative evaluation of dose distributions. Med Phys 1998;25:656–61.
2. McDermott L, Wendling M, Van Asselen B, Stroom J, Sonke J, Van Herk, M, Mijnheer B, Med. Phys 2006:33:3921–3930

O028 Use of machine learning to predict the chamber-measured point dose for patient-specific quality assurance

A. Xing[1,2,3], A. Hidar[2,3], P. Vial[1,2,3], L. Holloway[1,2,3]

[1]Liverpool and Macarthur Cancer Therapy Centres, Sydney, NSW Australia; [2]Ingham Institute for Applied Medical Research,

Liverpool, NSW Australia; [3]South Western Sydney Clinical School, University of NSW, Liverpool, NSW Australia.
aitang.xing@health.nsw.gov.au (Presenting author); a.haidar@unsw.edu.au; Philip.Vial@health.nsw.gov.au; Lois.Holloway@health.nsw.gov.au

Introduction Machine learning has been used for patient-specific quality assurance since 2016 and various studies have been done to predict the Gamma pass rate based on different detectors.(1) In our centre, the point dose in the high-dose planning volume region (PTV) was measured along with the planar dose. The purpose of this study is to use machine learning to predict the point dose based on the data of past patients.
Method 4010 patients were treated using Volume-modulated radiotherapy, Stereotactic body radiotherapy, and Stereotactic ablative radiotherapy using 6MV and 10MV flattening-filter free beam cross different sites. The dose at a point in PTV is measured using a CC13 thimble chamber and compared to the treatment planning system calculated mean dose of small volume corresponding to the chamber's volume. Except for the mean dose, the following dose-volume histogram parameters of this volume are recorded: maximum dose, minimum dose, standard deviation, global maximum dose, and total monitor unit (MU). The machine learning model XGBoost (2) was used and the patient data divided into a training dataset (90%) and test dataset (10%). The feature variables mean dose, minimum dose, maximum dose, global maximum dose, standard deviation, total MU, energy, treatment sites, and machine. The predicted variable is the measured point dose.
Results The optimal module tuning parameters are n_estimators = 106, learning_rate = 0.23527, subsample = 0.84399, colsample_Bytree = 0.7914. R2-score, MSE, and EVS of the model are 0.999507, 0.08998, and 0.999505, respectively. The minimum, mean and maximum difference between the predicted dose and actual measured dose are -0.000143 Gy, 0.00004098 Gy, and 0.696 Gy. The standard deviation across the test dataset is 0.0763. 92.3% of predictions are within 3% of the measured dose with the mean percentage difference of 1.3%.
Conclusion The chamber-measured point dose can be predicted accurately using a tree-based ensemble learning model for patient-specific quality control.
References

1. Chan M F, Witztum A and Valdes G (2020) Integration of AI and Machine Learning in Radiotherapy QA. Front. Artif. Intell. 3:577,620.
2. Chen T,Guestrin, C. (2016). XGBoost: A Scalable Tree Boosting System. In Proceedings of the 22nd ACM SIGKDD International Conference on Knowledge Discovery and Data Mining (pp. 785–794). New York, NY, USA: ACM. https://doi.org/10.1145/2939672.2939785

O029 Comparison of global and local gamma evaluation with isodose levels

Nancy Yu[1], Tanya Kairn[1], Scott Crowe[1]

[1]Royal Brisbane and Women's Hospital. nancy.yu@health.qld.gov.au (Presenting author)

Introduction Gamma analysis usually reports a single pass rate for the entire dose distribution. Sometimes it might be beneficial to evaluate its performance within certain dose ranges separately for investigation purposes. This study has evaluated the performance of global and local gamma analyses with various isodose levels.

Method Global and local gamma analyses were performed using an in-house developed gamma code on patient-specific quality assurance (PSQA) plans generated from Eclipse v13.7 Treatment Planning System (TPS) and delivered on an ArcCheck phantom, for 100 volumetric modulated arc therapy (VMAT) arcs and 100 helical tomotherapy (HT) plans. Isodose levels were set from zero to 100% of maximum dose with 10% increments. Gamma pass rates were evaluated on each isodose level and compared with the total pass rate.
Results Minimal differences were observed between the results of evaluating all VMAT arcs separately and those of evaluating VMAT plans by combining arcs, other than a slightly increased skew towards higher pass rates for the global gamma evaluation. Generally, the VMAT results showed average pass rates that increase with decreasing isodose level, for both global and local gamma evaluations. The HT results differed systematically from the VMAT results, with the results of performing global and local gamma evaluations agreeing more closely at all isodose levels and with the highest gamma pass rates being achieved at intermediate dose levels, between the 40 and 70% isodose levels. These results demonstrate the complex of relationships between global and local gamma evaluations that can arise when clinical PSQA data are analysed and exemplify how the local gamma evaluation does not necessarily produce disproportionately reduced gamma pass rates in low dose regions.

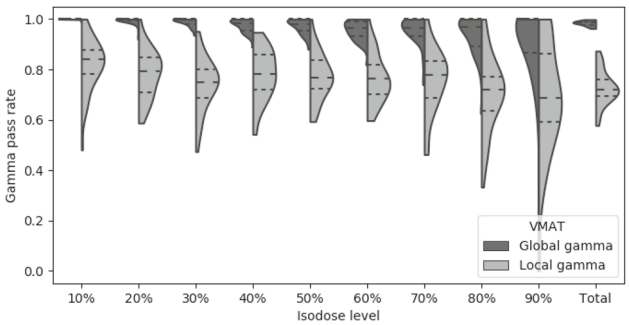

Fig 1. Violin plot of global (dark grey) and local (light grey) gamma pass rates versus isodose levels for 41 VMAT plans (100 arcs)

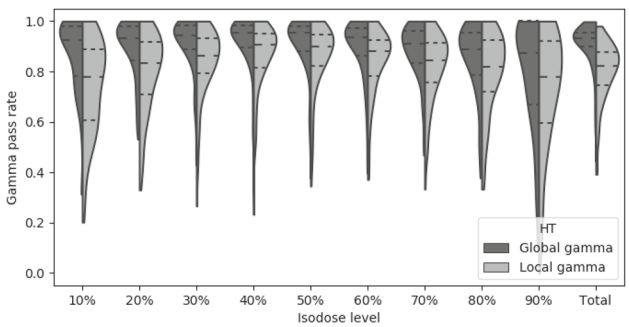

Fig 2. Violin plot of global (dark grey) and local (light grey) gamma pass rates versus isodose levels for 100 HT plans

Conclusion Performing gamma evaluation with different isodose levels is suggested as a useful method to improve understanding of specific PSQA data as well as the broader features of gamma evaluation results.

References

1. Bailey DW, Nelms BE, Attwood K, Kumaraswamy L, Podgorsak MB. Statistical variability and confidence intervals for planar dose QA pass rates. Medical physics. 2011;38(11):6053–6064.
2. Barber J, Vial P, White P, et al. A survey of modulated radiotherapy use in Australia & New Zealand in 2015. Australasian physical & engineering sciences in medicine. 2017;40(4):811–822.
3. Binny D, Kairn T, Lancaster CM, Trapp JV, Crowe SBJMD. Photon optimizer (PO) vs progressive resolution optimizer (PRO): a conformality-and complexity-based comparison for intensity-modulated arc therapy plans. 2018;43(3):267–275.
4. Crowe S, Kairn T, Middlebrook N, et al. Examination of the properties of IMRT and VMAT beams and evaluation against pre-treatment quality assurance results. 2015;60(6):2587.
5. Crowe SB, Sutherland B, Wilks R, et al. Relationships between gamma criteria and action levels: Results of a multicenter audit of gamma agreement index results. 2016;43(3):1501–1506.
6. Depuydt T, Van Esch A, Huyskens DPJR, oncology. A quantitative evaluation of IMRT dose distributions: refinement and clinical assessment of the gamma evaluation. 2002;62(3):309–319.
7. Fraass B, Doppke K, Hunt M, et al. American Association of Physicists in Medicine Radiation Therapy Committee Task Group 53: quality assurance for clinical radiotherapy treatment planning. Medical physics. 1998;25(10):1773–1829.
8. Hunter JD. Matplotlib: A 2D graphics environment. Computing in science & engineering. 2007;9(3):90–95.
9. Hussein M, Clark C, Nisbet AJPM. Challenges in calculation of the gamma index in radiotherapy–towards good practice. 2017;36:1–11.
10. Low DA, Dempsey JF. Evaluation of the gamma dose distribution comparison method. Medical physics. 2003;30(9):2455–2464.
11. Low DA, Harms WB, Mutic S, Purdy JA. A technique for the quantitative evaluation of dose distributions. Medical physics. 1998;25(5):656–661.
12. Miften M, Olch A, Mihailidis D, et al. Tolerance limits and methodologies for IMRT measurement-based verification QA: Recommendations of AAPM Task Group No. 218. Medical physics. 2018;45(4):e53-e83.
13. Mijnheer B, Olszewska A, Fiorino C, et al. Quality assurance of treatment planning systems: practical examples for non-IMRT photon beams. Vol 1: Estro Brussels; 2004.
14. Nelms BE, Chan MF, Jarry G, et al. Evaluating IMRT and VMAT dose accuracy: practical examples of failure to detect systematic errors when applying a commonly used metric and action levels. Medical physics. 2013;40(11):111,722.
15. Nelms BE, Zhen H, Tomé WA. Per-beam, planar IMRT QA passing rates do not predict clinically relevant patient dose errors. Medical physics. 2011;38(2):1037–1044.
16. Oliphant TE. A guide to NumPy. Vol 1: Trelgol Publishing USA; 2006.
17. Petoukhova A, Van Egmond J, Eenink M, Wiggenraad R, Van Santvoort JJPiM, Biology. The ArcCHECK diode array for dosimetric verification of HybridArc. 2011;56(16):5411.
18. Poppe B, Looe H, Luellau T, Willborn K, Allgaier B, Harder D. SU-E-T-139: Note on the Underestimation of the Dosimetrical Significance of Detected IMRT Verification Deviations Using the Gamma-Index Method and a Global Acceptance Criterion Based on the Number of Passing Points. Medical Physics. 2011;38(6Part12):3518–3518.
19. Stasi M, Bresciani S, Miranti A, Maggio A, Sapino V, Gabriele P. Pretreatment patient-specific IMRT quality assurance: a correlation study between gamma index and patient clinical dose volume histogram. Medical physics. 2012;39(12):7626–7634.
20. Stathakis S, Myers P, Esquivel C, Mavroidis P, Papanikolaou N. Characterization of a novel 2D array dosimeter for patient-specific quality assurance with volumetric arc therapy. Medical physics. 2013;40(7).
21. Steers JM, Fraass BA. IMRT QA: Selecting gamma criteria based on error detection sensitivity. Medical physics. 2016;43(4):1982–1994.
22. Stojadinovic S, Ouyang L, Gu X, Pompoš A, Bao Q, Solberg TD. Breaking bad IMRT QA practice. Journal of applied clinical medical physics. 2015;16(3):154–165.
23. Van Rossum G. Python Programming Language. Paper presented at: USENIX Annual Technical Conference2007.
24. Virtanen P, Gommers R, Oliphant TE, et al. SciPy 1.0: fundamental algorithms for scientific computing in Python. 2020; 17(3):261–272.
25. Waskom M BO, Gelbart M, et al.,. mwaskom/seaborn: v0.11.0 (September 2020), Zenodo. Available at: https://doi.org/10.5281/zenodo4019146. 2017.
26. Wendling M, Zijp LJ, McDermott LN, et al. A fast algorithm for gamma evaluation in 3D. 2007;34(5):1647–1654.
27. Yu L, Kairn T, Trapp J, Crowe SB. A modified gamma evaluation method for dose distribution comparisons. Journal of applied clinical medical physics. 2019;20(7):193–200.
28. Zhen H, Nelms BE, Tomé WA. Moving from gamma passing rates to patient DVH-based QA metrics in pretreatment dose QA. Medical physics. 2011;38(10):5477–5489.

O030 Development of 3D-printed radiotherapy shielding for superficial radiotherapy

S. B. Crowe[1,2,3,4], W. Li[3], S. Cleland[5], E. Simpson-Page[1], N. Cassim[1], S. K. Maxwell[1], P. Charles[2,3,4], T. Kairn[1,2,3,4]

[1]Cancer Care Services, Royal Brisbane and Women's Hospital, Brisbane, Queensland, Australia; [2]Herston Biofabrication Institute, Metro North Hospital and Health Service, Brisbane, Queensland, Australia; [3]School of Information Technology and Electrical Engineering, University of Queensland, Brisbane, Queensland, Australia; [4]School of Chemistry and Physics, Queensland University of Technology, Brisbane, Queensland, Australia; sb.crowe@gmail.com (Presenting author); weizheng.li@uq.net.au; [5]Radiation Oncology Princess Alexandra Raymond Terrace, Brisbane, Queensland, Australia. susannah.cleland@health.qld.gov.au; emily.simpson-page@health.qld.gov.au; naasiha.cassim@health.qld.gov.au.; sarah.maxwell@health.qld.gov.au; paul.charles@health.qld.gov.au; tanya.kairn@health.qld.gov.au

Introduction Kilovoltage radiotherapy is sometimes used for treatments of complex anatomical sites, such as the ears, nose and eyes; where other treatments such as electron radiotherapy and surgery may not be desired due to dosimetric and cosmetic disadvantages. Historically, these treatments have involved the use of moulded lead (Pb) shielding of sufficient thickness to reduce dose to 5%. High density non-toxic 3D-printable materials provide an alternative method to produce a patient-matched shield.

Method Two composite filaments, Copperfill (Cu-PLA) and 3DShield (W-PLA), were investigated in this study. The thickness required to reduce dose to 5% of unshielded value was estimated for 7

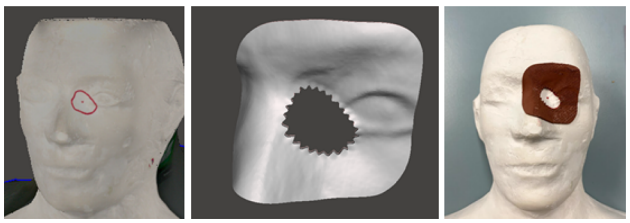

Fig. 1 (Left) marked up phantom, (centre) designed shielding, (right) printed shielding

kilovoltage beams, ranging from 70 kV / 1.2 mm Al to 300 kV / 3.88 mm Cu. The transmission factor, or ratio of shielded and unshielded dose, was estimated for a 2 cm diameter applicator based on iterative attenuation of the primary beam determined using SpekPy, and backscatter and mass energy transfer calculations using AAPM TG 61 data (incorporating changes in beam quality) [1]. Calculations were verified by measurement. Shielding has subsequently been designed using images acquired with 3D and CT scanning, using Autodesk Meshmixer, and printed on a consumer-grade Creality Ender 5 3D printer.

Results The required thickness of shielding ranged from 1.9–8.0 mm Cu-PLA and 0.3–0.8 mm Wu-PLA for $\leq$ 100 kV beams, and 4.0–4.9 Wu-PLA for 300 kV beams. A serrated shield designed for a 3D-scanned plaster phantom and fabricated in Cu-PLA is shown in Fig. 1.

Conclusion 3D-printing techniques can be used to design patient-matched shielding for kilovoltage radiotherapy treatments.

Acknowledgements This work was made possible by the Herston Biofabrication Institute Cancer Care Services programs, supported by the Metro North Hospital and Health Service.

References

1. Crowe, S. B., Charles, P. H., Cassim, N., Maxwell, S. K., Sylvander, S. R., Smith, J. G., Kairn, T., 2021. Predicting the required thickness of custom shielding materials in kilovoltage radiotherapy beams. Physica Medica 81: 94–101.

O031 Lessons learnt on the road to fabricating materials that are bone-equivalent in both kilovoltage and megavoltage photon beams

T. Kairn[1,2,3], A. Buddhavarapu[4], N. Cassim[1], P. H. Charles[2,3,5], L. Jessen[6], S. B. Crowe[1,2,3,5]

[1]Cancer Care Services, Royal Brisbane and Women's Hospital, Brisbane, Qld, Australia; [2]School of Information Technology and Electrical Engineering, University of Queensland, Brisbane, Qld, Australia; [3]School of Chemistry and Physics, Queensland University of Technology, Brisbane, Qld, Australia; t.kairn@gmail.com (Presenting author); [4]Ballarat Austin Radiation Oncology Centre, Ballarat, Vic, Australia; [5]Herston Biofabrication Institute, Metro North Hospital and Health Service, Brisbane, Qld, Australia; [6]Lund University, Lund, Sweden

Introduction Fabrication of bone-equivalent materials for use in radiotherapy phantoms is an area of growing research interest, with substantial practical challenges [1, 2]. While we have made much of our recent successes in the area of fabricating bone-equivalent materials [3,4,5], it is important to share our early failures, as a guide to others who may be investigating these same questions. Given the risk of inadvertently producing a material that was bone-equivalent at kilovoltage (kV) photon energies but not at megavoltage (MV) photon energies [6], and therefore unsuitable for use in radiotherapy phantoms, this work was focussed on mixing approximately tissue-equivalent materials (wax/fat, sawdust/cellulose) with materials chemically similar to bone (shells, plaster, calcium carbonate) with the aim of achieving bone-equivalence across the kV-MV range.

Method Attempts were made to fabricate materials that were bone-equivalent at both kV and MV photon beams, using materials listed in the lower half of Table 1. The upper half of Table 1 shows reference materials for comparison; a nominally bone-equivalent plug from a Gammex CT calibration phantom and a sample of human skull bone. Bone equivalence was assessed using computed tomography (CT) imaging using a 120 kV beam from a Siemens Somatom Confidence CT scanner and 3.5 MV imaging beam from a Tomotherapy Hi-Art unit. Hounsfield units (HU) from these kV CT and MV CT scans were converted to relative electron densities (RED) using existing HU-RED relationships for these two imaging systems.

Table 1 Summary of materials investigated and corresponding observations.

Fabrication method	RED from kV CT	RED from MV CT	Comment	Illustration
Gammex bone B200 in water (nominal RED = 1.10)	1.11 ± 0.01	1.10 ± 0.02	kV & MV results within uncertainties of nominal	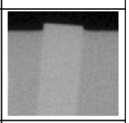
Gammex bone B200 in air (nominal RED = 1.10)	1.02 ± 0.01	1.08 ± 0.03	MV result within uncertainty of nominal. kV over-corrected for beam hardening.	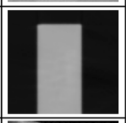
Human skull bones in water	1.9 ± 0.3	1.5 ± 0.1	kV & MV results agree within uncertainties, close to RED of cortical bone	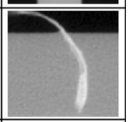
Human skull bones in air	1.5 ± 0.3	1.2 ± 0.3	kV & MV results agree within uncertainties, though kV more affected by air around	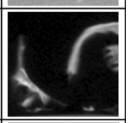
Sea shells in air	1.2 ± 0.6	0.8 ± 0.3	Very heterogeneous, lots of air between shells	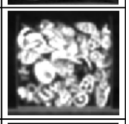
Sea shells mixed with wax	1.3 ± 0.4	1.2 ± 0.2	Very heterogeneous, though wax did get between shells.	
Plaster of Paris mixed with sawdust	1.1 ± 0.1 at top of sample 1.6 ± 0.2 at bottom of sample	1.1 ± 0.1 at top of sample 1.3 ± 0.1 at bottom of sample	Could be an acceptable model for bone, if suspension was achieved	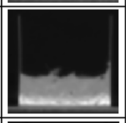
$CaCO_3$ in wax	1.7 ± 0.1	1.36 ± 0.07	$CaCO_3$ –wax mixtures could be model denser bone in MV, though kV result is inconsitent.	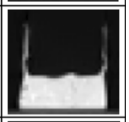
$CaCO_3$ in resin (samples with 30% and 50% $CaCO_3$)	1.17 ± 0.07 at top of 30% 1.4 ± 0.2 at top of 50%	N/A (Not imaged due to obvious sedimentation)	Samples containing less $CaCO_3$ could be suitable, if suspension was achieved	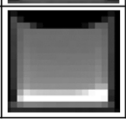

Results Converting mass density data from ICRP 23 [7] suggests that RED values for bone should range from approximately 1.13 (spongiosa) to 1.77 (cortical). Results summarised in Table 1 suggest that many materials used in this study could fall into this range, although issues with heterogeneity and sedimentation need to be resolved and kV imaging of samples without surrounding material (eg. water) should be avoided due to unrealistic beam hardening corrections [8].

Conclusion Some results of this work are promising enough to warrant further refinement, while the overall concept of combining bone-like materials with tissue-like materials to achieve variable "bone" densities may also inspire further work. It is hoped that this open discussion of "failures" will lead other groups to achieve successes in fabricating alternative bone-equivalent materials in the future.

Acknowledgements S B Crowe and P H Charles' contributions to this work were supported by a Metro North Hospital and Health Service funded Herston Biofabrication Institute Programme Grant.

References

1. Grehn M, Stille M, Ziemann C, Cremers F, Rades D, Buzug TM (2019) A new phantom for individual verification of the dose distribution in precision radiotherapy for head-and-neck cancer. Anticancer Res 39(12): 6931–6938.
2. Šemnická J, Spěvácek V, Veselský T, Konček O, Novotný Jr J (2009) Designing phantom for head-and-neck treatment verification: Feasibility tests with bone and bone equivalent material incorporated into polymer gel. J Phys Conf Se 164: 012,065.
3. Kairn T, Zahrani M, Cassim N, Livingstone AG, Charles PH, Crowe SB (2020) Quasi-simultaneous 3D printing of muscle-, lung- and bone-equivalent media: a proof-of-concept study. Phys Eng Sci Med 43: 701–710.
4. Webb LK, Crowe SB, Heseltine L, Kairn T, Charles PH (2021) 3D printed tissue and bone equivalent anthropomorphic head phantom for electron beam validation, Engineering and Physical Sciences in Medicine conference, Brisbane 2021 (submitted)
5. Charles PH, Kairn T and Crowe SB (2021) "An unexpected change in the density of 3D printed PLA: on the importance of e-step calibration and QA to the clinical workflow." Engineering and Physical Sciences in Medicine conference, Brisbane 2021 (submitted)
6. Crowe SB, Bennett J, Lathouras M, Lancaster CM, Sylvander SR, Chua B, Bettington CS, Lin CY, Kairn T (2020) Impact of radiopacified bone cement on radiotherapy dose calculation. Phys Imaging Radiat Oncol 14: P12-P16.
7. Snyder WS, Cook MJ, Nasset ES et al. (1975) ICRP Publciation 23: Report on the task group on reference man. Pergamon Press, Oxford
8. Inness EK, Moutrie V, Charles PH (2014) The dependence of computed tomography number to relative electron density conversion on phantom geometry and its impact on planned dose. Australas Phys Eng Sci Med 37(2): 385–391.

O032 Quality 3D printing in poly-ether-ether-ketone

W. T. Lewin[1], N. Suchowerska[2], D. R. McKenzie[2,3]

[1]Surgical and Sarcoma Research Centre, Chris O'Brien Lifehouse, Sydney, Australia. will.lewin@lh.org.au (presenting author); [2]VectorLAB, Chris O'Brien Lifehouse, Sydney, Australia. Natalka.Suchowerska@lh.org.au; [3]School of Physics, University of Sydney, Sydney, Australia. david.mckenzie@sydney.edu.au

Introduction 3D printing is increasingly being used to customise implants to suit patient anatomy and therapeutic needs. Poly-ether-ether-ketone (PEEK) is a material with desirable mechanical properties and biocompatibility for use in health. However, there are several challenges for printing with PEEK, including high process temperatures and cooling control. The aim of this study is to develop process parameters and procedures to maximise PEEK printing quality and be able to meet regulatory requirements for production of orthopaedic implants.

Method The figure below shows the two 3D printing technologies available to this study, the AON M.2 (left), a fused filament fabrication (FFF) printer, and the EOS P800 (right), a selective laser sintering (SLS) printer. To optimise printing in PEEK, the specific parameters that need to be controlled were identified. The dominant parameters were:

FFF

1. Warmup temperatures and times
   - Extrusion/retraction settings
   - Nozzle to platform offsets

SLS

- Process chamber temperature
- Beam offset

Results Quality is defined by the specific application. For example, in dental applications, surface roughness is an important property to control, while for orthopaedic bone-replacement scaffolds, fine porosity must be achieved. The table below shows preliminary assessment results, showing the SLS process achieves a good approach to the modulus and ultimate tensile strength of bulk PEEK and the FFF approach achieves the small pore size for PEEK orthopaedic scaffolds.

Property	FFF	SLS	Bulk
Modulus (GPa)	–	4.865	3.6
Ultimate Tensile Strength (Mpa)	–	89.63	100
Elongation at break (%)	–	2.49	35
Surface roughness	–	–	–
Minimum lattice pore size	0.5 mm	1 mm	NA

Conclusion A detailed workflow was produced to obtain reproducible implants from PEEK. Although PEEK is a difficult material to use in additive manufacturing, the quality of the print can be optimised with careful attention to the customer requirements and behaviour of the material during manufacturing processes.

References/Acknowledgements

- Commonwealth of Asutralia
- The Pierce Armstrong Foundation for AON Printer donation
- 1966 Foundation for AON Printer donation
- The Goodridge Foundation for AON Printer donation

O033 Clinical Implementation of a Quality Assurance Program For 3D Printed Devices

A. G. Livingstone[1], E. M. Simpson-Page[1], T. Poroa[1], S. B. Crowe[1,2,3,4]

[1]Cancer Care Services, Royal Brisbane and Women's Hospital, Brisbane, Queensland, Australia. alexander.livingstone@health.qld.gov.au; emily.simpson-page@health.qld.gov.au; tania.poroa@health.qld.gov.au; [2]Herston Biofabrication Institute, Metro North Hospital and Health Service, Brisbane, Queensland, Australia. [3]School of Information Technology and Electrical Engineering, University of Queensland, Brisbane, Queensland, Australia. [4]School of Chemistry and Physics, Queensland University of Technology, Brisbane, Queensland, Australia; sb.crowe@gmail.com

Introduction As 3D printing becomes more affordable and accessible, 3D printed devices will become more prevalent in the radiotherapy treatment process. As these devices directly impact patient treatment, a robust quality assurance program ensuring their quality is required. This study details the QA program put in place at the Royal Brisbane and Women's Hospital and a review of initial results over its first year of operation.

Method Once the device has been designed, it is typically printed on a Raise 3D Pro 2 dual extrusion printer tuned to print water-equivalent densities. A CT scan of each object is analysed by in-house software which segments the device, analyses the distribution of HU values within, and generates an STL object from the slices. This STL is then compared to the original using the meshlab software to assess geometrical accuracy, which along with the mean RED is used to determine clinical suitability.

Results A total of around 60 devices have been printed and successfully used clinically since the implementation of the program. The mean RED of most of these devices falls within the clinically acceptable range of 0.95–1.05. Geometric accuracy is typically very good, with agreement within 0.5 mm across the surface of the device in most cases. A device where the incorrect infill settings were used (resulting in mean RED of 0.49) was successfully identified by the process, preventing mistreatment. Print settings were tuned when device REDs were trending outside of the acceptable range. The mean RED of the devices that were deemed acceptable was 1.00 ± 0.04 (Figs. 10, 11).

Conclusion A quality assurance program assessing the quality of 3D printed devices to be used during patient treatments has been implemented at the RBWH. Good density and geometric agreement for most devices has been observed, with printing errors also being able to be identified before clinical use.

Acknowledgements This work was supported by the Herston Biofabrication Institute Cancer Care Services program, funded by the Metro North Hospital and Health Service.

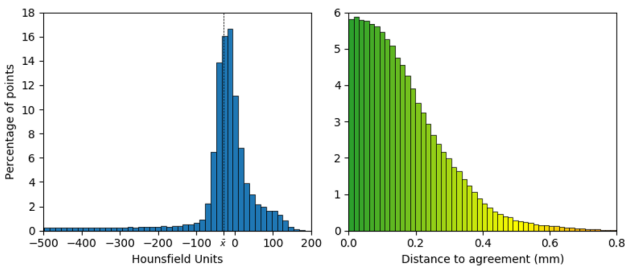

Fig. 10 Example of density (left) and geometric (right) accuracy results for a 3D printed device

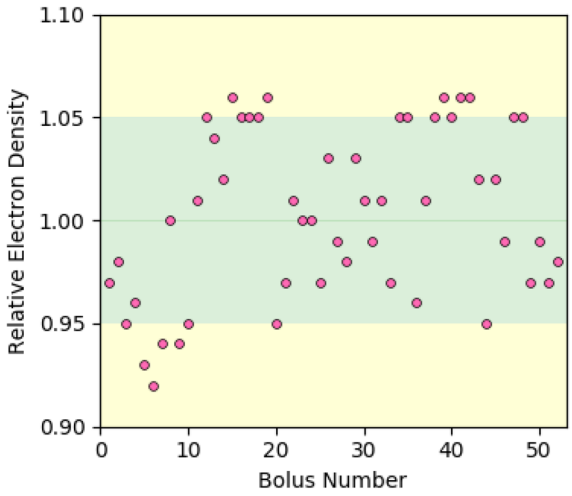

Fig. 11 REDs for the printed devices assessed since the implementation of the program (not including fail)

O034 A feasibility study—3D printed patient specific bolus generated with Fuel3D surface scanner in radiation therapy

P. Narayanan[1], V. Peng[1], J. Mathew[1], N. Hardcastle[1], B. Ha[2], H. M. Deloar[1], T. Kron[1]

[1]Department of Physical Sciences, Peter MacCallum Cancer Centre, Australia. Pradush.Narayanan@petermac.org (Presenting author); Valery.Peng@petermac.org; Joby.Mathew@petermac.org; Nick.Hardcastle@petermac.org; [2]Petermac Bendigo Radiotherapy Centre, Peter MacCallum Cancer Centre, Australia; Bruce.Ha@petermac.org; Deloar.Hossain@petermac.org; Tomas.Kron@petermac.org

Introduction Cancers arising near the skin treated by radiotherapy may require bolus to enhance the skin dose distribution. Usually, patient specific 3D bolus is designed in TPS using the planning CT of the patient. Therefore, the customised bolus will not be readily available during CT simulation. To overcome this, a method is proposed to design a 3D bolus using Fuel3D surface scanner which can be used during CT simulation.

Method right364490The feasibility study aims to simulate a clinical treatment to generate the customised 3D bolus of the anthropomorphic phantom using Fuel3D surface scanner. 3D surface of the phantom was created by acquiring pictures using surface scanner around the head phantom (Fig. 1). The Fuel3D software was used to post process the surface images into required thickness of reconstructed bolus.

The bolus is printed with Ultimaker™ printer using 100% infill density of PLA material which is adjusted to tissue equivalence. For comparison, another 3D printed patient specific bolus was generated using TPS which is currently used clinically.

To evaluate the clinical feasibility, boluses printed with both methods were attached to the correct position of the phantom and rescanned individually. The results of density, bolus thickness, geometry and contour fit were verified by overlaying both CT Images of the anthropomorphic phantom.

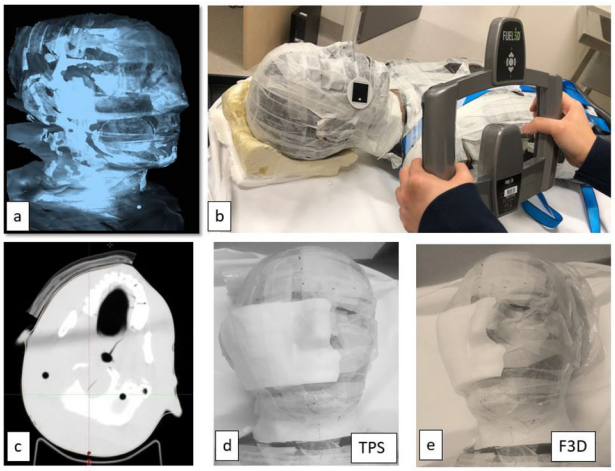

(Fig1) a)Surface reconstructed stich image from Fuel3D software b) Image capture using Fuel3D scanner c)Overlayed CT Images of F3D and TPS Bolus d&e) 3D printed bolus constructed using both methods

Results The differences of density, bolus thickness and geometry were within 20HU, 0.3 mm and 0.1 mm. Contour fit were matching when overlaid between the Image sets. The results were satisfactory when compared with the TPS fabricated bolus and it can accurately create customised bolus potentially acceptable for clinical use.
Conclusion 3D bolus generated with surface scanner was established and it can be used during the CT scanning used for planning. This bolus will perfectly fit on irregular body contour which avoids any air gap that produces accurate dose calculation in treatment planning.
References

1. Canters, R. A. et al. Clinical implementation of 3D printing in the construction of patient specific bolus for electron beam radiotherapy for non-melanoma skin cancer. Radiother Oncol.121, 148–153 (2016)
2. Pugh, R., Lloyd, K., Collins, M. & Duxbury, A. The use of 3D printing within radiation therapy to improve bolus conformity: a literature review. J. Radiother Pract.16, 319–325 (2017).
3. Kim, S. W., Shin, H. J., Kay, C. S. & Son, S. H. A customized bolus produced using a 3-dimensional printer for radiotherapy. PLoS One.9, 1–8 (2014)

O035 Towards enhancing treatment accuracy in prostate radiotherapy using an inhouse developed position monitoring system

Sankar Arumugam[1,2], Viet Do[3], Karen Wong[4], Tony Young[1,5], Phillip Chlap[1,2], Mark Sidhom[2,3]

[1]Department of Medical Physics, Liverpool and Macarthur Cancer Therapy Centres and Ingham Institute, Sydney, New South Wales, Australia; [2]South Western Clinical School, University of New South Wales, Sydney, New South Wales, Australia. Sankar.Arumugam@health.nsw.gov.au (Presenting author); [3]Department of Radiation Oncology, Liverpool and Macarthur Cancer Therapy Centres, Sydney, New South Wales, Australia. Viet.Do@health.nsw.gov.au; [4]Department of Radiation Oncology, Liverpool and Macarthur Cancer Therapy Centres and Ingham Institute, Sydney, New South Wales, Australia. Karen.Wong@health.nsw.gov.au; [5]Institute of Medical Physics, School of Physics, University of Sydney, Sydney, New South Wales, Australia. Tony.Young@health.nsw.gov.au; Tony.Young@health.nsw.gov.au; Mark.Sidhom@health.nsw.gov.au

Table 1 Gating Events for each Seedtracker tolerance level

Tolerance	Treatment fractions	GEs		
		Total	Maximum in one patient	Maximum in one fraction
5 mm	200	27	11	2
4 mm	219	101	31	6
3 mm	200	102	22	4

Introduction Real-time target monitoring ensures the accurate positioning of the target volume during treatment delivery and enables the reduction of safety margins used in radiotherapy (RT). The purpose of this study was to implement the implanted fiducial based real-time position monitoring for prostate radiotherapy using an x-ray image based position monitoring system, SeedTracker[1–3], and quantify its impact on treatment accuracy and overall treatment time.
Method Thirty prostate cancer patients receiving RT were enrolled for this two centre study (ACTRN12618001421224). VMAT plans with a PTV margin of 7 mm were generated for treatment on Elekta linacs. Planar x-ray images acquired at a gantry spacing of 9° were processed by the SeedTracker system to determine the real-time target position. The position tolerance for monitoring was reduced from 5 to 4 mm to 3 mm in 10 patient cohorts. The impact of observed intrafraction motion on the dose to CTV and Rectum was studied by incorporating the effects of position deviation into the treatment plan.
Results The Gating Events (GE) observed in each tolerance category is shown in Table 1. The mean(stdev) time taken to perform position correction and resume treatment where GE occurred was 1.2(0.4)minutes. If the position corrections were not performed V60 and V40 to Rectum would have increased by a maximum of 2 cc and 2.7 cc respectively and D98 to CTV would have decreased by a maximum of 1.5% in the studied patients.
Conclusion Real-time target monitoring with SeedTracker has improved the accuracy of Prostate RT with a minimal increase in overall treatment time.
References

1. Arumugam S, Sidhom M, Xing A, Holloway L. An online x-ray based position validation system for prostate hypofractionated radiotherapy. Med Phys 2016;43:961–74.
2. Arumugam S, Sidhom M, Truant D, Xing A, Udovitch M, Holloway L. Variable angle stereo imaging for rapid patient position correction in an in-house real-time position monitoring system. Phys Medica 2017;33:170–8.
3. Arumugam S, Pavey D, Oar A, Holloway L, Sidhom M, Lee M. The first real-time intrafraction target position monitoring in pancreas SBRT on an Elekta linear accelerator. Phys Eng Sci Med. 2021 May 21. https://doi.org/10.1007/s13246-021-01007-0.

O036 EPID-based verification of DIBH accuracy for breast VMAT

M. Carr[1], B. Zwan[2], M. Gargett[1], C. Stanton[1], J. Booth[1,3]

[1]Northern Sydney Cancer Centre, Royal North Shore Hospital, St Leonards NSW. Michael.Carr@health.nsw.gov.au (Presenting author); [2]Central Coast Cancer Centre, Gosford Hospital, Gosford

NSW. Benjamin.Zwan@health.nsw.gov.au; Maegan.Gargett@health.nsw.gov.au; Cameron.Stanton@health.nsw.gov.au; [3]Institute of Medical Physics, School of Physics, University of Sydney, Sydney NSW. Jeremy.Booth@health.nsw.gov.au

Introduction Deep inspiration breath-hold (DIBH) is a breathing control method used in adjuvant breast radiotherapy to reduce heart and lung dose [1]. Given the reliance on external motion surrogates during DIBH, previous studies have employed time-resolved EPID imaging to verify the internal chest wall (CW) anatomy during treatment [2, 3]. However, such studies have been constrained to 3D conformal radiotherapy where the CW is not obstructed by MLC motion. With literature supporting use of VMAT as best practice for breast radiotherapy, this study sought to develop a method to verify the accuracy of CW anatomy during VMAT breast DIBH.
Method This method focuses on monitoring the position of the CW in EPID images captured during treatment and comparing these to planned CW positions in digitally reconstructed radiographs (DRRs) generated at the same angle. Feasibility of the method was characterised by determining the percentage of dose delivered to the target volume that can be monitored. The accuracy of the system was computed by applying the method to a phantom. Finally, treatment data was collected for 7 left-sided breast cancer patients and the method was used to assess DIBH accuracy.
Results In the treatment plans studied, the CW could be monitored during delivery of 88% of the dose to the target volume. Phantom measurements determined that the accuracy of the system was better than 1 mm. 7 patients (23 fractions) were analysed with the software finding the CW to be within 5 mm of the planned position for 95% of measurements.

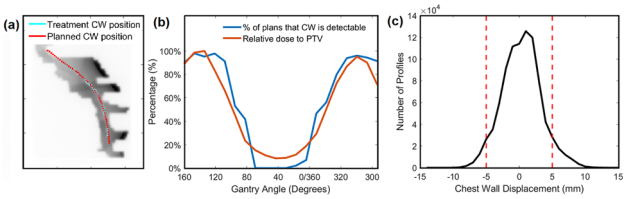

Fig 1: [a] An EPID image with the measured and planned CW position superimposed. [b] Comparison of the visibility of the CW and the relative dose delivered to PTV per gantry angle. [c] Histogram of the measured CW displacement at every horizontal profile for all patients. The displacement is given by the distance between the planned and measured CW positions.

Conclusion A novel method has been developed to assess the accuracy of breast DIBH during VMAT. The feasibility of the method was demonstrated and the technique has been applied to phantom and patient data. This work has the potential, in a real-time or offline setting, to improve the accuracy of DIBH for breast VMAT.

References

1. Bergom C, Currey A, Desai N, Tai A, Strauss JB (2018) Deep Inspiration Breath Hold: Techniques and Advantages for Cardiac Sparing During Breast Cancer Irradiation. Frontiers in oncology, 8, 87. https://doi.org/10.3389/fonc.2018.00087
2. Jensen C, Urribarri J, Cail et al. (2014) Cine EPID evaluation of two non-commercial techniques for DIBH. Med Phys 41: 021,730. https://doi.org/10.1118/1.4862835
3. Doebrich M, Downie J, Lehmann J (2018) Continuous breath-hold assessment during breast radiotherapy using portal imaging. Physics and imaging in radiation oncology, 5, 64–68. https://doi.org/10.1016/j.phro.2018.02.006

O037 Developing in-house corrections suitable for high-quality upright CBCT reconstruction

S. Hegarty[1], J. Korte[2,3], N. Hardcastle[2], R. Franich[1]

[1]RMIT University, Melbourne Australia. s3654771@student.rmit.edu.au; [2]Peter MacCallum Cancer Centre, Melbourne Australia; [3]Department of Biomedical Engineering, School of Engineering, University of Melbourne, Melbourne Australia. james.korte@petermac.org; nick.hardcastle@petermac.org; rick.franich@rmit.edu.au

Introduction Upright radiation therapy requires treatment planning image acquisition in the treatment position. Cone beam computed tomography (CBCT) of an upright patient can be acquired on a standard linac but requires high image quality for planning purposes and cannot be reconstructed using existing vendor software. In this study, we have designed and evaluated an in-house reconstruction and artefact correction pipeline suitable for upright CBCT.
Method CBCT reconstruction was based on the reconstruction toolkit (RTK) using the FDK algorithm [1]. Empirical corrections for bowtie filter induced beam hardening were derived by measuring the change in linear attenuation as a function of changing incident location through the filter [2]. Scatter correction was performed using a Monte Carlo (MC) method [3, 4]. Ring artefacts were corrected using an algorithm adapted from Sijbers [5]. We compared our reconstruction with a fan beam CT (FBCT) and CBCT images acquired of an anthropomorphic phantom with a Varian TrueBeam linac.
Result Fig. 1 compares the FDK reconstruction with and without corrections, with the FBCT and vendor based CBCT. Line profiles in Fig. 2 show convergence of the CT numbers to that of the FBCT, and better lung agreement than the vendor CBCT, when the three corrections were applied to the FDK reconstruction.
Conclusion Introducing corrections for bowtie induced beam hardening, scattered radiation and ring artefacts results in an FDK reconstruction with similar CT numbers to those of the FBCT and vendor CBCT.

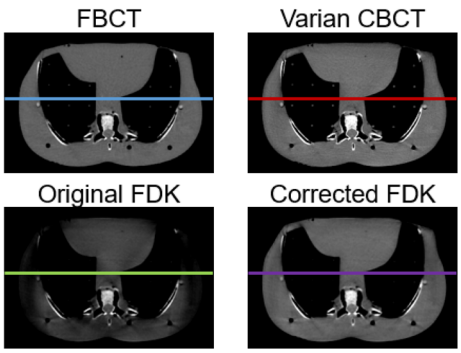

Figure 1: Reconstructions of an anthropomorphic phantom comparing FDK with and without corrections to a FBCT and vendor CBCT.

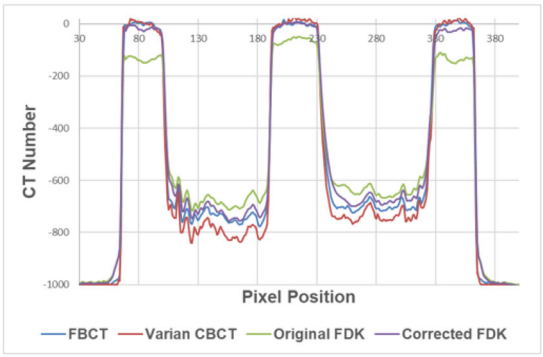

Figure 2: Line profiles comparing the CT number of FDK with and without corrections to a FBCT and vendor CBCT.

References

1. Feldkamp, L.A., L.C. Davis, and J.W. Kress, Practical cone-beam algorithm. Journal of the Optical Society of America. A, Optics, image science, and vision, 1984. 1(6): p. 612.
2. Cai, M., et al., Decoupling of bowtie and object effects for beam hardening and scatter artefact reduction in iterative cone-beam CT. Physical and Engineering Sciences in Medicine, 2020. 43.
3. Mainegra-Hing, E., Fast monte carlo calculation of scatter corrections for cbct images. Journal of Physics: Conference Series, 2008. 102(1): p. 012,017.
4. Thing, R.S., et al., Hounsfield unit recovery in clinical cone beam CT images of the thorax acquired for image guided radiation therapy. Physics in Medicine & Biology, 2016. 61(15): p. 5781.
5. Sijbers, J. and A. Postnov, Reduction of ring artefacts in high resolution micro-CT reconstructions. Physics in medicine and biology, 2004. 49 14: p. N247-53.

O038 Evaluation of the Intel Realsense™ LiDAR camera L515 for monitoring patient position in radiotherapy

J. Kim[1], A. K. Pandey[1], A. L. Fielding[1]

[1]Queensland University of Technology (QUT), Faculty of Science, School of Chemistry and Physics, Brisbane, Qld, Australia. jayeon.kim@hdr.qut.edu.au (Presenting author); a2.pandey@qut.edu.au; a.fielding@qut.edu.au

Introduction Variations in patient position from the planned treatment position between or during radiotherapy fractions can compromise dosimetric coverage of the tumour and organ-at-risk tissue sparing. The suitability of the new Intel Realsense LIDAR based depth camera has been investigated for use in monitoring patient position and movement during radiotherapy treatment delivery.

Method Controlled measurements were made to characterise the accuracy and precision of depth data from an Intel Realsense™ LiDAR camera. Depth data acquisition was carried out at 30 fps using the Realsense™ SDK 2.0 software with MATLAB**.** Depth measurements were taken for a static and sinusoidally moving object with camera-surface distances between 400 and 2000 mm, and compared with other depth cameras [1].

Results Fig. 1(a) shows the variation of measured depth values over 1800 continuously acquired frames of data for one minute for fixed camera-object distances ranging from 400 mm – 2000 mm. The variation increased with distance, but the precision was less than 1 mm even at 2000 mm. Figure 1(b) illustrates the measurement of the object surface undergoing sinusoidal motion with a residual better than 2 mm at 2000 mm distance without applying filters. The LIDAR based L515 camera demonstrated a reduction in the measured depth variation for both static and sinusoidal motion measurements compared to other Realsense depth camera technologies.

Fig. 1 *(a)* Distribution of measured depth values at different distances over 1800 frames. *(b)* measurement of the sinusoidal motion with 2.5 mm amplitude and 0.25 Hz over 900 frames at 2000 mm distance.

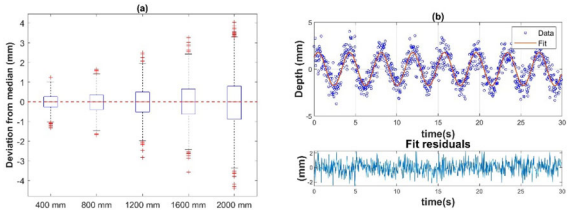

Conclusion We have previously demonstrated the suitability of the stereo-based Realsense depth camera for measuring the motion of a surface [1]. The reduction in the frame-to-frame variability of depth measurements with the LIDAR based Realsense camera makes it worthy of further investigation as a tool for patient position monitoring during radiotherapy treatment delivery.

Reference

1. A. L. Fielding et al., "Preliminary study of the Intel RealSenseTM D415 camera for monitoring respiratory like motion of an irregular surface," *IEEE Sens. J.*, pp. 1–1, 2020.

O039 Extended Length Cone Beam Computed Tomography (CBCT) on Varian TrueBeam

J. Miller[1], T. Markwell[1]

[1]Radiation Oncology – Princess Alexandra Hospital Raymond Tce (ROPART), South Brisbane, QLD, Australia. Julie-Anne.Miller@health.qld.gov.au (presenting author)

Introduction ROPART installed two Varian TrueBeam v2.7 machines in 2020–2021. The Extended Length CBCT (EL-CBCT) function in clinical mode allows the user to merge multiple CBCTs[1], with a two centimetre overlap region[2]. Scans can also be merged in the advanced reconstructor mode, but this cannot be used for online patient set up. The couch automatically moves longitudinally between scans. Individual scans can have different fields of view, reconstruction algorithms, gantry trajectories and slice widths.

Method A straight piece of PVC pipe placed diagonally along the couch was used to assess Z (longitudinal) geometric accuracy. The Catphan 604[3] was used to measure geometric accuracy in the XY (lateral) and Z (longitudinal) directions, as well as CT number, high

contrast resolution and uniformity. Four different scan combinations were acquired, varying the scan direction sequence, field of view, gantry trajectory and slice width.

Table 1 Scan settings

Scans	Slice width (mm)	Direction acquired	Tests
Head/ Thorax	1	Superior- Inferior	1.0–1.4
	2	Inferior-Superior	1.0
Pelvis/ Pelvis	2	Superior- Inferior (couch weighted for 1.1)	1.0–1.4
		Inferior-Superior	1.0

Results

Test 1.0: Geometric accuracy in the Z direction for entire volume—The scans of the pipe showed no significant distortions inside or outside of the merged volume. The ends of the pipe were "clipped" at the Z cone edges[2].

Test 1.1: CT number—All HUs measured were within the range quoted in the Catphan 604 manual ± 1 HU.

Test 1.2: Distortion—All measurements were 50 ± 0.1 mm.

Test 1.3: High contrast resolution—The Pelvis scan was 4 LP/cm, which was the same as the reference scan. The Head/Thorax scan was 5 LP/mm, which was the average of the Head and Thorax unmerged scans.

Test 1.4: Uniformity—All scans were less than ± 25 HU.

Conclusion EL-CBCT showed adequate geometric accuracy, CT number, high contrast resolution and uniformity in the merged region with no significant differences to the reference (unmerged) scans. The EL-CBCT showed no significant artefacts or offsets when a pipe, greater than the total longitudinal length of the scan, was scanned.

References

1. TrueBeam Instructions For Use (2018)
2. TrueBeam Technical Reference Guide—Volume 2: Imaging (2018)
3. The Phantom Laboratory Catphan 604 manual (2015)
4. Mohamathu Rafic K, Balasingh S, Peace T, Manu M, Arvind S, Ravindran P (2019) A Rationale for Cone Beam CT with Extended Longitudinal Field-of-View in Image Guided Adaptive Radiotherapy. Physica Medica 62:129–139

O040 Improving Elekta XVI CBCT image quality using an in-house Flexmap calibration procedure

Christopher Noble[1] (Presenting author), Luke Webb[1], Catherine Jones[1], Prabhakar Ramachandran[1]

[1]Radiation Oncology, Princess Alexandra Hospital, Ipswich Rd, Brisbane, Australia; Christopher.Noble@health.qld.gov.au; Luke.Webb@health.qld.gov.au; Catherine.Jones@health.qld.gov.au; Prabhakar.Ramachandran@health.qld.gov.au

Introduction It has been previously recognised that the default Elekta XVI flexmap calibration procedure results in a consistent offset of 0.5 to 1.0 mm for medium and large field of view presets with a corresponding reduction in image quality.

Method A Python script was developed to independently generate flexmap files using the raw projection data from the flexmap calibration scans. Each projection in the data set was thresholded and segmented to locate the ball bearing and the position written to the flexmap file. A Catphan 504 phantom was scanned using small, medium and large fields of view to assess the effect of correcting the flexmap files.

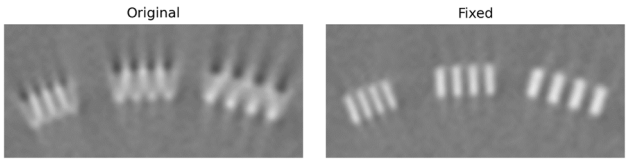

Fig. 12 LFOV CBCT images of Catphan CTP528 module reconstructed using the original and corrected flexmaps

Results Fig. 12 shows a portion of the reconstructed image of the CTP528 module of the Catphan phantom acquired with a large field of view. The image acquired with the flexmaps acquired with the Elekta flexmap calibration procedure shows obvious artefacts and low spatial resolution. The image acquired with the corrected flexmaps shows no artefacts and a much higher spatial resolution.

Conclusion The flexmap files that are produced by the Elekta XVI calibration procedure consistently have an offset for the medium and large fields of view. These offsets affect the spatial resolution and geometric scaling of the reconstructed images and should be corrected for optimal performance of the CBCT system. The Python script detailed in this presentation can be used to correct and verify the flexmaps.

O041 Are 0.35 mm Pb equivalent aprons sufficient for cardiologists?

George Antoniou[1], Chris Boyd[1], Dr Daniel Badger[1]

[1]Medical Physics & Radiation Safety, South Australia Medical Imaging, Adelaide, Australia. george.antoniou@sa.gov.au (presenting author); chris.boyd2@sa.gov.au; daniel.badger@sa.gov.au

Introduction Fear-based marketing techniques for radiation targeted personal protective equipment (PPE) [1] has instigated concerns from cardiologists regarding the extent of radiation protection needed to keep them 'safe'. As a result, there has been a recent push towards communicating the need for evidence-based PPE—such as varying lead equivalent apron thicknesses. The aim of this study is to explore if 0.35 mm lead equivalent aprons are sufficient to keep radiation exposure of cardiologists as low as reasonably achievable (ALARA). This work will help communicate the risks associated with doses received by cardiologists whilst wearing
0.35 mm lead equivalent aprons, in comparison to the more prevalent risk of musculoskeletal injuries likely attributed with wearing heavier lead equivalent aprons [2].

Method A retrospective analysis of dose reports from 57 cardiologists was conducted, each provided with 0.35 mm lead equivalent aprons between 2016 and 2021. Radiation readings below detection limits were disregarded, as cardiologists wearing dosimeters for clinical case-loads will likely exceed this minimum radiation exposure threshold. The dose reports provided from quarterly chest badges included personal dose equivalent readings for the skin,, and effective dose,.

Results A total of 97 and 110 values above the minimum detectible limits were analysed, resulting in mean quarterly values of 0.14 ± 0.02 mSv and 0.13 ± 0.02 mSv respectively. Boxplots summarising these results is shown in Fig. 13.

Conclusion The use of 0.35 mm lead equivalent aprons is sufficient to keep cardiologist radiation doses to a small fraction of occupational radiation exposure limits during clinical caseloads. This work should

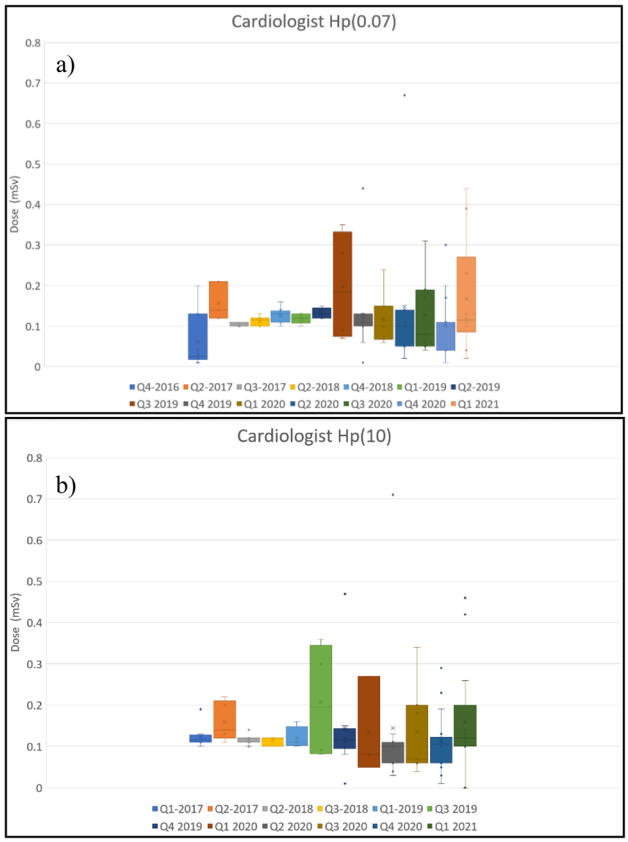

Fig. 13 **a** Skin () and **b** effective () personal dose equivalent readings per quarter from 2016 to 2021. Error bars indicate two standard deviations

provide peace-of-mind to cardiologists that currently provided PPE is adequate for optimising personal harm.

References

1. Marsh RM, Balter S, Mahesh M (2018) Personal protective equipment in interventional fluoroscopy: Distinguishing evidence from hype. J. Am. Coll. Radiol. 15(2):322–324. https://doi.org/10.1016/j.jacr.2017.08.017.
2. Klein et al. (2015) Occupational health hazards of interventional cardiologists in the current decade: Results of the 2014 SCAI Membership Occupational Health Survey. Catheter Cardiovasc. Interv. 86(5):913–924. https://doi.org/10.1002/ccd.25927.

O042 Optimizing the use of CT localizer radiographs for protective gown QA

D. J. Garrott[1], D. Carrick[1]

[1]Biomedical Technology Services, Gold Coast University Hospital, QLD, Australia; david.garrott@health.qld.gov.au (Presenting author); deborah.carrick@health.qld.gov.au

Introduction The use of CT localizer radiographs to image protective gowns as a part of a quality assurance (QA) program provides several potential benefits when compared to the more common use of fluoroscopy and general radiography. Greater imaging field-of-view (FOV) enables an entire garment to be captured in one image, images can be easily exported and stored for later review, staff are not required to be in the room during an exposure and the imaging time per garment is reduced. One of the biggest hurdles to this approach is ensuring confidence that the images will be of sufficient quality to identify any significant damage. The goal of this project is to investigate the image quality of scanned gowns and to quantify the minimum resolution and signal to noise ratio necessary to detect whether a garment is currently fit for use and whether a garment is likely to remain fit for use until it is next examined.

Method A gown phantom was made from a cracked section of an old lead impregnated vinyl gown and used to assess image quality for a range of scan parameters and conditions. Qualitative assessment was performed by visual inspection of the images against the known quality of the phantom, and quantitative assessment was performed by measuring signal to noise and resolution metrics.

Results Results from the testing scenarios were used to identify minimum quantitative image quality parameters of the CT localiser radiograph that correspond with confident, visual detection of significant cracks and damage in the protective gowns.

Conclusion With optimal scan parameters and careful setup, it is possible to confidently assess the quality of protective gowns (and other protective garments) using CT localizer radiographs.

O043 Inspection of Lead Aprons: Updated Rejection Criteria

C. Jeffries[1]

[1]Medical Physics & Radiation Safety, South Australia Medical Imaging, Adelaide, Australia. cameron.jeffries@sa.gov.au

Introduction Lambert and McKeon [1] is widely used as the basis for lead apron rejection criteria [2]. These criteria assess cost of averted dose as justification for replacement of a lead apron. Dose was determined using tissue weighting factors from ICRP Publication 60 [3]. Costs are assumed to be based on 2001 US dollars. This paper will update the rejection criteria based on ICRP Publication 103 [4]. The paper will further adjust the rejection criteria for inflation and current lead apron cost in Australian dollars. A significant change since the original rejection criteria were developed is the widespread use of two piece lead aprons.

Method The Lambert and McKeon method was used to revise the rejection criteria. This method determines additional dose due to a crack in a lead apron based on unattenuated whole body dose (D), tissue weighting factor (w_t), transmission fraction (f), defect area (a), and lead apron (or organ) area (A) [1]. The reasonable cost of $1000 per averted mSv [1] was corrected for inflation and converted into Australia dollars. Rejection criteria were determined with consideration of thyroid, gonads and lungs as critical organs.

Results The revised reasonable cost was estimated to be A$2200 per averted mSv.

Rejection Criteria Defect area (mm^2)	Whole Body	Thyroid	Gonads	Lungs
Original	670	11	15	N/A
Original + ICRP103	670	13	46	N/A
This study (Cost + ICRP103)	850	40	25	500

Conclusion The revised rejection criteria developed on a conservative cost model potentially increases the service life of PPE. This is partially due to revisions to the dose model in ICRP103 [4] that occurred since the original criteria were published. The lower radiation sensitivity of the gonads requires further consideration. Additional work on the cost benefit analysis will be undertaken.

References

1. Lambert, K and McKeon, T (2001) Inspection of Lead Aprons: Criteria for Rejection, Operational Radiation Safety, Supplement to Health Physics, 80, suppl 5, May 2001, S67- S69.
2. Department of Human Services, Victoria (2011) Testing Lead Aprons used in Diagnostic Radiology Departments, http://www2.health.vic.gov.au/about/publications/policiesandguidelines/Testing-lead-aprons-used-in-diagnostic-radiology-departments Accessed 7 June 2021
3. ICRP, 1991. 1990 Recommendations of the International Commission on Radiological Protection. ICRP Publication 60. Ann. ICRP 21 (1–3).
4. ICRP, 2007. The 2007 Recommendations of the International Commission on Radiological Protection. ICRP Publication 103. Ann. ICRP 37 (2–4)

O044 Medical Occupational Radiation Exposure (ORE) online training (– reassuring staff, assisting regulatory requirements and free!)

Alan Mason[1], Zoe Brady[2], Donald McLean[3]

[1]Medical Radiation Services, Australian Radiation Protection and Nuclear Safety Agency (ARPANSA). alan.mason@arpansa.gov.au (Presenting author); [2]Alfred Hospital, Melbourne. z.brady@alfred.org.au; [3]Canberra Hospital, Canberra. donald.mclean@act.gov.au

Introduction Occupational radiation safety is important, but not well understood by most facility staff, often resulting in unwarranted concerns and inadequate attention to best practice. In producing its Radiation Protection of the Patient (RPOP) material, ARPANSA staff visited medical facilities across the country. While RPOP addressed some issues for patient radiation safety, facility staff lamented that there was little accessible, authoritative and suitable occupational training material. ARPANSA's Occupational Radiation Exposure (ORE) material provides individually tailorable content, addressing potential concerns and providing advice and direction on best practice. The navigation is innovative, the content uses contemporary learning techniques and the modules are underpinned by scientific rigour.

Method ARPANSA adopted a collaborative, iterative approach to ORE's development, with input from regulators, professional colleges, peak bodies, facility experts and end users. A modular approach was chosen to allow for additional material and the ability to 'mix and match' to meet different needs. Development used industry standard programs and a user-friendly end product.

Results Released in 2021, ORE is being used by public and private facilities of all sizes. Early adopters, the Alfred Hospital in Melbourne and Canberra Hospital have identified multiple benefits for staff, including better radiation safety understanding, reduced anxiety and greater focus on best practice principles, as well as greater reach and training availability. The ability for individual staff to tailor their own program is novel and engaging. The multiple download options provide flexibility for training staff. The interactive nature of the material is more engaging than traditional approaches and its adoption encourages a common language and national uniformity.

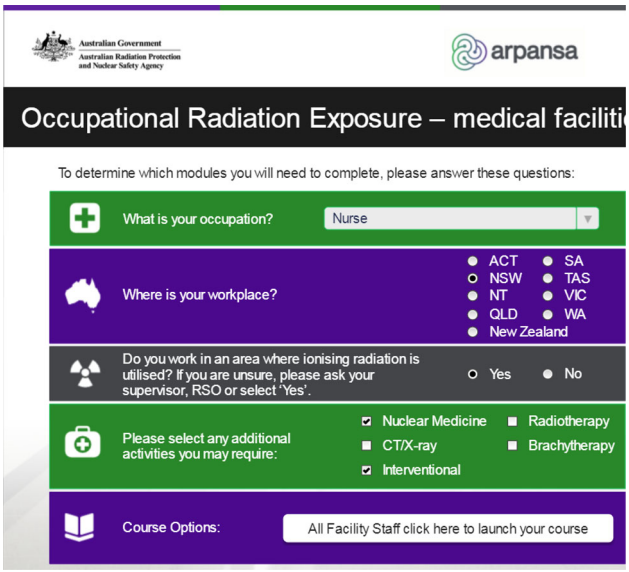

Conclusion ORE assists facilities in providing basic occupational radiation safety training for all staff, from cleaners and administrators to nurses and radiologists. Medical physicists, RSOs, trainers etc. are encouraged to make use of ORE and user feedback will be used to provide further improvements.

References/Acknowledgements Both RPOP and ORE are available via ARPANSA's website at: https://www.arpansa.gov.au/our-services/training

O045 The benefit of collaborations: The Australian Cancer Data Network

Lois Holloway[1,2,3,4]

[1]Liverpool and Macarthur Cancer Therapy Centres and Ingham Institute; [2]South Western Sydney Clinical School, University of New South Wales; [3]Institute of Medical Physics, University of Sydney; [4]Centre for Medical Radiation Physics, University of Wollongong

For every cancer patient there are many, many decisions to be made during the course of diagnosis, treatment and for life afterwards. Although there are also many randomised controlled clinical trials that have been undertaken to answer specific questions, the eligibility for these trials is tight and thus for some patients the results from these trials may not be directly relevant. There is also more and more data being accrued in our clinical practice which includes all patients, not just those eligible for clinical trials. This data provides an opportunity to develop models, learn and gain knowledge, however, the challenge is that large datasets are needed to ensure broad applicability and confidence in these models.

The Australian computer assisted theragnostics (AusCAT) distributed data network was established to enable learning from large datasets without the data leaving individual institutions. This approach enables data to be updated in an ongoing and timely manner and addresses some privacy and ethics concerns particularly with international collaborations. This network currently spans six Australian centres and a number of international collaborators. As part of an Australian Research Data Commons (ARDC) platform grant this network is being expanded and linked to Cancer Alliance QLD and the Cancer [Treatment|Outcomes] Variation project.

Work undertaken with this network requires strong collaborations between centres and different health professionals. Through these

collaborations it is possible to support consistent ontologies and definitions of data; develop patient outcome models, supporting treatment decisions; assess variation in practice, highlighting the need for changes in practice or further research; assess the potential to use imaging data to support diagnostic and outcome decisions and assess the clinical impact of clinical trials and other practice influencing research.

O046 New advances in Ultra-high field (7 T) MRI for state-of-the-art Neuroscience

Bradford Moffat[1]

[1]Principal Research Fellow, The University of Melbourne

The 7T MRI scanner at the Melbourne Brain Centre Imaging Unit (MBCIU) has recently undergone a major upgrade, bringing opportunities for Australian neuroscientists to have access to state-of-the-art human brain imaging technology. This talk will give an overview and examples of this technology, including advances in:

Parallel transmit (pTx) RF.

High resolution compressed sensing imaging (CSI) for superior MRA.

High resolution multi-echo MP2RAGE for combined anatomical imaging, quantitative relaxometry (T1 and T2*) and susceptibility mapping (QSM).

Quantitative metabolic imaging and spectroscopy.

Quantitative high-resolution diffusion tractography.

O047 Detection of increased dosimetric uncertainty in OSLD readouts using in-house quality control metrics

F. Kadeer[1], **A. Alves**[1], **C. Davey**[1]

[1]Australian Clinical Dosimetry Service, ARPANSA, VIC.
Fayz.Kadeer@arpansa.gov.au (Presenting author);
Andrew.Alves@arpansa.gov.au; Cate.Davey@arpansa.gov.au

Introduction The ACDS level I mail-out audit determines absorbed dose to water under facility reference conditions for all clinical beams in Australia using InLight® nanoDot™ optically stimulated luminescence dosimeters (OSLDs) and microStar/ii readers (Landauer Inc., Glenwood, Ill, USA). Clinical in in-vivo dosimetry [1] also relies on the same equipment. Quality control (QC) which can detect dosimetric errors due to malfunction is essential, both in the context of the national audit service and in clinical in-vivo dosimetry where undetected increases in dosimetric uncertainty could erroneously impact clinical practice. The ACDS has developed in-house QC to routinely assess the uncertainty.

Method Readers are calibrated during every readout session, containing ~ 160 measurement OSLDs, and 16 control OSLDs irradiated with a known dose of ~ 1 Gy. Readout sessions last 2 h. The average relative standard deviation (RSD) of the session's calibration OSLDs is 1.2%. This value is the primary QC metric for each session.

For sessions to pass QC, the following criteria must be met:

1. At least 12 calibration OSLDs must pass individual readout QC.
- The exclusive calibration (RSD) must be less than 2.1%.

Results Calibration (RSD) has been tracked since 2016 to monitor reader wear (up to ~ 9500 individual OSLD reads per year). The data is provided in Fig. 1. In 220 sessions, 15 have exceeded the QC threshold, thus demonstrating sporadic increases in reader uncertainty which are greater than a factor of 2 above the accepted value.

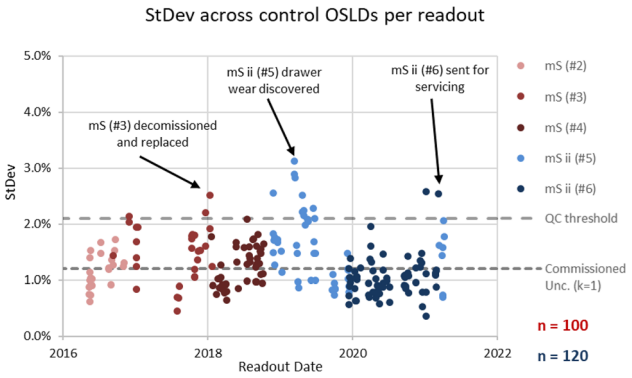

Fig. 1 Reader uncertainty over time assessed from Calibration (RSD) across multiple readers and types

Conclusion The magnitude of QC failures observed by the ACDS has justified OSLD readout negation and for reader decommissioning leading to repair or replacement. This QC demonstrates sensitivity to mechanical reader malfunction, while the sensitivity of the internal optical engine based microStar QC has not been assessed by the ACDS. Adapters/drawers become worn from many OSLD reads. All clinical protocols that rely on OSL dosimetry must maintain QC that routinely quantifies uncertainties and test the full readout chain.

References/Acknowledgements

1. Mrčela I, Bokulić T, Izewska J, Budanec M, Fröbe A and Kusić Z (2011) Optically stimulated luminescence in vivo dosimetry for radiotherapy: physical characterization and clinical measurements in 60Co beams. Phys Med Biol 56:6065–6082

O048 A Direct Comparison of the OSL Properties of BeO and Al_2O_3 for use in Clinical In-Vivo Dosimetry

Benjamin Broadhead[1,2] **(Presenting Author), Christopher Noble (Presenting author)**[1], **Prabhakar Ramachandran**[1]

[1]Radiation Oncology, Princess Alexandra Hospital, Ipswich Road, Brisbane, Australia; [2]Faculty of Science, Queensland University of Technology, Brisbane City, Australia.
Ben.broadhead@connect.qut.edu.au;
Christopher.Noble@health.qld.gov.au;
Prabhakar.Ramachandran@health.qld.gov.au

Introduction The current clinical standard and only commercially available optically stimulated luminescent dosimeter (OSLD) designated for clinical use is Al_2O_3:C [1]. This study aimed to compare the key OSL features of sensitivity and linearity of response in a clinical setting for a potential alternative, BeO.

Method All measurements were performed using a Lexsygsmart Automated TL/OSL Reader and a set of ten OSLD, consisting of five, beryllium oxide (Thermalox® 995) ceramic chips, and five carbon-doped aluminium oxide (Landauer nanoDot™). All OSLD were irradiated at the same time, performed using a Versa HD Elekta linear accelerator, with bleaching performed after each exposure and signal reading. Sensitivity testing was performed by reading OSL signals after repeated dosages of 1 Gy. Linearity was tested by taking several exposures between 0.2–10.0 Gy.

Results While BeO shows large differences in sensitivity between OSLD, even from the same batch, this difference in measurement was

found to be systematic, and by individual normalisation a high accuracy and precision was achieved.

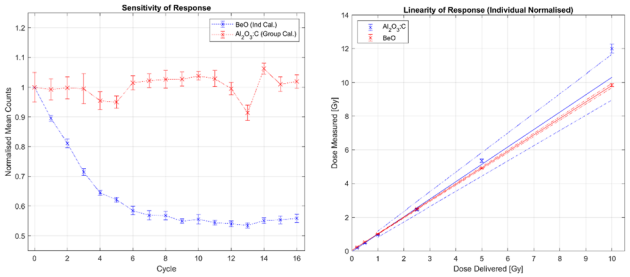

Conclusion While Al_2O_3:C showed good precision when calibrated to a group mean value, and is simple and direct to use, BeO must be calibrated individually and requires an initial 'conditioning' period for new OSLD to achieve signal stability. However, after stability is reached, BeO appeared to provide not only a higher precision, but a more consistent and linearity dose response, particularly for doses above 5 Gy.

References

1. Kry, S., Alvarez, P., Cygler, J., et al. (2019) AAPM TG 191: Clinical use of luminescent dosimeters: TLDs and OSLDs. *Medical Physics*, Vol. 47(2) https://doi.org/10.1002/mp.13839

O049 Water depth uncertainty and its influence on dosimetry

Guangli Song[1], Dhanushia Rajaratnam[1], Sherly Saju[1], Nikki Caswell[1], Athreya Buddhavarapu[1]

[1]Ballarat Austin Radiation Oncology Centre, 1 Drummond Street North, Ballarat, Victoria 3350, Australia. guangli.song@bhs.org.au; dhanushia.rajaratnam@bhs.org.au; sherly.saju@bhs.org.au; nikki.caswell@bhs.org.au; athreya.buddhavarapu@bhs.org.au

Introduction To introduce a simple method to investigate the variation of water level and true chamber depth due to servo submersion in the scanning water phantom and its influence on dosimetry uncertainties.

Method An optical reticle with 0.1 mm scale was attached to the external wall of the water phantom. A mobile phone camera held on a selfie stick with remote control was used for reading and recording. A 1D and a 3D-scanning phantom were investigated. A Farmer-type chamber was mounted on the servo. In-house and published dosimetry data were used for assessment of the influence on dose calibration.

Results Water level changes up to 0.8 mm, actual depth more than designated depth, were observed for the 1D-phantom. Less variation was observed for the 3D-phantom. Lower dose readings were due to the small PDD/TPR decrease. The relative variation to the reference dose is about 0.4%, 0.5%, 0.4% for 6, 6FFF & 10 MV photon, 0.2% & 0.3% for 16 & 20 MeV electron, and 1–2% for kV beams (HVL 3 & 4 mm Al). This results in a systematic increase in the dose at the true calibration depth for this 1D-scanning phantom. The scale is comparable to other correction factors like k_{pol}, k_s, k_n (non-uniformity). The actual amount varies with tank design and needs be assessed by physicists. Corrections can be made by using the corrected chamber position or through a correction factor k_w.

Conclusion The variation of the water level with moving parts and its influence on the dose accuracy needs be assessed for reference dosimetry and other measurements with such techniques. The magnitude of this uncertainty is small and of similar influence to other correction factors, however large enough to warrant inclusion in the reference dosimetry.

References

Andreo P, Burns DT, Hohlfeld K, Huq MS, Kanai T, Laitano F, Smith VG and Vynckier S (2006) Absorbed dose determination in external beam radiotherapy: an international code of practice for dosimetry based on standards of absorbed dose to water, IAEA Technical Report Series No 398, International Atomic Energy Agency, Vienna

Almond PR, Biggs PJ, Coursey BM, Hanson WF, Huq MS, Nath R and Rogers DW (1999) AAPM's TG-51 protocol for clinical reference dosimetry of high-energy photon and electron beams, Med Phys 26:1847–70

McEwen M, DeWerd L, Ibbott G, Followill D, Rogers DWO, Seltzer S and Seuntjens J (2014) Addendum to the AAPM's TG-51 protocol for clinical reference dosimetry of high-energy photon beams, Med Phys 41:041,501

Lye JE, Butler DJ, Oliver CP, Alves A, Lehmann J, Gibbons FP, and Williams IM (2016) Comparison between the TRS-398 code of practice and the TG-51 dosimetry protocol for flattening filter free beams, Phys Med Biol 61:N362-N372

Australian Clinical Dosimetry Service "FFF dosimetry ACDS fact sheet" (https://www.arpansa.gov.au/sites/default/files/acds-sup-9027-v2_fff_fact_sheet.pdf)

Arib M, Medjad T and Boudouma Y (2006) Study of the influence of phantom material and size on the calibration of ionization chambers in terms of absorbed dose to water, J Appl Clin Med Phys 7:55–64

Saenz D, Roring J, Crus W, Sarkar V, Papanikolaou N, Stathakis S (2016) Commissioning and cross-comparison of four scanning water tanks, Int J Cancer Ther and Oncol 4:1–9

O050 Characterization of MOSFET sensors for dosimetry in alpha particle therapy

Fang-Yi Su[1], Giordano Biasi[1,2], Linh T. Tran[1], Vladimir Pan[1], Mitchell Lielkajis[1], Marco Petasecca[1], Michael L.F. Lerch[1], Dean L. Cutajar[1], Zeljko Pastuovic[2], Joel Poder[3], Michael Jackson[4], Joseph Bucci[3], Anatoly B. Rosenfeld[1]

[1]Centre for Medical Radiation Physics, University of Wollongong, NSW, Australia. fys768@uowmail.edu.au (Presenting author); [2]Peter MacCallum Cancer Centre, Melbourne, VIC, Australia. gbiasi@uow.edu.au; tltran@uow.edu.au; vp881@uowmail.edu.au; mdl038@uowmail.edu.au; marcop@uow.edu.au; mlerch@uow.edu.au; deanc@uow.edu.au; [2]Centre for Accelerator Science, Australian Nuclear Science and Technology Organization, Lucas Heights, NSW, Australia. zkp@ansto.gov.au; [3]St George Private Hospital, Kogarah, NSW, Australia. jp132@uowmail.edu.au; [4]Prince of Wales Hospital Public Hospital, Randwick, Australia. Michael.Jackson2@health.nsw.gov.au; jbugeja@uow.edu.au; anatoly@uow.edu.au

Introduction Alpha particle therapy exploits the short range and high linear energy transfer (LET) of alpha particles to destroy cancer cells locally with minimal damage to surrounding healthy cells. This is the basis for both targeted alpha particle therapy (TAT) and diffusing alpha-emitters radiation therapy (DaRT) [1]–[6]. Metal–oxide–semiconductor field-effect transistors (MOSFETs) are well known to be

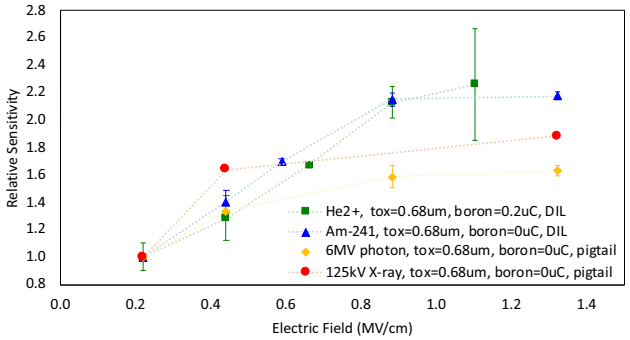

Fig. 14 MOSFET sensitivity to alpha particles emitted by ^{241}Am, He_{2+} ions, a 6 MV photon beam, 125 keV x-rays. X-rays data is extracted from [7]

suitable for dosimetry in megavoltage (MV) and kilovoltage (kVp) x-rays radiotherapy [7]–[9]. In this study, we investigated if MOSFETs are also suitable for dosimetry in alpha particle therapy.

Method Irradiations were performed with an Americium-241 (^{241}Am) source and a mono-energetic helium ion (He^{2+}) beam of 5.5 MeV, on MOSFETs featuring three different thicknesses of the SiO_2 (0.55, 0.68, and 1.0 µm). We investigated how MOSFET sensitivity varies as a function of electric field in the SiO_2 electrode (the sensitive volume) during irradiation, in the range between 15 to 75 V (0.2–1.4 MV/cm).

Results The 0.55 µm- and 0.68 µm- MOSFETs showed good reproducibility and good linearity response for alpha doses up to 26 Gy. Figure 14 shows the sensitivity of 0.68 µm-MOSFETs irradiated with alpha particles and photons, as a function of electric field in the SiO_2. In each case, sensitivity was normalized to the sensitivity recorded with a gate bias of 15 V that is corresponding to electric field 0.2 MV/cm.

Conclusion The MOSFETs investigated in this study had a good sensitivity and a linear dose–response when irradiated with alpha particles, similarly to when irradiated with x-rays. However, based on results, a higher bias was required to reach maximum sensitivity to alpha particles. This is due to the denser ionization track created in the SiO_2 by alpha particles.

References

1. M. Lassmann, D. Nosske, and C. Reiners, "Therapy of ankylosing spondylitis with 224Ra-radium chloride: Dosimetry and risk considerations," *Radiat. Environ. Biophys.*, vol. 41, no. 3, pp. 173–178, 2002.
2. G. Vaidyanathan and M. R. Zalutsky, "Targeted therapy using alpha emitters," *Phys. Med. Biol.*, vol. 41, no. 10, pp. 1915–1931, Oct. 1996.
3. L. Arazi, T. Cooks, M. Schmidt, Y. Keisari, and I. Kelson, "The treatment of solid tumors by alpha emitters released from 224 Ra-loaded sources—internal dosimetry analysis," *Phys. Med. Biol.*, vol. 55, no. 4, pp. 1203–1218, Feb. 2010.
4. L. Arazi, T. Cooks, M. Schmidt, Y. Keisari, and I. Kelson, "Treatment of solid tumors by interstitial release of recoiling short-lived alpha emitters," *Phys. Med. Biol.*, vol. 52, no. 16, pp. 5025–5042, Aug. 2007.
5. L. Arazi, "Diffusing alpha-emitters radiation therapy: approximate modeling of the macroscopic alpha particle dose of a point source," *Phys. Med. Biol.*, vol. 65, no. 1, p. 015,015, Jan. 2020.
6. A. Popovtzer et al., "Initial Safety and Tumor Control Results From a 'First-in-Human' Multicenter Prospective Trial Evaluating a Novel Alpha-Emitting Radionuclide for the Treatment of Locally Advanced Recurrent Squamous Cell Carcinomas of the Skin and Head and Neck," *Int. J. Radiat. Oncol. Biol. Phys.*, vol. 106, no. 3, pp. 571–578, 2020.
7. G. Biasi et al., "On the Combined Effect of Silicon Oxide Thickness and Boron Implantation under the Gate in MOSFET Dosimeters," *IEEE Trans. Nucl. Sci.*, vol. 67, no. 3, pp. 534–540, Mar. 2020.
8. A. B. Rosenfeld, A. Rosenfeld, T. Kron, F. d'Errico, and M. Moscovitch, "Advanced Semiconductor Dosimetry in Radiation Therapy," vol. 48, no. July, pp. 48–74, 2011.
9. A. B. Rozenfeld, G. Biasi, M. Petasecca, M. L. F. Lerch, G. Villani, and V. Feygelman, "Semiconductor dosimetry in modern external-beam radiation therapy," *Phys. Med. Biol.*, no. May, pp. 0–14, Jun. 2020.

O051 Lorentz Forced Problem Solving: Overcoming challenges commissioning the Australian MRI-Linac

J. Begg[1,2,3]

[1]Department of Medical Physics, Liverpool and Macarthur Cancer Therapy Centre, Sydney, Australia; [2]Ingham Institute for Applied Medical Research, Sydney, Australia; [3]South Western Sydney Clinical School, School of Medicine, University of New South Wales, Sydney, Australia. jarrad.begg@health.nsw.gov.au (Presenting author)

Introduction The Australian MRI-Linac Program [1, 2] was established in 2010 to help drive forward the research into MRI-linacs and the clinical practice of radiation oncology. The program has an aim to perform world class research with a global impact on the science and clinical practice of cancer radiotherapy. Themes within the program are to (1) Enable real-time cancer imaging and radiation targeting to improve tumour control and reduce treatment side-effects, (2) Enable and explore the clinical benefit of selectively targeting tumour physiology and (3) Discover synergies with combined modality therapies. Much of the investigations in the MRI-Linac bunker have involved transferring benchtop simulations and investigations into clinically useable equipment. As part of this, the optimisation of both the image acquisition and radiation beam has been investigated. This presentation will review the interesting and complicated challenges surrounding the characterisation of the radiotherapy components on the Australian MRI-Linac including magnetic shielding optimisation[3], alignment[3], collection of basic beam data [3], calibration of the beam [3], treatment planning system modelling, quality assurance tests and end-to-end dose verification for patient treatments. Each step of the journey, from a small radiotherapy device in a giant bunker, to treating rats under clinical conditions [4], to the first clinical trial has posed questions for the investigators to overcome. The solutions obtained have not only helped commission the Australian MRI-Linac, but have provided lessons relevant to conventional clinical equipment.

References/Acknowledgements

1. Keall PJ, Barton M, Crozier S, Australian MRI-Linac Program including contributors from Ingham Institute for Applied Medical Research, Illawarra Cancer Care Centre, Liverpool Hospital, Stanford University, Universities of Newcastle, Queensland, Sydney, Western Sydney, and Wollongong (2014) The Australian magnetic resonance imaging-linac program. Semin Radiat Oncol 24 (3):203–206. https://doi.org/10.1016/j.semradonc.2014.02.015
2. Liney GP, Dong B, Begg J, Vial P, Zhang K, Lee F, Walker A, Rai R, Causer T, Alnaghy SJ, Oborn BM, Holloway L, Metcalfe P, Barton M, Crozier S, Keall P (2016) Technical Note:

Experimental results from a prototype high-field inline MRI-linac. Med Phys 43 (9):5188. https://doi.org/10.1118/1.4961395
3. Jelen U, Dong B, Begg J, Roberts N, Whelan B, Keall P, Liney G (2020) Dosimetric Optimization and Commissioning of a High Field Inline MRI-Linac. Frontiers in Oncology 10 (136). https://doi.org/10.3389/fonc.2020.00136
4. Liney GP, Jelen U, Byrne H, Dong B, Roberts TL, Kuncic Z, Keall P (2019) Technical Note: The first live treatment on a 1.0 Tesla inline MRI-linac. Medical Physics 46 (7):3254–3258. https://doi.org/10.1002/mp.13556

O052 The current state of motion management in Australia and New Zealand – results of the ACDS respiratory motion management survey

A. Burton[1], S. Beveridge[2], N Hardcastle[3], J. Lye[4], R. Franich[5]

[1]Australian Clinical Dosimetry Service (ACDS)/RMIT University/ Peter MacCallum Cancer Centre. Alex.burton@petermac.org (presenting author); [2]Australian Clinical Dosimetry Service (ACDS). Sabeena.beveridge@arpansa.gov.au; [3]Peter MacCallum Cancer Centre. Nick.hardcastle@petermac.org; [4]Olivia Newton John Cancer and Wellness Centre. Jessica.lye@austin.org.au; [5]RMIT University. Rick.franich@rmit.edu.au

Introduction The Australian Clinical Dosimetry Service conducted a survey capturing patterns of practice of respiratory motion management (MM) for the purpose of defining the required scope of a MM audit.

Method The survey was distributed via REDCap (v10.8) to all radiation therapy facilities in the region. Firstly, participants indicated which MM was used: breath-hold gating (BHG), internal target volume (ITV), free-breathing gating (FBG), mid-ventilation, and tumour tracking (TT). Responses focussed on three main treatment locations (lung/thorax, liver/upper abdomen, and kidney/lower abdomen) and two fractionation schedules (stereotactic ablative body radiation (SABR) and conventional). Responses for conventional breast radiotherapy using BHG were excluded. For each combination of MM technique, site, and fractionation, participants described specific practices including use of motion limitation strategies and planning dataset used for dosimetric calculation. The final section asked participants to provide their perspectives on why MM is or isn't used in the clinic. Responses were extracted from REDCap and anonymised for analysis with Python (v3.8).

Results 87/112 (78%) participants provided complete responses, 97.7% of which utilise at least one form of MM. 100% of MM users utilise the ITV method, applied most commonly in lung SABR (89.4%—Fig. 1). While 41.2% of MM users utilise BHG, these responses were dominated by SABR treatments. FBG and TT are utilised sparingly (16.5%, 7.1% of MM users respectively), and mid-ventilation is not used. Motion limitation strategies are not widely used outside of abdominal compression for SABR in the upper abdomen. Choice of planning dataset for dose calculation is largely influenced by MM technique (Fig. 2).

Conclusion The survey highlighted that thoracic and upper abdominal SABR treatment sites primarily utilise the ITV and BHG methods, which will be prioritised for audit development. Practices within each MM technique (use of motion limitation, choice of planning dataset etc.) were fairly homogenous, which may streamline the auditing process.

References/Acknowledgements
Study data were collected and managed using the secure, web-based Research Electronic Data Capture (REDCap) hosted at Peter MacCallum Cancer Centre.

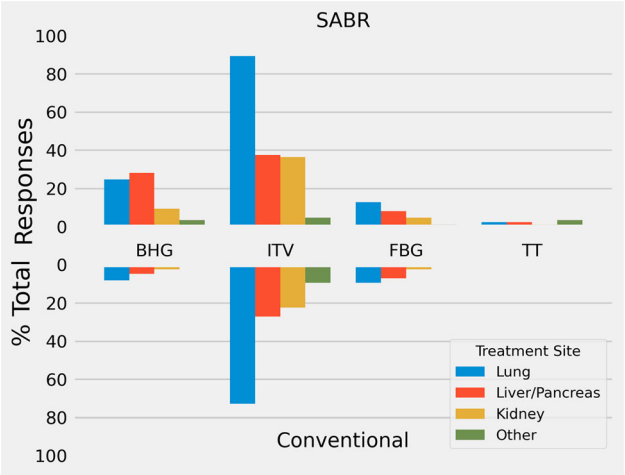

Fig. 1 Proportion of total responses utilising each MM method by treatment site for both SABR and conventional fractionation

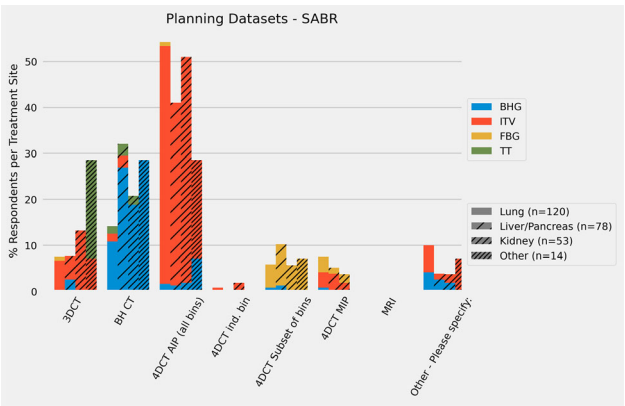

Fig. 2 Patterns of use of planning datasets for all combinations of SABR treatment site and motion limitation strategy

O053 The BRAVEHeart clinical trial: A comparison of motion management systems for deep inspiration breath-hold breast cancer radiation therapy

H. L. Byrne[1], C. Stanton[2], B. Zwan[3], M. Gargett[2], E Steiner[4], K Makhija[1], J. Atyeo[2], K. Richardson[2], L. Ambrose[2], M. Carr[2], R. Bromley[2], J. Booth[2], M. Morgia[2], G. Lamoury[2], P. J. Keall[1]

[1]ACRF Image X Institute, School of Health Sciences, The University of Sydney, Australia. hilary.byrne@sydney.edu.au (Presenting author); [2]Northern Sydney Cancer Centre, Royal North Shore Hospital, Australia. cameron.stanton@health.nsw.gov.au; [3]Central Coast Cancer Centre, Gosford Hospital, Australia. benjamin.zwan@health.nsw.gov.au; maegan.gargett@health.nsw.gov.au; [4]LK Wiener Neustadt, Austria. elisabeth.steiner@wienerneustadt.lknoe.at; kuldeep.makhija@sydney.edu.au; john.atyeo@health.nsw.gov.au; kylie.richardson@health.nsw.gov.au; leigh.ambrose@health.nsw.gov.au; Michael.carr@health.nsw.gov.au; regina.bromley@health.nsw.gov.au; jeremy.booth@health.nsw.gov.au;

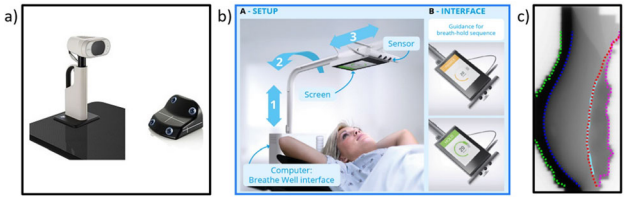

Fig. 1 a) RPM abdominal monitoring system; b) Breathe Well chest surface monitoring system; c) Chest wall detection from beams-eye-view images taken during treatment

marita.morgia@health.nsw.gov.au;
gillian.lamoury@health.nsw.gov.au; paul.keall@sydney.edu.au

Introduction Breast cancer patients treated in free breathing are at increased risk of cardiovascular complications in later life from heart dose during radiotherapy. Deep Inspiration Breath-Hold (DIBH) displaces the target away from the heart, reducing heart dose. To improve treatment accuracy in DIBH, visual feedback is provided to the patient [1]. Emerging technologies provide visual feedback based on surface guidance of the chest. The BRAVEHeart (Breast Radiotherapy Audio Visual Enhancement for sparing the Heart) trial compares a novel chest surface monitoring device using optical depth imaging (Breathe Well) with abdominal monitoring using Varian's RPM marker block system (Fig. 1).
Method Patients underwent 1:1 randomisation to use visual feedback from either the chest surface or abdominal monitoring system. After daily CBCT image match, beams-eye-view EPID images captured continuously were processed to determine treatment accuracy, defined as the chest wall displacement during treatment relative to the planned position [2]. Inter-fraction accuracy is defined as the mean of the chest wall displacement per fraction and intra-fraction accuracy the standard deviation [3].
Results Fig. 2 shows the per-patient inter-fraction accuracy for an initial 8 patients. Averaged across all patients, median inter-fraction accuracy was 0.02 mm and -0.68 mm while intra-fraction accuracy was 0.78 mm and 0.50 mm for the chest surface and for abdominal monitoring respectively.
Conclusion From the analysed treatments, accuracy was acceptable for both devices, with some patients showing larger variability than others attributed to random errors and reproducibility of baseline. Complete patient results for the BRAVEHeart trial (completion due in September) will be presented.
References

1. Cerviño LI, Gupta S, Rose MA, Yashar C & Jiang SB (2009) Using surface imaging and visual coaching to improve the reproducibility and stability of deep-inspiration breath hold for left-breast-cancer radiotherapy. *Phys. Med. Biol.* **54**, 6853–6865

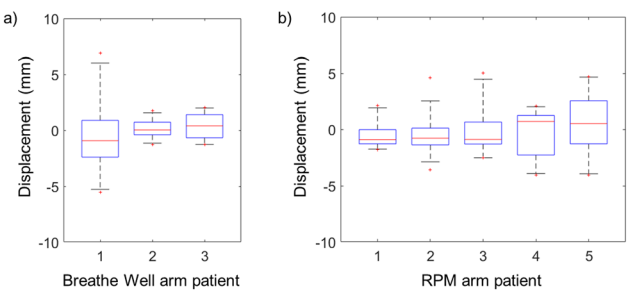

Fig. 2 Inter-fraction accuracy for a) chest surface monitoring; b) abdominal monitoring. Whiskers show 5th to 95th percentile

2. Jensen C et al. (2014) Cine EPID evaluation of two non-commercial techniques for DIBH. *Medical Physics* **41**, 021,730
3. van Herk M (2004) Errors and margins in radiotherapy. *Seminars in Radiation Oncology* **14**, 52–64

O054 Development of a semi-automatic visual inspection tool for ground truth definition in markerless lung tracking

D. Chrystall[1], M. Gargett[1], M. Mueller[2], A. Briggs[1], P. Keall[2], D. T. Nguyen[1,2], J. Booth[1,3]

[1]Northern Sydney Cancer Centre, Royal North Shore Hospital, Australia. Danielle.Chrystall@health.nsw.gov.au (Presenting author); Maegan.Gargett@health.nsw.gov.au; [2]ACRF Image X Institute, University of Sydney, Australia. Marco.Mueller@sydney.edu.au; Adam.Briggs@health.nsw.gov.au; Paul.Keall@sydney.edu.au; DoanTrang.Nguyen@uts.edu.au; [3]Institute of Medical Physics, University of Sydney, Australia. Jeremy.Booth@health.nsw.gov.au

Introduction Markerless tracking technology is under development as an alternative to the use of implanted fiducial markers to monitor tumour motion during radiotherapy [1]. The technology will be implemented in upcoming lung SBRT clinical trials at Royal North Shore Hospital. This work aims to develop and evaluate a semi-automatic visual inspection tool for estimating the ground truth tumour position, as validation of the markerless tracking software.
Method A 3D-printed, anatomically accurate thorax phantom was placed on a programmable motion platform. Kilovoltage fluoroscopic images were acquired during MV beam on, while four patient measured tumour motion traces were applied to the platform. The gross tumour volume (GTV) contour, segmented on planning CT images, was forward projected onto the kilovoltage frames. Manual correction of the GTV contour position was made for each frame and accepted or rejected as ground truth based on visual inspection. The geometric accuracy (mean difference) and precision (1 standard deviation) of the GTV position estimation method were measured and analysed with reference to the required tolerance of 1 mm [2, 3].
Results The accuracy and precision of the GTV position estimation method, averaged over all motion traces, was -0.2 ± 1.8 mm, -0.1 ± 1.5 mm and 0.1 ± 1.5 mm in LR, SI and AP, respectively. The average [5th, 95th] percentile accuracy values were [− 3.4, 1.5] mm, [− 2.1, 3.0] mm and [− 2.3, 2.9] mm in LR, SI and AP, respectively. The tumour was delineated for 16%–60% of kilovoltage frames. Figure 1 shows the tumour GTV for the High Frequency motion trace.
Conclusion The semi-automated visual inspection method of defining tumour position showed an average geometric accuracy < 0.5 mm and precision < 2.0 mm in all directions. Further refinement is required to improve precision and percentage of frames delineated before its use in markerless lung tracking clinical trials.

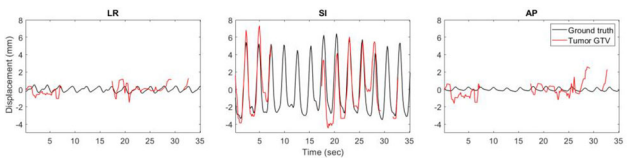

Fig. 1 Comparison between the programmable motion ground truth trace (black) and tumour GTV (red) in left–right (LR), superior-inferior (SI) and anterior–posterior (AP) directions for the High Frequency motion trace

References

1. Mueller, M., et al., The first prospective implementation of markerless lung target tracking in an experimental quality assurance procedure on a standard linear accelerator. Phys Med Biol, 2020. 65(2): p. 025008.
2. Ng, J.A., et al., Quality assurance for the clinical implementation of kilovoltage intrafraction monitoring for prostate cancer VMAT. Med Phys, 2014. 41(11): p. 111712.
3. Willoughby, T., et al., Quality assurance for nonradiographic radiotherapy localization and positioning systems: report of Task Group 147. Med Phys, 2012. 39(4): p. 1728-47.

O055 Patient experience with LEILA: real-time measurements of the mid lung depth in EPID images of tangential breast fields

E. Vasina[1], N. Kong[2], P. Greer[1,2], G. Govindarajulu[2], J. Ludbrook[2], J. Lehmann[1,2,3]

[1]School of Mathematical and Physical Sciences, University of Newcastle, NSW, Australia. Elena.Vasina@newcastle.edu.au (Presenting author); [2]Radiation Oncology Department, Calvary Mater Newcastle, Newcastle, NSW, Australia. Natalie.Kong@calvarymater.org.au; Peter.Greer@newcastle.edu.au; Geetha.Govindarajulu@newcastle.edu.au; Jane.Ludbrook@calvarymater.org.au; [3]Institute of Medical Physics, University of Sydney, Sydney, NSW, Australia. Joerg.Lehmann@calvarymater.org.au

Introduction In DIBH treatments of breast cancer it is critical to guide the patient's inspiration level to achieve optimal alignment of the treatment beam with the anatomy ensuring optimal target coverage and sparing of the heart or liver. Current commercial systems all suffer from the same major limitation being the reliance on surrogates of inspiration level. We have designed and phantom tested our system to directly observe the internal anatomy using real time analysis of EPID images [1]. We report on the initial patient experience with LEILA.

Method LEILA assesses the position of the chest wall relative to the beam aperture in EPID images of tangential breast fields in real time. LEILA is currently being tested with patients in our clinic with DIBH monitored and controlled with Varian's RPM system or C-RAD's Catalyst + HD. In both systems the treatment window (TW) of the chest motion is 5 mm. This report focuses on LEILA measurements of mid lung depth (MLD). Planning values for MLD were obtained from DRR images.

Results MLD was recorded with LEILA for 12 patients. Results are discussed for 3 RPM patients treated for right breast cancer. The average values of MLD, $< \text{MLD} >$, measured with LEILA were compared with planning values for each beam.

For 48 beams of patient A, 33 had $< \text{MLD} >$ below TW (0.7–8.5 mm). Of 18 beams of Patient B (Fig. 1), 4 had $< \text{MLD} >$ outside TW: maximum deviations being + 3.4 mm and − 4.2 mm. Patient C (Fig. 2) often needed multiple breath holds per beam. Of 30 beams, 27 had $< \text{MLD} >$ below TW (0.1–16.3 mm).

Conclusion Real-time measurements of MLD with LEILA are feasible. They have confirmed that RPM-based DIBH-monitoring technique can lead to appreciable deviations from the planned treatment which have been shown to have relevant dosimetric impact [2].

Acknowledgements This work was supported by National Health and Medical Research Council (NHMRC) grant 1,147,533 of the Australian Government. The contents of the published material are solely the responsibility of the authors and do not reflect the views of NHMRC. The authors are grateful to the radiation therapists of Calvary Mater Newcastle.

Ethical statement The involvement of patients in this work has been reviewed and approved by the Hunter New England Human Research Ethics Committee, Australia (2020/ETH00720).

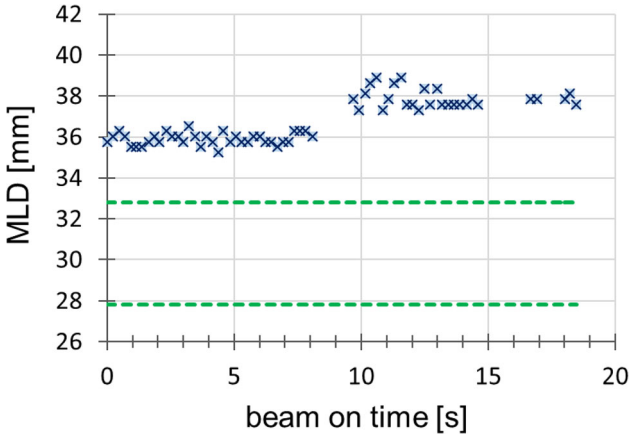

Fig. 1 MLD data of Patient B measured with LEILA for one beam (crosses). The tolerance window (TW, dashed green lines) indicates 2.5 mm either side of expected MLD value. At the start of the beam, MLD was already above TW. Mid-way of the beam, RPM system prompted the patient to breathe in more air. The gaps between groups of crosses are caused by beam hold

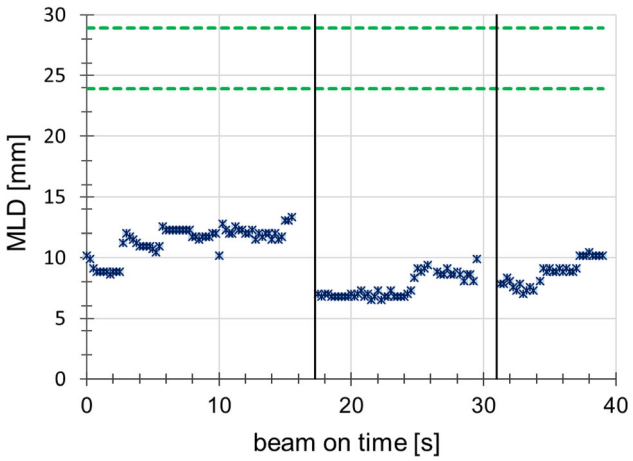

Fig. 2 MLD data (crosses) of Patient C measured with LEILA for all 3 beams of one fraction. During all 3 beams the measured MLD was below TW shown by the dashed green lines

References

1. Vasina E, Greer P, Lehmann J. Verification of new software for assessment of the quality of deep inspiration breath hold (DIBH) in radiotherapy of breast cancer. Real-time measurements of the lung depth with radiotherapy phantoms. HCRA 2020, poster presentation. https://doi.org/10.1111/ajco.13473
2. Doebrich, M., Downie, J., & Lehmann, J. (2018). Continuous breath-hold assessment during breast radiotherapy using portal imaging. *Physics and Imaging in Radiation Oncology*, *5*, 64.

O056 KIMView: An open-source real-time tumour motion, dose, and anatomy visualisation tool for radiotherapy

J. Selvaraj[1,2], C. Sengupta[3], P. Keall[3]

[1]Faculty of Medicine, University of New South Wales, Sydney, NSW, Australia; [2]Medical Physics & Radiation Engineering, Canberra Health Services, ACT, Australia. Jothy.Selvaraj@act.gov.au; [3]ACRF Image X Institute, University of Sydney Central Clinical School, Sydney, NSW, Australia

Introduction IGRT typically focuses on measuring geometric errors in patient's anatomy, especially tumor position and methods to account for it. Geometric accuracy is an indirect measure of treatment quality. The metric of most interest in radiotherapy that correlates directly with clinical outcomes is dose to tumour and critical organs [1]. The goal of this project is to develop an open-source real-time tumour motion, dose, and anatomy visualisation tool for radiotherapy so the treatment team can see the dose being delivered to the dynamic patient. To demonstrate this, kilovoltage intra-fraction monitoring (KIM) system which provides real-time tumor position is used in this work [2].

Method Patient's DICOM objects are read using in-house developed tools [3]. Tumor positions are received in user datagram protocol format from KIM software at 50 ms intervals. A 4 × 4 transformation matrix is constructed based on real-time tumour position. This transformation is applied to each vertex in the 3D polygonal mesh to convert the mesh coordinates and other visualization related attributes. A mesh cutting algorithm cuts the mesh at corresponding position in orthogonal views. To display images and dose, an image slicing algorithm maps raw data to grey and RGB colours using colour lookup tables respectively. The workflow is shown in Fig. 1.

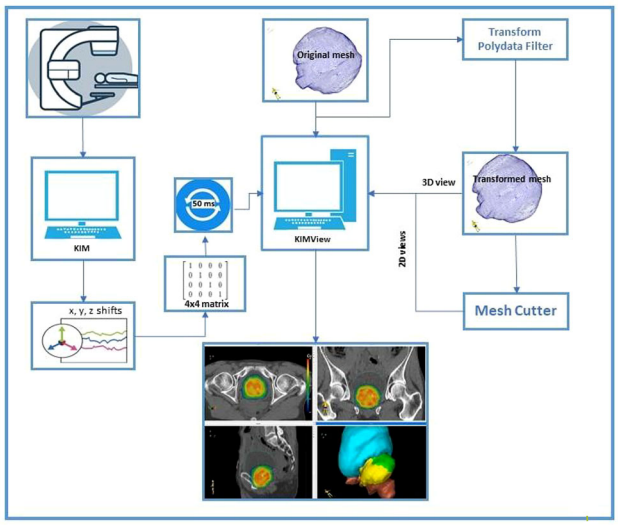

Figure 1: Workflow of KIMView and mesh transformation process

Results An open-source real-time tumour motion, dose and anatomy visualisation tool for radiotherapy has been developed [4]. The tumour positions are updated based on the shifts sent by KIM every 50 ms with other OARs and static tumour (Fig. 2).

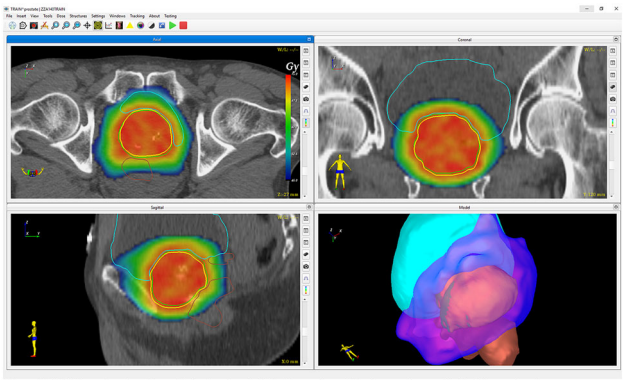

Figure 2: KIMView showing dynamic (yellow) and static (green) prostate tumor along with bladder and rectum

Conclusion Real-time tumour position visualization tool that is adaptable to any real-time image-guidance system such as MR-Linac, Calypso, ExacTrac has been demonstrated. Future work involves clinical evaluations in TROG 17.03 Liver Ablative Radiotherapy with KIM (LARK) trial and inclusion of additional dynamic data visualisation objects such as dose adaptation and anatomic deformation.

References

1. Bentzen, Søren M., et al. "Quantitative Analyses of Normal Tissue Effects in the Clinic (QUANTEC): an introduction to the scientific issues." International Journal of Radiation Oncology* Biology* Physics 76.3 (2010): S3-S9.
2. Keall, Paul, et al. "Real-time image guided ablative prostate cancer radiation therapy: results from the TROG 15.01 SPARK Trial." International Journal of Radiation Oncology* Biology* Physics 107.3 (2020): 530–538.
3. Selvaraj, J. Modelling the effect of geometric uncertainties, clonogen distribution and IMRT interplay effect on tumour control probability. Diss. University of Liverpool, 2013. https://github.com/Jothy/KIMView.git

O057 Six Degrees of Freedom Intrafraction Motion Monitoring during Stereotactic Liver Radiation Therapy in TROG 17.03 LARK Trial: Higher accuracy in half the treatment time than the current standard of care

C. Sengupta[1], D. T. Nguyen[1,2,3], T. Moodie[4], T. Wang[4], Y. Y. Lee[5], Ricky O' Brien[1], J. Booth[3], P. Keall[1]

[1]ACRF Image X Institute, Faculty of Medicine and Health, The University of Sydney, NSW, Australia. Chandrima.Sengupta@sydney.edu.au; [2]University of Technology, NSW, Australia; [3]North Sydney Cancer Centre, Royal North Shore Hospital, NSW, Australia; [4]Crown Princess Mary Cancer Centre, NSW, Australia. [5]Princess Alexandra Hospital, QLD, Australia

Introduction SBRT requires accurate knowledge of the tumour location during a treatment. Intrafraction liver tumour motion may significantly deteriorate the planned dose to the tumour volume and overdose nearby risk-organs. In the LARK trial, we employed a real-time 6 degrees-of-freedom (DoF) motion management technology named Kilovoltage Intrafraction Monitoring (KIM) [1] to directly measure the internal tumour motion and compared KIM-guided treatment accuracy and delivered dose with simulated no-tracking treatment accuracy and delivered dose.

Method Twelve liver cancer patients were treated at breath-hold (8 patients) or free-breathing (4 patients). Three fiducial markers were implanted near the tumour volume and used as surrogates of the tumour motion. KIM-measured tumour motion of 3 mm or more from the planned position triggered a couch correction. KIM-guided treatment time was assessed from KIM-generated log files and standard-of-care treatment time was assessed from the Record-and-verify system providing duration of a treatment including the pre-treatment CBCTs. The geometric accuracy of KIM in all the 6-DoF was evaluated against a kV-MV triangulation method. The summed delivered dose over the course of the treatment with KIM-guided SBRT and simulated delivered dose without KIM-guidance were calculated using dose reconstruction [2].
Results The average KIM-guided treatment time was 20 ± 12 min as compared to 40 ± 15 min[3] in the current standard-of-care. The mean and standard deviation of the targeting error of KIM is 0.4 ± 0.6 mm, 0.1 ± 0.8 mm and 0.1 ± 0.9 mm in the superior-inferior, left–right and anterior–posterior directions respectively and 0.4° ± 1.0°, 0.1° ± 0.7°, 0.1° ± 0.8° in roll, pitch and yaw respectively, averaged over all the treatment fractions. With KIM-guided SBRT, the summed delivered dose to PTV D95 was closer to the planned dose by an average of 1.5% (range: 0–10.6%) compared to simulated no-tracking (Fig. 1). Without KIM-guidance, overdose of one or more organ-at-risk by > = 10% was found.
Conclusion KIM-guided liver SBRT improved geometric and dosimetric accuracies.

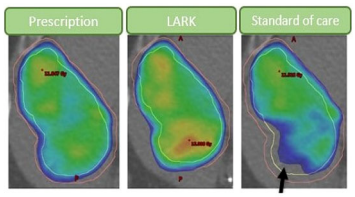

Figure 1: Dose map showing planned dose, dose delivered using KIM-guidance in the LARK trial, and, simulated no-tracking dose to the tumour volume for one of the LARK patients. A part of the tumour volume will be missed if motion correction was not adopted as indicated by the black arrow.

References

1. Keall et al., "Real-Time Image Guided Ablative Prostate Cancer Radiation Therapy: Results from the TROG 15.01 SPARK Trial", Int. J. of Rad. Onc. Biol. Phys. 107 (2020).
2. Poulsen et al., "A method of dose reconstruction for moving targets compatible with dynamic treatments", Med. Phys. 39 (2012).
3. Based on the measured practice at Crown Princess Mary Cancer Centre and Nepean Cancer Care Centre.

O058 Geometric Distortion evaluation on 1.5 T MRI-Simulator at ONJ

Reza Alinaghizadeh[1], Nikki Shelton[1], Jessica Lye[1], Glenn Cahoon[1], Rob Behan[1], Leah McDermott[1], Sandra Fisher[1]

[1]Olivia Newton John Cancer Research and Wellness Centre, Austin Health, Melbourne reza.alinaghizadeh@austin.org.au (Presenting author); nikki.shelton@austin.org.au; jessica.lye@austin.org.au; glenn.cahoon@austin.org.au; rob.behan@austin.org.au; Leah.McDermott@austin.org.au; sandra.fisher@austin.org.au

Introduction The geometric accuracy of any imaging modality used for planning radiotherapy is crucial to the accuracy of dose delivery. MRI provides great soft tissue contrast, which can improve the target and OAR delineation, but geometric (geo-)distortion needs to be evaluated carefully. Distortions in MRI images used as primary or secondary imaging for radiotherapy can compromise treatment efficacy [1]. The aim was to evaluate geo-distortions in the recently installed 1.5 T MRI-Simulator at the Olivia Newton John Cancer and Wellness Centre.
Method Various methods and phantoms were used, based on availability at different stages of commissioning. The Philips Geo-Distortion phantom was tested initially, but had limited utility as the first software analysis tools did not provide quantitative results. The CIRS MR-CT abdomen phantom was then used, with rigid and deformable registration, to quantify the geo-distortion present using different MRI sequences. Finally, the QUASAR Modus phantom was used to quantify the geo-distortion from B0 inhomogeneity and gradient linearity, as well as the combined distortion from both these parameters.
Results Despite a lack of quantified data for the Philips Geo-Distortion test, initial results from both rigid and deformable registration with CIRS MR-CT abdomen phantom provided similar distortion estimates: mean ≤ 1.5 mm within 200 mm from imaging isocentre. The QUASAR Modus phantom results showed an overall geo-distortion of mean = 0.43 mm, max = 1.36 mm and SD = 0.17 mm within 200 mm from imaging isocentre on 633 Hz bandwidth (Fig. 1). The Philips newer analysis tools also provided max = 1.48 mm within 200 mm from imaging isocentre, confirming the results from the alternative assessment methods.

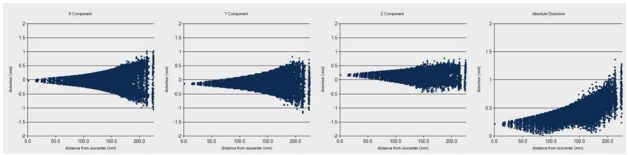

Fig. 1 Geo-distortion from Modus phantom in 3 different directions and their combined distortion
Conclusion Geo-distortion of the 1.5 T magnet was evaluated and baselined for routine and post-service checks during the commissioning process. Results from Philips Geo-Distortion phantom and QUASAR Modus phantom were within recommended tolerances.
Reference

1. Carri K. Glide-Hurst, Eric S. Paulson2, Kiaran McGee3, Neelam Tyagi4, Yanle Hu5, James Balter6, John Bayouth AAPM TG 284 report: Magnetic Resonance Imaging Simulation in Radiotherapy: Considerations for Clinical Implementation, Optimization, and Quality Assurance Med Phys 2021 https://doi.org/10.1002/MP.14695

O059 Evaluating the feasibility of 3D Chemical Exchange Saturation Transfer (CEST) MRI in prostate cancer at 3T

N. Gholizadeh[1], M. Kumar[2], J. Goodwin[1,2]

[1]Faculty of Science, The University of Newcastle, AU. neda.gholizadeh@newcastle.edu.au (Presenting author); [2]Calvary Mater Newcastle, AU. Mahesh.Kumar@calvarymater.org.au; jonathan.goodwin@newcastle.edu.au

Introduction Chemical exchange saturation transfer (CEST) MR is an imaging technique that is sensitive to metabolic state and macromolecule concentration in the human body [1]. This imaging

technique has been applied to evaluate tissue abnormalities, cell proliferation and pH [2,3]. Recent CEST studies have shown reduced amide proton transfer (APT) associated with various diseases [4,5]. In this study, the feasibility of APT-CEST was evaluated for prostate cancer detection by optimizing the saturation parameters using simulation and computing contrast using a Z-spectrum fitting approach.
Method A 75-year-old patient with biopsy-proven prostate cancer was imaged using an 18-channel receive coil on a Siemens 3 T before radiation therapy. Three dimensional APT-MR imaging was acquired with the following parameters: TR/TE = 2 /4.5 ms; Matrix = 128 × 104 mm^2; Slice thickness = 5 mm; Number of signal averages = 1. The saturation pre-pulse was composed of a train of pulses, each with a pulse length of 31 ms and saturation amplitude of 1.8 μT. The WASABI spectrum was prepared by one rectangular RF pulse of amplitude B1 = 3.5 μT and 5 ms length.
All image processing and data analysis were performed using in-house developed programs written in MATLAB.
Results B_0 shimming was performed with least square error optimization using manual segmentation of the prostate gland. APT-CEST images were corrected for inhomogeneities according to the acquired B_0 and B_1 inhomogeneity map from the WASABI (Fig. 1).

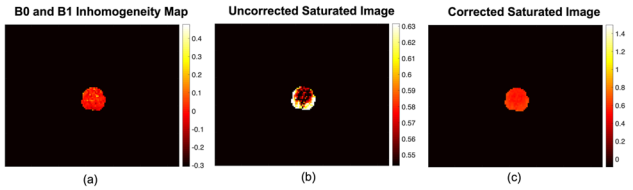

Fig. 1 **a** inhomogeneity map of the prostate gland derived from WASABI, **b** uncorrected and **c** corrected CEST MR image

A four-pool Lorentzian-fit model was used to achieve a reliable separation of the different contributions to the Z-spectrum. Cancer region showed higher asymmetry ratio at 3.5 ppm than healthy peripheral zone region, indicating elevated mobile protein levels in prostate cancer (Fig. 2).
Conclusion APT-MR imaging is feasible in prostate cancer detection. This study demonstrated that APT-CEST has the potential to discriminate between cancer and non-cancer tissues.
References

1. Jones KM, Pollard AC, Pagel MD (2018) Clinical applications of chemical exchange saturation transfer (CEST) MRI. J Magn Reson Imaging 47:11–27.
2. Zaiss M, Xu J, Goerke S, et al. (2014) Inverse Z-spectrum analysis for spillover-, MT-, and T1-corrected steady-state pulsed CEST-MRI–application to pH-weighted MRI of acute stroke. NMR Biomed 27:240–52.
3. Goldenberg JM, Pagel MD (2019) Assessments of tumor metabolism with CEST MRI. NMR Biomed 32:e3943.
4. Paech D, Dreher C, Regnery S, et al. (2019) Relaxation-compensated amide proton transfer (APT) MRI signal intensity is associated with survival and progression in high-grade glioma patients. Eur Radiol 29:4957–67.
5. By S, Barry RL, Smith AK, et al. (2018) Amide proton transfer CEST of the cervical spinal cord in multiple sclerosis patients at 3 T. Magn Reson Med 79:806–14.

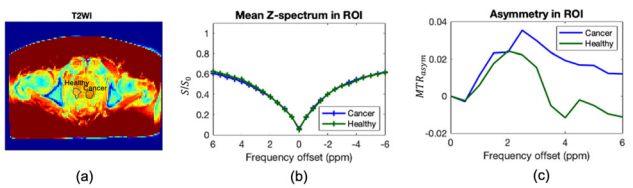

Fig. 2 **a** T2WI of a 75-year-old patient with biopsy-proven prostate cancer in left side of the peripheral zone, **b** Z-spectrum of cancer and healthy tissues and corresponding **c** asymmetry results

O060 Mobility of the choroid plexus as observed in MRI images of the brain

T. Kairn[1,2,3,4], S. B. Crowe[3,4,5], C. S. Bettington[1,6]

[1]Cancer Care Services, Royal Brisbane and Women's Hospital, Brisbane, Qld, Australia; [2]Herston Biofabrication Institute, Metro North Hospital and Health Service, Brisbane, Qld, Australia; [3]School of Information Technology and Electrical Engineering, University of Queensland, Brisbane, Qld, Australia; [4]School of Chemistry and Physics, Queensland University of Technology, Brisbane, Qld, Australia. t.kairn@gmail.com (Presenting author); [5]Herston Biofabrication Institute, Metro North Hospital and Health Service, Brisbane, Qld, Australia; [6]Faculty of Medicine, Queensland University of Technology, Brisbane, Qld, Australia

Introduction The choroid plexus may be deliberately be treated with radiation in cases of choroid plexus papilloma [1,2,3], choroid plexus carcinoma [1,2,4] or metastasis [2]. The choroid plexus is not routinely regarded as an organ-at-risk (OAR) for the purpose of radiotherapy treatment planning, though the functional importance of this structure [5,6] is sufficient to justify such treatment. Whether the choroid plexus is treated as the target or regarded as an OAR for cranial radiotherapy, the potential extent of inter-fraction motion of this structure is an important and under-studied variable.
Method T2-weighted turbo spin echo (TSE) MR images of the brains of 12 healthy volunteers were obtained as part of an ethics approved study into anatomical variation of CNS anatomy [7]. Images were acquired with each participant lying prone and supine, to provide a worst-case indication of choroid plexus mobility. The position of each choroid plexus within the right or left ventricle of each brain was measured and differences between prone and supine images of each participant were recorded.
Results An obvious shift in the position of the choroid plexus, within the right and left ventricles of the brain, was observed for the six oldest participants (over 30 years old), whose ventricles were large enough to allow substantial choroid plexus motion. Figure 1 exemplifies how the choroid plexus hung superior-posteriorly when each participant was imaged in the supine position (left-hand images) and flopped anteriorly when each participant was imaged in the prone position (right-hand images). Some of these shifts were observed to exceed 5 mm.
Conclusion Whereas cranial anatomy is often considered fixed within the skull, the choroid plexus is clearly exceptional in the range and extent of motion that it can display. Substantial shifts are possible, especially in older patients with larger ventricles, which should be considered when determining margins for radiotherapy of the choroid plexus or surrounding anatomy.
Acknowledgements S B Crowe's contribution to this work was supported by a Metro North Hospital and Health Service funded Herston Biofabrication Institute Programme Grant. MRI imaging series used in this study were provided by the Herston Imaging Research Facility (HIRF) via the Herston Biofabrication Institute.
References

1. Bettegowda C, Adogwa O, Mehta V, et al. (2012) Treatment of choroid plexus tumors: a 20-year single institutional experience. J Neurosurg Pediatr 10(5): 398–405

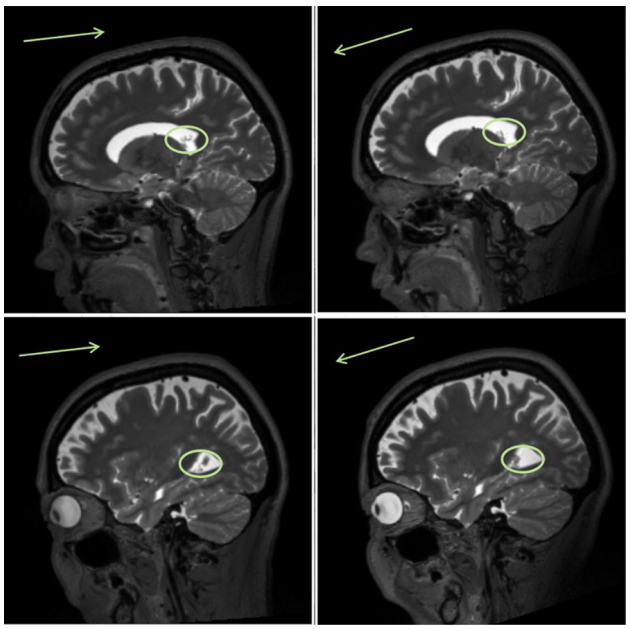

Fig. 1 Example images of one participant showing choroid plexus position (circled, dark line within lateral ventricle) in supine (left) and prone (right) MRI images

2. Wolff J E, Sajedi M, Coppes M J, et al. (2002) Choroid plexus tumours. British Journal of Cancer 87: 1086–1091
3. Schiopu S R, Habl G, Häfner M, et al. (2017) Craniospinal irradiation using helical tomotherapy for central nervous system tumors. J Radiat Res 58(2): 238–246
4. Mazloom A, Wolff J E, Paulino A C (2010) The impact of radiotherapy fields in the treatment of patients with choroid plexus carcinoma. Int J Radiat Oncol Biol Phys 78(1): 79–84
5. Javed K, Lui K F (2019) Neuroanatomy, Choroid Plexus, In StatPearls [Internet]. (StatPearls Publishing) https://www.ncbi.nlm.nih.gov/books/NBK538156/ Accessed April 2020
6. Lun M P, Monuki E S, Lehtinen M K (2015) Development and functions of the choroid plexus–cerebrospinal fluid system. Nature Rev Neurosci 16(8): 445–457
7. Kairn T, Berry C, Campbell L, et al. (2020) Appearance and minimisation of respiratory motion artefacts in thoracic MRI images of prone patients. Phys Eng Sci Med 43(1): 461–462 https://doi.org/10.1007/s13246-019-00826-6

O061 MRI motion artefact reduction in the radiotherapy context

Jessica Lye[1], Reza Alinaghi[1], Nikki Shelton[1], Glenn Cahoon[1], Sandie Fisher[1]

[1]Olivia Newton John Cancer Research and Wellness Centre, Austin Health, Melbourne. jessica.lye@austin.org.au (Presenting author); reza.alinaghizadeh@austin.org.au; nikki.shelton@austin.org.au; glenn.cahoon@austin.org.au; Sandie.fisher@austin.org.au

Introduction MRI offers superb soft tissue contrast but can be susceptible to motion artefacts such as ghosting/blurring [1]. Innovative MR sequences manipulating the phase encoding are commercially available that minimise these artefacts resulting in high image quality. During treatment the motion will still be present and contoured tumours must be linked to the correct breathing phase for ITV generation or gated deliveries. The purpose of this work is exploring MR sequences and developing processes for 4D sequence testing.

Method The CIRS MR-CT abdomen motion phantom tested the sequences; including a 3D T2 with Navigator (cylindrical excitation pulse to visualise the diaphragm) [2]; and a 2D T2 MultiVane ZOOM [3]. In MultiVane, data acquisition is performed with rotating "blades" in k-space. The motion will affect the low frequencies in the centre of k-space and can be corrected for with the oversampled central space.

Results Fig. 8 shows the transverse view of a target with sinusoidal 2 cm SI motion imaged with (a) no motion management, (b) T2 Navigator, and (c) T2 MultiVane ZOOM. The Navigator effectively reduces blurring and the MultiVane demonstrates superior image quality in this plane.

Figure 9 shows the sagittal view with regular 4 s breathing motion. Trigger delays of 1 and 3 s selected the inhale and exhale phases in the Navigator sequence. The Auto setting selects the inhale phase on the phantom (inverted due to phantom diaphragm surrogate). The MultiVane with external Vitaleye trigger with default delay selected the mid-phase and truncated the target length in SI direction. With 1 s delay the exhale phase was selected and full target size was visualised.

Conclusion Multiple sequences are available that will provide superior image quality with motion, but the imaged breathing phase will be dependent on the precise sequence configuration, trigger options, and breathing trace.

References

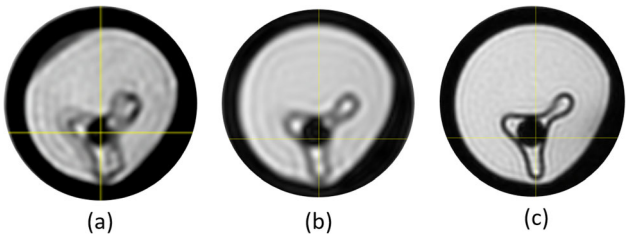

Fig. 15 The transverse view of a target with 2 cm SI sinusoidal motion with **a** Standard T2 imaging with no motion management, **b** T2 Navigator image, and **c** T2 MultiVane ZOOM image

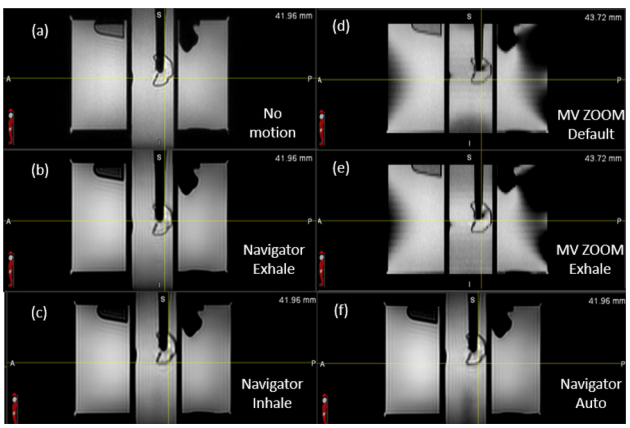

Fig. 16 (a) is the reference image with no motion which is the mid-phase. (b), (c) and (f) show the Navigator with trigger set to Inhale, Exhale, and Auto triggering respectively. (d) and (e) show the MultiVane with default time delay and set to Inhale respectively

1. Motion Artefacts in MRI: a Complex Problem with Many Partial Solutions, J Magn Reson Imaging. 2015 Oct; 42(4): 887–901.
2. Maxim Zaitsev et al. Shreyas S. Vasanawala et al. Navigated Abdominal T1 MRI Permits Free-Breathing Image Acquisition with Less Motion Artifacts, Pediatr Radiol. 2010 Mar; 40(3): 340–344.
3. Kyung A Kang et al., T2-Weighted Liver MRI Using the MultiVane Technique at 3 T: Comparison with Conventional T2-Weighted MRI, Korean J Radiol. 2015 Sep-Oct; 16(5): 1038–1046

O062 Implementation of an MR safety program into a radiation oncology center

Nikki Shelton[1], Reza Alinaghi[1], Sweet Ping Ng[1], Brad Moffat[2], Glenn Cahoon[1], Briana Farrugia[1], Drew Smith[1], Jessica Lye[1], Sandra Fisher[1], Kym Rykers[1]

[1]Olivia Newton John Cancer Research and Wellness Centre, Austin Health, Melbourne nikki.shelton@austin.org.au (Presenting author); reza.alinaghizadeh@austin.org.au; sweetping.ng@austin.org.au. [2]Senior Research Fellow—MRI Science Radiology, University of Melbourne. bmoffat@unimelb.edu.au; glenn.cahoon@austin.org.au; Briana.farrugia@austin.org.au; Drew.Smith@austin.org.au; Olivia Newton John Cancer Research and Wellness Centre, Austin Health, Melbourne; Jessica.lye@austin.org.au; sandra.fisher@austin.org.au; kym.rykers@austin.org.au

Introduction 2020 saw the introduction of two MRI systems into the Radiation Oncology department at the ONJ Centre in Melbourne. As the pandemic disrupted all of the department's established workflows, newly appointed staff and roles required new solutions for the implementation of novel technologies. As the role of safety in radiation oncology traditionally sits with the physics department, it was felt that the initial introduction of an MR safety program would also fall under the responsibility of the physicists; however, it soon became clear that a multi-disciplinary approach would be essential. This presentation explores the methods and outcomes that culminated in the development of a comprehensive MR safety program.
Method We sought and received substantial assistance from our neighboring Radiology department along with other external MRI experts, prior to the employment of our own MRI radiographer. Following the RANZCR[1] guidelines, a comprehensive MR safety program was developed prior to magnet ramp up. All meetings and document development was forced to occur online, in line with hospital policies to work remotely as much as possible due to physical distancing and infection controls.
Results Outcomes include the introduction of new staff definitions in line with the RANZCR Guidelines, the development and execution of associated levels of training for MR safety, a comprehensive MR safety document specific to our RT environment as well as relevant personnel and patient screening programs. The addition of a radiographer to the team fast tracked clinical protocols, contrast and device management policies.
Conclusion Introducing a new paradigm and new staff into an established program brings about its own challenges. Adding the impact of a pandemic to the ability to teach and adopt new standards has brought with it an opportunity to adopt change by focusing on common goals and highlighting the importance of good communication.
References/Acknowledgements

1. MRI Safety Guidelines, Version 2.0

O063 Radiomics for tumor characterization in nuclear medicine: the good, the bad and the ugly

Irène Buvat[1]

[1]Research Director, CNRS, Institut Curie

As an analogy to genomics, proteomics, and all omics specialties, radiomics was introduced a decade ago as a novel approach to comprehensively exploit the content of medical images. Despite the incredibly fast increase in radiomics-related publications since 2010, radiomics fails short in being clinically translated. We will explain the rationale for developing radiomics, how radiomics is performed, but also the reasons why it has not reached the initial expectations yet. We will discuss why the future of radiomics remains bright, as well as the connexion of Radiomics with the Artificial Intelligence hype.

O064 Comparison of rigorous and approximate calculations of close contact restrictions for patients who received radioiodine therapy for differentiated thyroid cancer

J. C. Forster[1], D. Badger[1], K. J. Hickson[1]

[1]Medical Physics & Radiation Safety, South Australia Medical Imaging, Adelaide SA, Australia. Jake.Forster@sa.gov.au (Presenting author); Daniel.Badger@sa.gov.au; Kevin.Hickson@sa.gov.au

Introduction Patients treated with radionuclide therapy may require restrictions on certain activities for a time following treatment to ensure that no member of the general public receives an exposure exceeding the legal dose limit. Software may be used to calculate necessary restriction periods for an individual based on longitudinal dose rate measurements from the time of administration. A Microsoft Excel spreadsheet called RNRTvPC14 created by John Cormack and Jane Shearer is one such software [1]. This spreadsheet has a limitation in that it uses an approximation in the calculation of dose from a contact pattern, which affects the restriction period.
Method A computer program called Morning Star (MS) was developed that provides the same functionality as the spreadsheet (including a graphical user interface), but implements the full, rigorous calculation of dose from a contact pattern [2]. Results from the spreadsheet and MS were compared for 35 patients who underwent radioactive I-131 therapy for differentiated thyroid cancer.
Results MS gave better curve fits to the dose rate measurements. The restriction periods for caring for infants, close contact with children and sleeping with a partner were typically about 12 h longer in MS than in the spreadsheet, but could be several days shorter or up to a month longer. By performing the rigorous calculation of dose for the restriction period, it was found that the restriction periods calculated in the spreadsheet frequently resulted in doses well above the dose constraints for the theoretical contact patterns considered (Figure). Note that some contact patterns do not apply to all patients and the true contact patterns vary considerably from patient to patient.

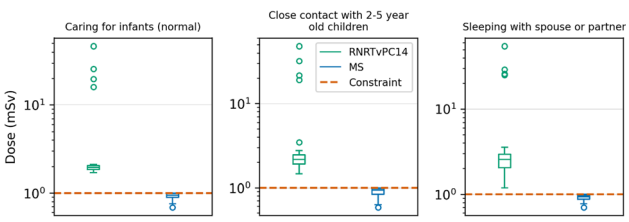

Conclusion If MS is used clinically, some patients will enjoy shorter restriction periods and, for other patients, the therapy provider can be more confident in their compliance with regulatory requirements and best practice.

References

1. Cormack J, Shearer J (2003) Computer generation of individually tailored radiation safety advice for radionuclide therapy patients. Flinders Medical Centre
2. Cormack J, Shearer J (1998) Calculation of radiation exposures from patients to whom radioactive materials have been administered. Phys Med Biol 43(3):501–51

O065 Performance evaluation of SPECT/CT systems with traditional scintillation detectors (NaI) and new semiconductor (CZT) detectors in low contrast studies

S. Gautam[1], O. Daskalovski[1], N. Hille[1], S. Gupta[1]

[1]Hunter New England Imaging, John Hunter Hospital, New Lambton Heights, NSW. sijan.gautam@health.nsw.gov.au (Presenting author); olivia.daskalovski@health.nsw.gov.au; nick.hille@health.nsw.gov.au; sandeep.gupta@health.nsw.gov.au

Introduction In a large number of clinical SPECT studies, low target to background activity concentration ratio (T:BG ratio) are often encountered including negative contrast e.g. brain SPECT studies. In many cases, the lesions are very small e.g. parathyroid studies. There is also a need to accurately quantify SPECT positive lesions for monitoring response to therapies. However, prior performance studies have used high T:BG ratios up to 8:1. Hence, there is a need to establish contrast recovery capabilities to help qualitative as well as quantitative assessments for such low contrast scenarios.

Method A series of scans of the NEMA IEC PET Body phantom was performed with two SPECT/CT systems, GE NM/CT 870 CZT (semiconductor detectors) and Siemens Symbia T2 (scintillation detectors), after initial sensitivity measurement and verification of both systems. Decremental T:BG ratios of ^{99m}Tc solution were used from 5:1 to 0.2:1. The images were processed according to NEMA NU2-2007 and percent contrast, percent background variability and relative lung error were calculated.

Results The maximum percent contrast were 63% and 55% for GE CZT and Siemens Symbia systems respectively, for the largest target sphere (37 mm diameter) which gradually decreased to under 10% for both systems for the smallest target sphere (10 mm diameter). The variation between percent contrasts at a given T:BG ratio was less for the larger spheres as compared to the smaller spheres. Background variability was between 3 and 9% for both systems, gradually decreasing as the sphere diameter increased.

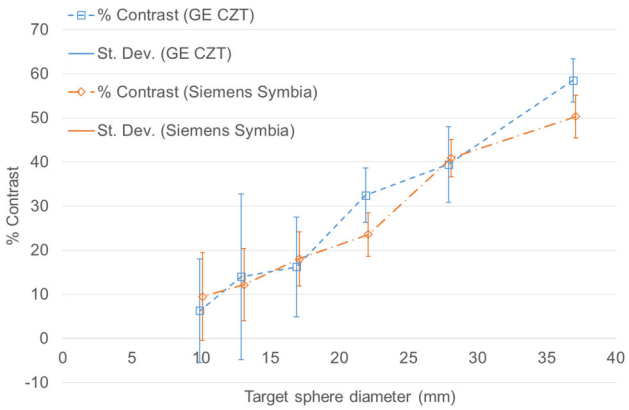

Fig. 1 Average % Contrast for the two SPECT/CT Systems with error bars representing the standard deviation

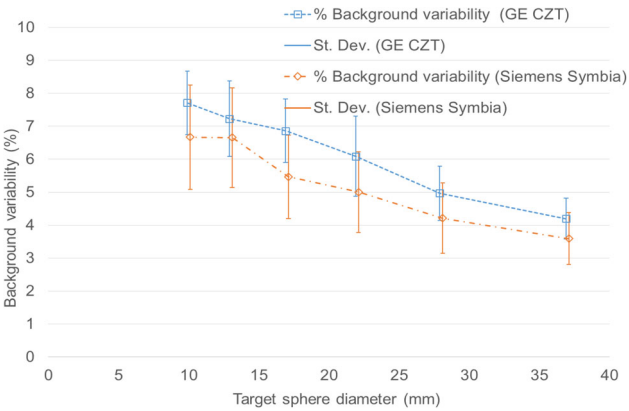

Fig. 2 Average % Background Variability for the two SPECT/CT Systems with error bars representing the standard deviation

Conclusion Accurate quantification of activity concentration, within acceptable margin of error, can be achieved with SPECT/CT for larger lesions, even at low T:BG ratios. However, lower contrast recoveries with higher fluctuations for smaller target spheres introduce higher errors. This renders quantitation unreliable for such small lesions. This can, however, aid physicians while interpreting small lesions that are indicated in planar imaging but not visible in SPECT.

Acknowledgement I would like to acknowledge Kevin Picton and the Nuclear Medicine department at John Hunter Hospital, Newcastle for facilitating the phantom scans on the clinical scanners.

O066 Radioactive Spill Practical Training and Quality Assessment for Nuclear Medicine Radiation Workers

K. E. Porumb[1], B. Crouch[1], C. Boyd[2]

[1]Medical Physics & Radiation Safety, South Australia Medical Imaging, Adelaide, Australia. Kirsten.Porumb@sa.gov.au (Presenting

author); Benjamin.Crouch@sa.gov.au; [2]South Australia Medical Imaging, Adelaide, Australia. Chris.Boyd2@sa.gov.au

Introduction Clinical nuclear medicine departments routinely work with unsealed radioactive isotopes, and as such, spills are inevitable. It is, therefore, necessary that staff know radioactive spill clean-up procedures. While information can be found in the organisation's Radiation Safety Manual, this only covers the theory of spill clean-up. Hands-on training is invaluable to improve staff's practical safety skills, knowledge and confidence. Structured assessment of technical clinical skills has previously been developed for the medical education of surgical residents, such as the OSTATS (Martin, 1997). OSTATS has also been applied to radioactive spills training in a nuclear medicine department (Hussain, 2015). Further third-party quality assessments are available through the IAEA via voluntary nuclear medicine quality management audits (IAEA, 2013).
Method The medical physics department of SA Medical Imaging developed practical radioactive spill clean-up scenarios tailored to the specific needs of each nuclear medicine department, maximising training currency and relevance (Graham, 2007). OSTATS helped to form the basis of SAMI's training framework; however, the evaluation was done on the training itself rather than the individual's abilities. This self-evaluation encourages and acknowledges the collaborative nature of nuclear medicine departments. The effectiveness of the session was assessed using a survey filled out before and after the training. Nonparametric statistical analysis was used to quantify the benefits of the training.
Results A positive trend was seen across all participants and sites. Individuals showed a positive attitude towards the training and felt it improved their confidence to clean-up a radioactive spill.
Conclusion The positive trend in participants opinions shows the training is improving the confidence of staff to attend a radioactive spill clean-up. This reassures SAMI they are providing their staff with the quality training their staff deserve, which creates a positive and safe workplace environment.
References

Graham MM, Metter DF. Evolution of nuclear medicine training: Past, present, and future. J Nucl Med 2007;48:257–68
Hussain RP. Management of Radioactive Spills in Nuclear Medicine: Teaching and Assessing with Objectively Structured Assessment of Technical Skills. World J Nucl Med 2015;14:89–94
Martin J, Regehr G, Reznick R, Macrae H, Murnaghan J, HutchisonC & Brown M: Objective Structured Assessment of Technical Skill (OSATS) for Surgical Residents. The British Journal of Surgery 1997; 84(2), 273–278.
Quality Management Audits in Nuclear Medicine Practices. IAEA; 2013. Available from: http://www.nucleus.iaea.org/HHW/NuclearMedicine/QualityPractice/QUANUM/QualityManagementAuditsinNuclearMedicinePractices/index.html.

Acknowledgements The authors would like to acknowledge all the staff that participated in the training.

O067 Addressing sonographer concerns regarding radioactive patients: a conservative approach

M. Vozzo[1], S Midgley[1]

[1]Medical Physics and Radiation Engineering, Canberra Health Services, Australia. Marie.A.Vozzo@act.gov.au (Presenting author); Stewart.M.Midgley@act.gov.au

Introduction A recent case at Canberra Hospital where a cardiac patient received an echocardiogram shortly after completion of a nuclear medicine procedure has renewed concerns regarding examination scheduling between departments, as well as concern for the yearly radiation exposure that may be received by sonographers who are not monitored as occupationally exposed workers.
Method To assess scheduling conflicts, a list of scans over the past year was obtained for all departments involved and scans were compared based on MRN, and date/time stamps to find ultrasounds occurring on the same day or day following a nuclear medicine or PET scan. Dose estimations were calculated for protocols which were found to be most used by the Nuclear Medicine Department. These calculations were performed using the AAPM TG108 dose estimation methodology (1). From these calculations a dose calculator was created for future use.
Results Data analysis showed that very few radioactive patients make it through to ultrasound within a 24-h period—about 4 per year (or 2–5% of patients who also receive a nuclear medicine scan). Conservative calculations assuming these 4 cases were performed by one sonographer estimated a total effective dose of 214 μSv. The dose calculator estimations were found to be conservative close to the patient and generally consistent with literature (2–6).
Conclusion While scheduling errors are a rare occurrence, administration processes should be improved to reduce these. The conservative, worst-case estimates of effective dose to sonographers remained below a quarter of the yearly dose limit to members of the public. Therefore, risk from radiation exposure to sonographers from radioactive patients at Canberra Hospital is considered very low to minimal. Furthermore, while the dose calculator will be a helpful tool for future calculations of conservative estimates, there is room for improvement by comparing the estimations with measured data.
Acknowledgements Leah Giles, Senior Cardiac Sonographer, for contributions regarding ultrasound positioning and procedures. Farshid Salehzahi, Head of Molecular and Nuclear Medicine Physics, for advice regarding risk assessment procedures in nuclear medicine and appropriate staff dose calculations. Stewart Midgley, Senior Diagnostic Imaging Medical Physicist, and Donald McLean, Head of Radiology Physics, for guidance regarding the approach to the risk assessment
References

1. Madsen MT, Anderson JA, Halama JR, Kleck J, Simpkin DJ, Votaw JR, Wendt III RE, Williams LE, Yester MV (2006) AAPM Task Group 108: PET and PET/CT shielding requirements. Medical Physics 33(1).
2. Griff M, Berthold T, Buck A (2000) Radiation exposure to sonographers from fluorine-18-FDG PET patients. J Nucl Med Technol. 28:186–187.
3. Güneş BY, Erez Ö, Gündoğan C, Ergül N (2019) The evaluation of external dose rate measurements of patients during and after F-18 FDG PET/CT imaging and appropriate discharge time from PET/CT department. İstanbul Med J 20(3):188–192.
4. Janssen J, Smart R, McKay E (2000) Sonographers and exposure to ionising radiation from nuclear medicine patients. Australasian Soc Ultrasound Med Bulletin 3(3):4–8.
5. Massalha S, Lugassi R, Raysberg E, Koskosi A, Lechtenberg G, Israel O, Kennedy JA (2018) Evaluation of staff radiation exposure during transthoracic echocardiography close to myocardial perfusion imaging. J Am Soc Echocardiogr 31(7):763–770.
6. Velchik MG (1990) Radiation exposure associated with the performance of radiologic studies in radioactive patients. J Nucl Med Technol. 18(3):211–213.

O068 A dosimetric comparison of CT and photogrammetry generated 3D printed surface molds for HDR brachytherapy

C. A. Bridger[1,2], M. J. J. Douglass[1,2], A. M. Caraça Santos[1,2], P. Reich[1,2]

[1]School of Physical Sciences, University of Adelaide, Australia; [2]Department of Medical Physics, Royal Adelaide Hospital, Australia.
corey.bridger@adelaide.edu.au (Presenting author); Michael.Douglass@adelaide.edu.au; Alexandre.Santos@adelaide.edu.au; Paul.Reich@sa.gov.au

Introduction In this study, we investigate whether an acceptable dosimetric plan can be obtained for a surface applicator designed using photogrammetry and compare the plan quality to a CT-derived applicator.
Materials and Methods The nose region of a RANDO phantom was selected as the treatment site due to its high curvature. Photographs were captured using a Nikon D5600 DSLR camera and reconstructed using Agisoft Metashape while CT data was obtained using an Aquillion LB scanner. Virtual surface applicators were designed in Blender and printed with ABS plastic. Treatment plans with a prescription dose of 3.85 Gy × 10 fractions with 100% dose to PTV on the bridge of the nose at 2 mm depth were generated using TG-43 and Acuros TG-186. PTV $D_{98\%}$, $D_{90\%}$ and $V_{100\%}$, and OAR $D_{0.1\ cc}$, D_{2cc} and $V_{50\%}$ dose metrics were evaluated, and their fit assessed by air-gap volume measurements.
Results Both surface applicators were printed with minimal defects and visually fitted well. Measured air-gap volume between the photogrammetry applicator and phantom surface was 44% larger than the CT-designed applicator, with a median air gap thickness of 3.24 and 2.88 mm, respectively. The largest difference in PTV and OAR observed was the PTV $V_{100\%}$ of − 1.27% using Acuros and skin $D_{0.1\ cc}$ of -1.38% using TG-43. PTV D_{98} and D_{90} and OAR D_{2cc} and V_{50} for the photogrammetry based plan were all within 0.5% of the CT based plan. No statistically significant difference between the TG-43 and Acuros dosimetric plans were observed as all dose metrics were within 1.1% of each other.
Conclusions 3D printed surface applicator for the nose was successfully constructed using photogrammetry techniques. Although it produced poorer conformity, its dosimetric plan was almost identical to the CT-designed applicator, showing its potential for future surface applicator construction.

O069 Failure modes and effects analysis guided commissioning and implementation of skin brachytherapy using Freiburg flap and 3D printed applicators

Kurt Byrnes[1], Francis Gibbons[1], Melissa Neal[1]

[1]Sunshine Coast University Hospital, QLD, Australia.
Kurt.byrnes@health.qld.gov.au (Presenting author); Francis.gibbons@health.qld.gov.au; Melissa.neal@health.qld.gov.au

Introduction An existing skin brachytherapy service using Valencia applicators with an Ir192 source was expanded to include larger superficial regions. As departmental staff had limited experience with brachytherapy, a thorough failure modes and effects analysis (FMEA) as described in the AAPM TG100 report was conducted. The commissioning and implementation based on this FMEA was performed. This included PSQA measurements for each patient's mould and in-vivo measurements using film. Applicators covering a surface up to 30 cm in length were created to hold up to 40 catheters. Both Freiburg Flap and 3D printed applicators were included in the commissioning.
Method The commissioning focussed on the following:

1. Catheter delineation and length measurement.
    - Comparison of different dwell spacings.
    - Positional accuracy of dwell positions in complex plans.
    - Ion chamber point dose and Gafchromic film profile measurements in solid water.
    - Ion chamber point dose and Gafchromic film profile measurements in anthropomorphic phantoms with artificial and actual patient plans.
    - 3D print material verification.
    - Patient and applicator setup using checklists.
    - Typical brachytherapy commissioning tests including end-to-end, TPS and source strength.

Fig. 17 Scalp treatment simulated using Steev phantom. Point dose measurement taken using PTW PinPoint chamber

Results Measurements showed a maximum dose difference of 1.4% between dwell spacing of 1 mm, 2 mm and 3 mm. Film measurements taken for PSQA and In-vivo measurements were qualitatively compared to predicted doses from the Oncentra TPS.

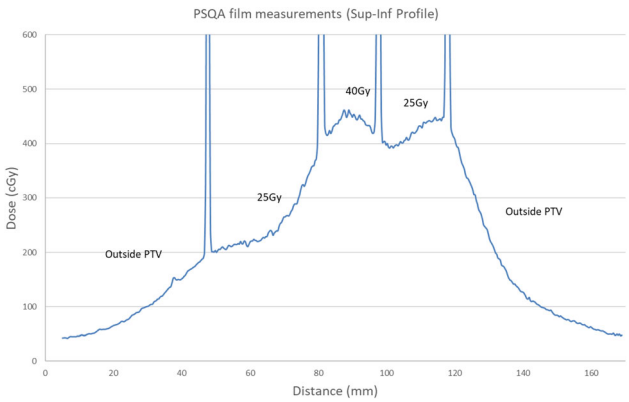

Fig. 18 Profile taken from film measurement used for PSQA for an actual patient plan. The 25 Gy and 40 Gy labels represent the prescribed dose in that region
Conclusion Although a thorough FMEA analysis was conducted using TG100, implementing the ideal processes for the simulation, planning and mould production was unsuccessful. These would have

deviated significantly from the processes used by the Radiation Therapists for EBRT. Through the commissioning tests, PSQA and in-vivo measurements the accuracy of individual dwells and total plans was found to be accurately delivered by the Flexitron afterloader. Involving all staff from the multidisciplinary team in PSQA and in-vivo measurements resulted in a high level of confidence in the safety and efficacy of the treatments. The use of checklists during patient setup were especially useful in maintaining confidence amongst inexperienced staff.

References/Acknowledgements

Frances Su, F.-C., & al, e. (2020). FMEA-guided transition from microSelection to Flexitron for HDR brachytherapy. American Brachytehrapy Society, 241–248.

Sayler, E., & al, e. (2015). Clinical implementation and failure mode and effects analysis of HDR skin brachytherapy using Valencia and Leipzig surface applicators. American Brachytherapy Society, 293–299.

O070 Impact of bladder filling protocols on bladder volume in HDR Cervix Brachytherapy

Guneet Kaur[1], Sharon Oultram[2], Claire Dempsey[3]

[1]Medical Physics Registrar, Calvary Mater Newcastle, NSW. Guneet.Kaur@calvarymater.org.au; [2]Senior Radiation Therapist Educator, Calvary Mater Newcastle, NSW. Sharon.Oultram@calvarymater.org.au; [3]Senior Medical Physicist, Calvary Mater Newcastle, NSW. Claire.Dempsey@calvarymater.org.au

Introduction High dose rate (HDR) brachytherapy is commonly used for management of cervical cancer with traditional organ-at-risk structures including the bladder and rectum. Currently, there are no consensus recommendations regarding bladder filling protocols for cervix brachytherapy [1]. The objective of this preliminary study is to investigate the impact of targeted bladder filling on both the overall bladder volume and inter-fraction bladder volume stability.

Method Cervix brachytherapy patients at the Calvary Mater Newcastle underwent two MRI imaging sequences, one with the patient having a free-draining, in-dwelling catheter and another with the bladder filled with sterile water in order to achieve a bladder volume close to 100 cm^3. A set of 13 patients with free draining and "filled" volume MRI datasets were analysed in this study. Contoured bladder volumes for each patient were used to investigate the consistency of bladder filling and the residual, free-draining volume both between individual patients and inter-fraction for each patient.

Results In almost all cases, the volume of saline placed in the bladder was more than required with a mean (range) filled bladder volume of 121.8 (84.3 – 188.5) mL. The mean (range) residual, free-draining volume across all patients was 64.1 (22.7 -118.3) mL. The reproducibility of both the residual and filled bladder volume for individual patient inter-fraction showed no significant trend with fraction to fraction variations of up to 60 mL (residual) and 72 mL (filled).

Conclusion Variation in residual bladder volume from patient-to-patient and fraction-to-fraction results in difficulties for bladder filling protocols to produce consistent bladder volumes for cervix brachytherapy patients at the time of treatment planning and further differences may also occur at the time of brachytherapy treatment. Evaluation of the dosimetric impact of changes to bladder filling on the bladder, and more specifically the bladder wall, is now required to determine the optimum workflow in the clinic.

Reference

1. Mahantshetty, U., Shetty, S., Majumdar, D., Adurkar, P., Swamidas, J., Engineer, R., & Chopra, S. (2017). Optimal bladder filling during high-dose-rate intracavitary brachytherapy for cervical cancer: a dosimetric study. *Journal of Contemporary Brachytherapy*

O071 pyTG43: An Open Source Brachytherapy Dose Verification Tool

A. G. Livingstone[1], S. Peet[1]

[1]Cancer Care Services, Royal Brisbane and Women's Hospital, Brisbane. alexander.livingstone@health.qld.gov.au (Presenting author); samuel.peet@health.qld.gov.au

Introduction Verification of doses calculated by treatment planning systems is an important step in treatment planning process for both external beam and brachytherapy treatments. There are several commercial software solutions available for 3D brachytherapy verification, most being either cumbersome to use or only providing point dose verification. pyTG43 is an open source, Python-based software package capable of full 3D dose verification of brachytherapy treatment plans.

Method Patient plan, dose, and structure set files are exported in DICOM format from the TPS and submitted through a GUI to pyTG43. Source dwell times and positions are extracted, along with the applicator structures. Source orientation at each dwell position is then calculated, allowing the angles and distances required by the TG-43 formalism to be easily determined, while also accounting for rotated datasets. ESTRO-supplied source specification data is then used for a TG-43 calculation at several points distributed throughout the structures supplied in the treatment plan. The software presents results in the form of a dose point comparison (if they are present in the treatment plan), as well as a dose-volume histogram.

Results The software has been routinely used as part of the planning process within the department for HDR/PDR gynaecological and HDR prostate patients. Calculations are typically completed within 10 to 15 s for gynaecological plans, with prostate plans taking on the order of 30 s due to the increased number of dwell positions. Comparisons have shown excellent agreement with the Varian BrachyVision planning system, with point dose difference being generally $< 0.2\%$, and DVH metric differences of $< 1\%$. PDF reports can be generated for record keeping.

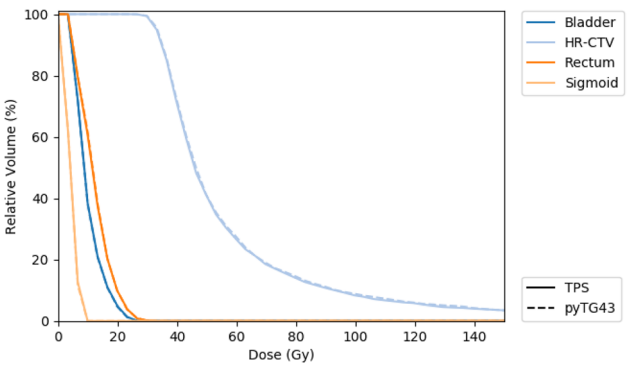

Fig. 19 DVH comparison for a PDR gynaecological plan

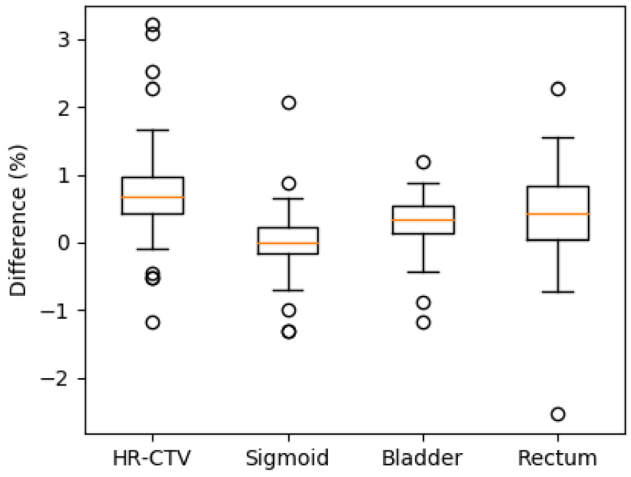

Fig. 20 Distribution of differences in D50 for various structures in 65 PDR gynaecological plans

Conclusion A Python-based dose verification tool for brachytherapy treatments using the TG-43 formalism has successfully been designed and implemented as part of the planning process at the RBWH, showing good agreement. The software is open source and available at http://github.com/livingag/pyTG43.

O072 Pixel-based Analysis of Urethra Dose Surface Maps for patients Treated with HDR Brachytherapy Boost

S. M. K. Author[1], V Panettieri[2,3], J. Crosbie[1], T. H. Qi[4], J. L. Millar[2,5]

[1]School of Science, RMIT University, Melbourne, Victoria 3001, Australia. snehamkuriyakose@gmail.com (Presenting author); [2]Alfred Health Radiation Oncology, Melbourne, Australia; [3]Medical Imaging and Radiation Sciences, Monash University, Clayton, Australia; [4]Department of Radiation Therapy, National Cancer Centre, Singapore; [5]Central Clinical School, Monash University, Melbourne, Australia

Introduction Urinary toxicity after radiation therapy for prostate cancer can reduce a patient's quality-of-life. Previous work correlated risk of urethral strictures and dose delivered during the treatment however, guidelines are not clear for this organ due to the variety of fractionation regimens and contouring methods used [1–4]. This project aimed at investigating the relationship between the spatial distribution to the urethra during High Dose Rate brachytherapy (HDRB) boost and the probability of urethral toxicity, using Dose-Surface-Maps (DSM).

Methods We retrospectively analysed clinical and dosimetric data from 206 patients who underwent HDRB boost at a single institution. Patients were treated with 18 Gy in 3, 19 Gy in 2, or 17 Gy in 2 fractions (between 2010–2013), and had urethral toxicity rate of 13.8%. Due to its tubular nature urethral DSM were constructed by sampling points at a fixed radius of 3 mm from the interpolated centroid of the urethral contour, and then unfolding along the posterior axis (MATLAB versionR2020a). Doses in each pixel were converted to Biological-Effective-Dose (BED) using $\alpha/\beta = 5$ Gy. Patients with urethra contours less than 55 mm in length were excluded. DSMs were compared between patients with and without toxicity, average doses calculated and difference in spatial patterns analysed with Wilcoxon-rank sum test ($p < 0.05$).

Results Average DSMs showed patterns of higher dose distribution closer to the apex of the prostate regardless of whether toxicity occurred (Fig. 1a, b). The toxicity group received higher doses with a maximum dose variation between apex and base of 57 Gy (BED). In the pixel-wise difference DSM (Fig. 1c), the patterns between 25 and 35 mm were statistically significantly correlated to urethral toxicity (p value < 0.05) (Fig. 1d).

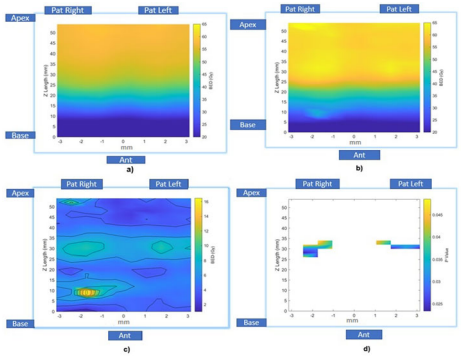

Figure1: (a) Average Dose Surface maps of 143 patients without urinary toxicity; (b) Average Dose Surface maps of 23 patients with urinary toxicity; (c) Mean difference in BED between patients with and without toxicity; (d) DSM with p value <0.05 for Wilcoxon rank sum test. The 0mm on the vertical, length axis represents the base of the prostate and the 55mm represents the apex and on the horizontal axis 0 mm corresponds to the anterior and the 3mm and -3mm corresponds to the posterior.

Conclusion The risk of urethral stricture is correlated to the dose received and could also be dependent on the area of the urethra irradiated. These results provide an improved understanding on local dose effects for the treatment of prostate cancer with brachytherapy.

References

1. Awad, MA, Gaither, TW, Osterberg, EC, Murphy, GP, Baradaran, N & Breyer, BN *'Prostate cancer radiation and urethral strictures: a systematic review and meta-analysis'*, Prostate Cancer Prostatic Dis. (2018) 21(2):168–174. https://doi.org/10.1038/s41391-017-0028-3
2. Sullivan, L, Williams, SG, Tai, KH, Foroudi, F, Cleeve, L & Duchesne, GM, *'Urethral stricture following high dose rate brachytherapy for prostate cancer'*, Radiother Oncol. (2009) 91(2):232–236. https://doi.org/10.1016/j.radonc.2008.11.013
3. Hindson BR, Millar JL, Matheson B. '*Urethral strictures following high-dose rate brachytherapy for prostate cancer: analysis of risk factors*.' Brachytherapy. (2013) 12:50–5. https://doi.org/10.1016/j.brachy.2012.03.004
4. Panettieri, V, Rancati, Onjukka, E, Ebert, M A, Joseph, DJ, Denham, J W, Steigler, A and M, Jeremy L. *'External Validation of a Predictive Model of Urethral Strictures for Prostate Patients Treated with HDR Brachytherapy Boost.'* Front in Oncol. (2020) 10:901 https://doi.org/10.3389/fonc.2020.00910

O073 Catheter generation using pathfinding algorithms for 3D-printed gynaecological brachytherapy moulds

S. M. Pleschka[1], R. Wilks[1,2,3], S. B. Crowe[1,2,3,4]

[1]Cancer Care Services, Royal Brisbane and Women's Hospital, Brisbane, Queensland, Australia. shaun.pleschka@health.qld.gov.au; [2]Herston Biofabrication Institute, Metro North Hospital and Health Service, Brisbane, Queensland, Australia; [3]School of Information Technology and Electrical Engineering, University of Queensland, Brisbane, Qld, Australia. rachael.wilks@health.qld.gov.au; [4]School

of Chemistry and Physics, Queensland University of Technology, Brisbane, Queensland, Australia. sb.crowe@gmail.com

Introduction Advancements in the 3D printing of bio-compatible materials has allowed the production of patient specific moulds with catheter channels optimised for improved DVH metrics. Unfortunately, the manual definition of a set of collision free, curvature constrained and DVH-optimised catheters using a treatment planning system may require hours of tedious planning. Pathfinding algorithms have been studied in a variety of disciplines, most notably robot motion planning with non-holonomic constraints, similar to the constraints associated with brachytherapy catheter generation. In particular, a highly customisable random sampling algorithm Rapidly-exploring Random Trees (RRT) has been modified and tested but never clinically implemented.
Method A customised RRT algorithm was implemented using the Python programming language. A CT-derived patient mould structure is imported at initialisation using pydicom. Random sampling bias was introduced to the RRT in the catheter exit zone to accelerate solution convergence. Cubic order Bezier curves were used instead of straight lines, as this was the simplest mathematical form a curve can take while allowing control over the required real world properties of the catheter such as continuity between generated segments, minimum radius of curvature and total torsion in the system. RRT algorithm parameters needed to be determined on a mould-specific basis, for example, based on mould length and width, for reliable high-quality solutions. The software produces a text file with the catheter locations and updates associated DICOM files.
Results All solutions meet or exceed the expected number of catheters of a manually planed treatment while satisfying 3D printing and catheter restrictions. The software has solution times under 15 min for 10 or less catheters.
Conclusion The software successfully addresses the planner's requirements and saves on time and resources during both the planning phase and the 3D-printing phase, by reducing the number of reprints required for successful catheter geometry.
Acknowledgements Rachael Wilk's contribution to this work was supported by a RBWH and RBWH Foundation Post Graduate Scholarship. Alexander Livingstone provided advice on the project

O074 Quantifying the isocentre accuracy of an Elekta Unity MR-linac through full gantry rotation

J. R. Hunt[1], P. Rowshafarzad[1], M. A. Ebert[2], H. L. Riis[3]

[1]School of Physics, Mathematics and Computing, The University of Western Australia, Crawley, WA 6009, Australia. Jamespb1@hotmail.com (Presenting author); Pejman.rowshanfarzad@uwa.edu.au; [2]Department of Radiation Oncology, Sir Charles Gairdner Hospital, Nedlands, WA 6009, Australia. Martin.Eber@health.wa.gov.au; [3]Radiofysisk Laboratorium, Odense University Hospital, Department of Oncology, Odense, Denmark. Hans.Lynggaard.Riis@rsyd.dk

Introduction Image-guided radiotherapy (IGRT) has shown continuous improvement in its capacity to treat target volumes whilst sparing organs at risk (OAR), due in part to the increased accuracy of linear accelerators (linacs). Recently, novel linacs are being developed with built-in magnetic resonance imagers, referred to as MRL. MRL offers great benefits for enhanced accuracy, but the capabilities of this new technology require testing. The primary aim of this project is to quantify the accuracy of Elekta's Unity MRL throughout gantry rotation.
Method A ball-bearing (BB) phantom is attached to the radiation head of the Unity, while a singular BB is placed at isocentre. Images are taken throughout rotation, using the MV imaging panel (MVIC). These images are enhanced using a robust Matlab program to reduce errors due to noise, and the positions of the BBs in the images are analysed to extract MVIC and radiation head sag data.
Results The robust Matlab program returned precise results with a mean standard deviation of 7 μm. The Unity radiation head was found to sag throughout rotation, resulting in a maximum course of movement of 0.59 mm. The sag pattern was time invariant over a period greater than one year but showed some dependence on gantry rotation direction.

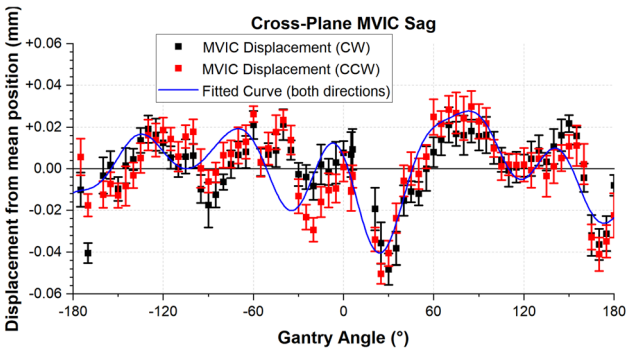

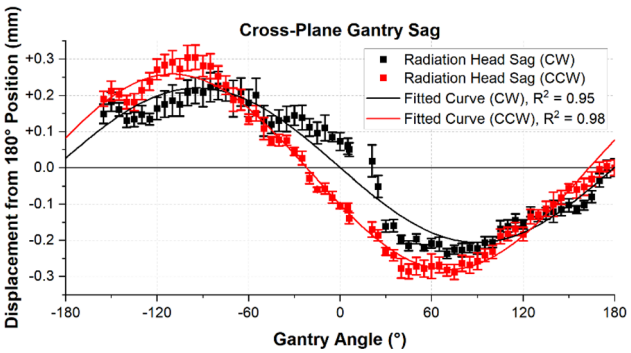

Conclusion While statistically significant, the course of movement found for the Unity was noticeably less than the courses of movement of conventional linacs found in the literature, demonstrating the precision of this MRL. The Matlab program was effective in minimising the effect of noise. Results were highly repeatable, presenting opportunities for further research in compensating for radiation head motion to increase MRL accuracy further.

O075 Setting up the periodic QA for the Elekta Unity MR linac using AQUA

U. Jelen[1], K. Condon[1], Z. Moutrie[1], M. G. Jameson[1]

[1]GenesisCare, The Mill, 41–43 Bourke Road, Alexandria, NSW, Australia. Urszula.Jelen@genesiscare.com (Presenting author); Kieran.Condon@genesiscare.com; Zoe.Moutrie@genesiscare.com; Michael.Jameson@genesiscare.com

Introduction AQUA (Elekta, Crawley, UK) is a web-based QA management tool designed to communicate with treatment delivery, imaging and simulation equipment, as well as QA measurement devices. The aim of this work is to report on our experience in

establishing and the first 12 months of use of a monthly QA program for MR Linac entirely encompassed by AQUA.

Method A set of vendor provided tests has been selected to encompass relevant aspects of regular QA: MR image quality, MV image quality, MR and MV isocentre congruence, Winston-Lutz test, panel based beam output and symmetry measurement, MLC performance and gantry angle mechanical stability. Additionally, tests to store dosimetric measurement results (ion chamber output and energy measurements and IC profiler beam shape measurements) have been developed in-house.

Results For nearly all tests, the baselines have been successfully set up prior to the commencement of clinical operation. For Winston-Lutz test, a new version was released at later date and the test has been re-validated and the baseline setting for the image-based Output and Symmetry test had required additional clarifications with the vendor which delayed its roll-out. Next, the work instructions were validated and tests have been executed by various staff members over 12 months.

Conclusion The use of AQUA provided (1) an efficient platform to harmonize, version control and access the procedure instructions, (2) enabled centralized result storage, easy way to view and interpret data trends and (3) increased productivity through automatization of certain image-based tests.

O076 Practical methods for reducing-, evaluating- and measuring electron streaming during treatment in a 1.5T magnetic field

Z. Moutrie[1], Urszula Jelen[1], Louise Hogan[1], J. de Leon[1], Stacy Alvares[1], David Crawford[1], C. Pagulayan[1], Nicolle Dunkerley[1], Conrad Loo[1], M. G. Jameson[1]

GenesisCare, St Vincent's Clinic, Darlinghurst, NSW.
Zoe.Moutrie@genesiscare.com (presenting author);
Urszula.jelen@genesiscare.com; lousie.hogan@genesiscare.com;
Jeremy.DeLeon@genesiscare.com; stacy.alvares@genesiscare.com;
david.crawford@genesiscare.com;
claire.pagulayan@genesiscare.com;
nicolle.dunkerly@genesiscare.com; conrad.loo@genesiscare.com;
Michael.Jameson@genesiscare.com

Introduction For MV photon radiation treatments in the presence of strong magnetic field, secondary electrons can experience the Lorentz force and spiral in the direction of the magnetic field away from the treatment area, this unwanted dose[1–4] should be minimised. Using the Elekta Unity MR linac workflow, each fraction the treatment plan changes. Limited patient immobilisation and set-up aids mean the absolute positioning of the patient within the treatment field can be less reproducible when compared with conventional radiotherapy. We developed robust solutions for predicting electron streaming, minimising the errant doses and evaluating the effectiveness via in-vivo dosimetry.

Method Custom thermoplastic bolus and non-patient specific jelly bolus were both evaluated for their effectiveness in absorbing electrons as well as their adaptability for each fraction. A beam model with no magnetic field (B = 0 model) was used to evaluate the required location and thickness of bolus material. Patients were CT scanned with bolus in situ, treatment plans were created using our clinical machine model and recalculated with the B = 0 model. EBT film placed at key locations under MR-visible markers was used to evaluate the TP predicted dosimetry.

Results A comparison of the clinical model with the B = 0 model predicted $\sim$ 2 Gy on the bolus and 0.05 Gy beneath the bolus, which was verified using in-vivo dosimetry placed under MR markers. Thermopalstic bolus and jelly bolus could not be visualised on MRI but did effectively minimize the dose. Additionally, the thermoplastic bolus could be used to aid the patient's chin position while jelly bolus was to be able to be adapted to any patient.

Conclusion Using the B = 0 machine model is an effective tool to predict electron streaming. Thermoplastic bolus and jelly bolus can be used with minimal interruption to the patient workflow to reduce electron streaming and this dose can be confirmed with in-vivo dosimetry using film.

Acknowledgements The authors wish to acknowledge Jason Arts and Elekta's support in providing a B = 0 field machine model for our clinic. The authors would like to thank the Townsville Physics team in providing technical advice on their experience with ESE.

References

1. Oborn B, Butson M, Metcalfe P, Rosenfeld A (2010) MRI Linear accelerators: impact of the electron return effect
2. Liu H, Ding S, Wang B, et al. (2020) In-air electron streaming effect for esophageal cancer radiotherapy with a 1.5 T perpendicular magnetic field: a treatment planning study. Frontiers in Oncology 10:
3. Malkov VN, Hackett SL, Wolthaus JW, et al. (2019) Monte Carlo simulations of out-of-field surface doses due to the electron streaming effect in orthogonal magnetic fields. Physics in Medicine & Biology 64:115,029
4. Nachbar M, Mönnich D, Boeke S, et al. (2020) Partial breast irradiation with the 1.5 T MR-Linac: First patient treatment and analysis of electron return and stream effects. Radiotherapy and Oncology 145:30–35

O077 Commissioning Liver Stereotactic Body Radiotherapy on the Elekta Unity MR-Linac

C. Pagulayan[1], Z Moutrie[1], S Alvares[1], J de Leon[1], M. G. Jameson[2]

GenesisCare, St Vincent's Clinic, Darlinghurst, NSW.
claire.pagulayan@genesiscare.com (presenting author);
Zoe.Moutrie@genesiscare.com; Stacy.Alvares@usa.genesiscare.com;
Jeremy.DeLeon@genesiscare.com; [2]GenesisCare, The Mill, 41–43 Bourke Road, Alexandria, NSW, Australia.
Michael.Jameson@genesiscare.com

Introduction There is emerging evidence for the efficacy and safety of liver SBRT in the treatment of malignant liver tumours[1]. However, liver tumours are prone to motion and difficult to visualise on standard X-Ray imaging. MR-Linacs enable better visualisation of liver tumours during treatment. This project aimed to commission free-breathing liver SBRT treatments on the Elekta MR-Linac (Elekta, Crawley, UK) at St Vincent's GenesisCare.

Method A diaphragm measurement is made on a cine MR scan (btFFE) to determine the magnitude of the patient's breathing amplitude. This is verified at each treatment session to ensure the internal target volume (ITV) is accurate. The CIRS MRgRT Motion Management phantom (CIRS Inc., VA, USA) was used to verify this. An amplitude of 15 mm was sent to the phantom and an MR scan acquired. Additionally, ten IMRT plans were created. The ArcCheck-MR (Sun Nuclear, FL, USA) and PTW SemiFlex (PTW, Freiburg, Germany) ionisation chamber (IC) in the ArcCheck-MR multiplug were used to measure the plans on the Elekta QA platform. The ArcCheck-MR plans were analysed with global gamma criterion of 3%/2 mm $\geq$ 95% and ion chamber $\leq$ 3% difference to the planned dose point.

Results The measurement tool gave an average result of (14.8 ± 0.3)mm. This accuracy was found to be acceptable. Nine plans passed with ArcCheck-MR and mean gamma pass rate of (98.7 ± 1.4)%. One yielded a fail result of 87%. This case required further measurements with the ArcCheck-MR placed directly on the couch with a lateral offset such that the SemiFlex aligned with the PTV, this yielded a pass result from the IC with -0.3% difference. This result is likely due to the ArcCheck-MR angular correction. Two off-axis SemiFlex measurements yielded pass-action results caused by set-up uncertainty of the ArcCheck-MR.

Conclusion Liver SBRT was successfully commissioned on the MR-Linac at St Vincent's GenesisCare.

Reference

1. Ohri N, Tomé WA, Romero AM, Miften M, Ten Haken RK, Dawson LA, Grimm J, Yorke E, Jackson A. Local control after stereotactic body radiation therapy for liver tumors. International Journal of Radiation Oncology* Biology* Physics. 2018 Jan 6.

O078 One pot synthesis of PEGylated bimetallic gold—silver nanoparticles for imaging and radiosensitization of oral cancers

Shameer Ahmed B[1], PhD Scholar, Dr Gunjan Baijal[2], MD, Radiation Oncologist Consultant, Prof Rudrappa Somashekar[3], PhD, Retired Professor, Prof Subramania Iyer[4], MS, MCh, HoD, Professor, Prof Vijayashree Nayak[1], PhD, Professor

[1]Department of Biological Sciences, Birla institute of Technology and Science, Pilani, K.K. Birla Goa Campus NH 17B, Bypass Road, Zuarinagar, Sancoale, Goa 403,726, India. p20170006@goa.bits-pilani.ac.in (Presenting author). [2]Department of Radiation Oncology, Manipal Hospital Goa, Panaji, Dr E Borges Rd, Dona Paula, Goa 403,004, India. gunjanbaijal.dr@gmail.com; [3]Centre for Materials Science and Technology, Vijnana Bhavan, University of Mysore, Mysore-570006, India. rs@physics.uni-mysore.ac.in; [4]Department of Head and Neck Oncology, Amrita Institute of Medical Sciences, Cochin -682 041, India. subu.amrita@gmail.com; vijayashree@goa.bits-pilani.ac.in

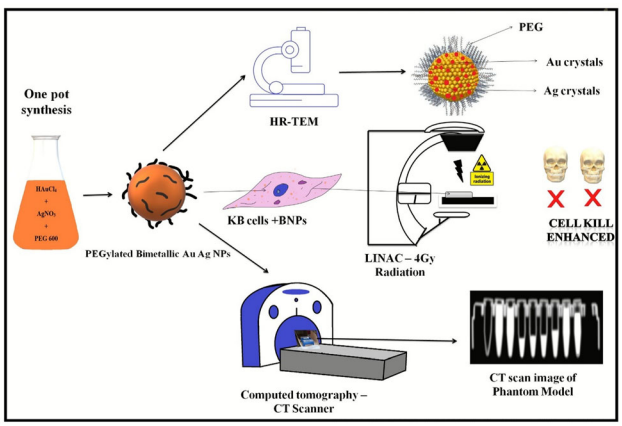

Introduction Radiotherapy a mainstay treatment for many types of head and neck squamous cell carcinomas. Nanomaterials comprised of high atomic number (Z) elements are novel radiosensitizers, enhance radiation injury by production of free radicals and subsequent DNA damage. Gold nanoparticles have emerged as promising radiosensitizers due to their high (Z), biocompatibility, and ease for surface engineering. Bimetallic nanoparticles have shown enhanced anticancer activity compared to monometallic.

Method PEG coated Au–Ag alloy nanoparticles (BNPs) were synthesized using facile one pot synthesis techniques. Size of ~ 50 ± 5 nm measured by dynamic light scattering. Morphology, structural composition and elemental mapping was analyzed by Electron Microscopy and SAXS (Small-Angle X-ray Scattering). The radiosensitization effects on KB oral cancer cells were evaluated by irradiation with 6MV X-rays on linear accelerator. Nuclear damage was imaged using confocal microscopy staining cells with Hoechst stain. Computed Tomography (CT) contrast enhancement of BNPs was compared to that of the clinically used agent Omnipaque.

Results BNPs were synthesized using PEG 600 as reducing and stabilizing agent. The surface charge of well dispersed colloidal BNPs solution was -5 mV. Electron microscopy reveals spherical morphology. HAADF-STEM and elemental mapping studies showed that the constituent metals were Au and Ag intermixed nanoalloy. Hydrodynamic diameter was ~ 50 ± 5 nm due to PEG layer and water molecules absorption. SAXS measurement confirmed BNPs size around 35 nm. Raman shift of around 20 cm^{-1} was observed when BNPs were coated with PEG. ^{1}H NMR showed extended involvement of ^{-}OH in synthesis. BNPs efficiently enter cytoplasm of KB cells and demonstrated potent in vitro radiosensitization with enhancement ratio ~ 1.5–1.7. Imaging Hoechst-stained nuclei demonstrated apoptosis in dose-dependent manner. BNPs exhibit better CT contrast enhancement ability compared to Omnipaque.

Conclusion This bimetallic intermix nanoparticles could serve a dual function as radiosensitizer and CT contrast agent against oral cancers, and by extension possibly other cancers as well.

Acknowledgements This work will be incorporated in thesis for PhD degree in Gold based Radiation Sensitizers and Drug delivery system. The study was financially supported by 'The Goa Cancer Society', project grant No (Ref.No.2/Research/GCS/2019–20). Also, one of the authors Shameer Ahmed B would like extent his gratitude to BITS Pilani KK Birla Goa Campus, Goa for Institute fellowship to do his PhD tenure. All the authors would like to thank University of Mysore for DLS and Raman Spectroscopy, IIT (Indian Institutes of Technology) Delhi for ICPMS, Centre for Nano Science and Engineering (CeNSE)- IISc (Indian Institute of Science), Bangalore for HRTEM, HAADF-STEM, EDX. Manipal Hospital, Goa for LINAC Irradiation and CT Scanning facilities. Prof. Vinod K. Aswal, Solid State Physics Division, Bhabha Atomic Research Centre, Trombay, Mumbai for the design, measurements and analyzed SAXS and SANS. Lastly, we thank Dr. Varsha. K. Pavithran, Rajah Muthiah Dental College and Hospital, Annamalai University, for assisting in statistical analysis of this research article.

References

1. Ahmed, S., Rao, A. G., Sankarshan, B. M., Vicas, C. S., Namratha, K., Umesh, T. K., … & Byrappa, K. (2016). Evaluation of Gold, Silver and Silver–Gold (bimetallic) nanoparticles as radiosensitizers for radiation therapy in cancer treatment. *Cancer Oncol. Res*, *4*, 42–51.
2. Teraoka, S., Kakei, Y., Akashi, M., Iwata, E., Hasegawa, T., Miyawaki, D., … & Komori, T. (2018). Gold nanoparticles enhance X-ray irradiation-induced apoptosis in head and neck squamous cell carcinoma in vitro. *Biomedical reports*, *9*(5), 415–420.
3. Mishra, S. K., & Kannan, S. (2017). Doxorubicin-conjugated bimetallic silver–gadolinium nanoalloy for multimodal MRI-CT-optical imaging and pH-responsive drug release. *ACS Biomaterials Science & Engineering*, *3*(12), 3607–3619.
4. Eriksson, D., & Stigbrand, T. (2010). Radiation-induced cell death mechanisms. *Tumor Biology*, *31*(4), 363–372.

O079 Incidence of Radiation Induced Epilation in Neurointerventional Procedures

D. A. Carrick[1]

[1]Biomedical Technology Services, Gold Coast University Hospital. deborah.carrick@health.qld.gov.au (presenting author)

Introduction The growth of fluoroscopically guided interventions (FGI) in recent years and subsequent reports of epilation and skin injuries, has raised awareness of the risk of tissue reactions in such procedures, necessitating estimation of skin dose and potential patient follow up for doses that exceed tissue reaction thresholds.
Method Gold Coast University Hospital (GCUH) is a major centre for neurointerventional procedures with over 100 procedures to treat cerebral aneurysms (embolisation, coiling, stenting) per year. Peak skin doses (PSD) are calculated when the reference air kerma (RAK) exceeds 3 Gy, and the calculations incorporate backscatter, table motion and tube rotation. A more robust patient follow-up procedure was introduced GCUH in 2020, with greater compliance in recording any skin effects.
Results ICRP states a threshold of 3 Gy for temporary epilation, with threshold dose defined as the dose resulting in 1% incidence of specified tissue reactions[1]. From 2020 to present (18 months), there have been 102 neurointerventional patients with RAK $>$ 3 Gy, and 43 with a calculated PSD $>$ 3 Gy. 9 patients were not followed up (deceased or unable to be contacted), and of the remaining 34 patients, there was a 50% incidence of temporary epilation at approximately 2–4 weeks post procedure. The median (max) PSD for patients with and without epilation, were 3.6 Gy (7.0 Gy) and 3.8 Gy (11.1 Gy) respectively.
Conclusion Results agree with published data that the scalp has high radiosensitivity to epilation and low radiosensitivity to skin damage[2]. Typically, dose thresholds for FGI are based more widely available published data from cardiac catheter laboratories and therefore do not consider variations in radiosensitivity of different skin regions. These results help provide more targeted information to patients undergoing neurointerventional procedures, to adequately explain the risks, and avoid potential distress due to epilation some weeks after the procedure.
References

1. ICRP, 2012. ICRP Statement on Tissue Reactions / Early and Late Effects of Radiation in Normal Tissues and Organs – Threshold Doses for Tissue Reactions in a Radiation Protection Context. ICRP Publication 118. Ann. ICRP 41(1/2)
2. Geleijns J et al. X-ray imaging and the skin: radiation biology, patient dosimetry and observed effects. Radiation Protection Dosimetry. 2005 114(1–3):121–125

O080 Fractionated radiotherapy and its effect on the tumour microenvironment: a small animal study

R. A. D'Alonzo[1,2,3], S. Keam[2,3,4], K. M. MacKinnon[1], A. M. Cook[2,3,5], A. Nowak[1,2,3], S. Gill[1,6], P Rowshanfarzad[1], M. A. Ebert[1,6,7]

[1]School of Physics, Mathematics and Computing, University of Western Australia, Australia; [2]National Centre for Asbestos Related Diseases, University of Western Australia, Australia; [3]Institute for Respiratory Health, Perth, Western Australia, Australia. rebecca.dalozno@research.uwa.edu.au (Presenting author); [4]Medical School, University of Western Australia, Australia. synat.keam@research.uwa.edu.au; kelly.mackinnon@research.uwa.edu.au; [5]School of Biomedical Sciences, University of Western Australia, Australia. alistair.cook@uwa.edu.au; anna.nowak@uwa.edu.au; [6]Department of Radiation Oncology, Sir Charles Gairdner Hospital, Australia. suki.gill@health.wa.gov.au; School of Physics, Mathematics and Computing, University of Western Australia, Australia. pejman.rowshanfarzad@uwa.edu.au; [7]5D Clinics, Claremont, Australia. martin.ebert@health.wa.gov.au

Introduction Malignant tumours have decreased oxygenation (hypoxia) due to malformed blood vessels. Hypoxia decreases the effectiveness of radiotherapy (RT), and the abnormal vessels prevent both systemic therapies and immune cells from reaching some areas of the tumour. Tumour hypoxia is associated with poorer prognosis. RT can alter the tumour microenvironment (TME), leading to vasculature normalisation and reoxygenation.
Method AB1-HA mesothelioma tumour cells were subcutaneously injected into BALB/cJAusbP mice. Mice with established tumours underwent RT fractionation with an X-RAD 225Cx small animal RT device, a pre-clinical translation of clinical linear accelerators. Starting 10 days post-inoculation, mice received one of the following fractionation schedules: 2 Gy $\times$ 1, 2 Gy $\times$ 2, 2 Gy $\times$ 3, 2 Gy $\times$ 4, 2 Gy $\times$ 5, 6 Gy x or 6 Gy $\times$ 2 fractions. On day 15 mice underwent hybrid optical and Doppler ultrasound imaging with a LAZR-X photoacoustic imaging instrument, to assess the spatial oxygen saturation concentration and the vasculature within the tumour. Imaging continued every second day, until day 29 post-inoculation, when mice were euthanised, and tumours harvested. Harvested tumour were stained for markers of hypoxia (pimonidazole) and vasculature (CD31 and pericytes).
Results Results showed alteration to the TME following different RT fractionation schedules. Imaging showed an increase in oxygen saturation and vascularisation with increasing dose, significantly for 2 Gy $\times$ 4, 2 Gy $\times$ 5 and 6 Gy $\times$ 2 fractions. These results were supported by tissue stains, which showed both an overall absolute increase in vasculature and improved vessel function. Hypoxia was decreased after RT, as shown by pimonidazole staining.
Conclusion RT fractionation can be used to modulate the TME. This has the potential to be exploited to prime the tumour for susceptibility to other treatments, for example immune checkpoint inhibitors.
Acknowledgements This study was supported by grant 1,163,065 from the Cancer Australia Priority-driven Collaborative Cancer Research Scheme.

O081 The silver bullet: using silver doped lanthanum manganite to selectively target deadly brain cancer

A. Khochaiche[1,2], M. Westlake[1,2], A. O'Keefe[1,2], E. Engels[1,2], S. Vogel[1,2], N. Li[1,2], M. Valceski[1,2], K. C. Rule[3], J. Horvat[4], K. Konstantinov[2,5], A. Rosenfeld[1,2], M. Lerch[1,2], S. Corde[1,2,6], M. Tehei[1,2]

[1]Centre for Medical Radiation Physics, University of Wollongong, AUS; [2]Illawarra Health and Medical Research Institute (IHMRI), University of Wollongong, Wollongong, AUS. abassk@uow.edu.au (Presenting author); myolamatt@gmail.com; aokeefe@uow.edu.au; elette@uow.edu.au; svogel@uow.edu.au; nanli4625@gmail.com; michaelv@uow.edu.au; [3]Australian Nuclear Science and Technology Organisation, Sydney, AUS. Kirrily@ansto.gov.au; [4]School of Physics, University of Wollongong, AUS. jhorvat@uow.edu.au; [5]Institute for Superconducting and Electronic Materials (ISEM), University of Wollongong, Wollongong. konstan@uow.edu.au; anatoly@uow.edu.au; mlerch@uow.edu.au; [6]Department

of Radiation Oncology, Prince of Wales Hospital, Sydney, AUS. Stephanie.CordeTehei@health.nsw.gov.au; moeava@uow.edu.au

Introduction Treatment of deadly cancers that are deep-seated within sensitive healthy tissue is limited to adequate targeting strategies. More specifically, brain and central nervous system cancers can be the most aggressive, have higher mortality rates and lower accessibility to chemotherapeutic drugs. This study introduces the first in-depth analysis on high silver doped lanthanum manganite (LAGMO) nanoparticles (NPs) as a brain cancer selective chemotherapeutic and radiation dose enhancer.
Method The magnetic, chemical and biological properties of LAGMO NPs at silver dopant levels of 0–10% were investigated. Free radicals and DNA damages were investigated using fluorescent imaging and flow cytometry. Phenotypic cellular analysis was examined using live cell imaging techniques. Biocompatibility and combinational treatment strategies involved in vitro biological end-point clonogenic assays and a cancer cell selectivity investigation.
Results Biocompatibility studies of LAGMO NPs with cancerous and non-cancerous cells displayed completely cancer cell selective toxic response while non-cancerous cell growth was promoted. The selective toxicity was regulated by the overproduction of free radicals causing DNA double strand breaks within the cell nucleus. Clonogenic assays revealed a significant decrease in long-term survival of cancer cells with NPs and radiation therapy compared to radiation alone.

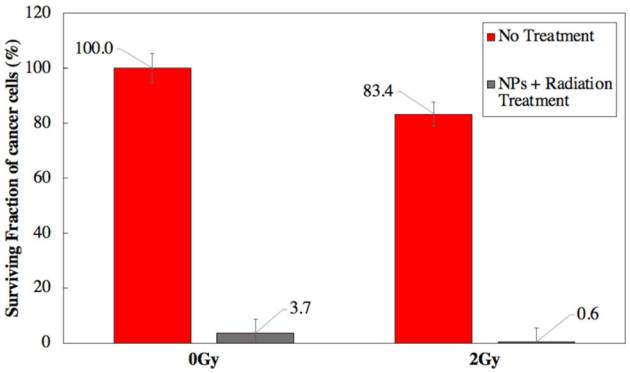

Conclusion LAGMO NPs have potential to significantly improve targeted cancer treatment strategies. Their unique magnetic properties introduce a potential to induce cancer cell hyperthermia alongside radiation treatment and improve clinical outcomes. Furthermore, they have been proven to promote non-cancerous cell growth while severely damaging cancer cells alongside radiation.
Acknowledgements We acknowledge time and access to the Prince of Wales Hospital, the Illawarra Health and Medical Research Institute (IHMRI), Wollongong, Australia, the Australian Centre for Neutron Scattering, and Australian Nuclear Science and Technology Organisation (ANSTO). We acknowledge the financial support of the Australian Government Research Training Program Scholarship, and Australian National Health & Medical Research Council (APP1084994).
References

1. Khochaiche A, Westlake M, O'Keefe A, Engels E, Vogel S, Valceski M, Li N, Rule K C, Horvat J, Konstantinov K, Rosenfeld A, Lerch M, Corde S, Tehei M (2021) First extensive study of silver-doped lanthanum manganite nanoparticles for inducing selective chemotherapy and radio-toxicity enhancement. Mater. Sci. Eng. C. 123:111,970. https://doi.org/10.1016/j.msec.2021.111970.

O082 Improved Therapeutic Ratio for Prostate using Spatially Modulated Radiation Therapy: A Radiation & Metabolomic Study

L. R. Rogers[1,*], B. B. Chen[2,*], K. Liu[2,*], A. Dona[3], D. R. McKenzie[1], A. H. Kwan[2], N. Suchowerska[1]

[1]VectorLAB, Chris O'Brien Lifehouse, Sydney, Australia and School of Physics, University of Sydney, Australia. linda.rogers@lh.org.au (Presenting author); [2]School of Life and Environmental Sciences, University of Sydney, Australia; [3]Sydney Nano Institute, University of Sydney, Australia; David.mckenzie@sydney.edu.au; Ann.kwan@sydney.edu.au; Natalka.suchowerska@lh.org.au; *These authors contributed equally

Introduction Grid and microbeam therapy use spatially modulated fields, where radiation is delivered in high and low dose regions to reduce damage to normal cells, while maintaining cancer toxicity [1]. The mechanisms behind the beneficial effects remain unknown. Here we examine the metabolome of cancer and normal cells with the aim of finding differences despite receiving the same dose.
Method A modulated or uniform field of 6MV photons was used to irradiate a prostate cancer (LNCaP) and a normal prostate (PNT1A) cell line. For the uniform field, the dose was equal to the valley, peak or the mean dose of the modulated field (Fig. 1). A clonogenic assay was performed and the metabolic profiles were examined using Mass Spectrometry and Nuclear Magnetic Resonance. A Principal Component Analysis (PCA) was performed to characterize the metabolite expression.

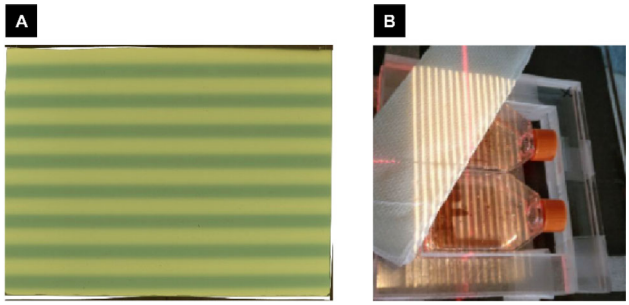

Figure 1: Irradiation set up for the clonogenic and metabolomic study. A photo showing the modulated field overlying two T25cm2 clonogenic study flasks surrounded by Perspex plates (A) and radiochromic film showing the modulated field created with the Varian™ HDmMLC on the Novalis Linear accelerator.

Results For cancer cells, the PCA showed a dose response to irradiation in uniform fields (Fig. 2A). However, the expressed cellular metabolites following modulated field exposure, separated from those of a uniform field exposure of the same total dose, but overlapped with those of a higher uniform dose. For cancer cells, the metabolites separating the metabolic profiles are correlated with stress signaling. For normal cells, the PCA did not reveal a significant separation in response between uniform and modulated irradiation, providing evidence that normal cells are not sensitive to the modulation of the field (Fig. 2B).

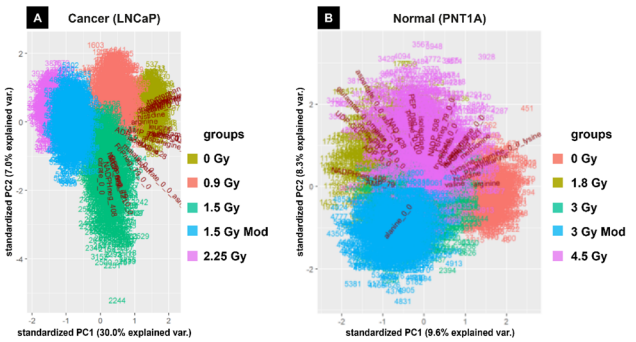

Figure 2: Principal Component Analysis plots for (A) prostate cancer cell line LNCaP and (B) normal prostate cell line PNT1A. In (A) there is a strong dose response relation and the modulated field aligns with the higher uniform dose, which does not occur in (B).

Conclusion We provide new evidence that normal cells appear insensitive to spatially modulated fields. However, cancer cells exposed to spatially modulated fields exhibit a biological response similar to that of uniform higher dose radiation fields, creating an opportunity to increase the therapeutic advantage.

Acknowledgements
We wish to acknowledge Ian & Margaret Bailey for funding this project.

Reference

1. Peng, V., Suchowerska, N., Rogers, L., Claridge Mackonis, E., Oakes, S. and McKenzie, D. Grid therapy using high definition multileaf collimators: realizing benefits of the bystander effect. Acta Oncol, 2017. 56(8): p. 1048–1059.

O083 Oxidative Damage to Mitochondria Enhanced by Ionizing Radiation and Gold Nanoparticles in Cancer Cells

F. Tabatabaie[1], M. Geso[2], B. Feltis[2], K. Quinn[2], R. Franich[1]

[1]School of Sciences, RMIT University, Melbourne, Australia. Farnaz.tabatabaie@rmit.edu.au (Presenting author); [2]School of Health & Biomedical Sciences, RMIT University, Victoria, Australia. Moshi.geso@rmit.edu.au; Bryce.Feltis@rmit.edu.au; Kylie.Quinn@rmit.edu.au; Rick.Franich@rmit.edu.au

Introduction Gold nanoparticles (AuNP) aided radiation-therapy can make tumour cells more sensitive to radiation damage via intracellular dose enhancement (1). In this study, the effects of radiation and AuNPs on mitochondrial reactive oxygen species (ROS) generation in cancer cells was assessed as a potential therapeutic target.

Method MM418-C1 and DU-145 cancer cell lines were irradiated with 6 MV x-rays at doses from 0–8 Gy, with and without AuNPs. Radiobiological damage to mitochondria was quantified via increased ROS activity, using the MitoSOX fluorescent dye, analysed by flow cytometry and Mitochondria stress level test using Seahorse Extracellular Flux (XF) assay.

Results ROS production by mitochondria in MM418-C1 cells was enhanced by the addition of AuNPs, reaching a peak at ~ 4 Gy before decreasing at higher doses (Fig. 1A). AuNPs increased the radiation-induced ROS by 78%. The XF assay showed that the oxygen consumption rate (OCR) peaked at 4 Gy representing a 27% enhancement of radiation-induced stress response. Similar results were seen for both MM418-C1 and DU145 cells.

Conclusion Indicators of mitochondrial stress were quantified using two techniques and were found to be significantly enhanced by the inclusion of AuNPs in both cancer cell lines. Mitochondria are also

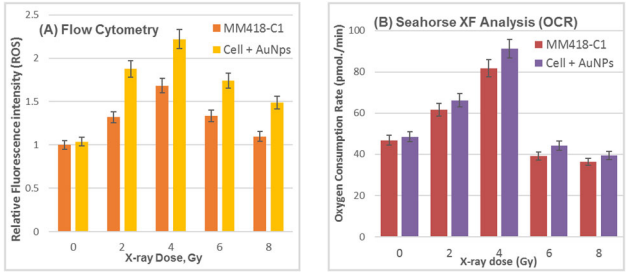

Fig. 1 AuNP enhanced Mitochondrial stress due to irradiation: two assay techniques

pivotal mediators of apoptosis in cells, and therefore they may offer an attractive target for functionally-guided nanoparticles

Acknowledgements We are thankful for the support of Dr Peter Harty, ARPANSA (Australian Radiation Protection and Nuclear Safety Agency) for irradiation assistance.

Reference

1. Kam, W. W. Y., & Banati, R. B. (2013). Effects of ionizing radiation on mitochondria. Free Radical Biology and Medicine, 65, 607–619.

O084 Expert-Augmented Machine Learning

E. D. Gennatas[1,*], J. H. Friedman[2], L. H. Ungar[3], R. Pirracchio[4], E. Eaton[3], L. G. Reichmann[5], Y. Interian[5], J. M. Luna[6], C. B. Simone 2nd[7], A. Auerbach[8], E. Delgado[9], M. J. Van der Laan[10], T. D. Solberg[1], G. Valdes[1]

[1]University of California San Francisco, Department of Radiation Oncology; [2]Stanford University, Department of Statistics; [3]University of Pennsylvania, Department of Computer and Information Science; [4]University of California San Francisco, Department of Anesthesia and Perioperative Care; [5]University of San Francisco, Data Institute; [6]University of Pennsylvania, Department of Radiation Oncology; [7]New York Proton Center, Department of Radiation Oncology; [8]University of California San Francisco, Division of Hospital Medicine; [9]Innova Montreal Inc; [10]University of California Berkeley, Division of Biostatistics

Abstract Machine Learning is proving invaluable across disciplines. However, its success is often limited by the quality and quantity of available data, while its adoption is limited by the level of trust afforded by given models. Human vs. machine performance is commonly compared empirically to decide whether a certain task should be performed by a computer or an expert. In reality, the optimal learning strategy may involve combining the complementary strengths of man and machine. Here we present Expert-Augmented Machine Learning (EAML)[1], an automated method that guides the extraction of expert knowledge and its integration into machine-learned models. Using RuleFit and a large dataset of intensive care patient data to derive 126 decision rules that predict hospital mortality. Using an online platform, we asked fifteen clinicians to assess the relative risk of the subpopulation defined by each rule compared to the total sample. We compared the clinician-assessed risk to the empirical risk and found that while clinicians agreed with the data in most cases, there were notable exceptions were they over- or underestimated the true risk. Studying the rules with greatest disagreement, we identified problems with the training data, including one miscoded variable and one hidden confounder. Filtering the rules based on the extent of disagreement between clinicians and empirical risk, we

improved performance on out-of-sample data and were able to train with less data. EAML provides a platform for automated creation of problem-specific priors which help build robust and dependable machine learning models in critical applications.

Reference

1. Gennatas, E. D. et al. Expert-augmented machine learning. *Proceedings of the National Academy of Sciences* (2020). https://www.pnas.org/content/early/2020/02/14/1906831117

O085 U-net semantic segmentation of carotid anatomy for stroke management: A pilot study

C. Boyd[1,2], G. Brown[1], T. Kleinig[3,4], J. Dawson[5,6], M. D. McDonnell[7], M. Jenkinson[8], E. Bezak[9,10]

[1]Allied Health and Human Performance, University of South Australia, Australia; [2]South Australia Medical Imaging, Adelaide, Australia. chris.boyd2@sa.gov.au (Presenting author); greg.brown2@unisa.edu.au; [3]Department of Neurology, Royal Adelaide Hospital, Adelaide, Australia; [4]Adelaide Medical School, The University of Adelaide, Adelaide, Australia. timothy.kleinig@sa.gov.au; [5]Discipline of Surgery, University of Adelaide, Adelaide, Australia; [6]Department of Vascular & Endovascular Surgery, Royal Adelaide Hospital, Adelaide, Australia. joseph.dawson@adelaide.edu.au; [7]Computational Learning Systems Laboratory, UniSA STEM, University of South Australia, Australia. mark.mcdonnell@unisa.edu.au; [8]Oxford Centre for Functional MRI of the Brain (FMRIB), University of Oxford, Oxford, UK. mark.jenkinson@ndcn.ox.ac.uk; [9]Cancer Research Institute, University of South Australia, Adelaide, Australia;[10]Department of Physics, University of Adelaide, Adelaide, Australia. eva.bezak@unisa.edu.au

Introduction Stroke is a globally leading cause of morbidity and mortality [1], with better management and prevention needed. One potential opportunity is the use of Computed Tomography Angiography (CTA) biomarkers, obtained with machine learning. A common cause of ischemic stroke, carotid atherosclerosis, is quantified using percentage narrowing (stenosis) of the internal carotid artery, to guide medical and surgical intervention [2]. Such measurements currently require medical specialists to hand-contour. This is associated with potential for human error, as well as, limiting large dataset development, impeding machine learning advancement [3].

Method Following ethical approval (HREC/19/CALHN/448), DICOM CTA of 96 carotid vessels equally distributed between four stenosis severities (none, mild, moderate and severe) were downloaded, anonymised and linearly re-sampled from 0.5 to 2.5 mm slice thickness. Fifty millimetres of vessel, centred on the internal carotid origin were hand-segmented by a vascular surgeon and neurologist, each with extensive stroke experience, using 3D Slicer™ [4]. A pre-existing [5] 'U-net' [6] machine learning model was heavily modified using TensorFlow™ 2.1.0 [7], to segment calcified plaque, non-calcified plaque and carotid vessel lumen. Development was performed using "Leave-p-Out" cross-validation ('LpO'), producing multiple models each trained on (96-p) vessels. Following this, the remaining 'p' vessels were segmented by the model to evaluate: accuracy, recall, precision, Dice and F1-score [8].

Results Despite expected performance variability with changes to epoch or optimisation and validation methods, segmentation of carotid anatomy and pathology by machine learning had performance approaching that of experienced medical specialists.

Conclusion 2D machine learning segmentation from CTA appears promising to provide a reproducible and accurate method for segmentation of clinically significant, stroke associate carotid anatomy and pathology, in a practically relevant timeframe.

References

1. World Health Organization. "The top 10 causes of death." World Health Organization,. https://www.who.int/news-room/fact-sheets/detail/the-top-10-causes-of-death (accessed 25/4/2019, 2019).
2. G. G. Ferguson et al., "The North American Symptomatic Carotid Endarterectomy Trial: surgical results in 1415 patients," *Stroke,* vol. 30, no. 9, pp. 1751–8, Sep 1999, https://doi.org/10.1161/01.str.30.9.1751.
3. C. Boyd et al., "Machine Learning Quantitation of Cardiovascular and Cerebrovascular Disease: A Systematic Review of Clinical Applications," *Diagnostics,* vol. 11, no. 3, Mar 19 2021, https://doi.org/10.3390/diagnostics11030551.
4. A. Fedorov et al., "3D Slicer as an image computing platform for the Quantitative Imaging Network," *Magn Reson Imaging,* vol. 30, no. 9, pp. 1323–41, Nov 2012, https://doi.org/10.1016/j.mri.2012.05.001.
5. F. T. Sancinetti, "PTC5750—Computer Tomography Scan segmentation using Convolutional Neural Networks," 2017.
6. O. Ronneberger, P. Fischer, and T. Brox, "U-Net: Convolutional Networks for Biomedical Image Segmentation," *MICCAI 2015. Lecture Notes in Computer Science*, N. Navab, J. Hornegger, W. Wells, and A. Frangi, Eds., 2015.
7. *TensorFlow: Large-scale machine learning on heterogeneous systems*. (2015). tensorflow.org. [Online]. Available: tensorflow.org
8. S. R. Hashemi, S. S. M. Salehi, D. Erdogmus, S. P. Prabhu, S. K. Warfield, and A. Gholipour, "Asymmetric Loss Functions and Deep Densely Connected Networks for Highly Imbalanced Medical Image Segmentation: Application to Multiple Sclerosis Lesion Detection," *IEEE Access,* vol. 7, pp. 721–1735, 2019, https://doi.org/10.1109/ACCESS.2018.2886371.

O086 Physics and Engineering methods for processing micro-CT data

Georgio Andrew Katsifis[1,2], Will Lewin[3], Hedi Kruse[4], David R. McKenzie[1,2], Natalka Suchowerska[1,2]

[1]University of Sydney, School of Physics, Australia; [2]VectorLAB, Chris O'Brien Lifehouse, Australia. gkat2146@uni.sydney.edu.au; [3]VectorLAB, Sarcoma and Surgical Research Centre, Chris O'Brien Lifehouse, Australia. will.lewin@lh.org.au; hedi.kruse@lh.org.au

Introduction The aim of this study is to assess the osseointegration of a 3D printed PEEK-bone implant from an animal trial. A micro-CT provides the spatial resolution required; however, it does not have established processes and protocols to quantify the osseointegration. Here we will describe how to acquire and process the data.

Method A MILABS micro-CT was used to image 3D-printed explants after 6–12 weeks in vivo. The customised stage was 3D printed on the RAISE3D Pro2Plus using PLA to a design created in Fusion360 (Fig. 1a). Stainless steel screws were inserted to adjust the tilt of the scaffold following an initial scan in the micro-CT. Fe-PLA filament is embedded into the stage structure at a known height to act as a fiducial marker, minimising image artefacts.

The mathematical analysis, carried out in MATLAB2021a, involves:

1. Using HU distribution to identify the thresholding range.
2. Using the Fe-PLA and thresholding techniques to locate the centre of mass of the PEEK scaffold.
3. Using circle detection software to locate the boundary of the circular PEEK implant and create an imaging mask.

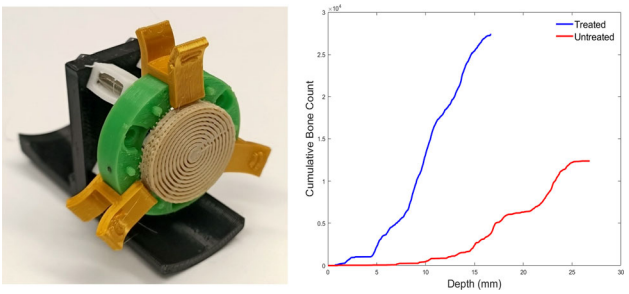

Fig. 1 a) 3D printed stage, holding the freshly 3D printed scaffold. b) Cumulative sum of bone mineral within cavities of scaffold with and without surface treatment

4. Check the alignment of the scaffold and correct the shape of the imaging masks to correct for any deformation of the circular cross sections.
5. Integrate through the slices of the CT for mineralised bone.

Results The explant positioning stage successfully aligned the implant with the imaging plane of the micro-CT. This enabled two examples of PEEK scaffolds to be analysed using the bespoke software. A cumulative histogram of the bone as a function of depth is shown in Fig. 1b.

Conclusion We have developed a procedure to quantify the osseointegration of a novel bone scaffold implant. This will enable us to find the best implant design for rapid and complete osseointegration.

References/Acknowledgements

Head and Neck Surgical Research Unit at Chris O'Brien Lifehouse, led by Professor Jonathan Clark
Sofie Trajanovska from the University of Sydney, Charles Perkins Centre, for valuable discussion relating to the Micro CT Commonwealth funding for Sarcoma and Surgical Research

O087 Photon Counting Detector CT Technology and Clinical Applications

Cynthia H. McCollough[1], PhD, DABR, FAAPM, FACR, FAIMBE

[1]*Brooks-Hollern Professor* and Professor of Medical Physics and Biomedical Engineering, CT Clinical Innovation Center, Department of Radiology, Mayo Clinic, 200 First Street SW, Rochester, MN, USA. e-mail: mccollough.cynthia@mayo.edu

The first patient CT exam was performed on October 1, 1971, forever changing the face of medicine. Since then, ongoing technical advances have made possible clinical applications only imagined by Hounsfield, who was awarded a Nobel Prize in Physiology and Medicine for his invention. Initial innovations in CT technology first revolved around the acquisition geometry, detector material, and rotation speed. Around 1990 and 1999, respectively, the introduction of spiral and multi-detector-row CT vastly expanded the range of clinical applications of CT, enabling vascular and cardiac imaging and providing highly detailed 3D—and 4D—representations of human anatomy. Around 2006, with the introduction of dual-source CT, a slow but steady development of dual-energy CT technology and clinical applications began. In parallel, concerns about radiation dose led to a number of dose management technologies, including the development of iterative reconstruction techniques fast enough for clinical use. Today, artificial intelligence (AI) methods are being used to guide data acquisition and provide further reductions in image noise. Now, photon-counting detector (PCD) technology is poised to be the next milestone in CT technical innovation. In 2014, the first whole-body PCD-CT system was installed at the Mayo Clinic. In 2020 and 2021, respectively, 2nd and 3rd generation PCD systems were installed at Mayo, where over 800 human subjects have been scanned. The technology is inherently spectral in nature, allowing temporally and spatially synchronous acquisition of multi-energy data. In addition, the lack of optical reflectors between detector pixels allows acquisition of 125-micron limiting spatial resolution data without a dose penalty. To date, studies covering the range of clinical applications have demonstrated measurable benefits relative to scintillating, energy-integrating detectors. This presentation will describe the state of the art in PCD CT scanners and present numerous examples of the clinical benefit derived from this latest innovation in CT technology.

O088 Volumetric breast density, compression pressure and dosimetry measurements with Volpara software at Breast Screen ACT

S. M. Midgley[1], J. Tse[2,3], J. Selvaraj[1,4], D. McLean[1,2], Y. Epping[5], T. Jain[5,6]

[1]Medical Physics and Radiation Engineering, Canberra Health Services, ACT. stewart.m.midgley@act.gov.au (Presenting author); [2]Faculty of Medicine and Health, University of Sydney, NSW, Australia; [3]Biomedical Technology Service, The Prince Charles Hospital, QLD, Australia. jason.tse@health.qld.gov.au; [4]Faculty of Medicine, University of New South Wales, Sydney, NSW, Australia. jothy.selvaraj@act.gov.au; donald.mclean@act.gov.au; [5]BreastScreen ACT, Department of Health, Australia. yvonne.epping@act.gov.au; Medical Imaging, Canberra health services, ACT. tarun.jain@act.gov.au

Introduction Breast density correlates with cancer risk. VolparaDensity software [1] was used to analyse raw mammograms delivering numerous measures of the breast. Derived parameters include Volumetric breast density (VBD) (ratio of fibroglandular tissue to total breast volume), compression pressure (ratio of force to contact area), and a composition specific Volpara estimate of mean glandular dose (VMGD).

The primary aim (P1) tested the hypothesis there is the same patient demographic (in terms of compressed thickness, contact area and VBD distributions) across 3 screening centres in the ACT. Secondary aims (S1-3) include analysis of the (S1) VBD reproducibility (a) for repeat images (same patient, side, and view), (b) for the same patient comparing different sides and views. (S2) distribution for compression pressures. (S3) difference between radiation dose reported as MGD (assumes 50/50 fat/gland) and VMGD accounting for patient specific composition quantified via VBD.

Method Ethical approval was gained to collect unprocessed DICOM images from three sites equipped with Sectra/Philips screening equipment. Task scheduler used XCOPY to harvest daily images to an external hard drive. The data was anonymised (using pydicom) before leaving the clinic. Volpara summary results are 112 column of parameters per image including DICOM tags for exposure and dosimetry, and the Volpara measurements. Sorting rules were developed to reject unwanted images such as QC and implants. We considered standard 4 view mammograms and upto one repeat, with good radiographic positioning. Results were sorted according to site (P1), patient (S1) or pooled (S2-3) and subject to appropriate statistical analysis.

Results and Conclusions Data for 2020 rejected 10% delivering 60 k images for 14 k patients, with good positioning for two thirds. Preliminary analysis indicates (S1) good VBD reproducibility amongst duplicate images for the same side and view, justifying future statistical analysis for aims P1 and S2, whilst (S3) VMGD differs from MGD by approximately ± 10%.

Acknowledgements We gratefully acknowledge the support of Volpara solutions limited (Wellington, NZ) in waiving licence fees to conduct this research, and Research analytics (Centre for Health and Medical Research, ACT Health) for sharing access to their pool of professional statisticians.

Reference

1. 'Robust Breast Composition Measurements', Highnam, Brady, Yaffe and Karssemeijer, International Workshop on Digital Mammography, Girona, Spain, June 2010.

O089 Optimisation of anode/filter material and tube potential selection for magnification imaging of larger breast thicknesses using digital mammography

A. J. Pascoe[1], T. A. Ireland[1]

[1]Biomedical Technology Service, Queensland Health, QLD, Australia. Alana.Pascoe@health.qld.gov.au (Presenting author); Timothy.Ireland@health.qld.gov.au

Introduction Through routine mammography performance testing it was identified that some x-ray tubes can fail to meet the technical standards for magnification imaging of 60 mm PMMA [1, 2]. Failing to meet signal difference to noise ratio (SDNR) and exposure time requirements can reduce contrast between pathology and background tissue, potentially reducing diagnostic sensitivity and breast cancer detection rates. The objective of this project was to provide an optimised set of exposure parameters for magnification imaging of PMMA thicknesses > 60 mm.

Method For each PMMA thickness, a range of tube potentials were evaluated for Mo/Rh and W/Rh anode/filter materials on a Siemens Mammomat Inspiration. Under automatic exposure control (AEC), the SDNR, relative mean glandular dose (rMGD), and exposure time were measured, and a visual image quality assessment performed using the ACR DM phantom. A figure-of-merit (FOM), defined as the $SDNR^2/rMGD$, was utilised as an optimisation metric [3]. Following the selection of an optimised set of exposure parameters, measurements were performed on several BreastScreen Queensland mammography systems to evaluate the clinical impact of the amending the default exposure parameters.

Results Preliminary data confirmed W/Rh was the optimal anode/filter selection. Clinical measurements confirmed changing from Mo/Rh to W/Rh significantly reduced patient dose, while maintaining similar image quality and exposure time for the selected thicknesses of PMMA. The optimised set of exposure parameters matched Siemens' recommendations at the time.

Conclusion These findings support the decision to amend the target/filter selection to W/Rh for magnification imaging of larger breast thicknesses on BreastScreen Queensland's Siemens Mammomat Inspirations.

Acknowledgements We would like to thank Queensland Health and BreastScreen Queensland for providing access to their facilities and equipment.

References

1. Heggie, J. C. P. et al. (2017) Position paper: recommendations for a digital mammography quality assurance program V4.0. Australas. Phys. Eng. Sci. Med. 40:491–543.
2. BreastScreen Australia National Quality Management Committee (2019) National Accreditation Standards.
3. Borg, M., Badr, I. & Royle, G. J. (2012) The use of a figure-of-merit (FOM) for optimisation in digital mammography: A literature review. Radiat. Prot. Dosimetry 151:81–88.

O090 Investigation of isocentre uncertainty from partial arc CBCT

O. L. Dancewicz (presenting author)[1], L. K. Webb[1], V. Seshadri[1], P. Ramachandran[1]

[1]Radiation Oncology, Princess Alexandra Hospital, Ipswich Road, Australia. Orrie.Dancewicz@health.qld.gov.au; Luke.Webb@health.qld.gov.au; Venkatakrishnan.Seshadri@health.qld.gov.au; Prabhakar.Ramachandran@health.qld.gov.au

Introduction Verification of patient setup is performed using a Cone-Beam Computed Tomography (CBCT) scan acquired with the X-ray Volume Imaging (XVI) system. Projection images are ideally acquired over a full 360° arc while the x-ray source and panel rotate around the patient. The projections are then reconstructed into a 3D dataset using filtered back-projection [1]. For specialised treatment techniques such as breath hold (DIBH/EEBH), image projections may be acquired using partial arcs while the patient is being treated, a technique known as Intra-fraction Imaging (IFI). kV & MV isocentre co-incidence is calibrated & assessed using full arc CBCT's. The aim of this study was to assess the uncertainty in XVI positioning associated with partial arcs and hence the impact on kV and MV isocentre co-incidence in these cases.

Method The kV-MV isocentre co-incidence of the linac was quantified using the standard Elekta bill ball bearing & flexmap tools. The MIMI phantom (Standard Imaging, Middleton, WI) was then positioned at the kV isocentre using the HexaPOD 6dof couch. Partial CBCT's were then acquired for a range of clinically relevant gantry angles, and the reconstruction registration was re-assessed.

Results Regular QA results show that the coincidence of the kV and MV isocentres assessed using a full-arc CBCT is consistently less than or equal to 0.3 mm in the lateral, longitudinal (superior-inferior) and vertical (anterior–posterior) directions. When CBCTs are acquired using a partial arc, offsets in the kV-MV isocentre of up to 0.5 mm were found in the lateral and vertical directions.

Conclusion Registration uncertainties of up to 0.5 mm in the lateral and vertical direction when partial-arc CBCTs are obtained are additive with kV-MV isocentre co-incidence and could result in patient positioning errors of up to 0.8 mm (without accounting for couch accuracy).

Reference

1. Elekta (2013) *XVI R5.0 Instructions for Use for: Elekta Synergy®, Elekta Axesse™, Elekta Infinity™, Versa HD™*, Elekta Limited, Crawley, UK

O091 Clinically significant MLC positional errors not detected by the treatment unit: A risk assessment

C. G. Lee[1], R. David[1], B. J. Zwan[1]

[1]Central Coast Cancer Centre, Gosford Hospital, NSW. Christopher.Lee@health.nsw.gov.au (Presenting author); Rajasekar.David@health.nsw.gov.au; Benjamin.Zwan@health.nsw.gov.au

Introduction Systematic MLC leaf positional errors up to 6 mm were observed on two Varian 21iX linear accelerators. The errors were not detected by the linac and no beam interlocks were asserted. As errors of only 2 mm can introduce a 10% dosimetric error for one leaf pair in a typical DMLC field [1], we performed a TG-100 [2] risk assessment and adjusted our MLC QA protocol accordingly. We compare our outcomes with published international recommendations for MLC QA [3–5]. This work highlights a shortcoming of relying on MLC trajectory log files alone for measuring MLC position.
Method The detectability, severity and occurrence of this fault was used to assess risk. The detectability was analysed by comparing the log files of the erroneous fields for which EPID images were acquired. The potential severity was assessed in the treatment planning system by inducing MLC leaf offsets from 1 mm up to 6 mm into SRS and SBRT treatment plans and comparing with the original plan. DVH analysis was used to demonstrate the magnitude of the induced error.
Results Qualitative MLC leaf position errors could be visualised on an EPID image immediately after acquisition during QA. Analysis of the log file data however, failed to accurately record the erroneous MLC positions for these faults. Figure 1 is a clinical example showing how the dose to the PTV and spinal cord increases as the leaf offset increases for a 2-fraction spine SBRT.
Conclusion We have demonstrated the possibility of adverse clinical outcomes resulting from this error. Relying on log files alone is an inadequate approach when trying to detect this fault. We recommend that the positional accuracy of each MLC leaf should be incorporated into a linac's daily QA schedule, with the ideal scenario being real-time MLC verification during treatment using EPID imaging.
References

1. LoSasso, T, Chui, CS, & Ling, CC. (2001) Comprehensive quality assurance for the delivery of intensity modulated radiotherapy with a multileaf collimator used in the dynamic mode. Med Phys, 28(11): 2209–2219 https://doi.org/10.1118/1.1410123
2. Huq, MS, Fraass, BA, Dunscombe, PB, Gibbons, JP, Jr., Ibbott, GS, Mundt, AJ, Mutic, S, Palta, JR, Rath, F, Thomadsen, BR, Williamson, JF, & Yorke, ED. (2016) The report of Task Group 100 of the AAPM: Application of risk analysis methods to radiation therapy quality management. Med Phys, 43(7): 4209 https://doi.org/10.1118/1.4947547
3. Klein, EE, Hanley, J, Bayouth, J, Yin, FF, Simon, W, Dresser, S, Serago, C, Aguirre, F, Ma, L, Arjomandy, B, Liu, C, Sandin, C, Holmes, T, & Task Group, AAoPiM. (2009) Task Group 142 report: quality assurance of medical accelerators. Med Phys, 36(9): 4197–4212 https://doi.org/10.1118/1.3190392

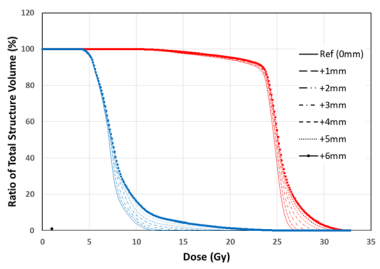

Spinal Cord D2cc (Gy)		PTV D95.0% (Gy)	
Ref (0mm)	7.951	Ref (0mm)	19.152
+1mm	8.115	+1mm	19.503
+2mm	8.364	+2mm	19.807
+3mm	8.7	+3mm	20.099
+4mm	8.989	+4mm	20.345
+5mm	9.215	+5mm	20.514
+6mm	9.413	+6mm	20.665

Fig. 1 DVH data (Spinal Cord—blue and PTV—red) for 1 mm incremental leaf offsets for a 2 fraction Spine SBRT, including Spinal Cord D2cc and PTV D95% data

4. Kirkby, C, Ghasroddashti, E, Angers, CP, Zeng, G, & Barnett, E. (2018) COMP report: CPQR technical quality control guideline for medical linear accelerators and multileaf collimators. J Appl Clin Med Phys, 19(2): 22–28 https://doi.org/10.1002/acm2.12236
5. van der Wal, E, Wiesma, J, Ausma, AH, Cuijpers, JP, Tomsej, M, Bos, LJ, Pittomvils, G, Murrer, L, & van de Kamer, J. (2013) Code of Practice for the Quality Assurance and Control for Intensity Modulated Radiotherapy. Netherlands Commission on Radiation Dosimetry, Report 22:

O092 Optimization of the Angles Used for Linac Collimator Radiation Isocentre Measurements

Y. Lyu[1], M. A. Ebert[1,2,3], G. M. Hassan[1], H. L. Riis[4,5], P Rowshanfarzad[1]

[1]School of Physics, Mathematics and Computer Science, University of Western Australia. 22623854@student.uwa.edu.au (Presenting author); [2]Department of Radiation Oncology, Sir Charles Gairdner Hospital, Nedlands, Western Australia; [3]5D Clinics, Claremont, Western Australia. martin.ebert@health.wa.gov.au; ghulam.hassan@uwa.edu.au; [4]Radiofysisk Laboratorium, Odense University Hospital, Department of Oncology, Odense, Denmark; [5]University of Southern Denmark, Department of Clinical Research, Odense, Denmark. hlynggaard@health.sdu.dk; hans.lynggaard.riis@rsyd.dk; pejman.rowshanfarzad@uwa.edu.au

Introduction A common method for measuring radiation isocentre of collimator rotation is 'star shot'. The conventional method is to expose a piece of film or EPID at a number of different collimator angles. The size of the radiation isocentre is determined by the maximum radius of the intersecting circles of all the triangles formed by the beam central axes. A finite number of collimator angles are randomly selected without supporting scientific evidence. This study aims to investigate the contribution of different collimator angles to radiation isocentre of collimator rotation of varying beam energies and gantry angles. This study will also aim to provide recommendations on selection of the collimator angles for accurate and efficient measurement of the collimator radiation isocentre.
Method Single beam images of different beam energies (6 and 18 MV), gantry angles and collimator angles were acquired on EPIDs. Gantry and collimator angles had a range of − 180° to 180°, in 30° increments. Images of the same beam energy and gantry angle but different collimator angles are digitally superimposed on one single image, and the size of the radiation isocentre is determined using an analytical solution. Overall, approximately 16,000 images were analysed in this study.
Results Preliminary results showed on one of the linacs investigated, collimator angles of − 30°, 30° and 60° had predominant contribution to radiation isocentre. Collimator angle of 0° is commonly one of the random selections for measurement of collimator isocentre, but has little effect on its size.
Conclusion Some collimator angles have more pronounced effect on the size of radiation isocentre. Using angles which have a larger effect on the size of radiation isocentre can make current measurement settings in clinical routine QA more efficient

O093 Linac reported steering error insensitive to 6 mv fff transverse beam position deviations

J. McAloney[1], S. Biggs[2], M Sobolewski[1,3]

[1]Riverina Cancer Care Centre, Wagga Wagga, NSW. jmcaloney@riverinacancercare.com.au (presenting author); Radiotherapy AI, Wagga Wagga, NSW. simon@radiotherapy.ai; [3]Norther Beaches Cancer Care, Frenchs Forest, NSW. msobolewski@riverinacancercare.com.au

Introduction Clinically significant beam position deviations were identified for a 6 MV FFF beam. Traditional physics workflow of a cardinal angle Winston-Lutz test was not able to identify this issue, nor was there significant reported transverse steering error from the machine ion chamber and nothing within the Elekta CAT highlighted the issue. Initial investigation using an electronic portal imaging device (EPID) revealed clinically significant penumbra shifts for small steering errors. This prompted investigation into further impact and possible solutions.

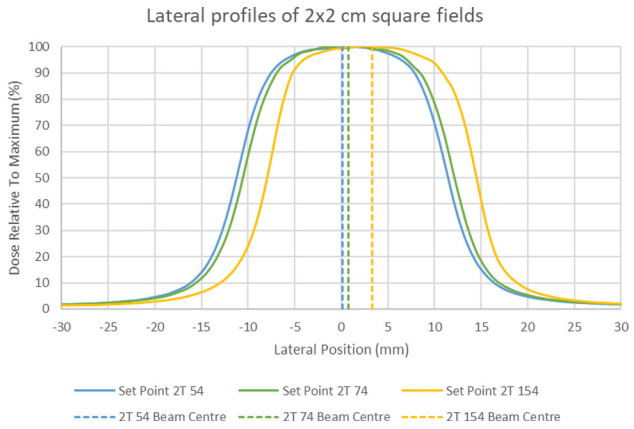

Fig. 12 × 2 cm profiles. Reported 2 T error (mm deviation): − 0.2 (0.1 mm), − 0.5 (0.8 mm), − 0.8 (3.2 mm)

Method We established testing set-points by adjusting transverse steering current to achieve introduced 2T steering errors. Tests at each set-point included profiles and EPID images. A proposed method for adjusting the 2T error sensitivity is explored via adjusting the 2T loop parameter such that a reported error corresponds to specific beam position deviations.

Results Large beam shifts were observed for small 2T reported beam steering errors. A suggested method for establishing 2T error sensitivity was successfully implemented.

Table 1 Results of EPID imaging

2TI ctrl	2T error	Central pixel coordinate	Position deviation (mm)
54	− 0.2	508	0
74	− 0.5	513	− 1.1
154	− 0.8	522	− 3.4
24	0.3	502	1.5
− 46	0.9	494	3.6

Conclusion This work has shown that existing vendor protocol for establishing beam steering error for 6 MV FFF beams can lead to clinical impacts on beam position without machine interlocks or significant reported steering errors. Not only does the method for establishing reported error sensitivity need addressing, this work supports a change in philosophy is required for 6 MV FFF beam steering: focus on positional accuracy as opposed to symmetry.

O094 Integrating Winston-Lutz tests into Daily QA during Machine Warm-Up

J. McAloney[1], S. Biggs[2]

[1]Riverina Cancer Care Centre, Wagga Wagga, NSW. jmcaloney@riverinacancercare.com.au (presenting author); [2]Radiotherapy AI, Wagga Wagga, NSW. simon@radiotherapy.ai

Introduction Morning linear accelerator warm-up includes both the delivery of photon beams of several hundred monitor units to an empty bunker, as well as taking a CBCT of a phantom and using image registration of its air gaps to perform couch shifts. It was proposed that the warm-up beams and the presence of a phantom at the imaging isocentre could be used for Winston-Lutz style tests. For the work-flow of the centre, changes to the procedure could not add much additional time cost.

Method Warm-up beams were adjusted to a field size to encompass the air-gap and delivered to an electronic portal imaging device (EPID). As the central air gap would have been moved to the kV isocentre following the CBCT, the discrepancy between the centre of the air gap and the centre of the radiation field on the EPID image provides a Winston-Lutz style test of kV to MV isocentre coincidence. Adapting prior in-house work regarding performing Winston-Lutz tests on an arc delivery to capture all gantry angles, the warm-up beams were adjusted to be delivered as static arcs.

Results The warm-up beams were replaced with half dose rate arcs (180° to –180° gantry angles). The EPID was run in movie mode acquiring frames approximately every 2°. In-house software was successfully adapted to identify the air-gap and present the results, see Fig. 2. In total, approximately 5 min was added to the warm-up procedure.

Conclusion Morning warm-up beams were successfully adjusted to provide Winston-Lutz type testing with gantry rotation. This provides daily kV to MV isocentre results as part of warm-up at a cost of 5 min to the workflow.

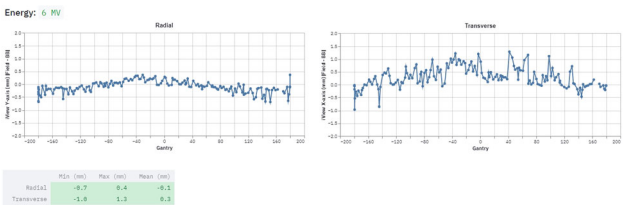

Fig. 2 In-house software kV to MV isocentre coincidence results

O095 Matching 10MVFFF beams on two different models of linacs for VMAT

Mahesh Mundayadan Chandroth[1,2], Anthony Venning[1,2]

[1]Medical Physics Specialist; [2]Mid North Coast Cancer Institute, Port Macquarie, NSW. Mahesh.Mundayadanchandroth@health.nsw.gov.au (Presenting author); Anthony.Venning@health.nsw.gov.au

Introduction Flattening Filter Free (FFF) beams were clinically released in Monaco® for IMRT treatments. The beam models were

generated from the data collected on PB2(Synergy^{TM}). Three linacs commissioned subsequently, all Versa HD^{TM} could not be beam matched to PB2 for 10MVFF. The largest discrepancy was identified for fields larger than 10 × 10cm^2 for the in-line beam profile. This study aims to find out the clinical significance of this variation on VMAT plans and the feasibility of patient transferability between the two models of linacs.

Method Monaco Commissioning Utility® (MCU) is used to compare the output factors, PDDs and profiles using the gamma analysis method. Also, 11 clinical plans were measured on both machines to compare the gamma scores. Another set of 5 SABR plans planned originally with 6MVFFF were recalculated with the other 3 photon beams (6MV, 15MV and 10MVFFF) retaining the beamlet shapes and MU. These 20 plans were measured on Versa HD using ArcCHECK® and compared the gamma scores. Also, the 16 10MVFFF plans are compared for average leaf pair opening (ALPO) and modulation factor (MF) with their gamma scores.

Results The output factors, PDDs and profiles were compared and tabulated (Tables 1, 2). The results of the 11 VMAT plans are in Table 3. The difference in gamma scores of the 20 recalculated plans is statistically insignificant. The 6MVFFF plan in the second set (plan 17) could not be delivered due to persistent 'Beam Timer' error on the linac. The gamma scores for the 16 10MVFFF plans were compared against ALPO and showed no correlation.

10MVFFF (Gamma scores - 1% 1mm)									
Field Size (cm^2)	Versa 1 Vs Versa 2			Versa 1 Vs Synergy			Versa 2 Vs Synergy		
	PDD	Profile - In plane	Profile - Cross plane	PDD	Profile - In plane	Profile - Cross plane	PDD	Profile - In plane	Profile - Cross plane
1x1	100.0	93.0	73.3	100.0			100.0		
2x2	100.0	94.8	78.5	100.0	100.0	71.6	100.0	97.1	100.0
3x3	100.0	100.0	98.8	100.0	100.0	100.0	100.0	100.0	100.0
4x4	100.0	99.1	100.0	100.0	97.9	92.9	100.0	86.4	94.9
5x5	100.0	99.3	100.0	100.0	62.7	96.6	100.0	71.1	89.2
10x10	100.0	100.0	100.0	100.0	25.7	43.3	100.0	38.7	45.7
30x30	100.0	100.0	100.0	100.0			100.0		

Table 1: Comparison of PDD and Profiles

Field Size (cm^2)	Measured Scp (10MV FFF CC-04)						
	Versa 1	Versa 2	Synergy	% Difference	Versa1 Vs Versa2	Versa1 Vs Synergy	Versa2 Vs Synergy
10x10	1.000	1.000	1.000		0.0	0.0	0.0
1x1	0.635	0.664	0.651		2.4	-2.0	-4.5
2x2	0.829	0.833	0.820		-1.0	-1.6	-0.5
3x3	0.891	0.893	0.885		-0.6	-0.9	-0.2
4x4	0.923	0.924	0.918		-0.5	-0.7	-0.2
5x5	0.942	0.944	0.939		-0.3	-0.5	-0.1
20x20	1.042		1.046		0.4		
40x40	1.061		1.068		0.7		

Table 2: Comparison of field output factors

Plan ID	Site	Gy/#	Segs	MU	ALPO(cm)	MF	Gamma pass					
							Clinical		Versa 1		Diff	
							3% 3mm	2% 2mm	3% 3mm	2% 2mm	3% 3mm	2% 2mm
1	RT LUNG	10.0	236	1576.48	2.82	0.591	96.7	91.8	99.8	95.8	3.1	4.0
2	L1	8.0	365	3348.42	2.32	0.329	97.5	92.6	99.2	95.7	1.7	3.1
3	L1	8.0	353	1942.32	3.07	0.557	99.4	94.3	97.2	92.8	-2.2	-1.5
4	RT PELVIS	8.0	201	2040.94	2.16	0.573	98.4	92.9	96.7	89.9	-1.7	-3.0
5	SPINE	8.0	393	1988.29	2.62	0.541	98.8	94.7	99.2	93.4	0.4	-1.3
6	LT NECK	5.0	104	654.18	3.17	0.643	95.5	85.6	98.9	93.3	3.4	7.7
7	FRONT BRAIN	5.0	87	577.89	2.97	0.932	99.4	96.1	97.9	93.9	-1.5	-2.2
8	MID BRAIN	5.0	141	668.43	2.61	0.816	98.7	91.1	95.7	87.0	-3.0	-4.1
9	PELVIS	4.0	189	971.50	4.50	0.473	98.1	91.1	96.1	87.2	-2.0	-3.9
10	LT HIP	8.0	139	1415.04	2.86	0.700	99.8	95.1	93.0	84.0	-6.8	-11.1
11	SPINE	8.0	259	2432.47	2.05	0.519	92.7	85.1	89.1	80.2	-3.6	-4.9

Table 3: Comparison of VMAT plan gamma pass rate between the clinically treated 10XFFF plans and Versa 1

Conclusion A new beam model is recommended to be generated for 10MVFFF for Versa HD. Considering the plan pass-rates on the two models, it is also recommended that patient specific QA be performed prior to treatment, on both models of linacs.

References

1. Commissioning & validation of 6MVFFF and 10MVFFF photon beams at MNCCI Port Macquarie, Physics Report
2. D Paynter et al., Characterisation of flattening filter free (FFF) beam properties for initial beam set-up and routine QA, independent of flattened beams, 2018 Phys. Med. Biol. 63 015021

O096 Technology Implementation On A National Scale During A Pandemic

Trent Aland[1,2]

[1]National Director of Medical Physics; [2]ICON Group

As the COVID-19 pandemic spread across the globe in early 2020 and Australia went into various lockdowns throughout the year, the Icon Group Medical Physics team pivoted to a largely working from home model. For a role that had traditionally been a hands on multi-disciplinary role, this was a challenge in itself to achieve.

These challenges were compounded by the fact that the Icon Group continued to expand its services and continued to implement technology across the network as well as into the Asia region. Despite this, in 2020, our team delivered on 5 major software projects, 6 major hardware projects, and implemented stereotactic techniques to a number of our centres. Continuing into 2021, our team plan to deliver on at least 5 major software projects, at least 10 major hardware projects, and further implementation of techniques to our centres.

In this presentation, we discuss how our team has delivered on these projects safely and also discuss how we have adapted to the challenges and how we have changed as a result of the challenges.

O097 A probabilistic U-Net for auto-segmentation of a gastric cancer clinical target volume modelling inter-observer variability

P. Chlap[1,2], H Min[1,3], R. Finnegan[4], J Dowling[1,3], M. Field[1,2], K. Cloak[1,2], M. Lee[5], T. Leong[6], J. Chu[6], J. Tan[6,7], P. Tran[6], T. Kron[6], A. Haworth[4], M. Ebert[8,9], S. K. Vinod[1,5], L. Holloway[1,2]

[1]South Western Sydney Clinical School, University of New South Wales, and Ingham Institute for Applied Medical Research, Australia; [2]Department of Medical Physics, Liverpool and Macarthur Cancer Therapy Centre, Australia. phillip.chlap@unsw.edu.au (Presenting author); [3]Australian e-Health Research Centre- CSIRO, Royal Brisbane Hospital, Australia. hang.min@csiro.au; [4]Institute for Medical Physics, School of Physics, The University of Sydney, Australia. robert.finnegan@sydney.edu.au; jason.dowling@csiro.au; matthew.field@unsw.edu.au; k.cloak@unsw.edu.au; [5]Liverpool and Macarthur Cancer Therapy Centre, Australia. mark.lee2@health.nsw.gov.au; [6]Peter MacCallum Cancer Centre, Australia. trevor.leong@petermac.org; julie.chu@petermac.org; [7]Sir Peter MacCallum Department of Oncology, The University of Melbourne, Australia. jennifer.tan@petermac.org; phillip.tran@petermac.org; tomas.kron@petermac.org; annette.haworth@sydney.edu.au; [8]Sir Charles Gairdner Hospital and University of Western Australia, Australia; [9]School of Physics, Mathematics and Computing, University of Western Australia, Australia. martin.ebert@uwa.edu.au; shalini.vinod@health.nsw.gov.au; lois.holloway@health.nsw.gov.au

Introduction When multiple experts contour a structure on a medical image they can often significantly disagree on the clinical definition of the structure, known as Interobserver variability (IOV). Auto-segmentation algorithms, such as U-Net, attempt to predict one boundary for a given structure and do not account for IOV. In this work we adopt a probabilistic U-Net which enables the sampling of multiple plausible contours on an unseen image.
Method The Clinical Target Volume (CTV) defined in the TOPGEAR clinical trial for treatment of gastric cancer is a complex structure [1]. Five Radiation Oncologists manually contoured this structure on the planning CT of 10 cases. These were deemed protocol compliant even though sections of these contours disagreed by up to 3 cm. We trained a probabilistic U-Net which, by combining a traditional U-Net with a variational auto-encoder, allows sampling of unlimited plausible CTV variants [2]. 8 cases were used for training and 2 cases for validation. One sample per observer was generated for each manual contour on the validation cases. The sampled contours were matched to the nearest manual contour based on the Dice Similarity Coefficient (DSC) to show that different samples can better represent IOV.
Results The DSC between the sampled contours and the matched manual contours was 0.86 ± 0.03 and with 2.88 ± 0.6 mm Average Surface Distance (ASD). This is an improvement over a traditional U-Net with a mean DSC of 0.85 ± 0.03 and ASD of 2.98 ± 0.59 mm (Fig. 1).
Conclusion The probabilistic U-Net shows promise in its ability to represent varying plausible contours. Future work will investigate extending the model to 3D and further validation on a test set.
References

1. Leong, T., Smithers, B. M., Michael, M., Gebski, V., Boussioutas, A., Miller, D., Simes, J., Zalcberg, J., Haustermans, K., Lordick, F., Schuhmacher, C., Swallow, C., Darling, G., & Wong, R. (2015). TOPGEAR: A randomised phase III trial of perioperative ECF chemotherapy versus preoperative chemoradiation plus perioperative ECF chemotherapy for resectable gastric cancer (an international, intergroup trial of the AGITG/TROG/EORTC/NCIC CTG). *BMC Cancer*, *15*(1). https://doi.org/10.1186/s12885-015-1529-x
2. Kohl SAA, Romera-Paredes B, Meyer C, et al. A probabilistic U-net for segmentation of ambiguous images. Adv Neural Inf Process Syst. 2018;2018-Decem(NeurIPS):6965–6975.

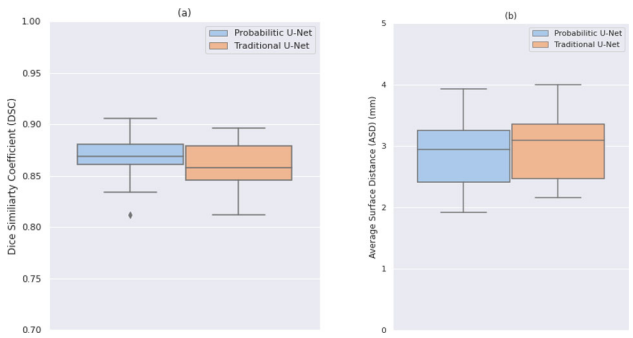

Fig. 1 Box plots of DSC (**a**) and ASD (**b**) computed on validation cases

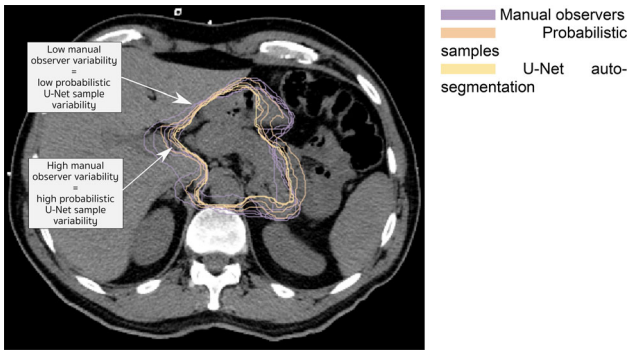

Fig. 2 Example of contours sampled using the probabilistic U-Net

O098 Characterisation of Artec Leo 3D scanner for radiotherapy applications

S. B. Crowe[1,2,3,4], J. Luscombe[1], T. Poroa[1], S. K. Maxwell[1], S. Cleland[5], T. Kairn[1,2,3,4]

[1]Cancer Care Services, Royal Brisbane and Women's Hospital, Brisbane, Queensland, Australia; [2]Herston Biofabrication Institute, Metro North Hospital and Health Service, Brisbane, Queensland, Australia; [3]School of Information Technology and Electrical Engineering, University of Queensland, Brisbane, Queensland, Australia; [4]School of Chemistry and Physics, Queensland University of Technology, Brisbane, Queensland, Australia. sb.crowe@gmail.com (Presenting author); jenna.luscombe@health.qld.gov.au; tania.poroa@health.qld.gov.au; sarah.maxwell@health.qld.gov.au; [5]Radiation Oncology Princess Alexandra Raymond Terrace, Brisbane, Queensland, Australia. susannah.cleland@health.qld.gov.au; tanya.kairn@health.qld.gov.au

Introduction 3D scanning techniques, including photogrammetry, stereo depth scanners and structured light scanners are cost-effective solutions to acquire 3D surface data of patients. These models can be used to facilitate the design of patient-matched medical devices and treatments. This project characterised the performance of a metrology-grade Artec Leo scanner in a radiotherapy setting.
Method The system was commissioned by scanning of objects of known dimensions and of different tones, to characterise precision, accuracy and limitations of the system, by comparison against known properties. Subsequently, 26 participants were scanned (HREC approval QRBW/66064) by investigators, with scans performed on various anatomical sites (e.g. face, bodies, arms) in multiple treatment positions (sitting, supine, prone, standing). Simple uniform thickness boluses covering the nose, eyes and cheekbones were 3D printed for participants where a face scan was performed. Space between the participant skin and the fitted device was assessed visually by the investigators.
Results More than 150 participant scans were performed, with an average scan time of 3.5 min. A selection of scanned models are presented in Fig. 1. Scanning of features occluded by other anatomy (e.g. behind the ear) required experimentation or instruction to perform successfully. The weight of the scanner (2.6 kg) resulted in operator discomfort with sustained use, particularly where the scanner needed to be elevated above supine subjects. Maintaining irregular standing positions for whole body scans was uncomfortable for some participants. Some participants were not comfortable keeping their eyes open, due to bright light. 95% of edges of the fitted device fit

Fig. 21 Photographs and textured and untextured reconstructed model screenshots

anatomy within 1 mm, with poorest agreement observed at eyebrow and nasal-facial crease.

Conclusion The scanner provided accurate 3D models of participants suitable for production of patient-matched devices such as bolus, immobilisation, shielding and superficial applicators.

Acknowledgements The investigators acknowledge the Royal Brisbane and Women's Hospital staff members who volunteered to be scanned by the investigators.

O099 Reframing Risk

Anna Ralston[1]

[1]St George Hospital Cancer Care Centre, Sydney, Australia. anna.ralston@health.nsw.gov.au

Introduction Active risk/benefit management has been used for many decades in for-profit industries such as construction and finance, however healthcare organisations typically enforce a centralised "one size fits all" framework of risk reduction.

There have been many medical physics publications on risk reduction, most notably the AAPM's 2016 TG100 report[1], however the majority of these do not address the importance of the relative risk/benefit ratio, nor do they take non-clinical risks and benefits into account, such as staff well-being.

Method To help evaluate the risk/benefit ratio of implementing new technologies and techniques, St George Hospital Cancer Care Centre (STGCCC) developed the Risk and Benefit Balance Impact Template (RABBIT)[2]. The implementation of stereotactic radiosurgery at STGCCC is presented as a case study[3].

Results The highest ranked potential risks identified for the implementation of SRS at STGCCC were: suboptimal image registration or contouring, poor quality plans, inaccurate patient positioning, and staff stress due to tight timelines or lack of training. The highest ranked benefits were: improved local control and less cognitive decline compared to whole brain radiotherapy, and patients no longer needing to travel to other hospitals for treatment. After reviewing the processes in place to reduce the risks and increase the benefits, the multidisciplinary team agreed that the benefits of SRS outweighed the risks. The technique was released for clinical use with initial limitations, including only one patient per week and a minimum PTV size of 15 mm. These limitations were periodically reviewed, and eventually relaxed in light of the good clinical outcomes the SRS program was achieving.

Conclusion The RABBIT is a simple system for ranking risks and benefits, both clinical and non-clinical. It provides a multidisciplinary team with a process to reach consensus on whether the local benefits of the new technology outweigh the local risks, which is a requirement for clinical release.

References

1. Huq MS, Fraass BA, Dunscombe PB, Gibbons JP, Ibbott GS, Mundt AJ, et al. The report of Task Group 100 of the AAPM: Application of risk analysis methods to radiation therapy quality management. Med Phys 2016; 43(7):4209–62.
2. Ralston A, Yuen J. Use of the AAPM Safety Profile Assessment tool to evaluate the change in safety culture after implementing the RABBIT prospective risk management system. Advances in Radiation Oncology 2019; 4(1):150–5.
3. Ralston A, Graham P, Poder J, Yuen J. The RABBIT risk-based approach to clinical implementation of new technology: SRS as a case study. Technical Innovations & Patient Support in Radiation Oncology 2020;14: 51–60

O100 A medical physics registrar joins the ICRP Task Group 116: experiences from the ICRP mentorship program

M. Djukelic[1], **T. Kron**[2], **C. J. Martin**[3]

[1]Medical Technology & Physics, Sir Charles Gairdner Hospital, Perth, Australia. Mario.Djukelic@health.wa.gov.au (presenting author); [2]Peter MacCallum Cancer Centre, Melbourne and University of Wollongong, Australia and ICRP Task Group 116 Member. Tomas.Kron@petermac.org; University of Glasgow, Glasgow, UK and ICRP Task Group 116 Chair. colin.j.martin@ntlworld.com

Introduction In 2020, the International Commission on Radiological Protection (ICRP) established a mentorship program to engage university students and early-career professionals and scientists as mentees in ICRP Task Groups (TG) with the guidance of an ICRP member as mentor. Currently there are eight different task groups accepting mentees.

Method A medical physics registrar (MD) applied for ICRP TG116"Radiological Protection Aspects of Imaging in Radiotherapy"; a task group under the ICRP Committee 3 chaired by Colin J Martin. The application included a CV, a letter of interest and a letter of endorsement from the registrar's employer. The duration of the mentorship is one year with possible extension. A total of seven mentees from all parts of the world joined the TG116 mentorship program.

Results The mentor and the mentee had regular virtual meetings to discuss general aspects of a task group such as allocation of tasks and chapters amongst the members, the reviewing process in the ICRP hierarchy, and meetings to discuss drafted chapters. MD conducted several literature reviews on certain aspects of utilizing imaging in radiotherapy. In collaboration with the other members and mentees, MD and his mentor worked on an international survey to determine imaging practices in radiotherapy in various countries. They were responsible for the data collection and analysis from Australia and New Zealand. Due to restrictions resulting from the COVID pandemic the mentorship was extended for another two years.

Conclusion The ICRP TG116 mentorship program is a valuable experience for early-career professionals to understand the complex logistics of an internationally based task group and the establishment of important radiation protection guidelines. Some of the work would be suitable for sign-offs within TEAP, particularly the radiation protection module. It is possible to incorporate the mentorship workload in a busy working schedule.

Acknowledgements Medical Technology & Physics for enabling resources to be able to participate in the ICRP mentorship program.

O101 Optimising Knowledge Sharing in Radiation Oncology

J. Green[1], E. Keating[1]

[1]NT Radiation Oncology, Alan Walker Cancer Care Centre, NT Australia. julia.green@nt.gov.au; elly.keating@nt.gov.au

Introduction Knowledge sharing is gaining increasing attention in healthcare due to positive impacts on organisational performance [1, 2]. Northern Territory Radiation Oncology (NTRO) is a small organisation in an inner regional location where knowledge sharing is critical to business continuity and developing resilience. This work aimed to optimise knowledge sharing at NTRO by measuring staff knowledge needs, perceptions and behaviours to identify opportunities for enhancing knowledge sharing for organisational performance.
Method A survey was designed to identify treatment planning knowledge gaps and examine the relationship between knowledge assets, psychological trust, innovation and knowledge sharing based on the work of Mura et al. [3]. Results were analysed to identify strengths, weaknesses and opportunities for knowledge sharing improvement. Recommendations arising from results and supporting literature were developed into knowledge sharing pilots.
Results Knowledge gaps in complex planning and problem solving were identified with most planning knowledge held by subject matter experts as tacit knowledge. Discrepancies between self-perceptions and manager perceptions of knowledge were identified where staff have good awareness of their treatment planning knowledge but less awareness regarding their knowledge for problem solving or quality improvement. Very high levels of relational social capital and trust were found while relatively lower levels of knowledge sharing and innovative work behaviour were reported. Of the knowledge sharing behaviours, sharing mistakes scored the highest while sharing best practices and seeking feedback scored lower.
Conclusion Treatment planning knowledge gaps, perceptions and knowledge sharing behaviours were measured and analysed. The relationship between knowledge assets, behaviours, trust and innovation as reported by Mura et al. [3] were demonstrated. Opportunities for increasing knowledge sharing and innovation were identified utilising existing high levels of relational social capital and trust. Recommendations were developed into pilots to be trialled for optimising knowledge sharing for innovation and quality, with future work planned to measure outcomes in these areas.
References

1. Ahmad F, Karim M (2019) Impacts of knowledge sharing: a review and directions for future research, J Workplace Learn 31(3):207–30
2. Popa I, Stefan SC (2019) Modeling the Pathways of Knowledge Management Towards Social and Economic Outcomes of Health Organizations, Int J Environ Res Public Health 16(7):1114.
3. Mura M, Lettieri E, Radaelli G, Spiller N (2016) Behavioural operations in healthcare: a knowledge sharing perspective, Int J Oper Prod Manag 36(10):1222–46

O102 Management: the missing module

M. Whitaker[1], B. Cooper[2], J. Green[3]

[1]Radiation Oncology, Chris O'Brien Lifehouse, NSW Australia. may.whitaker@lh.org.au (Presenting author); [2]Radiation Oncology, Canberra Hospital, ACT Australia. ben.cooper@act.gov.au; [3]Radiation Oncology, Alan Walker Cancer Care Centre, NT Australia. julia.green@nt.gov.au

Introduction Medical Physics training and education focusses on the requisite knowledge and competence to become an independent Medical Physics Specialist. As careers progress, the development of managerial skills and functions becomes necessary, however the TEAP program only includes 'professional awareness' as an ancillary module. This leaves a large gap in the skills, training and knowledge required for good management and leadership, which then begs the question of how to fill this gap for those Medical Physicists taking on management roles.
Method Three (relatively) newly appointed medical physics directors from vastly different geographic areas, in both public and private hospitals, formed a weekly peer support meeting via videoconferencing to discuss and share acquired knowledge, skills, and experiences in conducting the management role of the medical physics director.
Results/Discussion Emerging from the discussions were a number of themes that Medical Physics directors, as technical leaders, must take on in their overall responsibilities: managing human and capital resources, developing strategic and financial directions, engaging in organisational and network building, and decision making and prioritisation. [1]The following items were identified as helpful in executing these duties: establishing role expectations with both subordinates and superiors to create transparency and understanding; formal education, such as a Masters of Business Administration, to build a foundation of management knowledge; developing relationships with knowledgeable mentors to add an experience-based dimension to formal education; and a support network of other managers to share experiences and insights.
Conclusion Medical Physics training is largely focussed on the technical aspects of the role, hence there is little formal training in management or managerial functions. This leaves a skills and knowledge gap for the senior physicist transitioning into a managerial role. Establishing expectations of the position and seeking training and mentoring from a variety of sources will assist the new manager in successfully navigating this complex role.
References/Acknowledgements

1. Hill, Linda A (1992) Becoming a Manager: Mastery of a New Identity. Harvard Business School Press, USA

O103 Collaboration and Resources to Increase the Consistency and Efficiency of Training NSW Public Radiation Oncology Medical Physics (ROMP) Registrars

L. Wilfert[1,2], E. Seymour[3], A. Gray[4,5,6], T. Erven[4], R Stensmyr[7], A. Wilfert[1]

[1]Department of Radiation Oncology, Calvary Mater Newcastle, NSW Australia; [2]School of Mathematical and Physical Sciences, University of Newcastle, NSW Australia. Lisa.Wilfert@calvarymater.org.au (Presenting author); [3]Central Coast Cancer Centre, Gosford, NSW Australia; [4]Liverpool and Macarthur Cancer Therapy Centres, Sydney, NSW Australia; [5]Ingham Institute for Applied Medical Research, Liverpool, NSW Australia; [6]South Western Sydney Clinical School, University of NSW, Liverpool, NSW Australia; [7]Crown Princess Mary Cancer Centre, Westmead, NSW Australia

Introduction Since 2004, NSW Public ROMP Registrars enrolled in TEAP have tripled and now comprise approximately one third of the Australian and New Zealand Registrar population. They are geographically spread across NSW in 18 departments. Half of our Registrars work outside Sydney; many limited in their ability to travel for training activities. The COVID-19 pandemic, whilst devastating in

terms of health and economic outcomes, did provide some opportunities for remote collaboration and resource sharing[1]. Concurrently, the ACPSEM decided to hold Registrars starting after 1st July 2020 to a 3 year clinical training period, prompting NSW to look for more efficiencies.

Method and Results The NSW TEAP Coordinator worked with the NSW/ACT Branch and departments to reduce duplication of effort and impact of restrictions by sharing teaching and resources, such as:

- Development of monthly, interactive tutorials and study groups
- Increased online training and assessment resources
- Online tutorial recordings

Guidance developed for departments included:

- Documents for grouping learning outcomes
- Worksheets to focus and shorten Registrar study notes
- Advice on streamlining assessment and increased collaboration on the development of training plans

Some NSW Departments are collecting interesting treatment plans and developing assignments to streamline the treatment planning module; one of the areas of training most impacted by the restrictions.

Conclusion Efficiencies in NSW's approach to TEAP were introduced, due to restrictions caused by the COVID-19 pandemic and ACPSEM's decision to more strictly police the time to completion, while a revised clinical training guide (and supporting resources) was still being developed. The goal was to protect our opportunistic clinical training approach, mental health and retention of Registrars, exam track record, as well as improve access to and consistency in training across NSW. To fully reduce duplication of effort, these initiatives would need to be implemented by ACPSEM on an Australasian wide basis.

Acknowledgements Thanks to the ROMPs in the public and private sectors who shared insight in to their own tutorial programs.

Reference

1. Hall AK, Nousiainen MT, Campisi P, Dagnone JD, Frank JR, Kroeker KI, Brzezina S, Purdy E, Oswald A. (2020) Training disrupted: Practical tips for supporting competency-based medical education during the COVID-19 pandemic, Med Teach, 42(7):756–761, https://doi.org/10.1080/0142159X.2020.1766669

O104 A 2020 Survey of the Australasian Diagnostic Imaging Medical Physics Workforce

L. Wilkinson[1], Z. Brady[2,3], H. Round[4]

[1]Dept. of Medical Engineering & Physics, St. Vincent's Hospital, Melbourne, Australia Luke.Wilkinson@svha.org.au (Presenting author); [2]Department of Radiology, Alfred Health, Melbourne, Australia; [3]Department of Neuroscience, Monash University, Melbourne, Australia; z.brady@alfred.org.au; [4]Australasian College of Physical Scientists and Engineers in Medicine (ACPSEM). howell.round@gmail.com

Introduction As part of a broader project aimed at assessing Diagnostic Imaging Medical Physics (DIMP) workforce requirements in the context of the Australian healthcare environment, a survey of the DIMP workforce was conducted in 2020.

Methodology A targeted medical physics survey was emailed to hospital sites and private consultants/companies across Australia and New Zealand (NZ). The list of survey participants was derived from ACPSEM records, local regulatory listings and personal knowledge of the medical physics community. Survey questions were designed to align with previous surveys conducted in 2006, 2009 and 2012 [1–3] to allow direct comparison to previous data.

Results The survey identified a total of 132.4 DIMP full-time equivalent (FTE) positions for Australia and 5.5 for NZ based in hospitals/imaging practices. The state-based FTE breakdown was ACT = 5.8, NSW = 33.6, QLD = 30.8, SA = 10.8, VIC = 25.7, WA = 24.7 and 1 FTE working Australia-wide. Of the medical physicists employed across these FTE, 43% were on the ACPSEM register, 27% were non-registered, 16% were radiology registrars, 7% nuclear medicine registrars and 7% physics support staff. Only two (of 63) registered physicists held dual ACPSEM certification with 40% of the remainder ACPSEM-certified in radiology, 40% ACPSEM-certified in nuclear medicine, and the final 17% holding mammography testing certification, or an international certification or unspecified. Private consultants/companies accounted for a further 12.3 FTE in Australia, 7.1 in NZ, 2.6 across both jurisdictions and 1 FTE unidentified. Of these, 33% were listed on the ACPSEM register. In hospitals, the gender breakdown was 60/30/10 (male/female/not specified) and in the private sector it was 61/26/13. In comparison with the 2012 survey, the overall Australian/NZ DIMP workforce has grown by 41%.

Conclusion Analysis of the data shows ongoing changes to the DIMP workforce in overall number and composition when compared to previous surveys. This data will be valuable for ongoing workforce planning in this sector.

Acknowledgements This project was supported by the Australian Government Department of Health.

References

1. Round WH (2007) A survey of the Australasian clinical medical physics and biomedical engineering workforce. Australas Phys Eng Sci Med 30: 13–24
2. Round WH (2010) A 2009 survey of the Australasian clinical medical physics and biomedical engineering workforce. Australas Phys Eng Sci Med 33(2):153–162
3. Round WH (2013) A 2012 survey of the Australasian clinical medical physics and biomedical engineering workforce. Australas Phys Eng Sci Med 36:147–157

O105 Regional Collaboration Initiative—from challenges to opportunities: perspective

Y. Yousif[1], J. Zifodya[1], J. McAloney[2], M. Sobolewski[2], A. Mishra[3], D Banjade[3]

[1]North West Cancer Centre, Tamworth, Australia. Yousif.Yousif@health.nsw.gov.au (Presenting author); Jackson.Zifodya@health.nsw.gov.au; [2]Reverina Cancer Care Centre (RCC), Wagga Wagga. jmcaloney@riverinacancercare.com.au; msobolewski@riverinacancercare.com.au; Ajeet.Mishra@health.nsw.gov.au; Central West Cancer Centre (CWCC), Orange Hospital; Dilli.Banjade@health.nsw.gov.au

Introduction Collaboration continuously plays a vital role in healthcare, particularly in regional settings, for a sustainable and high-quality service delivery. This has been witnessed clearly during the recent pandemic time. Although the pandemic has brought up unprecedented challenges, great opportunities appeared, adopted and incorporated into our routine practices. This work aims to present the Regional Collaboration Initiative (RCI), highlight the challenges that regional Medical Physicist faces, and propose some solutions to tackle these challenges.

Challenges In late 2020, Radiation Oncology Medical Physicists (ROMPs) from three Regional centres: North West Cancer Centre

(NWCC) in Tamworth, Central West Cancer Centre (CWCC) in Orange and Reverina Cancer Care Centre (RCCC) in Wagga Wagga, came together to establish a forum to discuss common challenges that Regional ROMPs face and share their experiences in how to address these challenges. The challenges identified were:

1. Continuous Professional Developments (CPDs) – attending training courses and workshops
    - Training and Education for registrars – limited to resources & trainers and supervisors experiences
    - Implementation of advanced Radiotherapy techniques
    - Career progression
    - staffing recruitment

Opportunities The RCI created a group email to facilitate regular meetings. The group adopted some innovative solutions widely used during the COVID-pandemic time (i.e.Zoom and Microsoft team) for communication. Activities include:

- CPDs
    - o Presenting informal departmental activities
    - o Improving workflow efficiency through software development
    - o Collaboration between centres and exchange the innovations
- TEAP
    - o Allowing registrar to participate in other departmental ATPs/ Commissioning activities
    - o Sharing departmental approaches in addressing challenges caused by the recent TEAP updates
    - o A forum for registrars to present their training competencies
    - o Networking
- Miscellaneous
    - o Allocation time for QA and research in limited resources
    - o Career progression

Conclusion RCI is a forum that has been established and managed successfully so far. A regional centres conference can be held in the future, allowing more regional centres to participate and share their experiences.

O106 There is no Physical basis for the current trend to favor Specific Energy (Dose to Medium) over Absorbed Dose (Dose to Water) for the prediction of Biological effect from MV External Beam Radiation

N. Bennie[1]

[1]North Coast Cancer Institute, Lismore, NSW, Australia. Nick.Bennie@ncahs.health.nsw.gov.au (Presenting author)

Introduction Several modern Radiotherapy Treatment planning systems now either calculate by default or offer the option to calculate the total energy deposited by radiation in a voxel divided by an estimate of the mass of the voxel. A voxel being an arbitrary volume of the Patient or phantom, usually a cube 2 or 3 mm in dimensions. It is noted that it is not always explicitly stated this is the case, however by examination of the results of the TPS computer programs, it can be determined that it is. This is commonly referred to as "Dose to Medium". This is consistent with the ICRU quantity "Specific Energy". This is a real quantity; in that it represents a real amount of energy in a volume with real dimensions. It is normal for the ICRU defined quantity "Absorbed Dose" to be used as the indicator of Biological effect. It is noted that it is defined as a point quantity. It is noted that in the limit of a small domain, the mean specific energy is equal to the absorbed dose. A further aspect is that for aggregate materials, such as clinical tissue, the absorbed dose for each type of particle of the aggregate is different, the type referring to the elemental composition. That is each type will absorb a different amount of energy from the radiation fluence (Stopping power) and will have a different mass factor (Z/A ratio). It is noted that Absorbed Dose is commonly referred to as "Dose to Water".

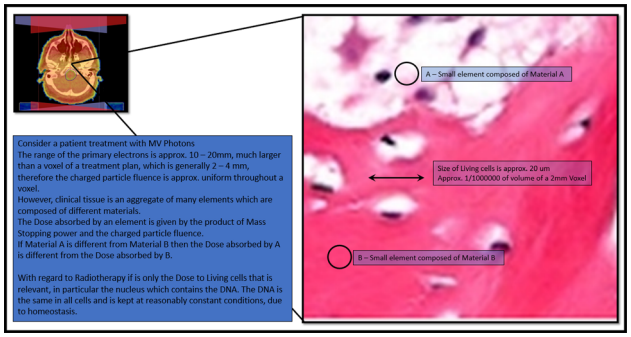

Expanded representation of a patient at a scale comparable to Living cells

Conclusion Specific Energy ("Dose to Medium") is an average of all contents of a voxel. For the prediction of effect in clinical tissue, it is only the energy absorbed by living cells that is of interest. There is no physical process, whereby the energy and particularly the mass of inert particles can affect living cells.

References

1. Khan, F. M. (1994). The Physics of Radiation Therapy. 2nd Edition. Lippincott Williams & Wilkins. (ISBN 0-683-04502-4)
2. ICRU Report 83. State of the art on dose prescription, reporting and recording in intensity-modulated radiation therapy. ICRU 2011 (Bethesda, MD)
3. ICRU Report 85. Fundamental quantities and units for ionizing radiation. ICRU 2011 (Bethesda, MD)
4. Elekta (Elekta AB, Stockholm, Sweden.) documents including: Monaco Dose Calculation Technical Reference and letter titled "SUMMARY OF DOSE TO WATER CALCULATIONS IN MONACO (V3.1 and later)" dist. Feb 2013.

O107 A multi-detector comparison to determine convergence of measured output factors for small field dosimetry

Do Duc Chi[1], **Tran Ngoc Toan**[2], **Robin Hill**[3]

[1]108 Military Central Hospital, Hanoi, Vietnam. chidd108@gmail.com (Presenting author); [2]Vietnam Atomic Energy Institute, Hanoi, Vietnam; [3]Department of Radiation Oncology, Chris O'Brien Lifehouse, Sydney, Australia and Institute of Medical Physics, School of Physics, The University of Sydney, NSW Australia

Introduction The IAEA TRS483 Code of Practice recommends to use at least 2 detector types for the calculation of relative output factors (ROF) in small fields [1]. More recently, there are new published data sets of small field correction factors covering both well-established and newly available detector. In this study, we review the convergence of ROFs using a range of IBA detectors (SFD, PFD-3G

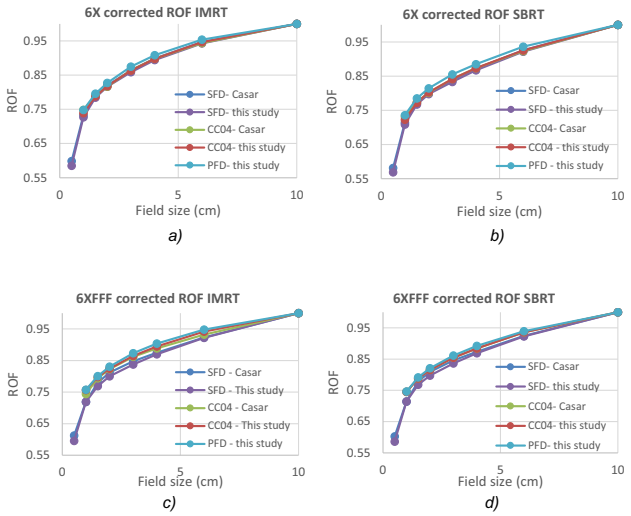

Fig. 1 Measured relative output factors in IMRT and SBRT mode using Casar's [3] and TRS483 correction factors

and CC04) as reference detectors to then determine small field correction factors.

Method 6X and 6XFFF photon beams from a Truebeam STx linear accelerator (Varian Medical System) with High Definition MLCs are selected to use in two modes IMRT (without jaw-tracking) and SBRT (with jaw-tracking) as described by IROC [2]. The calculated ROF from reference detectors were then used to calculate ROF correction factors for 3 new generation small field detectors: IBA Razor Nano Chamber (RNIC), IBA Razor Ionization Chamber (RIC) and IBA Razor Diode (RD).

Results The results showed that there is a certain convergence in calculation of relative output factor between reference detectors as shown in Fig. 1. Except at field size 0.5 × 0.5 cm, standard deviation between corrected ROF was largest being 1.7% and 2.7% for 6X and 6XFFF beams respectively at field size 1 × 1 cm. Small field correction factors for RNIC, RIC and RD were calculated but showed larger variations

Conclusion The convergence of ROF for the established detectors was very good. Further work is required to determine small field correction factors for the newer-generation detectors RNIC, RIC and RD.

Acknowledgements Do Duc Chi acknowledges support through the IAEA CRP E24022 doctoral training program and Pavel Kazantsev, Dosimetry Laboratory, IAEA, Vienna for helpful discussions.

References

1. IAEA, "Dosimetry of Small Static F ields Used in External Beam Radiotherapy: An International Code of Practice for Reference and Relative Dose Determination," 2017.
2. D. S. Followill et al., "The Radiological Physics Center's standard dataset for small field size output factors," *J. Appl. Clin. Med. Phys.*, vol. 13, no. 5, pp. 282–289, 2012.
3. B. Casar, E. Gershkevitsh, I. Mendez, S. Jurković, and M. Saiful Huq, "Output correction factors for small static fields in megavoltage photon beams for seven ionization chambers in two orientations—perpendicular and parallel," *Med. Phys.*, vol. 47, no. 1, pp. 242–259, 2020.

O108 Calibration and Inter-comparison of a Range of High-Resolution Diode Array Detectors for Stereotactic Radiotherapy

Simon K. Goodall[1,2,3], Katrina Biggerstaff[4], Leon Dunn[5]

[1]Genesis Care WA; [2]School of Physics, Mathematics, and Computing, Faculty of Engineering and Mathematical Sciences, [3]University of Western Australia, Crawley, WA, Australia; simon.goodall@genesiscare.com (Presenting Author); [4]Genesis Care QLD. Katrina.biggerstaff@genesiscare.com; [5]Genesis Care VIC. Leon.Dunn@genesiscare.com

Introduction The frequency of Stereotactic Radiosurgery and Stereotactic Body Radiotherapy treatments are increasing in clinical practice. These techniques, referred to in general as Stereotactic Radiotherapy (SRT), utilise high precision, steep dose gradients and dose escalation within the targets. The treatment targets themselves are typically small and treatment fields are therefore also required to be very small. To achieve the required accuracy during Patient Specific QA (PSQA), devices are required which provide high spatial resolution and high dosimetric accuracy. One such device is the SRS MapCHECK (Sun Nuclear Corporation, Melbourne, Florida), which has been shown to be suitable for SRT PSQA.

Method Following a detailed characterisation of a single SRS MapCHECK device, a series of simple tests were selected to commission and compare a further seven devices. All devices were calibrated and commissioned following the same process and evaluated to intercompare their performance. The tests were designed to evaluate the quality of the calibration and determine the range of performance seen across like devices.

Results It was shown that calibrations could be obtained which allowed variations of less than 1.0% in the measured dose during rotations and inversions of the device under invariant irradiation conditions. No dependence was observed between error in individual diode calibration factor with distance from device centre, or magnitude of required calibration factor. Variations between device performance for linearity and dose rate dependence were seen to be less than 0.5%. Angular dependence and small field measurement variations were greater, exceeding 5% under specific situations.

Conclusion All devices were shown to perform within specification and at a level acceptable for clinical practice. A series of baselines were established along with a range of inter device performances which can be used to characterise the performance of new devices in a single measurement session

References/Acknowledgements

1. Halvorsen, P.H., et al., AAPM-RSS Medical Physics Practice Guideline 9.a. for SRS- SBRT. Journal of applied clinical medical physics, 2017. 18(5): p. 10–21.
2. Miften, M., AAPM TG218: Measurement Methods and Tolerance Levels for Patient-Specific IMRT Verification QA. Medical Physics, 2016. 43(6): p. 3852–3853.
3. Palmans, H., et al., Dosimetry of small static fields used in external photon beam radiotherapy: Summary of TRS-483, the IAEA–AAPM international Code of Practice for reference and relative dose determination. Medical physics (Lancaster), 2018. 45(11): p. e1123-e1145.
4. Rose, M.S., et al., Multi-institution validation of a new high spatial resolution diode array for SRS and SBRT plan pretreatment quality assurance. Med Phys, 2020. 47(7): p. 3153–3164.
5. Zhang, G., E. Moros, and V. Feygelman, Comprehensive evaluation of the high-resolution diode array for SRS dosimetry. Journal of Applied Clinical Medical Physics, 2019. 20.

6. Lassot, M., et al., 67 Study of a new detector for stereotactic treatments: The SRS MapCheckTM. Physica medica, 2019. 68: p. 41–41.
7. Parsons, D., et al., Characterization and Validation of SRS MapCheck for Patient Specific QA On CyberKnife M6. 2019

O109 An evaluation of the performance of three film dosimetry methods for stereotactic radiosurgery quality assurance

L. M. L. Smyth[1], K M Collins[1], S. Beveridge[1], A. Alves[1]

[1]Australian Clinical Dosimetry Service, Australian Radiation Protection and Nuclear Safety Agency, Yallambie, VIC. lloyd.smyth@arpansa.gov.au (Presenting author); km4collins@gmail.com; sabeena.beveridge@arpansa.gov.au; andrew.alves@arpansa.gov.au

Introduction In film dosimetry, methods of calculating net optical density (netOD) vary in accuracy, complexity, and cost. This study evaluates the performance of three film dosimetry methods using EBT3 and EBT-XD at stereotactic radiosurgery (SRS) doses.
Method Three netOD methods were analysed; 'stock-to-stock' (S–S, background OD taken from any piece of unirradiated film from the same lot), 'film-to-film' (F-F, background OD taken from a region-of-interest on the same piece of film prior to irradiation) and 'pixel-to-pixel' (P-P, netOD determined on a per-pixel basis by geometric registration of pre- and post-irradiation film scans). Calibration curves were generated using 12 doses ranging from 0 to 3600 cGy. In the first experiment, n = 10 sets of three 'check-films' per film type were irradiated with control doses (10–30 Gy) and agreement between the film-measured doses and control doses was assessed. Second, clinical SRS plans were delivered to an anthropomorphic head phantom containing a film-slot and co-located microdiamond detector. Agreement between film and microdiamond dose was evaluated. Finally, dose-difference maps were generated to compare EBT3 and EBT-XD for the three netOD methods.
Results The F-F method marginally improved the film-dose to control-dose agreement (mean ± standard error) compared to S–S for EBT3 (2.8 ± 0.3% versus 2.9 ± 0.3%) while substantial improvements were observed for EBT-XD (2.5 ± 0.3% versus 4.1 ± 0.6%) (Fig. 1). The blue channel had the poorest performance for EBT-XD

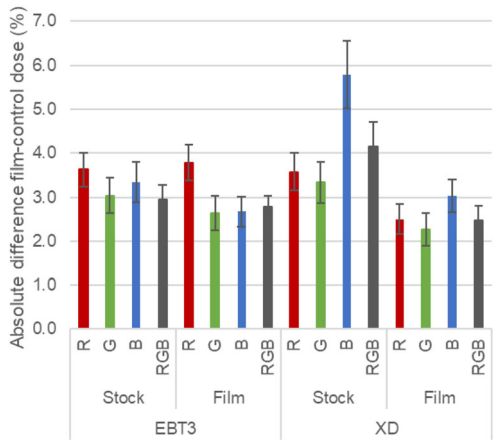

Fig. 1 Absolute percentage difference between film- and control-dose (mean ± standard error)

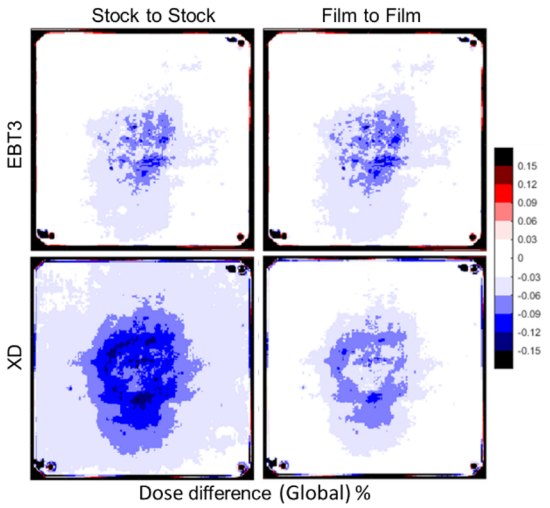

Fig. 2 Representative dose-difference maps (plan versus film) for a 20 Gy SRS delivery using the three netOD methods

with a S–S method (5.8 ± 0.8%). Representative dose-difference maps (plan versus film) for a 20 Gy SRS delivery are shown in Fig. 2.
Conclusion Preliminary data suggests that EBT3 is non-inferior to EBT-XD when using a F-F method and more robust when using a S–S method. A F-F method should be utilised for EBT3-XD to account for the poor performance of the blue channel. Data for the pixel-to-pixel method is under analysis.

O110 Effects of air gaps when using 3D printed bolus for small field VMAT treatments

E. Spelleken[1,2], T. Kairn[2,3,4], S. Crowe[1,2,4], J. Hellyer[5]

[1]GenesisCare, Rockhampton Base Hospital, Rockhampton; [2]School of Information Technology and Electrical Engineering, University of Queensland. Emma.spelleken@genesiscare.com (Presenting Author); [3]Cancer Care Services, Royal Brisbane and Women's Hospital; [4]Herston Biofabrication Institute, Metro North Hospital and Health Service; [5]GenesisCare, Macquarie University Hospital

Introduction This study investigated the effect of small beam segments and air gaps when using 3D printed bolus for wide field VMAT treatments. Wide field VMAT was introduced to treat the ever-increasing number of cases presenting with extended skin conditions. These treatments pose a unique challenge as the fields are large as they are requiring the treatment of whole legs, arm and backs. The bolus that is used for these treatments is 3D-printed for each patient and can be rigid and patients can swell during treatment, which can cause significant air gaps, up to 1 cm. Currently, no investigations has occurred into the effect that air gaps have on these unique treatment fields.
Methods Film was used to take surface dose measurements on solid water, using foam to create air gaps, with 1 cm of jelly bolus placed on top. A range of field sizes from 10 × 10cm^2 to 1 × 1cm^2 and slit fields of 3 × 20cm^2 and 0.5 × 20cm^2, varying air gap of 0-1 cm, depth of measurement at surface and 1 cm depth and gantry angles from 0^0 to 30^0 were taken using a 6MV beam energy.
Results Fig. 1 shows the results of gantry angle and varying air gap and its effect on surface dose. The values for Fig. 1 are compared to gantry 0° measurements. Figure 2 shows the effects of surface dose with slit fields and varying air gap thickness. The results showed that

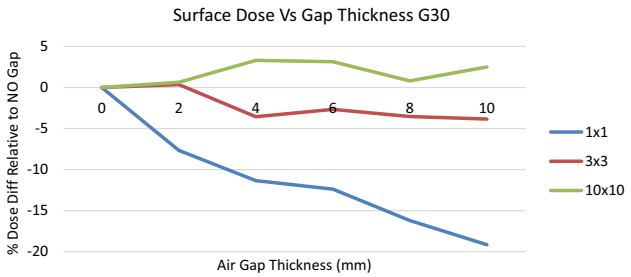

Fig. 1 Comparison of surface dose measurements for varying gap thicknesses at gantry angle of 30 degrees

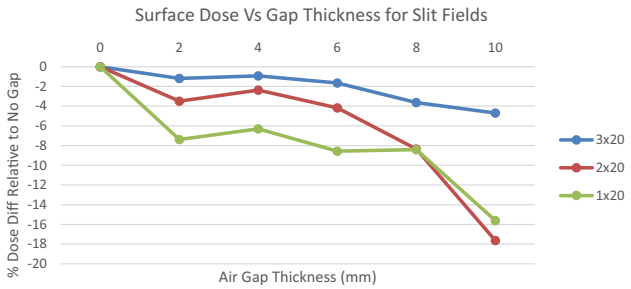

Fig. 2 Surface dose differences for slit fields with varying air gap

by increasing the gantry angle and air gap, the surface dose for small fields down to a 1 × 1cm^2 field significantly decreased. A 3 × 3cm^2 field showed a decrease in surface dose of approximately 4% whereas a 1 × 1cm^2 field shows a decrease of almost 20%. Increasing the air gap and decreasing field sizes also showed a similar result, with a 1 cm air gap and 1 × 20cm^2 field showing a decrease in surface dose of up to 18%.

Conclusion When air gaps of up to 0.5 cm are present in these treatment plans, it is recommended to try and decrease the size of the air gap, particularly when there are small field sizes and varying gantry angles.

References

Butson M et al.1998. Measurement of off-axis and peripheral skin dose using radiochromic film. *Phys. Med. Biol.* 43:2647–2650

Charles P et al.2012. The effect of very small air gaps on small field dosimetry. *Phys Med Biol* 57:6947–6960

Chung J et al.2012. Surface Dose Measurements from Air Gaps under a Bolus by Using a MOSFET Dosimeter in Clinical Oblique Photon Beams. *Journal of the Korean Physical Society*. 61(7):1143–1147

Khan Y et al.2013. Clinical and Dosimetric Implications of Air Gaps between Bolus and Skin Surface during Radiation Therapy. *Journal of Cancer Therapy*, 4:1251–1255

Wong et al., 'Volumetric modulated arc therapy (VMAT) for extensive skin field cancerisation (ESFC) – exploring the limits of treatment volumes with a case series of backs' *Int J Radiol Radiat Ther*, vol 7(6), pp 184–192, Nov 2020

O111 Applying spatially dependent density corrections to film data

A. Alves[1], M. Shaw[1]

[1]Australian Clinical Dosimetry Service, Australian Radiation Protection and Nuclear Safety Agency, Yallambie, VIC. andrew.alves@arpansa.gov.au; maddison.shaw@arpansa.gov.au

Introduction The ACDS offers end-to-end dosimetry audits of SABR and techniques to radiotherapy facilities. The audit utilises a thorax phantom and Gafchromic film to measure dose in lung, spine and soft tissue targets. Returning dose in the presence of changing density media requires different portions of the film to be corrected according to the medium the film is embedded in because the in-water calibration is not applicable in non-water-equivalent media. The ACDS film is inserted to take a cross-section of dose at boundaries between high- and low-density media (lung, soft tissue and bone). The corrections are derived from an EGS MC model of a cube structure which has returned different values for different media (Fig. 1a).

Method The film must be spatially registered so that the density dependent corrections can be applied to the correct portions of the film. The film is first matched to locating peg features that are visible in the CT of the phantom (Fig. 1b). The phantom has constant geometry so universal density masks are matched with the standard film cut-out to define the locations of features: soft tissue, cortical and trabecular bone, lung and lung tumour (e.g. Figure 1c is the spine detail).

Results The film-to-CT match has precision of 0.3 mm for CT resolution of 1 mm. The universal density mask-to-film match has sub-pixel precision (< 0.35 mm). A 3-pixel Gaussian blur (∼ 1 mm) to the correction mask was required to account for dose blurring which arises from density uncertainty.

Conclusion The planned dose is calculated using density derived from the CT. The blurring of the correction mask has been set to account for doses in typical plans where some density blurring should be expected from clinical CTs.

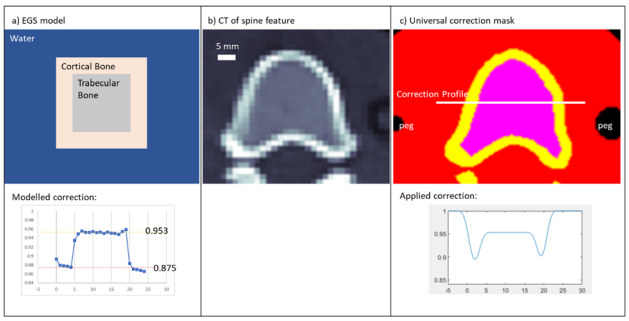

Fig. 1 **a** the EGS model to calculate correction factors. **b** CT data. **c** The universal mask used to apply the film correction

O112 Varian Portal Dosimetry commissioning: new model with Truebeam Golden Beam Data matched linacs

P. Fogg[1], H. Stephens[1], C. Challens[1]

[1]Genesis Care, Qld, Australia. Penny.Fogg@genesiscare.com (Presenting author); Holly.Stephens@genesiscare.com; Cameron.Challens@genesiscare.com

Introduction Varian™ provides a generic portal dosimetry (PD) beam model for treatment plan and delivery quality assurance. The vendor provided PD did not provide the desired quality assurance, therefore a new PD model specific to linacs used and typical treatment sites in GenesisCare was created.
Method The PD model was created on Varian Eclipse V15.6 treatment planning system for plans calculated using the 6MV AcurosXB (dose to medium) and AAA beam models. The model fields were delivered on a Varian Truebeam linac fitted with standard 120 MLCs and aS1200 port imaging panel. Reproducibility, linearity, dose rate and output factors were verified. Thereafter PD quality assurance was performed on a selection of TG119 and clinical plans of various complexity for the two 6MV beam models (AXB and AAA). The PD results were compared with SNC ArcCheck quality assurance of the same plans.
Results Clinical plan results for four matched TB across 11 plans with a total of 28 fields were 99.8 ± 0.4% and 97.7 ± 4.5% for gamma criteria 3% 3 mm and 2% 2 mm with 10% Threshold respectively.
Comparison results with SNC Perfraction of 17 clinical plans and 50 fields 99.9 ± 0.4%, 99.5 ± 1.0% and 99.7 ± 0.6% for Perfraction, PD (AAA) and PD (AXB) respectively with the gamma criteria of 3% 3 mm 10% Threshold. The new PD model also showed good agreement with the SNC ArcCheck for the TG119 and challenging cases. There were significant improvements with the new model for the challenging cases compared to the provided PD model.
Conclusion Clinically acceptable results were confirmed using a single new model for beam matched TB linacs with standard 120 MLC. A range of clinical plans including some larger fields showed improvement with our own model compared to the vendor provided model. The ARIA based workflow and distributed QA on beam matched TB was verified.

O113 Gamma Criteria of Large Field VMAT Quality Assurance at SSD 65 cm

S. F. Liu, A. Mehta[1], B. Perrett[1], A. Kazi[1]

[1]Radiation Oncology, Princess Alexandra Hospital, Ipswich Road, Australia. SauFan.Liu@health.qld.gov.au (Presenting author); Akash.Mehta@health.qld.gov.au; Ben.Perrett@health.qld.gov.au; Aleksandra.Kazi@health.qld.gov.au

Introduction Electronic Portal Imaging Device (EPID) in-air measurement is a time saving option for Volumetric Modulated Arc Therapy (VMAT) quality assurance (QA). To avoid irradiating the EPID electronics, another QA method is required if any jaw field dimension is greater than 13 cm in a VMAT plan. The maximum field size of Octavius1500 array is 27 cm × 27 cm. To avoid shifting the Octavius1500 array in four different directions (left, right, superior, and inferior) for individual large field measurements, the Octavius1500 array measurements with plastic water at SSD 65 cm were investigated with different 2D gamma criteria.
Method A Pinnacle script was created to reset gantry and couch angles to zero with SSD 65 cm to the surface of plastic water. The dose was also validated with ion chamber measurements. Patient plan QA was repeated with the Octavius1500 array and plastic water at SSD 65 cm, instead of SSD 95 cm. With the loss of spatial resolution at SSD 65 cm, different 2D gamma criteria were investigated for clinical cases and two failed cases.
Results The dose difference between ion chamber measured dose and the Pinnacle calculated dose was within 1%. These calculated dose maps were compared to 2D measurements with the Octavius1500 array at SSD 65 cm.
Table 2 Dose comparisons between ion chamber measured dose and TPS calculated dose

100 MU, 10 cm × 10 cm field, SSD 65 cm	6 MV	10 MV
Measured dose with chamber and plastic water	2.34 Gy	2.29 Gy
TPS calculated dose at 5 cm depth	2.36 Gy	2.31 Gy
Dose difference	0.8%	0.7%

Table 3 Gamma pass rate comparisons of different Octavius arrays measurements with different gamma criteria

Clinical case Case	Octavius1500 Beam	SSD 65 cm 2D 3%/2 mm	SSD 65 cm 2D 3%/1.4 mm	SSD 65 cm 2D 3%/1.2 mm	SSD 65 cm 2D 3%/1 mm	SSD 95 cm 2D 3%/2 mm
1	Arc 1	100.0%	100.0%	99.6%	98.9%	98.2%
	Arc 2	100.0%	100.0%	99.0%	98.6%	97.9%
2	Arc 1	99.6%	99.6%	99.2%	98.8%	99.6%
	Arc 2	100.0%	99.6%	98.7%	95.7%	98.5%
	Arc 3	100.0%	99.6%	99.6%	99.6%	98.7%
	Arc 4	99.5%	98.5%	98.0%	97.4%	98.2%
3	Arc 1	99.7%	98.3%	97.9%	97.6%	96.9%
	Arc 2	99.6%	99.6%	98.9%	98.2%	97.5%
	Arc 3	100.0%	96.0%	95.7%	92.8%	98.7%
	Arc 4	99.7%	99.1%	98.1%	96.9%	97.5%
	Arc 5	99.7%	99.7%	99.7%	99.7%	97.3%
	Arc 6	98.7%	97.5%	96.2%	95.5%	98.1%

Clinical case Case	Octavius1500 Beam	SSD 65 cm 2D 3%/2 mm	SSD 65 cm 2D 3%/1.4 mm	SSD 65 cm 2D 3%/1.2 mm	SSD 65 cm 2D 3%/1 mm	SSD 95 cm 2D 3%/2 mm
Very large field						
4	Arc 1	100.0%	100.0%	100.0%	99.5%	100%/100%
	Arc 2	100.0%	100.0%	100.0%	98.8%	98.7%/98.7%
5	Arc 1	100.0%	100.0%	100.0%	100.0%	100%/100%
	Arc 2	100.0%	99.8%	99.8%	99.4%	99.7%/99.4%

Failed case Case	Octavius1500 Beam	SSD 65 cm 2D 3%2 mm	SSD 65 cm 2D 3%1.4 mm	SSD 65 cm 2D 3%1.2 mm	SSD 65 cm 2D 3%1 mm	SSD 95 cm 2D 3%2 mm	Iso 3D 3%2 mm
6	arc1	96.2%	93.3%	89.5%	84.8%	73.2%	87.2%
	arc2	97.1%	93.1%	92.2%	89.2%	78.0%	85.7%
7	arc1	100.0%	94.3%	91.5%	85.8%	94.2%	78.1%
	arc2	93.1%	88.2%	85.3%	84.3%	92.0%	88.6%

Failed case Case	Octavius1000 Beam	SSD 65 cm 2D 3%/2 mm	SSD 65 cm 2D 3%/1.4 mm	SSD 65 cm 2D 3%/1.2 mm	SSD 65 cm 2D 3%/1 mm	SSD 95 cm 2D 3%/2 mm	Iso 3D 3%/2 mm
6	Arc 1	70.5%	53.0%	47.9%	41.6%	83.0%	94.5%
	Arc 2	74.1%	52.5%	46.6%	40.9%	88.7%	93.8%
7	Arc 1	70.5%	47.6%	44.1%	36.9%	98.9%	94.1%
	Arc 2	69.1%	50.6%	48.6%	45.4%	93.2%	95.8%

Conclusion Gamma criteria of 3%/1.4 mm with 10% threshold and global normalization showed the Octavius1500 array at SSD 65 cm sensitive enough to pick up the failed cases compared to other QA methods. These SSD 65 measurements save the time of shifting the Octavius1500 array to different selected positions for individual fields. This advantage comes at the cost of spatial sensitivity. The Octavius1500 array alignment, collimator angle, and gantry angle need to be accurately set as small setup errors translate to significant shifts at 65 cm SSD.

O114 Impact of Detector spacing and characteristics on Gamma Passing Rates

J. Ukath[1], L. Webb[1], C. E. Jones[1], V. Seshadri[1], P. Ramachandran[1]

[1]Radiation Oncology, Princess Alexandra Hospital, Ipswich Road, Australia. Jaysree.Ukath@health.qld.gov.au (Presenting author); Luke.Webb@health.qld.gov.au; Catherine.Jones3@health.qld.gov.au; Venkatakrishnan.Seshadri@health.qld.gov.au; Prabhakar.Ramachandran@health.qld.gov.au

Introduction Various QA solutions are available for patient specific QA in radiotherapy. EPID-based software SunCHECK^{TM}, Gafchromic EBT3 film coupled with inhouse analysis software, ArcCHECK, Octavius 1500 and OCTAVIUS SRS 1000 (OS1000) are the QA tools employed in this project. OS1000 offers reasonable spatial resolution of 2.5 mm to verify high dose distributions characteristic of the modulated stereotactic ablative radiotherapy (SABR) in its central 5.5 × 5.5 cm^2. The detectors placed peripheral to the above offers a lower resolution of 5 mm. The aim of this study was to compare conventional VMAT plan QA using three different QA systems. The 'Merge Feature' of the VeriSoft software was used to combine two sets of measurements: one taken at isocentre and the second shifted by half the detector spacing in the longitudinal axis.

Method Five regular VMAT cases belonging to different anatomical sites were chosen for comparison using the three QA modalities. 2D coronal plane Gamma analysis obtained from OS1000 were compared with those obtained using film and SunCHECK measurements. The universal tolerance Gamma Passing rate of $> = 95\%$ for 3% 2 mm with 10% threshold as recommended by TG 218 was used for comparing the three methods.

Results All the three QA methods gave similar pass rates above 95% for a 3% 2 mm gamma at 10% Threshold. Since the plans selected were regular VMAT plans, this criterion was reasonable. The EPID-based and film-based methods have uncertainties in gamma passing rates due to panel calibrations and handling procedures, respectively.

Conclusion 'Merge feature' in VeriSoft can be used to increase the resolution in the peripheral region. For the fields verified in this study, the merge feature did not affect the gamma pass rates significantly. The high spatial resolution ensures adequate measurements of dose profiles in regular and highly modulated photon beams, especially when targets are near OARs. Although Film and EPID offered better resolution compared to array, the uncertainties associated with these methods needs to be considered.

References

Tolerance limits and methodologies for IMRT measurement-based verification QA: Recommendations of AAPM Task Group No. 218 Moyed Miften, Arthur Olch, Dimitris Mihailidis, Jean Moran, Todd Pawlicki, Andrea Molineu, Harold Li, Krishni Wijesooriya, Jie Shi, Ping Xia, Nikos Papanikolaou, Daniel A Low *Med. Phys. 45 (4), April 2018*

O115 Patient-specific and modular oral positioning stents for potential use during head-and-neck radiotherapy treatments

T. Kairn[1,2,3], S. Cleland[4,5], J. Dawes[1], A. G. Livingstone[1], S. B. Crowe[1,2,3,4]

[1]Cancer Care Services, Royal Brisbane and Women's Hospital, Brisbane, Qld, Australia; [2]School of Information Technology and Electrical Engineering, University of Queensland, Brisbane, Qld, Australia; [3]School of Chemistry and Physics, Queensland University of Technology, Brisbane, Qld, Australia. t.kairn@gmail.com (Presenting author); [4]Herston Biofabrication Institute, Metro North Hospital and Health Service, Brisbane, Qld, Australia; [5]Now at: Radiation Oncology Princess Alexandra Hospital Raymond Terrace, Brisbane, Qld, Australia

Introduction Oral positioning stents can play an important role in head-and-neck radiotherapy, helping to isolate targeted tissues and push sensitive tissues out of the path of the radiation beam [1]. While warm wax can be used to form comfortable stents that exactly match patient anatomy [1,2,3], concerns have been raised regarding the robustness and resulting positioning reproducibility achievable using wax stents [1, 2]. In this work, MRI imaging was used to investigate the potential for robust 3D printed stents to achieve stable and reproducible positioning without substantially reducing patient comfort.

Method Oral positioning stents were fabricated using the standard local wax moulding process [1], replicated using 3D printing [1], and constructed from modular 3D printed components, for one healthy participant (volunteer senior member of the research team), who was then MRI imaged 20 times with different stents in situ. Geometric analysis of resulting images was performed using MIM Maestro (MIM Software Inc, Cleveland, USA) and RayStation (RaySearch Laboratories AB, Stockholm, Sweden).

Results After repeat MRI imaging, taking approx. 4 min per stent, the participant reported issues with small pieces of wax remaining attached to teeth and hard palate after removal of wax stents, discomfort due to excessive smoothness of 3D printed replicas (perceived need to clench jaw to stabilise), and "surprisingly" increased comfort from 3D printed modular stents. The example image analysis shown in Fig. 1 shows different positioning but similar reproducibility achieved with a wax and a 3D printed modular stent.

Conclusion This study demonstrated the potential for replacing a process of constructing patient-specific oral positioning stents using wax with a process of selecting from a small library of 3D printed modular components, to achieve desired positioning using a more robust material with minimal (generally positive) effects on patient comfort.

Acknowledgements S B Crowe and S Cleland's contributions to this work were supported by a Metro North Hospital and Health Service funded Herston Biofabrication Institute Programme Grant. MRI image acquisition was made possible by a grant from the Herston Imaging Research Facility—Project Support Scheme 2020.

References

1. Cleland S, Chan P, Chua B, et al. (2021) Dosimetric evaluation of a patient-specific 3D-printed oral positioning stent for head-and-neck radiotherapy. Phys Eng Sci Med. In press. https://doi.org/10.1007/s13246-021-01025-y
2. Lee VSK, Nguyen CT, Wu J (2019) The fabrication of an acrylic repositioning stent for use during intensity modulated radiation therapy: a feasibility study. J Prosthodont 28(6): 643–648.

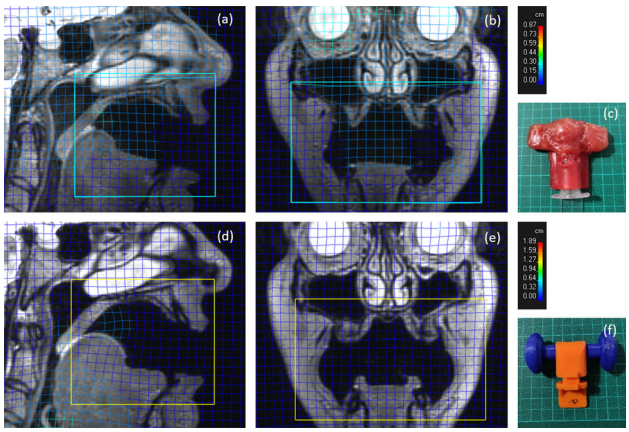

Fig. 1 Sagittal and coronal MRI slices showing deformation matrices obtained from registering repeat images with the same stent, for wax stent (top row) and modular 3D printed stent (bottom row)

3. Norfadilah MN, Ahmad R, Heng SP, et al. (2017) Immobilisation precision in VMAT for oral cancer patients. J Phys Conf Ser 851: 012025.

O116 Bone cell response to 3D printed implant materials: rough vs smooth, PEEK vs titanium

H. V. Kruse[1], W Lewin[1], D. R. McKenzie[2], N Suchowerska[1]

[1]VectorLAB, Department of Radiation Oncology, Chris O'Brien Lifehouse, Australia. hedi.kruse@lh.org.au (Presenting author); will.lewin@lh.org.au. [2]Applied and Plasma Physics, School of Physics, The University of Sydney, Australia. david.mckenzie@sydney.edu.au; natalka.suchowerska@lh.org.au

Introduction We examined the bone cell response to two different 3D printed implant materials: commercially available hydroxyapatite-coated titanium and plasma-activated polyether ether ketone. We also examine the method of printing with the PEEK objects being either fused filament fabricated (FFF) with a smooth surface finish or selective laser sintered (SLS) presenting a rougher surface. The titanium specimen were selective laser (SLM) molten and supplied in four different roughnesses by the manufacturer, two being smooth or extra smooth and two being rough and extra rough.

Method We analysed initial bone cell adhesion and proliferation using cell viability assays and bone cell spreading using scanning electron microscopy. In vitro cell responses are indicative of osseointegration potential of the implant material.

Results

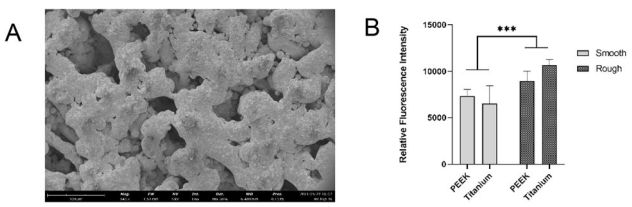

Fig. 1 A Scanning electron microscope image of 3D printed titanium with high surface roughness. **B** Osteoblast adhesion after 2 h hours of incubation to smooth and rough PEEK and titanium specimen. Shown is the mean value and standard deviation of six replicates. Three-star significance was reached with a two tailed paired t-test comparing smooth and rough surfaces.

Conclusion Our results indicate that rough surfaces are able to retain more bone cells compared to their smooth counterparts. Furthermore, we show that FFF or SLS printed PEEK is a viable alternative to commercially available titanium with equivalent osseointegration potential. This offers an opportunity to form a composite of the two materials depending on the local needs of the site of implant.

References/Acknowledgements We thank Dr William Parr from 3DMorphic for the provision of the titanium specimen.

O117 3D Printed PTW TRUFIX-Compatible Detector Holders

A. G. Livingstone[1]

[1]Cancer Care Services, Royal Brisbane and Women's Hospital, Brisbane. alexander.livingstone@health.qld.gov.au (Presenting author)

Introduction PTW TRUFIX is a patented detector position system, which helps to precisely adjust the effective point of measurement for PTW ion chambers and solid state detectors in a PTW water phantom. Once setup, detectors can be exchanged without the need to set a new zero point by placing the effective point of measurement (EPOM) of all detectors to the water surface using specific holders and caps. The required hardware can be purchased from PTW, but only PTW branded detectors are officially compatible. This study details the design and 3D printing of TRUFIX-compatible hardware.

Method Dimensions of official TRUFIX detector holders were measured using calipers. Along with schematics of the detectors, the relationship between the EPOM and the TRUFIX attachment point could then be calculated. A holder for the PTW Farmer (horizontal orientation) and a setup cap for the microDiamond (vertical orientation) were then designed in the Tinkercad software using this relationship. These holders were then printed on a Raise 3D Pro 2 dual extrusion printer, using standard 1.75 mm PLA filament. PDDs were compared between the Advanced Markus (official TRUFIX) and microDiamond (printed TRUFIX) to verify EPOM placement. Setup using the printed Farmer holder was verified visually in the water tank.

Results Two detector holders were successfully printed and both interface well with the official TRUFIX hardware. PDD comparison between the Advanced Markus and microDiamond showed very good agreement, indicating correct positioning of the EPOM using the 3D printed cap. The Farmer holder has successfully been used multiple times for absolute dose measurements, with users indicating excellent agreement between TRUFIX and where they would position the chamber manually.

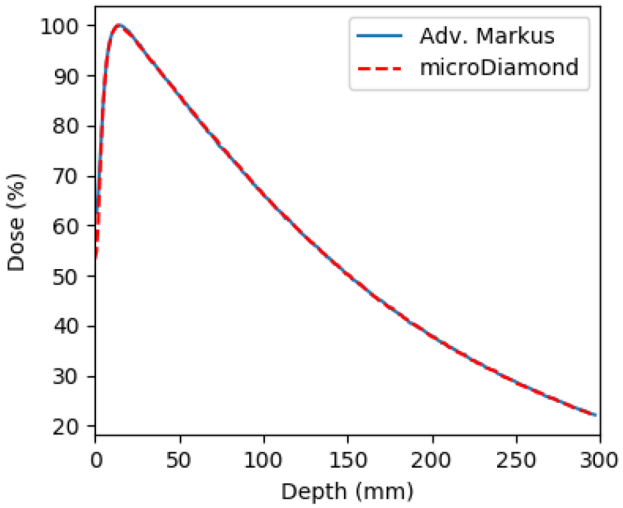

Fig. 22 PDD comparison between PTW (Adv. Markus) and 3D printed (microDiamond) TRUFIX

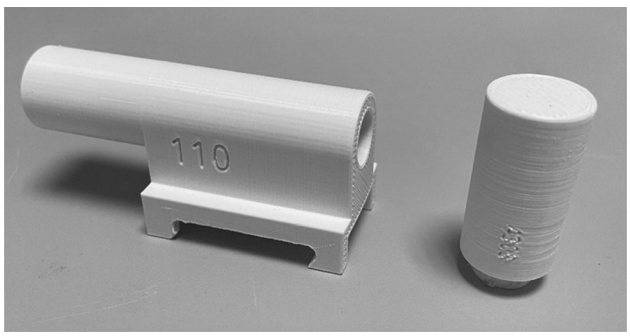

Fig. 23 3D printed holders for Farmer (left) and microDiamond (right)

Conclusion TRUFIX-compatible holders for two PTW detectors were designed and 3D printed. This process can then be repeated in the future for any non-PTW detector to become TRUFIX-compatible if the position of its EPOM is well-characterized.

O118 3D printed tissue & bone equivalent anthropomorphic head phantom for electron beam validation

L. K. Webb[1], **S. B. Crowe**[2,3,4,5], **L. Heseltine**[2], **P. H. Charles**[3,4,5], **T. Kairn**[2,3,4,5]

[1]Radiation Oncology, Princess Alexandra Hospital, Ipswich Road, Australia. luke.webb@health.qld.gov.au (Presenting author); [2]Cancer Care Services, Royal Brisbane and Women's Hospital, Brisbane, Qld, Australia; [3]Herston Biofabrication Institute, Metro North Hospital and Health Service, Brisbane, Qld, Australia; [4]School of Information Technology and Electrical Engineering, University of Queensland, Brisbane, Qld, Australia; [5]School of Chemistry and Physics, Queensland University of Technology, Brisbane, Qld, Australia

Introduction Commissioning of treatment planning algorithms culminate in end-to-end validation in anthropomorphic phantoms,

simulating both patient anatomy & heterogeneities. Finding a suitable phantom to undertake such a task for electron beams proved difficult, so one was 3D printed. This process has been explored in depth for photon beams [1], but is rarely considered for electron beams.

Method The phantom was designed using CT data of a total body irradiation patient in a recumbent position. 3D models of the three primary tissue compositions (tissue, bone & air) were segmented and smoothed in 3DSlicer (version 4.1). Mesh operations & slicing of the 3D models into 5 mm slabs with alignment rods were performed in Python using the Pymesh module. The slabs were prepared for printing on a Raise3D Pro 2 using ideaMaker (version 3.6.1). Tissue & bone-equivalent regions were printed using eSun PLA + (85% infill) and StoneFil Concrete (100% infill) respectively to achieve the desired tissue equivalence [2]. The phantom underwent CT simulation and was transferred to Monaco 5.51, where a 9 MeV electron treatment with 14 × 14 cm^2 applicator, 12.6 cm circle cut-out and 99 cm SSD was planned using the eMc dose algorithm. EBT3 film was cut and positioned at a depth of 2 cm. Film was compared to the TPS fluence at the same depth using a 5%/3 mm gamma criteria.

Results The completed phantom (Fig. 1-left) was validated using MVCT achieving a nominal RED of 0.97 ± 0.03 and of 1.38 ± 0.04 for the tissue and bone regions. Gamma analysis between film measured in the phantom and simulated dose from the TPS using the stated REDs achieved a pass rate of 95.2% (Fig. 1-right).

Conclusion Custom 3D printed tissue & bone equivalent anthropomorphic phantoms can be printed which enable the validation of electron treatment beams in scenarios closer to the complexities (anatomical shape & heterogeneities) found in real patients.

References/Acknowledgements

1. S. Crowe, "Personalized phantoms through 3D printing", Radiotherapy and Oncology 133(S1): s362, 2019
2. Kairn T, Buddhavarapu A, Cassim N, Charles PH, Jessen L, Crowe SB (2021) Lessons learnt on the road to fabricating materials that are bone-equivalent in both kilovoltage and megavoltage photon beams. Engineering and Physical Sciences in Medicine conference, Brisbane 2021 (submitted)

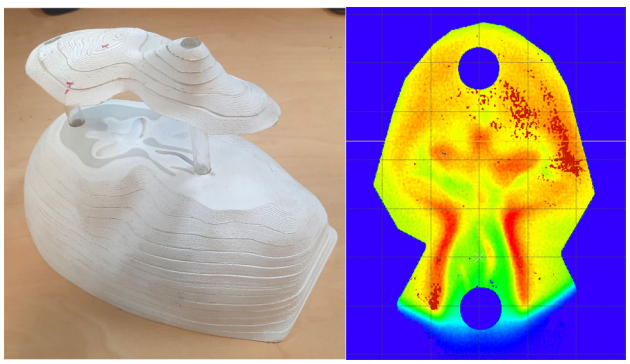

Fig. 24 (Left)—completed anthropomorphic phantom shown with alignment rods, (Right) Gamma Analysis results overlaid onto film

O119 An evaluation of solid state detectors for the relative dosimetry of Kilovoltage x-ray beams

J. Daniel[1], Y. Yousif[1], W.-L. Hsieh[1], J. Zifodya[1], R. Hill[2,3]

[1]North West Cancer Centre, Tamworth, Australia. John.Daniel@health.nsw.gov.au (Presenting author); Yousif.Yousif@health.nsw.gov.au; WenLong.Hsieh@health.nsw.gov.au; Jackson.Zifodya@health.nsw.gov.au; [2]Department of Radiation Oncology, Chris O'Brien Lifehouse, Sydney, Australia; [3]Institute of Medical Physics, School of Physics, University of Sydney, Australia. Robin Hill Robin.Hill@lh.org.au

Introduction Kilovoltage (KV) x-ray beams are an important modality in radiotherapy(1). Solid-state detectors are widely available in radiotherapy departments, but their use for KV dosimetry has been limited to date. The purpose of this study was to evaluate the dosimetric performance of a range of solid-state detectors for KV dosimetry.

Method Percentage depth doses (PDDs) and output factors (OFs) were measured in a PTW-MP1 water-tank on an XStrahl 300 unit (XStrahl-Ltd., UK) using the 100kVp (HVL 2.86 mm-Al) and 300kVp (HVL 3.08 mm-Cu) beams. Circular applicators with field sizes of 2–10 cm diameters and SSD-30 cm and square applicators with field sizes of 10 × 10 and 20 × 20 cm and SSD-50 cm were used for 100 kVp and 300 kVp beams, respectively. PTW radiation detectors used were; Advanced-Markus, 3D-Pinpoint, Semiflex chambers, Photon, Electron and SRS diodes and micro-Diamond detector. All PDDs were normalized at 5 mm depth, and OFs were measured at 3 mm depth to avoid collisions with the applicators. OFs measured using chambers were corrected for polarity and ion-recombination effects.

Results PDDs for the 100 kVp beam showed good agreement between all diodes and the chambers over the full-depth except in the first few mm near the surface. However, for the 300 kVp, all diodes over-responded as compared to reference advanced-Markus PDDs (Fig. 1). Diode's OFs were relatively higher compared to the advanced-Markus at 100KVp. The magnitude of these differences is inversely proportional to the field sizes. The P-diode showed the highest variation of up to 15% in the OF compared to the advanced-Markus.

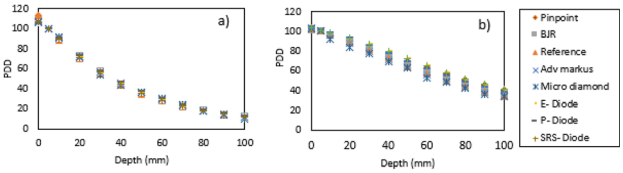

Fig 1. (a): PDDs for a 100 kVp x ray beam (HVL of) with a 10 cm diameter and an FSD of 30 cm. (b): PDDs for 300 kVp x-ray beam with a 10x10 cm field size and an FSD of 50 cm.

Conclusion PDD measurements showed that diode detectors could be a suitable for lower energy x-ray beams but not for higher beam energies. A large variation in the measured OFs at lower energies for the diodes showed they might not be suitable as a direct replacement for ionization chambers.

Reference

1. Li XA, Salhani D, Ma C. Characteristics of orthovoltage x-ray therapy beams at extended SSD for applicators with end plates. Physics in Medicine & Biology. 1997;42(2):357.

O120 Dosimetric impact of absorber purity in the measurement of half value layer (HVL) for kilovoltage radiotherapy

I. Peters[1], A. Gray[1,2,3], V Nelson[1]

[1]Liverpool and Macarthur Cancer Therapy Centres, Sydney, NSW. Iliana.peters@health.nsw.gov.au; [2]Ingham Institute for Applied Medical Research, Liverpool NSW; [3]South Western Sydney Clinical School, UNSW, Liverpool NSW. Alison.Gray@health.nsw.gov.au; Vinod.Nelson@health.nsw.gov.au

Introduction Beam quality for kilovoltage beams is specified by the peak potential (kVp) and the half value layer (HVL) absorber thickness. The HVL is important for determining parameters used for monitor unit calculations and reference dosimetry. The 2018 ACPSEM kilovoltage position paper recommends an absorber purity > 99.9%, based on the AAPM dosimetry protocol. Other protocols (IPEMB, IAEA) recommend 'high purity' absorbers. Absorbers of different purity are available, however 99.99% purity is over 15 × the price of the 99% purity. A 99% purity aluminium absorber set was available locally but 99.99% absorbers were purchased to comply with the recommendations. A comparison of HVL measured with the sets was completed and the dosimetric impact of the change assessed.

Method ACPSEM recommendations were followed for all methodology. HVL measurements utilising the two absorber sets were conducted. The 99% values were compared to the 99.99% reference value. The absorbed dose to water was also calculated based on the two sets of results. The measurement uncertainty was estimated using repeated measurements for one beam quality.

Results The HVL thicknesses measured for beams of 40–150 kVp ranged from 0.8–6.6 mm Al.

The maximum absolute HVL difference between the two purity sets was 0.07 mm Al for the 5.09 mm Al (120 kVp) beam. The maximum percentage difference was -1.7% for the 2.38 mm Al (80 kVp) beam (Fig. 1). The average absolute difference for all beams was 0.8% ± 0.6% (1SD). The maximum difference in absorbed dose to water calculated was 0.13%.

Conclusion The HVL variation between the 99% and 99.99% purity absorbers was within 2%, resulting in an absolute dose determination difference of < 0.2%. Based on these results, a 99% aluminium absorber may be considered for HVL measurement if a higher purity set is unavailable.

Acknowledgements Thanks to the Macarthur Cancer Therapy Centre Physics team for assisting with measurements.

References

1. Hill R, Healy B, Butler D, Odgers D, Gill S, Lye J, Gorjiara T, Pope D, Hill B. Australasian recommendations for quality assurance in kilovoltage radiation therapy from the kilovoltage Dosimetry Working Group of the Australasian College of Physical Scientists and Engineers in Medicine. Australas Phys Eng Sci Med. 2018 Dec;41(4):781–808
2. Ma CM, Coffey CW, DeWerd LA, Liu C, Nath R, Seltzer SM, Seuntjens JP (2001) AAPM protocol for 40–300 kV X-ray beam dosimetry in radiotherapy and radiobiology. Med Phys 28(6):868–893
3. Prepared by Klevenhagen SC, Aukett RJ, Harrison RM, Moretti C, Nahum AE, Rosser KE (1996) The IPEMB code of practice for the determination of absorbed dose for X-rays below 300 kV generating potential (0.035 mm Al-4 mm Cu HVL; 10–300 kV generating potential). Phys Med Biol 41(12):2605–2625
4. IAEA (2006) Absorbed dose determination in external beam radiotherapy: An international code of practice for dosimetry based on standards of absorbed dose to water v.12. International Atomic Energy Agency, Vienna

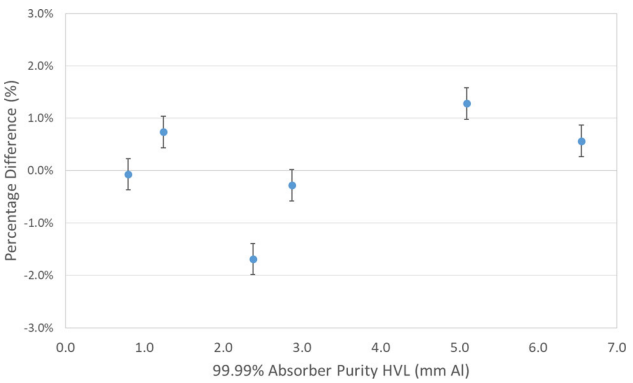

Fig. 25 Difference in HVL between 99% and 99.99% absorber purity

O121 Changing Penumbras: Assessment of variation in kV lead shield edge effects

E. Simpson-Page[1], S. Maxwell[1], N. Cassim[1], T. Kairn[1,2,3,4], S. B. Crowe[1,2,3,4]

[1]Cancer Care Services, Royal Brisbane and Women's Hospital, Brisbane. Emily.simpson-page@health.qld.gov.au (presenting author); sarah.maxwell@health.qld.gov.au; naasiha.cassim@health.qld.gov.au; [2]Herston Biofabrication Institute, Metro North Hospital and Health Service, Brisbane, Queensland, Australia; [3]School of Information Technology and Electrical Engineering, University of Queensland, Brisbane, Queensland, Australia; [4]School of Chemistry and Physics, Queensland University of Technology, Brisbane, Queensland, Australia. tanya.kairn@health.qld.gov.au; scott.crowe@health.qld.gov.au

Introduction Superficial and orthovoltage treatments with lead shields can result in increased dose at the field edge, due to electron contamination. These 'edge effects' can be up to three times the central dose for 300 kV beams [1]. At Royal Brisbane & Women's Hospital, lead shields are created with serrated edges, nominally used to avoid a sharp dose fall off to prevent abrupt hyperpigmentation or inflammation. However, these serrations have been reported to increase electron contamination dose [1]. The aim of this study was to characterise edge effects for various serrations and to observe whether rotation of serrated edges with variation in clinical positioning over a standard fractionation scheme contributes to the reduction of edge effects.

Method EBT3 measurements were performed for 3 shielding options using a WOmed T300 superficial unit, for two beam qualities; 100 kV 4.13 mm Al and 300 kV 2.4 mm Cu. For each measurement, four rotationally-shifted profiles were averaged to simulate shield rotation. A physical rotation measurement was performed for verification of this approach.

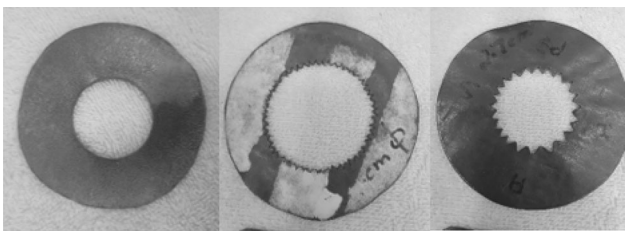

Fig. 26 Variations in serrations at RBWH. From left to right: No serration (2 cm field), Small Serration (3 cm field) and Large serration (2 cm field)

Results The edge effect was effectively removed with a single physical rotation in measurements for the large serration shield. For the 300 kV beam, the small teeth 3 cm field and large teeth 2 cm field had reduced edge effects with rotation applied. The edge effects were not present in the 100 kV beam but were increased in the 300 kV beam for all field sizes.

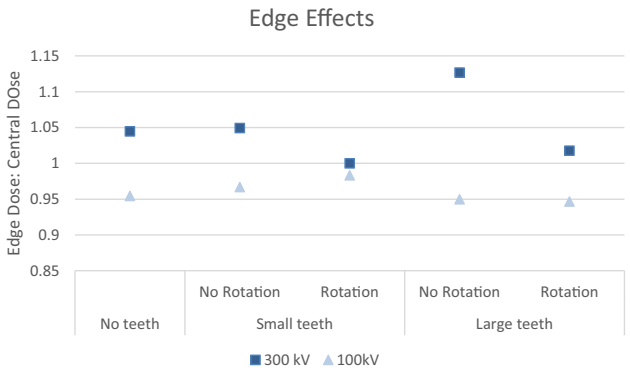

Fig. 27 Edge effects for each shield, with no rotation and averaged over four rotations

Conclusion No edge effects were observed for the 100 kV beam, due to limited electron range. For the 300 kV beam, the edge effect was most prominent for large serrations with no rotation. This was greatly reduced with applied rotations. Variations in clinical positioning of the shield can reduce the edge effect, and should be considered if designing shields with high positional reproducibility (e.g. patient-matched 3D-printed shielding).

Reference

Lye JE, Butler DJ, Webb DV (2010) Enhanced epidermal dose caused by localized electron contamination from lead cutouts used in kilovoltage radiotherapy. *Med Phys 37*(8): 3935–3939.

O122 An evaluation of Ion recombination and polarity effect for ionization chambers in Kilovoltage X-ray beams

Y. Yousif[1], J Daniel[1], W-L Hsieh[1], J. Zifodya[1], R. Hill[2,3]

[1]North West Cancer Centre, Tamworth, Australia. Yousif.Yousif@health.nsw.gov.au (Presenting author); John.Daniel@health.nsw.gov.au; WenLong.Hsieh@health.nsw.gov.au; Jackson.Zifodya@health.nsw.gov.au; [2]Department of Radiation Oncology, Chris O'Brien Lifehouse, Camperdown, NSW 2050, Australia; [3]School of Physics, Institute of Medical Physics, University of Sydney, Sydney, NSW 2006, Australia. Robin.Hill@lh.org.au

Introduction Ionization chambers are commonly used for routine measurements in kilovoltage x-ray dosimetry. The recommendations for the need to apply ion recombination and polarity corrections vary in different dosimetry codes of practice. In addition, there is limited data on absolute values of these corrections for some ionization chambers. In this study, five different ionization chambers were investigated for the measurements of the ion recombination and polarity effect for kilovoltage x-ray beams.

Methods Two PTW plane-parallel chambers, the Roos and Advanced Markus and three PTW cylindrical chambers, Pinpoint, Semiflex and Farmer, were employed to measure Ion recombination and polarity factors for kilovoltage beams produced from an Xstrahl 300 unit (Xstrahl Ltd., UK). All measurements were acquired at 2 cm depth in PTW-MP3 water-tank for beams between 60 kVp (HVL 1.29 mmAL) and 300 kVp (HVL 3.08 mmCu), and field sizes of 2–10 cm diameter for 30 cm SSD and 4 × 4 cm2—20 × 20 cm2 for 50 SSD. The chambers were connected to a PTW-UNIDOS electrometer and the ion recombination was determined using the two-voltage method and the polarity effect determined as per AAPM TG-61.[1]

Results All chambers exhibited a negligible ion recombination effect; the maximum recorded value was 0.2% for Advanced Markus. Results revealed large polarity effects, up to 9% and 11%, for the advanced Markus and Pinpoint, respectively. In comparison, the polarity corrections were 0.9%, 0.4% and 0.1% for the Roos, Semiflex and Farmer, respectively. The magnitude of the polarity effect increases with the increase in the field size, beam energy and is strongly depended on the chamber's sensitive volume. Overall, the results agreed well with the published literature.[2]

Conclusion Ionization chambers exhibited large polarity effects, particularly for those with smaller volumes. Therefore, polarity correction should be considered when performing relative dose measurements in kilovoltage x-ray beams.

References

1. Ma CM, Coffey CW, DeWerd LA, et al. AAPM protocol for 40–300 kV x-ray beam dosimetry in radiotherapy and radiobiology. *Med Phys.* 2001;28(6):868–893.
2. Dowdell S, Tyler M, McNamara J, Sloan K, Ceylan A, Rinks A. Potential errors in relative dose measurements in kilovoltage photon beams due to polarity effects in plane-parallel ionisation chambers. *Phys Med Biol.* 2016;61(23):8395–8407.

O123 Commissioning a Monte Carlo model of a kilovoltage radiotherapy unit

S. B. Crowe[1,2,3,4], E. Simpson-Page[1], P. Charles[2,3,4], T. Kairn[1,2,3,4]

[1]Cancer Care Services, Royal Brisbane and Women's Hospital, Brisbane, Queensland, Australia; [2]Herston Biofabrication Institute, Metro North Hospital and Health Service, Brisbane, Queensland, Australia; [3]School of Information Technology and Electrical Engineering, University of Queensland, Brisbane, Queensland, Australia; [4]School of Chemistry and Physics, Queensland University of Technology, Brisbane, Queensland, Australia. sb.crowe@gmail.com (Presenting author); emily.simpson-page@health.qld.gov.au; paul.charles@health.qld.gov.au; tanya.kairn@health.qld.gov.au

Introduction The determination of dose for kilovoltage radiotherapy treatments is typically limited to a surface reference point, without consideration of the patient anatomy. This prevents informed clinical decision making and comparisons of kilovoltage therapy to other superficial treatment techniques (i.e. electrons, VMAT and brachytherapy). Monte Carlo algorithms provide a means to accurately calculate dose but require the optimisation of a source model. This study describes a simple, accessible and robust method for commissioning an EGSnrc model of a WOmed T-300 unit (with energies 50–300 kV).

Method Geometric and material data for the treatment unit head and applicator were taken from vendor material, physical measurements

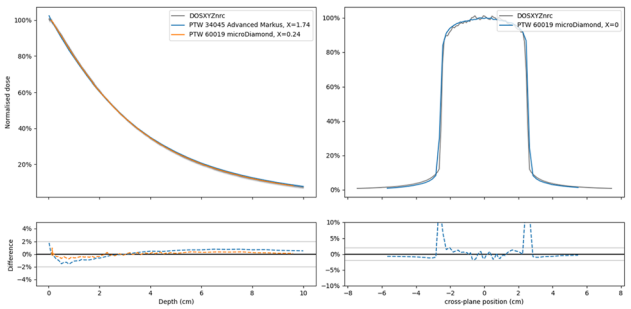

Fig. 1 (Left) percentage depth dose, (right) off-axis profile

and published data; with no specific request made for specifications from vendors. Software was developed using Python to automatically create EGSnrc input files with variable initial electron energies, batch submission scripts, and to characterise and plot agreement for percentage depth-dose and off-axis profiles. Agreement between measured and simulated data was characterised using reduced chi-squared statistics. Isodose data was subsequently simulated to supplement existing basic planning data, due to time required to perform these measurements for each energy, filter and applicator combination.

Results Simulated optimal energies were within 5% of nominal x-ray tube energies for all beams, with reduced chi-squared statistics calculated for a reference 5 cm diameter applicator being between 0.2 and 1.3 (where ≤ 1 is agreement within statistical uncertainties). Results for a nominal 100 kV 2.90 mm Al HVL beam are shown in Fig. 1. Improved agreement was observed between microDiamond and simulation results, compared to Advanced Markus measurements.

Conclusion Monte Carlo simulations allow accurate estimation of dose to supplement measurements or on a patient-specific basis, and models can be optimised without detailed vendor specifications.

O124 Development of a Monte Carlo model to evaluate the angular dependence of a 2-D high spatial resolution silicon array detector used for dosimetry in stereotactic radiotherapy

I. Filipev[1], G. Biasi[1,2], S. Guatelli[1], T Kron[2], A. Rosenfeld[1]

[1]Centre for Medical Radiation Physics, University of Wollongong, Wollongong, NSW, Australia. if889@uowmail.edu.au; [2]Peter MacCallum Cancer Centre, Melbourne, VIC, Australia. gbiasi@uow.edu.au; susanna@uow.edu.au; Tomas.Kron@petermac.org; anatoly@uow.edu.au

Introduction The aim of this study was to develop a beam-detector model, based on the Octa, a 2-D array of 512 silicon diodes with a spatial resolution of 0.3 mm, designed at the Centre for Medical Radiation Physics, and to use the model for the evaluation of the detector angular dependence and as a core model for future studies on the "Octa" for stereotactic radiotherapy (SRT) [1].

Methods The GEANT4 toolkit was used for Monte Carlo (MC) simulations [2]. The radiation source was modelled using phase-space files provided by the IAEA (CyberKnife System 10 mm beam with IRIS collimator) [3]. The "Octa" model was placed in the centre of a water-equivalent phantom (30 cm in diameter, 30 cm in length), both placed at the isocentre, and irradiated at angles from 0 to 90 degrees (at 0 degrees the beam is normal to the detector surface), source-to-centre-of-detector distance was 100 cm. Results were compared with previous experimental studies [4] and additional modelling was done

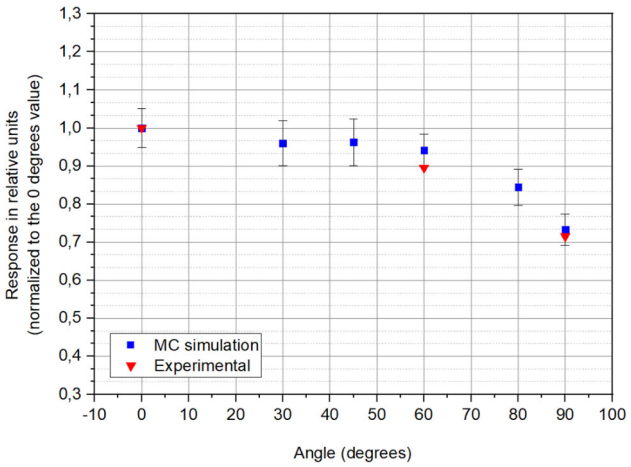

Fig. 1 Relative response of "Octa" central diodes as a function of the radiation-beam incidence angle: MC simulation of deposited energy averaged over the nine central diodes (error bars – standard error) and experimental measurements under similar conditions [4]

to analyse the influence of different detector components and geometry on the angular dependence.

Results Characterization of the "Octa" and its irradiation under the CyberKnife beam was achieved with the developed model. The detector angular dependence was assessed and showed good agreement with the experiment (Fig. 1). Additional MC studies of how different detector components and geometry influence angular dependence will be discussed.

Conclusion A working MC model for the irradiation of the "Octa" detector with sources used for SRT was developed and will constitute an essential component in the studies of the "Octa", and of similar detectors for SRT dosimetry.

Acknowledgements Gross Foundation.

References

1. Biasi G, Petasecca M, Guatelli S, Hardcastle N, Carolan M, Perevertaylo V, et al. (2018) A novel high-resolution 2D silicon array detector for small field dosimetry with FFF photon beams. Physica Medica. 45:117–26.
2. Agostinelli S, Allison J, Amako Ka, Apostolakis J, Araujo H, Arce P, et al. (2003) GEANT4—a simulation toolkit. Nuclear instruments and methods in physics research section A: Accelerators, Spectrometers, Detectors and Associated Equipment. 506(3):250–303.
3. Capote R, Jeraj R, Ma C, Rogers DW, Sánchez-Doblado F, Sempau J, et al. (2006) Phase-space database for external beam radiotherapy. Summary report of a consultants' meeting.
4. Biasi G, Hardcastle N, Petasecca M, Guatelli S, Perevertaylo V, Kron T, et al. (2018) On the instantaneous dose rate and angular dependence of monolithic silicon array detectors. IEEE Transactions on Nuclear Science. 66(1):519–27.

O125 Evaluation of the effectiveness of steel for shielding photoneutrons produced in medical linear accelerators: A Monte Carlo particle transport study

L. Moghaddasi[1,2], C. J. Colye[3]

[1]Department of Medical Physics, Austin Health, Ballarat, Victoria, Australia; [2]School of Physical Sciences, University of Adelaide,

Adelaide, Australia. leyla.moghaddasi@austin.org.au (Presenting author); [3]GenesisCare, Kurralta Park, South Australia. christopher.colyer@genesiscare.com

Introduction In the context of radiation shielding for linear accelerator bunkers, there is little information on the effectiveness of steel for shielding neutrons. This study hopes to confirm the effectiveness of steel as a material for shielding photoneutrons produced in medical linear accelerators (linac) and report values for neutron first and second tenth value layer (TVL) to be used as radiation protection quantities.
Method Monte Carlo code Geant4 was used to simulate transport of photoneutrons through primary barriers containing layers of concrete and steel. The photoneutron spectrum generated in high energy linac head components was simulated and projected to barriers of different thicknesses of steel including a control case of no barrier. To derive the TVL, absorbed dose was evaluated at 1 cm depth in a water phantom outside the barrier. The fluence and energy spectrum of neutrons leaking outside the barrier were also calculated. The neutron model was used to quantitatively assess the neutron shielding for a newly designed bunker to be installed.
Results For a 10 MV photon beam produced by a linear accelerator, the first and second TVLs for steel as a neutron shielding material were determined to be 16.8 cm and 25.3 cm respectively. The lateral distribution of neutrons outside of steel barriers is shown to narrow with increasing thickness. Investigation of neutron energy spectrum outside barrier demonstrated that steel predominantly absorbs the fast neutron component of a photoneutron spectrum, resulting in production of thermal and epithermal neutrons, whose numbers increase with increasing steel thickness up to approximately 30 cm, Fig. 1.
Conclusion This paper agrees with previous studies for Pu-Be sources, and we would advocate using these values for the purposes of linear accelerator bunker design. In addition, it was shown that the newly designed bunker provides sufficient shielding against photoneutrons produced by the linac.

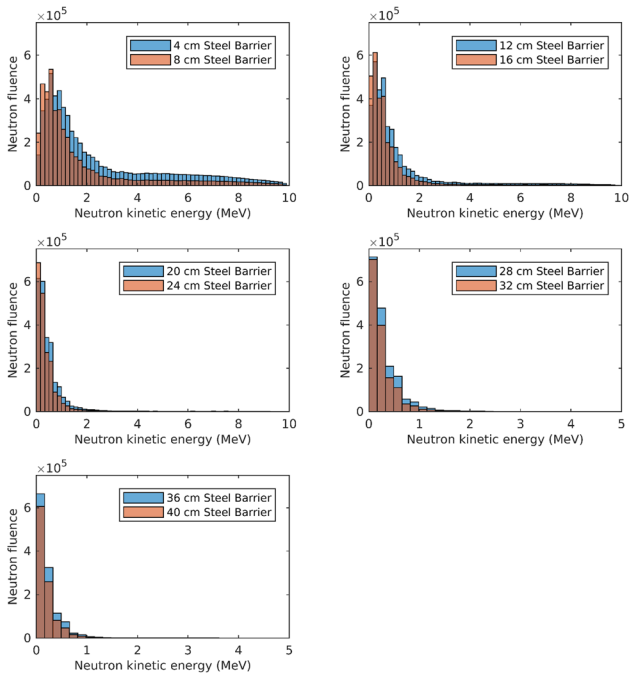

Fig. 1 Neutron energy spectrum calcualted at 10 cm outside steel barrier of different thicknesses

O126 Implementing cloud based Monte Carlo calculations for radiotherapy – the Amazon Web Service experience

J. E. Morales[1], Chris O'Brien Lifehouse[2]

[1]Department of Radiation Oncology, Sydney, Australia. johnny.morales@lh.org.au (Presenting author); [2]Queensland University of Technology, Brisbane, Australia

Introduction Monte Carlo calculations for radiation transport in radiotherapy are fundamental for accurate dose calculations in tissue and other different human body tissues such as lung and bone where electronic equilibrium is lost. However, these calculations demand high computing processing power. In this poster, work is presented on the use of cloud based services, such as the Amazon Web Service (AWS), to facilitate high computing power without the need of buying expensive servers that usually require clean rooms and a lot of air conditioning.
Method A linux server was created using one of the instances available on the AWS. An instance is referred to a specific machine type which can in turn be configured with a specific operating system. The EGSnrc (NRC, Canada) packaged was installed and configured to run on this server. Calculations were performed to simulate a Varian TrueBeam (Palo Alto, USA) linear accelerator. The space phase files used for these calculations were obtained from Varian Medical Systems and were based on the IAEA format. Calculations were performed for percentage depth doses and cross profiles for a 6 MV WFF beam of 10×10 cm^2 field size at 100 cm SSD.
Results Fig. 1 shows the PDD and cross profiles obtained for the 10×10 cm^2 field size on a $40 \times 40 \times 40$ cm square box water phantom. These calculations were repeated using different AWS Instances to compare the speed of calculations and the cost required for each Instance.
Table 1 Shows the different AWS Instance configurations, time take to perform a DOSXYZnrc calculation and possible cost involved for these calculations.

AWS Instance	Available vCPU	vCPUs used for calc	No of histories	Time (sec)	Approx. Cost (AUD)/hr
c5.18xlarge	64	64	1,500,000,000	1264	3.9960
c5.18xlarge	72	1	1500	7.9	3.9960
t3a.2xlarge	8	1	1500	12.1	0.3802
c4.8xlarge	32	1	1500	8.2	2.0850

Conclusion The results obtained in this work provide a practical overview of what Instance would be most appropriate for different situations and the cost incurred in each situation.

O127 Monte Carlo simulation of the RefleXion™ X1 radiotherapy machine

Oluwaseyi M. Oderinde[1], Daniel Zaks[1], Cal Huntzinger[1], Shervin M. Shirvani[1], Thomas Laurence[1], Gopinath Kuduvalli[1], Minghui Lu[1]

[1]RefleXion Medical, Hayward, CA, USA. ooderinde@reflexion.com (Presenting author); dzaks@reflexion.com; cal@reflexion.com;

sean@reflexion.com; thomas.laurence@reflexion.com; gkuduvalli@reflexion.com; mlu@reflexion.com

Introduction The RefleXion™ X1 radiotherapy machine is a novel combination of positron emission tomography (PET) and computed tomography (CT) technologies with a 6 MV linear accelerator, with the intent of using tumor-PET to guide beamlet delivery in real-time. The present work developed an accurate Monte Carlo (MC) model of the RefleXion™ X1 machine.
Method The EGSnrc user code was utilized in this study. The linear accelerator head was modeled for 1.25, 2.5, 5, 10, 20, and 40 cm MLC opening leaves with 1 and 2 cm jaw openings defined at source-to-surface distance of 85 cm. The phase space file scored downstream the backup jaws was used for simulating the dose distribution in a virtual water phantom of 60 × 30x24 cm^3 with ~ 100 billion histories. The percentage depth doses (PDDs), lateral dose-profiles, and relative output factors were calculated using 1 × 1x1 mm^3 voxel size and compared with measurements. The measurements were done using Standard Imaging Exradin D1H Diode detector in a Blue phantom Helix. The difference between the MC calculation and the measurement data was analyzed using the local percentage difference for relative Outputs (ROFs) and gamma criteria of 2%/2 mm for PDDs and lateral beam profiles.
Results There was good agreement between measurements and MC simulation ROFs, with differences less than 2% for all measured parameters. In addition, MC simulated PDDs and lateral beam profiles had an average gamma pass rate of 99.08% ± 0.05% and 96.36% ± 6.17%, respectively. The deviation between the measurement and MC lateral beam profiles was pronounced within the penumbra region, which increases with an increase with depth in the virtual water phantom.
Conclusion This study shows that the MC model is accurate for the RefleXion X1 machine. The model has the potential to be used for further dosimetric studies such as secondary dose check and patient treatment plan quality assurance.

O128 Monte Carlo simulation of small fields for megavoltage photon beams

N. P[1], P. Ramachandran[2,3], V. Seshadri[3,4], B. Perrett[5], A. Fielding[6]

[1]Research Assistant, Princess Alexandra Hospital, QLD. Nazia.parveen@health.qld.gov.au (Presenting Author); [2]Director of Therapeutic Physics; [3]Princess Alexandra Hospital, QLD. Prabhakar.Ramachandran@health.qld.gov.au; [4]Medical Physicist, Treatment Team Leader. Venkatakrishnan.seshadri@health.qld.gov.au; [5]Senior Medical Physicist, Princess Alexandra Hospital, QLD. Ben.Perrett@health.qld.gov.au; 6Senior Lecturer, Queensland University of Technology

Introduction The aim of this study is to simulate the beam characteristics of small fields produced on a Versa HD linear accelerator and compare the results against a W2 scintillator.
Method The W2 scintillator detector was used to measure the inline and crossline profiles and the output factors at 10 cm depth and 90 SSD for 6MV photon beams. The field sizes ranged from 0.5 cm × 0.5 cm to 5 cm × 5 cm. Reference profiles were simulated using the EGSnrc-based Monte Carlo codes: BEAMnrc and DOSXYZnrc. Gamma analysis was performed to compare between simulated profile data and data measured with the W2.
Result Gamma analysis of the crossline profiles showed a pass rate of 100% at gamma criteria 3%/1.5 mm for 0.5 cm × 0.5 cm, 96% for 3 cm × 3 cm, 93% for 4 cm × 4 cm and 97% for 5 cm × 5 cm at the same criteria. The percentage difference in the output factor of the W2 scintillator detector and simulated data was measured to be 1% for 3 cm × 3 cm and 2 cm × 2 cm, 2% for 1 cm × 1 cm.
Conclusion The lateral beam profiles measured with the W2 scintillator detector had excellent agreement with the Monte Carlo simulation inside the treatment field but exhibited a small variation in the penumbral region which becomes more evident as the field sizes decreases. Excellent agreement between the W2 measured and simulated output factors was observed for field sizes greater than 0.6 cm × 0.6 cm. The variation for field size less than 0.6 cm × 0.6 cm field size could be attributed to the small field conditions.

O129 Radiation-Induced Second Cancer Risk from Proton Beam Therapy for Paediatric Cranial Cancer: Age and Sex Impact on Out-of-Field Organs

Mikaela Dell'Oro[1,2], Dylan David Peukert[3], Michala Short[1], Puthenparampil Wilson[2,4], Eva Bezak[1,5]

[1]Cancer Research Institute, University of South Australia, Adelaide, SA 5001, Australia; [2]Department of Radiation Oncology, Royal Adelaide Hospital, Adelaide, SA 5000, Australia. mikaela.delloro@mymail.unisa.edu.au (Presenting author); [3]ARC Training Centre for Integrated Operations for Complex Resources, University of Adelaide, Adelaide, SA 5005, Australia. dylan.peukert@adelaide.edu.au; michala.short@unisa.edu.au; [4]UniSA STEM, University of South Australia, Adelaide, SA 5001, Australia. puthenparampil.wilson@unisa.edu.au; [5]Department of Physics, University of Adelaide, Adelaide, SA 5005, Australia. eva.bezak@unisa.edu.au

Introduction Proton beam therapy (PBT) is the optimal radiotherapy for treating paediatric cranial malignancies based on the superior physical properties. PBT reduces radiation-induced side effects including second primary cancer (SPC) induction and consequently improves overall quality of life. Despite the high number of paediatric patients treated with radiotherapy, specific risk factors for SPC are still not fully understood. This study aims to estimate the risk of radiation-induced SPC as a function of age and sex for out-of-field organs (e.g. salivary gland and small intestine) following scattering and scanning PBT for select paediatric cranial irradiation.
Method A total of 108 intensity-modulated PBT plans were robustly optimised in Eclipse (Varian, version 13.7) for tumour volumes using age-specific paediatric CT scans (5, 9 and 13 years-of-age). Dose-volume data were extracted for a range of simulated tumour volumes and plans. Scattered and scanning PBT neutron dose equivalents were sourced from Polf et al. [1] and Schneider et al. [2] respectively. Values adjusted for doses delivered were then input into Schneider et al.'s [3] model using MATLAB (R2020B) to calculate the lifetime attributable risk (LAR) of SPC per organ distance.
Results Preliminary results for scanning PBT [2] demonstrated smaller LAR risk of SPC (Table 1) compared to scattering PBT [1] (Table 2). Expectantly scattering PBT produced a higher LAR of SPC. Both scanning and scattering PBT depended on age and sex gender, increasing the LAR of SPC for 5-year-old females. However, outliers exist for the estimation of LAR with scattering PBT for the lung, stomach, liver, rectum. Further investigation is warranted.
Conclusion The study compared latest clinically relevant scanning and scattering PBT across age and sex-specific simulated clinical scenarios. Modified LAR calculations can be used to predict risk of SPC and matched back to clinical data.
Acknowledgements St. Jude Children's Research Hospital.
References

Table 1 Organ-specific LAR estimates for Scanning Pencil Beam Proton Therapy presented by sex and age [2]

Organ	Female (per 10 000 person years)			Male (per 10 000 person years)		
	5	9	13	5	9	13
Mouth	76.9	44.4	43.9	41	32	33.2
Salivary Gland	38.8	20.5	18.9	20.7	16	14.5
Thyroid	217	80	54.3	90	52.9	32.9
Oesophagus	13.2	5.6	5.5	5.2	3.9	2.9
Lung	80.2	37.8	38.2	35	26.9	21.2
Breast	279	111	91.5	128	78.7	55
Stomach	37.6	20.1	17.8	20.1	14.8	10.9
Liver	29	13.2	13	13.5	9.8	5.9
Colon	89.6	46.7	30.2	55	27.7	19.1
Small Intestine	79.7	39.7	30.1	43.3	28.6	14.1
Rectum	1.8	0.9	0.6	1	0.6	0.4
Bladder	9	4.6	3.5	5.1	3	1.9
Reproductive organs	3.3	1.7	1.1	1.3	0.7	0.4

Key: Reproductive organ for males is testes and for females it is ovaries

Table 2 Organ-specific LAR estimates for Scattering Proton Therapy [1]

Organ	Female (per 10 000 person years)			Male (per 10 000 person years)		
	5	9	13	5	9	13
Mouth	158	147.8	140.5	104.2	98.9	94.4
Salivary Gland	59.9	57.7	54.9	40	38.4	36.6
Thyroid	935	758	621	627	516	421
Oesophagus	102	98	100	65.9	66.1	66
Lung	771	768	817	495	511	523
Breast	2875	2487	2216	1905	1683	1478
Stomach	169	175	181	113	117	122
Liver	69.7	71.8	69.5	47	46.9	48.2
Colon	196	190	174	129	125	120
Small Intestine	71.7	65.4	57.2	47.2	42.4	43.2
Rectum	0.4	0.5	0.6	0.3	0.3	0.4
Bladder	94.9	113	115	67	75.6	82.5
Reproductive organs	1.4	1.3	1.1	1	0.9	0.8

Key: Reproductive organ for males is testes and for females it is ovaries

1. Polf, J.C., Newhauser, W.D., 2005. Calculations of neutron dose equivalent exposures from range-modulated proton therapy beams. Phys Med Biol 50(16), 3859–3873.
2. Schneider, U., Agosteo, S., Pedroni, E., Besserer, J., 2002. Secondary neutron dose during proton therapy using spot scanning. Int J Radiat Oncol Biol Phys. 53(1), 244–251.
3. Schneider, U, Sumila, M, Robotka, J, 2011. Site-specific dose–response relationships for cancer induction from the combined Japanese A-bomb and Hodgkin cohorts for doses relevant to radiotherapy. Theor Biol Med Model. 8(27), 1–21.

O130 Turbo charging radiotherapy with plasma activated liquid

J. C. H. Author[1], L. Rogers[2], N Suchowerska[2], D. McKenzie[1]

[1]School of Physics, The University of Sydney and VectorLAB, Chris O'Brien Lifehouse. jhar9271@uni.sydney.edu.au (Presenting author); [2]VectorLAB, Chris O'Brien Lifehouse and The School of Physics, The University of Sydney. Linda.Roger@lh.org.au; Natalka.Suchowerska@lh.org.au; david.mckenzie@sydney.edu.au

Introduction Gas plasma is an emerging cancer therapy. Like radiation therapy, it produces reactive species, which are toxic to cells (Ji et al. 2019). We have shown in previous work that delivering a priming radiation dose before a second radiation dose increases cell death in prostate cancer. However, in clinical practice, delivering

such a treatment in partial fractions is cumbersome. Using the idea of a priming dose, we propose to replace the first partial fraction with a plasma activated liquid (PAL) treatment with the aim of improving the cytotoxicity of radiation treatment.

Method For the radiation treatment, DU145 prostate cancer cells in 6-well plates were exposed to a Varian 6MV photon beam to 2.5 Gy. PAL was a physical plasma treated Hartmann's solution, which for treatment was transferred to cells in 6-well plates for 30 min. For the combination treatment, the PAL was delivered 1 h prior to the radiation treatment. All plates were incubated for a further 7 days to assess clonogenic survival fraction.

Results The Figure shows the survival fraction of DU145 after treatment with PAL, with radiation and their combination.

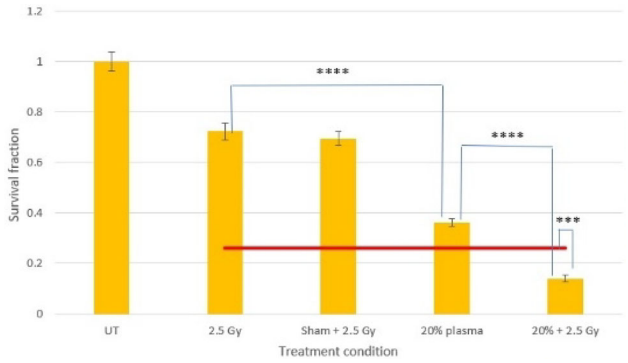

The expected survival (red line) is higher than that observed, showing synergy.

Conclusion We have found strong synergy between PAL and radiation therapy ($p < 0.001$) presenting the opportunity to significantly improve patient outcomes without increasing radiation dose. Furthermore, using PAL and radiotherapy in this manner is feasible in clinical practice.

Acknowledgements Australian Commonwealth Government Funding; Funding from the Bailey Family; Commonwealth Government RTP Scholarship

References

Ji, W.-O., Lee, M.-H., Kim, G.-H., and Kim, E.-H. (2019). Quantitation of the ros production in plasma and radiation treatments of biotargets. *Scientific Reports*, 9(1):1–11.

O131 Gravitational effects of patient rotation on the position of the eye within the orbit

T. Kairn[1,2,3,4], P. C. W. Chan[1,5], L. Sim[6], S. B. Crowe[1,2,3,4]

[1]Cancer Care Services, Royal Brisbane and Women's Hospital, Brisbane, Qld, Australia; [2]Herston Biofabrication Institute, Metro North Hospital and Health Service, Brisbane, Qld, Australia; [3]School of Information Technology and Electrical Engineering, University of Queensland, Brisbane, Qld, Australia; [4]School of Chemistry and Physics, Queensland University of Technology, Brisbane, Qld, Australia. t.kairn@gmail.com (Presenting author); [5]Faculty of Medicine, Queensland University of Technology, Brisbane, Qld, Australia; [6]Radiation Oncology Princess Alexandra Hospital Raymond Terrace (ROPART), Brisbane, Qld, Australia

Introduction There has recently been an increase in interest in the use of patient rotation as an alternative to gantry rotation during photon radiotherapy [1,2,3,4], occurring in parallel with a resurgence of interest in novel patient positioning as an alternative to the use of gantries for proton radiotherapy [5,6]. This study aimed to contribute to this growing area of research by investigating the gravitational effects of patient rotation on an anatomical site for which precision treatments are needed [7] and which is a well-established target of static-beamline proton treatments for seated patients [8]; the eye.

Method T2-weighted turbo spin echo (TSE) MR images of the facial anatomy of 12 healthy volunteers were obtained as part of an ethics approved study into anatomical variation of CNS anatomy [9]. Images were acquired with each participant lying prone and supine, to provide a worst-case indication of tissue mobility. Resulting gravitational effects on the position of the eye and surrounding tissues were assessed by measuring distances from the superior, inferior and posterior surfaces of the eye to the orbit bone, in the prone and supine MRI images.

Results Shifts in eyeball position of up to 2 mm were detected for six participants, shifts exceeding 2 mm were detected for two participants, and negligible shifts (undetectable at this resolution) were found for the remaining three cases. Figure 6 exemplifies these results, showing a case with zero shift in the top row and a case with a 2.1 ± 0.2 mm shift in the bottom row.

Conclusion It may be inadvisable to use images acquired in the supine position alone, when planning photon radiotherapy treatments to rotating patients or proton radiotherapy treatments to seated patients. It cannot be assumed that the eye does not move when the patient orientation changes. In some cases, the eye muscles seem to fix the eye position, even with the substantial change from supine to prone positioning, but in other cases gravitational effects may shift the treatment target to a degree that could result in a geometric miss in treatment delivery.

Acknowledgements S B Crowe's contribution to this work was supported by a Metro North Hospital and Health Service funded Herston Biofabrication Institute Programme Grant. MRI imaging series used in this study were provided by the Herston Imaging Research Facility (HIRF) via the Herston Biofabrication Institute.

References

1. Kairn T (2018) Patient rotation during linac-based photon and electron radiotherapy. J Med Imaging Radiat Oncol 62(4): 548–552 (2018)
2. Liu PZY, O'Brien R, Heng SM, et al. (2019) Development and commissioning of a full-size prototype fixed-beam radiotherapy system with horizontal patient rotation. Med Phys 46(3): 1331–1340.

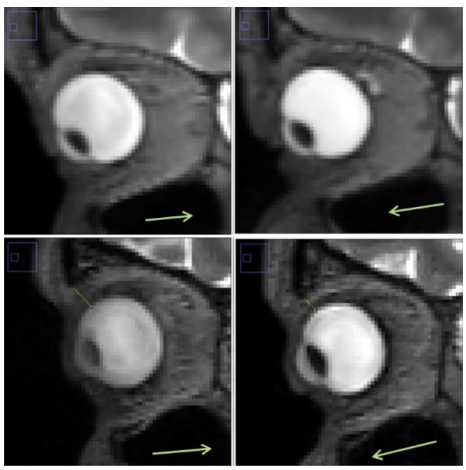

Fig. 1 Example images of two participants (one in each row) showing eye position in supine (left) and prone (right) MRI images. Top row shows zero shift, bottom row shows 2 mm shift and arrows show direction of gravity

3. Buckley JG, Smith AB, Sidhom M, et al. (2021) Measurements of human tolerance to horizontal rotation within an MRI scanner: Towards gantry-free radiation therapy. J Med Imaging Radiat Oncol 65(1): 112–119.
4. Effeney B, Biggs J, Brady C, et al. (2019) Considerations and adaptions to the modulated arc total body irradiation technique: dosimetry description. J Med Radiat Sci 66(4): 284–291.
5. Devicienti S, Strigari L, D'Andrea M, et al. (2010) Patient positioning in the proton radiotherapy era. J Exp Clin Cancer Res 29(1): 47.
6. Yan S, Lu HM, Flanz J, et al. (2016) Reassessment of the necessity of the proton gantry: analysis of beam orientations from 4332 treatments at the Massachusetts General Hospital proton center over the past 10 years. Int J Radiat Oncol Biol Phys 95(1): 224–233.
7. Antony R, Herschtal A, Todd S, et al. (2017) A pilot study on geometrical uncertainties for intra ocular cancers in radiotherapy. Australas Phys Eng Sci Med 40(2): 433–439.
8. Goitein M, Miller T (1983) Planning proton therapy of the eye. Med Phys 10: 275–283.
9. Kairn T, Berry C, Campbell L, et al. (2020) Appearance and minimisation of respiratory motion artefacts in thoracic MRI images of prone patients. Phys Eng Sci Med 43(1): 461–462 https://doi.org/10.1007/s13246-019-00826-6

O132 A New Model for Dose–Response Relations in Hadron Therapy

M A McIntyre[1], Dr A. Kızılersü[1], Prof. A. Thomas[1], Dr M. Kreer[2]

[1]Department of Physics, The University of Adelaide. melissa.mcintyre@adelaide.edu.au (Presenting author); ayse.kizilersu@adelaide.edu.au; anthony.thomas@adelaide.edu.au; Department of Physics, Universität Frankfurt am Main in Germany. mkreer@web.de

The advantages of hadron therapy compared to conventional, photon-based radiation treatments are well known amongst the radiation therapy community. Studies have shown that as low as 11% of cancer patients that receive proton therapy experience severe health side effects compared with 28% of photon cancer treatment patients. With our increasing understanding of the underlying mechanisms and stochastic processes involved with proton and ion radiation-induced cell death, we can continue reduce these uncertainties. In this talk I will present a new stochastic dose–response model based on a fractional Poisson count process, which is a generalisation of the standard Poisson count process.

The model was tested on a range of experimental data obtained from the literature and Monte Carlo simulated dose response data generated using the TOPAS-nBio software toolkit. Its performance was compared with current established radiobiological models based on a standard Poisson count process. We observed the model's performance by considering cell response data at different stages including distributions of lethal DNA or chromosomal lesions per cell, cell survival probability curves and predictions of relative biological effectiveness.

A rigorous residual error and regression analysis of the model fits to the data yielded an extremely accurate fit. When compared to other established radiobiological models, they performed similar for low doses of low linear energy transfer radiation, whilst our proposed model performed much better for all doses of high linear energy transfer radiation and high doses of low LET radiation for experimental and simulated cell survival and lethal lesion distribution data.

O133 Implementation of microdosimetry in proton therapy clinical practice

Linh T. Tran[1], Benjamin James[1], David Bolst[1], Dirk Wagenaar[2], Marc-Jan van Goethem[2], Stefan Both[2], Michael L. F. Lerch[1], Marco Petasecca[1], Susanna Guatelli[1], Zeljko Pastuovic[3], Ceri Brenner[3], Marco Povoli[4], Angela Kok[4], Verity Ahern[5], Michael Jackson[6], Anatoly B. Rosenfeld[1]

[1]Centre for Medical Radiation Physics, University of Wollongong, NSW, Australia. tltran@uow.edu.au; bj197@uowmail.edu.au; dbost@uow.edu.au; [2]Department of Radiation Oncology, University Medical Center Groningen, University of Groningen, Groningen, The Netherlands. d.wagenaar@umcg.nl; m.j.van.goethem@umcg.nl; s.both@umcg.nl; mlerch@uow.edu.au; marcop@uow.edu.au; susanna@uow.edu.au; [3]Centre for Accelerator Science, Australian Nuclear Science and Technology Organization, Lucas Heights, NSW, Australia. zkp@ansto.gov.au; brennerc@ansto.gov.au; [4]SINTEF, Norway. Marco.Povoli@sintef.no; Angela.Kok@sintef.no; [5]Westmead Hospital, Australia. Verity.Ahern@health.nsw.gov.au; [6]University of New South Wales, Australia. Michael.Jackson2@health.nsw.gov.au; anatoly@uow.edu.au (Presenting author)

Introduction In Australia, more than 100 children aged 0–14 are diagnosed with malignant brain tumours each year. Brain cancer survival rates in children are good, with 75% surviving 5 years compared to 20% of adults. Survival rates have improved significantly in the last 30 years, making the avoidance of long-term complications even more important. Proton therapy decreases radiation exposure to normal parts of the brain compared to conventional X-ray therapy, thereby improving long-term cognitive outcomes. The radiobiological efficiency (RBE) of protons depends on their linear energy transfer (LET) which varies throughout the treatment volume [1]. Conventional proton therapy planning assumes a constant RBE of 1.1, while biologically optimized robust planning is a paradigm shift taking into account variable LET. However, its clinical implementation requires a new quality assurance capability called dose averaged LET_D verification.

Method The Centre for Medical Radiation Physics, University of Wollongong, developed an award winning microdosimeter called MicroPlus for verification of LET_D in proton and heavy ion therapy [2, 3]. MicroPlus is the only device in the world and is patented, licensed, and currently used in eleven of the world's leading proton therapy centres.

Results At the University Medical Center Groningen, MicroPlus was tested in an anthropomorphic head phantom to verify the LET_D calculated by the RaySearch treatment planning system for brain, nasal and head and neck tumours. We demonstrated that the RBE actually increases up to 1.5, this would lead to 40% overdosing at interfaces between the tumor and normal tissue [4] suggesting that dose weighting optimized robust planning is important clinically.

Conclusion Introduction of LET_D optimized planning and its quality assurance using MicroPlus will allow Australia to provide the best proton therapy treatment at the Bragg Centre for Proton Therapy being built in Adelaide and the planned National Particle Treatment and Research Centre at Westmead.

References

1. H. Paganetti, "Relative biological effectiveness (RBE) values for proton beam therapy. Variations as a function of biological endpoint, dose, and linear energy transfer", Phys. Med. Biol., vol. 59, no. 22, 2014
2. L. T. Tran, L. Chartier, D. Bolst, David Bolst, Marco Povoli, Anand Summanwar, Angela Kok, Alex Pogossov, Marco Petasecca, Susanna Guatelli, Mark I. Reinhard, Michael Lerch,

Mitchell Nancarrow, Naruhiro Matsufuji, Michael Jackson and Anatoly B. Rosenfeld, "Thin silicon microdosimeter utilizing 3D MEMS technology: Charge collection study and its application in mixed radiation fields," IEEE Transactions on Nuclear Science, vol. 65, no. 1, pp. 467–472, Oct 2017.
3. Linh T. Tran, Lachlan Chartier, David Bolst Alex Pogossov, Susanna Guatelli, Dale A. Prokopovich, Marco Petasecca, Michael L. F. Lerch, Mark I. Reinhard, Benjamin Clasie, Nicolas Depauw, Hanne Kooy, Jay Flanz, Aimee McNamara, Harald Paganetti, Chris Beltran, Keith Furutani, Vladimir L. Pereverzaylo, Michael Jackson and Anatoly B. Rosenfeld, Characterisation of proton pencil-beam scanning using a high spatial resolution solid state microdosimeter, Med Phys. 2017 Nov; 44(11):6085–6095
4. D. Wagenaar, L. T. Tran, A. Meijers, GG Marmitt, K Souris, D Bolst, B James enjamin James, Giordano Biasi, Marco Povoli, Angela Kok, Erik Traneus, Marc-Jan van Goethem, Johannes A Langendijk, Anatoly B Rosenfeld, "Validation of linear energy transfer computed in a Monte Carlo dose engine of a commercial treatment planning system", Phys. Med. Biol., vol. 65, no. 2, 2019

O134 Towards IMRT without no moving parts: Bayesian optimization of a novel X-ray collimation concept

B. M. Whelan[1], J. Wang[2], R. Fahrig[3], M. Shumail[4], Stefania Trovati[5], J. Perl[4], S. Tantawi[4], P. J. Keall[1], B. W. Loo[6]

[1]ACRF Image-X, School of Health Sciences, University of Sydney, Australia. Brendan.whelan@sydney.edu.au (presenting author); [2]Department of Radiation Oncology, Stanford University, Stanford, California (Currently at Varian medical systems, Palo Alto, California); [3]Tibaray, Sunnyvale, California; [4]SLAC National Accelerator Laboratory, Stanford University, Menlo Park, California; [5]Department of Radiation Oncology, Stanford University, Stanford, California (Currently at Lawrence Berkley National Lab, Berkley, California); [6]Department of Radiation Oncology, Stanford University, Stanford, California

Introduction SPHINX (scanning pinhole intensity modulated x-ray source) is a novel X-ray collimation concept consisting of an array of small collimator channels in conjunction with X/Y scanning magnets[1] (Fig. 1). The magnets scan the electron beam across the channels, allowing intensity modulated dose deposition. This concept could enable IMRT with no moving parts, as well as ultra-fast (FLASH) treatments. The goal of this work is robust and rapid optimisation of the SPHINX geometry for a given situation.

Method TopasMC[2] was used to simulate SPHINX designs with a given set of input parameters. This simulation incorporates a magnetic field map from a given scanning magnet, and electron phase space from a given linac. This functionality was passed to a Bayesian optimiser[3], which finds an optimal parameter set by fitting a prior model to an underlying cost function; the prior is updated at each iteration based on the measured data. The entire workflow was scripted in python for plug and play functionality. The cost function consisted of terms to maximise dose rate, minimise cross talk between collimator channels, minimise amount of tungsten used, and generate a specified beamlet width, here 7 mm.

Results The Bayesian optimisation solution was found in 32 iterations and achieved a dose rate 2.4 times higher than the previous best (manual) solution. Each iteration took around 6 min on a high-end cloud cluster using 24 cores. The returned beamlet width was 8 mm instead of the requested 7 mm; this could be improved by higher weighting of the beamlet width term in the objective function.

Conclusion A parametric simulation framework to model and optimise SPHINX has been developed. The utility of the software to rapidly generate optimal parameter sets for a given objective function has been demonstrated. This also facilitates rapid prototyping if for instance the Linac design changes.

References

1. Maxim, P. G., S. G. Tantawi and B. W. Loo Jr (2019). "PHASER: A platform for clinical translation of FLASH cancer radiotherapy." Radiotherapy and Oncology 139: 28–33.
2. Perl, J., J. Shin, J. Schümann, B. Faddegon and H. Paganetti (2012). "TOPAS: an innovative proton Monte Carlo platform for research and clinical applications." Medical Physics 39(11): 6818–6837.
3. Nogueira, F. (2021). Bayesian Optimization: Open source constrained global optimization tool for Python. https://github.com/fmfn/BayesianOptimization

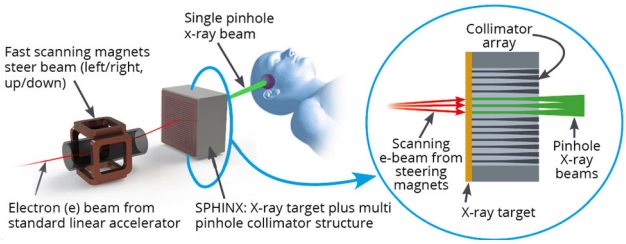

Fig. 28 The SPHINX concept consists of an array of collimators in conjunction with a bremsstrahlung target plate. The electron beam is rapidly scanned over the target plate using fast scanning magnets. By illuminating different channels within the collimator array, an intensity modulated dose distribution can be created

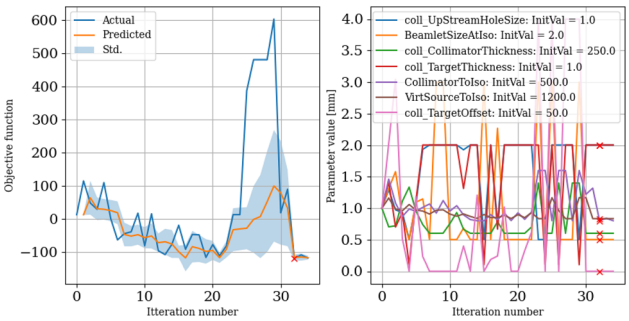

Fig. 29 Convergence plot for the Bayesian optimiser. Left: Objective function versus iteration. The predicted objective function is based on a Gaussian Process prior which is updated at each iteration to best fit the observed data. Right: Parameter values at each iteration, relative to the initialisation value shown in the legend. The red marker in each plot shows the best solution found

O135 Clinical Implementation of Automatic Proximal Bronchial Tree Contouring

Tony Young[1,2], Wsam Ghandourh[3,4], Roya Merie[4,5], Philip Chlap[1,4], Joselle Faustino[1,4], Vicky Chin[1,4], Lois Holloway[1,2,4,6]

[1]Liverpool and Macarthur Cancer Therapy Centres and Ingham Institute, Sydney, Australia; [2]Institute of Medical Physics, School of Physics, University of Sydney, Sydney, Australia. Tony.Young@health.nsw.gov.au (Presenting author); [3]Ingham Institute, Sydney, Australia; [4]University of New South Wales, Sydney, New South Wales, Australia; [5]Liverpool and Macarthur Cancer Therapy Centres, Sydney, Australia; [6]Centre for Medical Radiation Physics, University of Wollongong, Wollongong, New South Wales, Australia

Introduction Stereotactic Body Radiotherapy (SBRT) is an effective treatment of lung tumours. From RTOG 0236 [1] and RTOG 0813 [2], a description of a 2-cm perimeter around the proximal bronchial tree (PBT) was used to determine appropriate SBRT fractionation. Treatment within this area has reported high toxicity [3]. Currently the PBT is manually contoured for each patient undergoing lung SBRT. Distance from treatment area to PBT is a vital consideration for the eligibility and safety of lung SBRT treatments. Automatic contouring of PBT using an algorithm that detects airways based on their CT density was previously introduced [4]. The aim of this project was to assess acceptability and time effectiveness of the automatic contours of PBT compared to the manual contours.
Method A retrospective study was completed with 30 patient datasets. Comparison of the automatically contoured PBT with the original clinically accepted manually contoured PBT was undertaken by 3 Radiation Oncologists (ROs) for suitability and appropriateness. A timing study was conducted for 10 patient datasets, with the PBT manually contoured and the automatically contoured PBT edited by two ROs until the PBT met clinical guidelines. The time taken to complete these were compared to assess time savings.
Results From the retrospective study, the automatically contoured PBT was scored "accurate" for most regions. Though the original clinical contour was scored better than the automatic contoured, it was not perfect either, with scoring indicating that regions were considered to deviate by up to 3 mm. From the timing study, on average, editing the automatic contours was 31% faster than manually contouring the PBT. This was a time saving of approximately 1.6 min per patient.
Conclusion The use of the automatic contouring method for the PBT is time saving and appropriate for clinical implementation.
References/Acknowledgements as applicable

1. Group RTO. RTOG 0236, A Phase II Trial of Stereotactic Body Radiation Therapy (SBRT) in the Treatment of Patients with Medically Inoperable Stage I/II Non-Small Cell Lung Cancer. Philadelphia (PA): RTOG. 2006.
2. Group RTO. RTOG 0813: Seamless phase I/II study of stereotactic lung radiotherapy (SBRT) for early stage, centrally located, non-small cell lung cancer (NSCLC) in medically inoperable patients. Philadelphia (PA): RTOG. 2009.
3. Timmerman R, McGarry R, Yiannoutsos C, Papiez L, Tudor K, DeLuca J, et al. Excessive toxicity when treating central tumors in a phase II study of stereotactic body radiation therapy for medically inoperable early-stage lung cancer. Journal of clinical oncology. 2006;24:4833–9.
4. Ghandourh W, Dowling J, Chlap P, Oar A, Jacob S, Batumalai V, et al. Assessing tumor centrality in lung stereotactic ablative body radiotherapy (SABR): the effects of variations in bronchial tree delineation and potential for automated methods. Medical Dosimetry. 2021;46:94–101.

O136 Correlation of contouring variability with simulated outcome for prostate bed radiation therapy

Viet Le Bao[1,2], Sankar Arumugam[1,3], Annette Haworth[4], Jason Dowling[1,5], Amy Walker[1,2,3,6], Kirrily Cloak[1,2], Andrew Kneebone[7], Lois Holloway[1,2,3,4,6]

[1]South Western Clinical School, UNSW, Sydney, Australia; [2]Ingham Institute for Applied Medical Research, Sydney, Australia. v.lebao@student.unsw.edu.au (Presenting author); [3]Liverpool and Macarthur Cancer Therapy Centres, Sydney, Australia. Sankar.Arumugam@health.nsw.gov.au; [4]Institute of Medical Physics, School of Physics, University of Sydney, Australia. annette.haworth@sydney.edu.au; [5]Australian e-Health Research Centre, CSIRO, Royal Brisbane and Women's Hospital, Herston, Australia. jason.dowling@csiro.au; [6]Centre for Medical Radiation Physics, University of Wollongong, Wollongong, Australia. amy.walker3@health.nsw.gov.au; k.cloak@unsw.edu.au; [7]Royal North Shore Hospital, Sydney, Australia. andrew.kneebone@health.nsw.gov.au; lois.holloway@health.nsw.gov.au

Introduction Variability in contouring remains one of the largest sources of uncertainty in radiation therapy (RT) [1, 2]. Currently, there are no consistently reported similarity metrics to quantify contour variability [3]. This study aims to recommend suitable similarity metrics by investigating the relationship between contouring variability and modelled outcome surrogates for prostate bed RT.
Method Two patient datasets were used in this study. Dataset 1 included 10 patient CT scans, with CTV, rectum, and bladder contoured independently by three experienced observers. STAPLE volumes were generated as the reference volume for each structure. Dataset 2 served as a benchmarking dataset and comprised one patient CT scan with 42 independent manual CTV contours. An in-house atlas-based segmentation tool, derived from dataset 2, was used to automatically generated 42 contours for each patient in dataset 1. A set of six contours were then generated by combining 42 contours into a probabilistic label, and taking thresholds at levels of agreement of 20%, 40%, 60%, 80%, 95%, and 100%. Plans were created for all target volumes on dataset 1. The impact of contouring uncertainty on dose distribution was then assessed using radiobiological metrics. The correlation between contouring similarity metrics and radiobiology metrics are reported using the Spearman's rank correlation coefficient.
Results Table 1 shows the correlation between contour variation and radiobiology metrics. Metrics based on surface agreement (95% HD) showed the highest correlation with CTV EUD ($\rho = -0.409$, $p < 0.01$). The strongest correlation for the rectum and bladder was found in MDA ($\rho = 0.599$, $p < 0.01$) and volume difference ($\rho = -0.401$, $p < 0.01$) respectively.
Conclusion The correlation between contouring similarity metrics and modelled outcome is dependent on the structure. Rectal NTCP showed moderate correlation with MDA, DSC and Jaccard metrics. Only weak correlations were found between contour variation and radiobiology metrics in the CTV and bladder.
References

1. Njeh CF, *Tumor delineation: the weakest link in the search for accuracy in radiotherapy*. J Med Phys., 2008. **33(4):136–40.**

Table 1 Spearman's rho for geometric variation and model radiobiology for all patients

		CTV		Rectum		Bladder	
		EUD	TCP	EUD	NTCP	EUD	NTCP
Volume	ρ	0.263	0.236	0.370	0.370	0.401	0.401
	Sig	0.012	0.025	0.00	0.00	0.00	0.00
95% HD	ρ	− 0.409	− 0.382	0.452	0.452	0.15	0.15
	Sig	0.00	0.00	0.00	0.00	0.16	0.16
MDA	ρ	− 0.369	− 0.352	0.599	0.599	0.222	0.222
	Sig	0.00	0.001	0.00	0.00	0.035	0.035
DSC	ρ	0.366	0.341	− 0.547	− 0.547	− 0.164	− 0.164
	Sig	0.00	0.001	0.00	0.00	0.123	0.123
Jaccard	ρ	0.366	0.341	− 0.547	− 0.547	− 0.164	− 0.164
	Sig	0.00	0.001	0.00	0.00	0.123	0.123

CTV: clinical target volume; EUD: equivalent uniform dose; TCP: tumour control probability; NTCP: normal tissue complication probability; HD: Hausdorff distance; MDA: mean distance to agreement; DSC: Dice similarity coefficient; Jaccard: Jaccard similarity

2. Feng M, Demiroz C, Vineberg KA, et al., *Normal tissue anatomy for oropharyngeal cancer: contouring variability and its impact on optimization*. Int J Radiat Oncol Biol Phys., 2012. **84(2):e245–e249.**
3. Vinod SK, Jameson MG, Min M, et al., *Uncertainties in volume delineation in radiation oncology: A systematic review and recommendations for future studies*. Radiother Oncol, 2016. **121**(2): p. 169–179.

O137 A structured and multidisciplinary approach to the release of scripting solutions into a clinical environment based on Monaco 6.0 API pilot release

Arek Mazurek[1,2], Luis Muñoz[3]

[1]GenesisCare; [2]Fiona Stanley Hospital Radiation Oncology Dept, Western Australia, Australia. Arek.Mazurek@genesisacare.com (presenting); [3]GenesisCare, Flinders Private Hospital, South Australia, Australia

Introduction Automated planning provides workflow efficiencies and safeguards[1,2]. In-house written software should undergo strict quality assurance when used in medical environment[3]. Planning Automation Module (PAM) utilizes the application programming interface (API) in Monaco 6.0 (Elekta, Sweden), this work details the safe application of Agile work practices for radiotherapy.

Method Agile software development practices are characterized by continuous iterative delivery and validation by prototype. PAM was guided using a high-level governance document, developed by a working group of software engineers and medical physicists. Changes were integrated into the code base via GitLab (GitLab Inc., USA) using clear short-term goals outlined in Jira (Atlassian, USA) cards within a 2-week sprints. Planning templates were developed by Radiation Therapists (RT), where the API applied a site-specific class solution to imported patient data sets. As the code base expanded, testing of code changes were verified in a User Acceptance Testing (UAT) environment that mirrors production server configuration with a separate patient database. Feedback by RT's on workflow behaviour and plan quality provided areas for further development. Performance and error monitoring in UAT and production were handled by Sentry, Datadog and a Status Page. This allowed timely triaging of errors during DICOM transfer and API performance. Access to a live status page logged plan creation as it progressed through various stages, providing escalation, and triaging of clinical errors to Physics. Nightly end to end testing vet the API and code performance against baseline. These workflows were also utilized before merging a new version of the code into master. Credentialing and training users in newly designed work practices focused on quality management ensured the standardisation of safe software development practises.

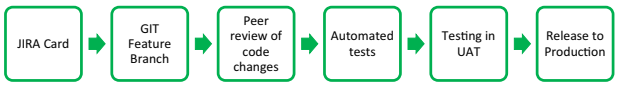

Fig. 1 Workflow for code release in PAM

Results Agile work practices were applied to the Monaco 6.0 API for clinical use, providing a scalable product with rapid deployment. This has been successfully rolled out across three states.

Conclusion Safe software development methods require documentation, quality assurance and end to end testing by a multidisciplinary approach in radiotherapy treatment planning.

Acknowledgements GenesisCare Australia have an Alpha agreement with Elekta and are part of the pilot program for Monaco 6.0.

References

1. Bamatov IM, Bamatov DM. The current and future role of automation in radiotherapy treatment planning. Paper presented at: Journal of Physics: Conference Series 2020.
2. Hussein M, Heijmen BJ, Verellen D, Nisbet A. Automation in intensity modulated radiotherapy treatment planning—a review of recent innovations. *The British journal of radiology*. 2018; 91(1092): 20180270.
3. Best-practice guidance for the in-house manufacture of medical devices and non-medical devices, including software in both cases, for use within the same health institution v1.0 – IPEM Task Group 2021

O138 When Patient Immobilisation Immobilises a Department: OmniBoard Implementation

K. Summerhayes[1], E. C. Cosgriff[1,2]

[1]Nepean Cancer Care Centre, Kingswood, NSW. Katie.summerhayes@health.nsw.gov.au (Presenting author); [2]Present address: Crown Princess Mary Cancer Centre, Westmead, NSW. Eireann.Cosgriff@health.nsw.gov.au

Introduction OmniBoard is a modular patient immobilisation system designed for every treatment site, offering setup reproducibility and efficiency. Carbon fibre patient immobilisation devices and couchtops have been shown to have non-negligible dosimetric impact even for VMAT beam deliveries [1, 2]. The dosimetric effect of the Omniboard (MacroMedics) when used in conjunction with the Evo Couchtop (Elekta) has been investigated, and the impact of the OmniBoard on treatment simulation, planning and delivery considered.
Method Cylindrical water phantom measurements were performed through the head, shoulder, and pelvis sections of the OmniBoard and EvoCouch combination at every 10° gantry rotation for 6, 10, and 18 MV beams of 5 × 5cm^2 and 10 × 10cm^2 field sizes. Corresponding beams were calculated in the TPS (Pinnacle^3) for comparison with the measurements. Additional measurements were performed to assess the attenuation of the polyoxymethylene (POM) patient positioning attachment connectors and the BreastBoard attachment. PDD measurements for the Omniboard and EvoCouch combination were performed using a Roos chamber in solid water at normal incidence.
Results The maximum measured attenuation factor for the OmniBoard and EvoCouch was 0.828 (6 MV, G = 130°) whilst the normal incident attenuation factor through the POM sections was 0.878. The Omniboard TPS model created agreed within 2% of the measured data and the TPS estimated the dose through the POM sections within 1%. PDD measurements were found to be representative of the literature findings [3]. For adequate data acquisition, large FoV reconstructions were required at treatment simulation and patient positioning at treatment required the development of new small FoV XVI presets.
Conclusion Careful consideration of all aspects of the treatment planning and delivery chain needs to be given when implementing an immobilisation device such as OmniBoard. Technical challenges have been overcome through process changes and iterative development of modelling and density overrides in the TPS.
References

1. Mihaylov, IB, Bzdusek, K, & Kaus, M (2011) Carbon fiber couch effects on skin dose for volumetric modulated arcs. Medical Physics (Lancaster), 38(5), 2419–2423. https://doi.org/10.1118/1.3576106
2. Zhang, RH, J Fleckenstein, J, Gao, YL, Miao, MC, Chi, ZF & Bai, WW (2019) Quantification and modelling of the dosimetric impact of the treatment couch in volumetric modulated arc therapy (VMAT). International Journal of Radiation Research, 17(2), 335–344. https://doi.org/10.18869/acadpub.ijrr.17.2.335
3. Poppe, B, Chofor, N, Rühmann, A, Kunth, W, Djouguela, A, Kollhoff, R, & Willborn, KC (2007) The Effect of a Carbon-Fiber Couch on the Depth-Dose Curves and Transmission Properties for Megavoltage Photon Beams. Strahlentherapie Und Onkologie, 183(1), 43–48. https://doi.org/10.1007/s00066-007-1582-8

O139 Physical properties comparison of Aquaplast and Polyflex thermoplastic bolus materials for radiotherapy

M. Wawrzak[1], L. Webb[1], B. Perrett[1], P Ramachandran[1]

Radiation Oncology, Cancer Services, Princess Alexandra Hospital, Brisbane, Australia. Michal.Wawrzak@health.qld.gov.au (Presenting author); Luke.Webb@health.qld.gov.au; Ben.Perrett@health.qld.gov.au; Prabhakar.Ramachandran@health.qld.gov.au

Introduction Thermoplastic bolus materials when heated up are easily molded to any surface shape. However, as they are quite rigid after cooling down, patient weight loss during radiotherapy may result in significant discrepancies between bolus and skin surface. This study compares physical properties of Aquaplast RT^{TM} and Polyflex thermoplastic boluses including influence of air gap on surface dose.
Method The homogeneity of the materials has been established using ImageJ software on CT images. The water relative electron density has been established using three methods: CT-ED curve, Montaseri formula and Moutrie method employing EPID imaging. The TPRs, transmission factors (TFs), and an influence of an airgap on the surface dose for both materials were measured for 5 × 5 cm^2 and 10 × 10 cm^2 6MV and 10MV photon and 10 × 10 cm^2 6 MeV, 9 MeV and 12 MeV electron fields and compared with corresponding values for the plastic water. All properties have been investigated pre and post molding.
Results The water relative electron density derived from CT-ED curve for Aquaplast^{TM} and Polyflex^{TM} was 1.03 and 1.08, calculated with Montaseri formula was 1.08 and 1.13 and established with Moutrie method was 1.11 and 1.10, respectively. The TFs for both materials were within 0.4% from TFs of the plastic water for all photon fields and 7.5%, 3.8% and 1.7% for Aquaplast^{TM} and 6.5%, 3.3% and 2.3% for Polyflex^{TM} below TFs of the plastic water for 6 MeV, 9 MeV and 12 MeV electron fields respectively. The 5 mm air gap caused surface dose decrease by 3.4% for 5 × 5 cm^2 and 1% for 10 × 10 cm^2 fields for both photon and electron beams.
Conclusion Aquaplast^{TM} and Polyflex^{TM} were found to be near water equivalent for electron and photon beams. The influence of air gap on surface dose has been found acceptable for clinical use.
References/Acknowledgements

Montaseri A, Alinaghizadeh M, Mahdavi SR. Physical properties of ethyl methacrylate as a bolus in radiotherapy. *IJMP*. 2012; 9(2): 127–134
Moutrie V. Exploration of a MVCT for use in radiation therapy planning. *Master of Science (research)*, University of Wollongong, 2014.

P001 A single centre audit of CT doses for radiotherapy procedures

Khalsa Al Shukaili[1,2], Elizabeth Claridge Mackonis[1], Robin Hill[1,3]

[1]Department of Radiation Oncology, Chris O'Brien Lifehouse, Sydney, Australia; [2]Department of Radiation Therapy, National Oncology Centre, Muscat, Oman. khalsa.alshukaili@gmail.com (Presenting author); elizabeth.mackonis@lh.org.au; [3]Institute of Medical Physics, School of Physics, University of Sydney, Australia. robin.hill@lh.org.au

Introduction CT scans are the primary imaging modality as used for radiotherapy treatment planning. The ICRP has implemented diagnostic reference levels (DRL) for radiological imaging to ensure ALARA principles are followed. However, CT imaging requirements for radiotherapy can be very different to those in the diagnostic setting and there is only limited reported DRLs from radiotherapy centres [1]. The purpose of this work is to review and audit the DRLs that are found on radiotherapy CT scanner.
Method DRL parameters $CTDI_{vol}$ and DLP were reviewed for patients who had radiotherapy CT scans on a Toshiba LB Aquilion

Table 1 The values of the $CTDI_{volume}$ and Total DLP for different scanning protocols

Scan protocol	$CTDI_{volume}$ (mGy)			Total DLP (mGy/cm)		
	Mean	Median	3rd Quartile	Mean	Median	3rd Quartile
SRS Cranial	86	76	104	4212	4788	5093
Head & Neck	17	16	17	698	691	764
Chest	16	16	17	742	760	782
Lung	28	20	28	1418	1170	2048
Breast	13	12	15	715	682	920
Abdomen	13	11	14	696	609	795
Pelvis	19	16	22	847	710	1072
Prostate	23	19	31	882	726	1215
Sarcoma	21	19	22	1508	1498	1636

CT scanner. Each treatment site had a specific CT scan protocol with a minimum of 20 patients per protocol. There were also specific scan protocols for SRS and SBRT planning purposes. The scanning region margins were anatomically defined by the departmental procedure and protocols.

Results The results of the mean, median and the 3rd quartile values of DLP and $CTDI_{vol}$ for the different scan protocols are shown in Table 1. The DRLs are consistent with other reported radiotherapy DRLs but using a different CT scanner [1] with exception of the cranial scanning protocols. The DRLs for these patients were much higher. This is due to the greater scan resolution and area of interest required for SRS planning purpose.

Conclusion In this study, we have demonstrated that radiotherapy CT DRLs are comparable to other published studies with exception of cranial SRS protocols. This data set provides a useful benchmark for other Australasian radiotherapy departments who would be interested in performing a similar review.

Acknowledgements This work would not have been possible without the financial support from Sultanate of Oman government.

References

1. Zalokar, N., Marciuš, V.Ž. and Mekiš, N., 2020. Establishment of national diagnostic reference levels for radiotherapy computed tomography simulation procedures in Slovenia. *European journal of radiology*, *127*, p.108979.

P002 1.5T Philips MRI commissioning process for Radiotherapy at ONJ

R. A. Author[1], N. Shelton[1], J. Lye[1], R. Behan[1], G. Cahoon[1], S. Fisher[1], K. Rykers[1]

[1]Olivia Newton John Cancer Research and Wellness Centre, Austin Health, Melbourne reza.alinaghizadeh@austin.org.au (Presenting author); Nikki.shelton@austin.org.au; jessica.lye@austin.org.au; Rob.behan@austin.org.au; Glenn.cahoon@suatin.org.au; sandra.fisher@austin.org.au; kym.rykers@austin.org.au

Introduction In June 2020, the Philips Ingenia 1.5T Magnetic Resonance Imaging Unit was installed in the Radiotherapy Department at ONJ. Its function is to provide patient MRI images for radiotherapy planning, addressing the overarching goal of improving the accuracy of target and OAR identification and delineation. MRI systems used for radiotherapy planning require high spatial accuracy for the patient alignment equipment, e.g. external lasers and table motion. In addition, a high level of importance is placed on characterizing any geometric distortions inherent in the system, to minimize the contribution of uncertainties to the patient treatment workflow.

Method To commission the MRI, various methods and phantoms were used in accordance with the vendor white paper [1] and international guidelines [2,3]. For mechanical integrity and virtual isocentre positioning, MRI-safe equipment and a LAP laser phantom were used. The vendor PIQT and ACR phantoms were used for image quality and system performance tests [4]. To evaluate the geometric fidelity of the system, vendor and third-party phantom were used. The QUASAR CT-MR 4D phantom was used for both motion management and geo-distortion evaluation on individual sequence testing.

Results Mechanical integrity and virtual positioning of the imaging isocentre revealed positional accuracy within $\pm$ 1 mm. Image quality tests were all within ACR guideline and vendor tolerances. Geometric distortion analysis showed maximum distortion $<$ 1.5 mm, within a 200 mm radius from the imaging isocentre. In addition, image quality and geometric fidelity were evaluated for all individual imaging sequences prior to clinical release.

Conclusion Commissioning tests were performed according to international guidelines. Quality systems were developed for daily, monthly, quarterly and annual QA of the MRI. Following acceptance of all tests, the MRI was released for clinical use at ONJ.

References

1. Commissioning of MR-only simulation for radiotherapy planning, Philips White paper, Gerald Schubert, Teuvo Vaara, Matti Lindstrom, Reko Kemppainen and Marieke van Grootel-Rensen
2. AAPM report 100 MR Subcommittee TG1; Acceptance Testing and Quality Assurance Procedures for Magnetic Resonance Imaging Facilities
3. The AAPM TG 284 Report: Magnetic Resonance Imaging Simulation in Radiotherapy: Considerations for Clinical Implementation, Optimization, and Quality Assurance.
4. The American Association of Physicists in Medicine (AAPM) and the American College of Radiology (ACR) Phantom Test Guidance for Use of the Large MRI Phantom for the ACR – MRI Accreditation Program

P003 Spatial accuracy of SRS cranial treatment in Australian radiotherapy: Results of the ACDS field trial audit

A. Alves[1], M. Shaw[1], J. Kenny[2], J. Lye[3], R Brown[1]

[1]Australian Clinical Dosimetry Service, ARPANSA, Melbourne, Australia. andrew.alves@arpansa.gov.au; maddison.shaw@arpansa.gov.au; [2]Medical Physics Specialists, Health Stem Solutions. John.kenny@healthstemsolutions.com; [3]Olivia Newtown John Cancer Wellness and Research Centre; jessica.lye@austin.org.au; rhonda.brown@arpansa.gov.au

Introduction We report the results from the Australian Clinical Dosimetry Service (ACDS) end-to-end stereotactic radiosurgery (SRS) audit. The audit includes dispersed targets, ranging from 0.15–8 cc. The audit is compatible with various treatment platforms and multi or single isocentre delivery and is used in credentialing for TROG trials [1, 2]. It is similar in scope to the IROC audit [3] where the gamma metric is 5%/3 mm. The audit method must be capable of resolving 1–2 mm errors in treatment to be in-line with typical PTV margins [1, 2].

Method An IMT MAX-HD^{TM} (IMT, New York) cranial phantom with tissue equivalent materials and bony anatomy suitable for IGRT is used. Facilities plan to ACDS requirements using departmental protocols, including clinical immobilization. GTV/PTV and OAR dose constraints are delineated from facility MR images or provided via RT structure set. Measurement is performed using Gafchromic EBT3 and XD film (Ashland Inc., Bridgewater NJ, USA). Eight film locations (axial or coronal) are investigated across three audit cases. Film-to-CT matching localises the film to the planned dose reference frame. Tilted dose plane extraction from DICOM data has been enabled.

Results Measurements have been conducted at 14 sites to-date. Spatial precision of the film-to-CT matching is estimated to be 0.3 mm when resolution of the facility CT scan is $\leq$ 1 mm. The spatial accuracy of the treatment has been assessed via distance to agreement (DTA) at 90% isodose from horizontal and vertical 1D profiles through the target and via distance to match (DTM) > 70% isodose from an auto-alignment algorithm.

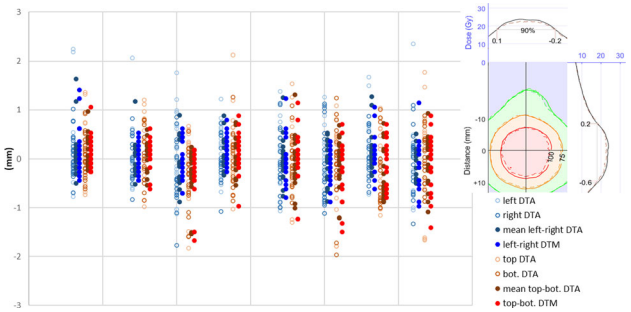

Fig. 1 Results of the DTA and DTM spatial precision metrics for 8 film location in 14 audits. (Inset: An example film-to-plan comparison with 90% DTAs)

Conclusion Single point DTA values have shown > 2 mm discrepancies, however, overall geometric precision is better represented by the mean DTA or DTM metrics. The audit achieves the required spatial precision to detect relevant geometric errors in SRS cranial treatments. A gamma scoring metric of 5%/1 mm is proposed.

Acknowledgements

The ACDS would like to acknowledge:

TROG Cancer Research for use of the TROG planning competition OAR structure set in the audit.

The facilities who have performed the audit.

References

1. Australian Cancer Trials Registry: Sydney (NSW): NHMRC Clinical Trials Centre, University of Sydney (Australia); 2005 -. Identifier ACTRN12616001265460. TROG 16.02 Local HER-O A study of local therapy for the treatment of brain metastases from Human Epidermal Growth Factor Receptor Type 2 (HER2) positive breast cancer 2016 Sep 8. http://anzctr.org.au/ACTRN12616001265460.aspx
2. ClinicalTrials.gov [Internet]: Bethesda (MD): National Library of Medicine (US) 2016 Jul 14 -. Identifier NCT03497767, TROG 17.02 Randomised phase II trial of Osimertinib with or without stereotactic radiosurgery for EGFR mutated NSCLC with brain metastases. 2016 Sep 8. https://clinicaltrials.gov/ct2/show/NCT03497767
3. Molineu, Andrea & Kry, Stephen & Alvarez, Paola & Hernandez, Nadia & Nguyen, Thien Tho & Followill, D. (2016). SU-G-TeP2-12: IROCHouston and MDAPL SRS Anthropomorphic Phantom Results. Medical Physics. 43. 3665–3665. https://doi.org/10.1118/1.4957047.

P004 Delivered dose assessment in Pancreas SBRT using real-time target position determined by SeedTracker

Sankar Arumugam[1,2], Mark Lee[3]

[1]Department of Medical Physics, Liverpool and Macarthur Cancer Therapy Centres and Ingham Institute, Sydney, New South Wales, Australia. [2]South Western Clinical School, University of New South Wales, Sydney, New South Wales, Australia. Sankar.Arumugam@health.nsw.gov.au (Presenting author); [3]Department of Radiation Oncology, Liverpool and Macarthur Cancer Therapy Centres, Sydney, New South Wales, Australia. Mark.Lee@health.nsw.gov.au

Introduction The accurate delivery of pancreas Stereotactic Body Radiotherapy(SBRT) is challenging due to abdominal organ motion. The purpose of this study was to assess the delivered dose accuracy in pancreas SBRT by incorporating the real-time target positon determined by an in-house position monitoring system.

Method An online image based position monitoring system,SeedTracker[1-3],was developed to monitor intrafraction radiopaque marker positions using monoscopic x-ray images, available from the Elekta XVI imaging system. This system was applied to patients receiving SBRT for pancreatic cancer on the MASTERPLAN Pilot trial (UTN: U1111-1202-7476). All patients were implanted with at least four peri-tumoral radiopaque markers before SBRT for target localisation. Each patient was planned for SBRT using a dual arc VMAT technique and five treatment fractions. During treatment delivery the marker positions were compared to expected positions delineated from the planning CT. The position tolerance of $\pm$ 3 mm from the expected position of the markers was set to trigger a gating event during treatment. The actual dose delivered during treatment was calculated by convolving the control point dose matrices of the treatment plan with the target position determined during treatment.

Results Eight patients were treated within this trial. The mean (range) difference between plan and delivered dose in target and organs at risk (OARs) for the actual delivery and simulated delivery, if position corrections were not performed in the absence of online monitoring, is shown in Table 1.

Conclusion Real-time target monitoring enabled the assessment of delivered dose by incorporating the actual target positions and improved the accuracy of dose delivered to target and OARs.

Table 1 Dose difference between plan and delivery

Structure	Metric	Difference between plan and delivered dose (Gy) Mean (min–max)	
		Actual delivery	Simulated delivery
GTV	D98	0.14(− 0.6–1.8)	− 1.2(− 10.9–1.2)
Duodenum	Dmax	1.1(− 0.7–3.3)	1.9(− 0.1–4.6)
	D2cc	0.0(− 0.5–0.6)	0.2(− 0.1–0.8)
Stomach	Dmax	− 0.5(− 1.6–1.2)	− 0.9(− 1.7–0.3)
	D2cc	− 0.4(− 1.4–0.6)	− 0.9(− 2.6–0.2)

References

1. Arumugam S, Sidhom M, Xing A, Holloway L. An online x-ray based position validation system for prostate hypofractionated radiotherapy. Med Phys 2016;43:961–74.
2. Arumugam S, Sidhom M, Truant D, Xing A, Udovitch M, Holloway L. Variable angle stereo imaging for rapid patient position correction in an in-house real-time position monitoring system. Phys Medica 2017;33:170–8.
3. Arumugam S, Pavey D, Oar A, Holloway L, Sidhom M, Lee M. The first real-time intrafraction target position monitoring in pancreas SBRT on an Elekta linear accelerator. Phys Eng Sci Med. 2021 May 21. https://doi.org/10.1007/s13246-021-01007-0.

P005 Repeatability of image features extracted from FET PET in application to post-surgical glioblastoma assessment

Nathaniel Barry[1], Pejman Rowshanfarzad[1], Roslyn J. Francis[2], Anna K. Nowak[2], Martin A. Ebert[3]

[1]School of Physics, Mathematics and Computing, University of Western Australia, Crawley, Western Australia. nathaniel.barry@outlook.com (Presenting author); pejman.rowshanfarzad@uwa.edu.au; [2]Medical School, University of Western Australia, Crawley, Western Australia and Department of Nuclear Medicine, Sir Charles Gairdner Hospital, Nedlands, Western Australia. roslyn.francis@uwa.edu.au; anna.nowak@uwa.edu.au; [3]School of Physics, Mathematics and Computing, University of Western Australia, Crawley, Western Australia and Department of Radiation Oncology, Sir Charles Gairdner Hospital, Nedlands, Western Australia. martin.ebert@health.wa.gov.au

Introduction Positron emission tomography (PET) imaging using the amino acid tracer O-(2- [^{18}F]fluoroethyl)-L-tyrosine (FET) has gained significant popularity within the past decade in the management of glioblastoma (GBM). Radiomics features extracted from FET PET images may be sensitive to variations when imaging at multiple time points. It is therefore necessary to assess feature robustness to test–retest imaging.

Methods Eight patients with histologically confirmed GBM that had undergone post-surgical test–retest FET PET imaging were recruited. In total, 1578 radiomic features were extracted from biological tumour volumes (BTVs) delineated using a semi-automatic contouring method. Feature repeatability was assessed using the intraclass correlation coefficient (ICC). The effect of both bin width and filter choice on feature repeatability was also investigated.

Results 59/106 (55.7%) features from the original image and 843/1472 (57.3%) features from filtered images had an ICC $\geq$ 0.85. Shape and first order features were most stable. Choice of bin width showed minimal impact on features defined as stable. The Laplacian of Gaussian (LoG, σ = 5 mm) and Wavelet filters (HLL and LHL) significantly improved feature repeatability ($p \ll 0.0001$, $p = 0.003$, $p = 0.002$, respectively). Correlation of textural features with tumour volume was reported for transparency.

Conclusion FET PET radiomic features extracted from post-surgical images of GBM patients that are robust to test–retest imaging were identified. An investigation with a larger dataset is warranted to validate the findings in this study.

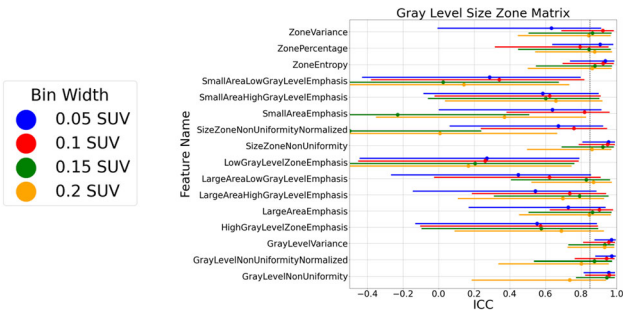

P006 Response of Beryllium oxide fiber optic dosimetry system to ^{18}F-FDG

S. Birajdar[1], K. Hickson[2], A. Santos[3,4], W. Zhang[1], S. Afshar V.[1]

[1]Laser Physics and Photonic Devices Laboratories, UNISA STEM, The University of South Australia, Mawson Lakes, SA 5095; birbm002@mymail.unisa.edu.au; [2]Medical Physics & Radiation Safety, SA Medical Imaging, Adelaide, SA 5000. Kevin.Hickson@sa.gov.au; [3]Department of Medical Physics, Royal Adelaide Hospital, Adelaide, SA 5000; [4]School of Physical Sciences, The University of Adelaide, Adelaide, SA 5005. alexandre.santos@sa.gov.au; wenqi.zhang@unisa.edu.au; Shahraam.AfsharVahid@unisa.edu.au

Introduction This study investigates the concept of a Fibre Optic Dosimetry system (FOD) for real-time dose measurement of radionuclides used in nuclear medicine. Given the small size of FODs, their applications to direct in-vivo measurement following radioembolization become feasible. The response of a beryllium oxide (BeO) scintillator to positron emitter ^{18}F is presented here.

Method Our system is based on a previously developed FOD [1] consists of a BeO cylinder with a volume of $\sim$ 0.8 mm^3 optically coupled to a 400 µm silica fibre. The detection system includes a photomultiplier tube (PMT), data acquisition card (USB-DAQ) and LabView software, which reads the counters of the USB-DAQ. For the irradiation, 334 MBq of ^{18}F-FDG (0.02 ml) was placed inside a polypropylene cap to create a point source. The BeO probe tip was placed opposite the cap in the immediate vicinity. Upon irradiation with ^{18}F, the BeO emits light via radioluminescence (RL) with intensity proportional to the activity of ^{18} F at that time. The RL light output data was collected for 8.3 h. Background readings were obtained by collecting the RL output in the absence of the point source.

Results RL output (count rate) response to the activity of ^{18}F, measured with the dose calibrator, showed a strong positive linear relationship (Fig. 1).

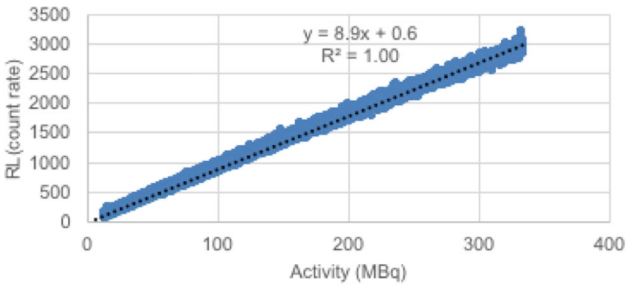

Fig. 1 RL count rate response to the activity of ^{18}F-FDG

After background correction of the RL count rate, the response linearity was assessed by calculating the measured half-life of ^{18}F from the ln (RL output) vs time plot. The measured half-life (110.59 min) was in good agreement with the actual half-life of ^{18}F (109.77 min).
Conclusion The linear response of a BeO FOD to ^{18}F positron emitter source has shown the feasibility of using real-time FOD in Nuclear medicine. Further studies are planned to develop a FOD to validate the image-based dosimetry used in Radioembolization.
Reference

1. Santos A.M.C., M. Mohammadi, Asp J., Monro T. M., and Afshar V. S. (2013). Characterisation of a real-time fibre-coupled beryllium oxide (BeO) luminescence dosimeter in X-ray beams. Radiation Measurements, (53–54), 1–7.

P007 Rapid 4D cone-beam CT in under 20 s with new generation linacs: a simulation study

S. J. Blake[1], O. Dillon[1], H. L. Byrne[1], R. T. O'Brien[1]

ACRF Image X Institute, School of Health Sciences, The University of Sydney, Australia. samuel.blake@sydney.edu.au (Presenting author); owen.dillon@sydney.edu.au; hilary.byrne@sydney.edu.au; ricky.obrien@sydney.edu.au

Introduction New generation linacs use a ring-mounted design that enables faster imaging and radiotherapy treatments. The kilovoltage x-ray imaging system integrated with the Halcyon 2.0 linac (Varian Medical Systems) is capable of rapid 3D cone-beam CT (3DCBCT) in 16.6 s [1]. By comparison, a conventional 4DCBCT acquires projections over 240 s to produce images of sufficient quality across the respiratory cycle. In this study, we demonstrate the feasibility of using rapid acquisitions to produce 4DCBCT images and quantify image quality relative to conventional 4DCBCT.
Method Two 4DCT images for each of 14 patients from the Cancer Imaging Archive 4D-Lung dataset were used in this study. One was considered a "planning" 4DCT and the other a "ground-truth" for 4DCBCT simulation and image quality quantification. Conventional and rapid CBCT acquisitions were simulated over 200 degrees using the Reconstruction Tool Kit by generating 1320 and 491 forward projections over 240 and 16.6 s, respectively, with a constant 13–15 breaths per minute respiratory rate. The 4D Feldkamp-Davis-Kress (4DFDK) algorithm [2] was used to reconstruct both acquisitions (Fig. 1). The rapid acquisition was also reconstructed using Motion Compensated FDK (MCFDK) by backprojecting data along curved paths to account for motion estimated from the planning 4DCT [3]. Image quality was quantified in terms of contrast-to-noise ratio

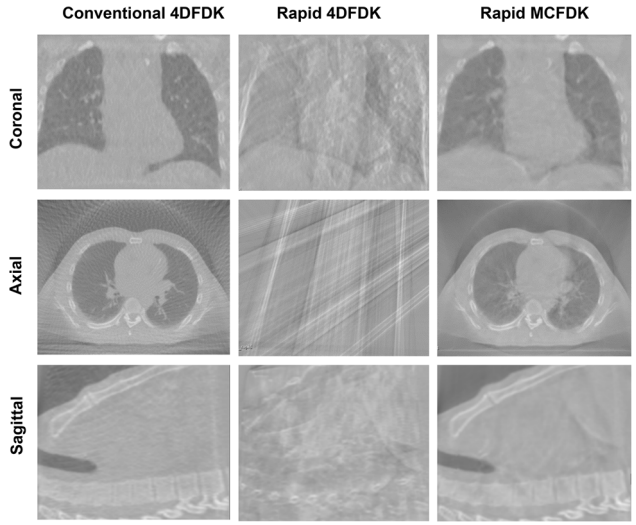

Fig. 1 Central slice reconstructions for each 4DCBCT acquisition and reconstruction method considered

(CNR), root-mean-square error to ground-truth (RMSE-GT) and structural similarity index to ground-truth (SSIM-GT).
Results The phase-averaged CNR, RMSE-GT and SSIM-GT for the conventional 4DFDK were 2.695, 78.93 and 0.415 respectively. The phase-averaged CNR, RMSE-GT and SSIM-GT for the rapid 4DFDK and MCFDK reconstructions were 2.006, 292.8, 0.072 and 2.864, 134.7, 0.205.
Conclusion Using motion compensated reconstruction, forward projections simulated for rapid CBCT protocols can be reconstructed to give 4DCBCT images of quality comparable to conventional protocols.
References

1. Cai B, Laugeman E, Mazur TR, Park JC, Henke LE, Kim H, Hugo GD, Mutic S, Li H (2019) Characterization of a prototype rapid kilovoltage x-ray image guidance system designed for a ring shape radiation therapy unit. Med Phys 46(3):1355–70. https://doi.org/10.1002/mp.13396
2. Feldkamp LA, Davis LC, Kress JW (1984) Practical cone-beam algorithm. J Opt Soc Am A 1:612–9. https://doi.org/10.1364/JOSAA.1.000612
3. Rit S, Wolthaus JWH, van Herk M, Sonke J-J (2009) On-the-fly motion-compensated cone-beam CT using an a priori model of the respiratory motion. Med Phys 36(6):2283–96. https://doi.org/10.1118/1.3115691

P008 Ultraviolet Germicidal Irradiation (UVGI) Laundry Prototype

Z. Brady[1,2], L Wilkinson[3], J. Crocker[1], K. Macmillan[4], A. Coustley[1], M. Law[1,2,5]

[1]Department of Radiology, Alfred Health, Melbourne, Australia; [2]Department of Neuroscience, Monash University, Melbourne, Australia. z.brady@alfred.org.au (Presenting author); [3]Dept. of Medical Engineering & Physics, St. Vincent's Hospital, Melbourne, Australia. Luke.Wilkinson@svha.org.au; j.crocker@alfred.org.au; [4]Surgical Services, Alfred Health, Melbourne, Australia. K.Macmillan@alfred.org.au; A.Coustley@alfred.org.au; [5]Department of Electrical and Computer

Systems Engineering, Monash University, Melbourne, Australia. meng.law@alfred.org.au

Introduction At the start of the COVID-19 pandemic, there were critical shortages of N95 filtering facepiece respirators (FFRs) worldwide. The efficacy of decontamination and re-use of respirators in healthcare using ultraviolet germicidal irradiation (UVGI) had not been widely assessed. For preparedness as a crisis capacity strategy [1], we developed an FFR UVGI decontamination "laundry" prototype [2].
Method UVGI inactivates microorganisms to block DNA and RNA replication [3–4]. A literature review was conducted to determine (1) the UVGI dose required to inactivate a single-stranded RNA viral load, (2) penetrability and effectiveness for FFRs, and (3) treatment effects on filtration, fit and strength of the FFR. Testing was undertaken to determine the irradiance level and intensity variation in the treatment field for two different UVGI devices, the appropriateness of UV measurement meters, and the orientation for hanging FFRs to maximise coverage and throughput while not compromising safety.
Results At the time of conducting the evaluation, UVGI inactivation of COVID-19 (SARS-CoV-2) on FFRs had not been confirmed directly [5]. The general consensus in the literature was that a UVGI dose of $\geq$ 1 J/cm^2 was required, that laundry workflow needed consideration due to remaining bio-burden, verification of the marginally acceptable dose within each treatment cycle and zone was necessary, and the maximum possible dose for multiple treatment cycles per FFR must not be exceeded due to potential integrity loss. Strict protocols were required in terms of infection control (COVID-19 contaminated masks being handled) and radiation protection (due to the UV-C hazards). It was found that 1,200 FFRs could be processed every 24 h with a treatment zone that exhibited 60% dose variation from the edges relative to the centre.
Conclusion Although never implemented, the UVGI laundry prototype was an important exercise in risk mitigation and management using new applications of technology during a crisis.
References/Acknowledgements

1. US Centres for Disease Control and Prevention (CDC), Decontamination and Reuse of Filtering Facepiece Respirators, https://www.cdc.gov/coronavirus/2019-ncov/hcp/ppe-strategy/decontamination-reuse-respirators.html, 9 April 2020.
2. Lowe JJ, Paladino KD, Farke JD et al. (2020) N95 Filtering Facemask Respirator Ultraviolet Germicidal Irradiation (UVGI) Process for Decontamination and Reuse, Nebraska Medicine. https://www.nebraskamed.com/sites/default/files/documents/covid-19/n-95-decon-process.pdf
3. Lindsley WG, Martin Jr SB, Thewlis RE et al. (2015) Effects of Ultraviolet Germicidal Irradiation (UVGI) on N95 Respirator Filtration Performance and Structural Integrity, J Occup Environ Hyg 12(8):509–517. https://doi.org/10.1080/15459624.2015.1018518
4. Kowalski W, Bahnfleth WP, Hernandez MT (2009) A Genomic Model for the Prediction of Ultraviolet Inactivation Rate Constants for RNA and DNA Viruses. IUVA News 11:15–28.
5. N95Decon Research Document. Version 1.2, Technical Report for UV-C-Based N95 Reuse Risk Management, 1 April 2020. https://www.n95decon.org/

P009 Survey of Medical Physics Radiation Risk Assessments for Research Trials

Z. Brady[1,2], L. Wilkinson[3]

[1]Department of Radiology, Alfred Health, Melbourne, Australia; [2]Department of Neuroscience, Monash University, Melbourne, Australia. z.brady@alfred.org.au (Presenting author); [3]Dept. of Medical Engineering & Physics, St. Vincent's Hospital, Melbourne, Australia Luke.Wilkinson@svha.org.au

Introduction A National Mutual Acceptance (NMA) system of scientific and ethical review of multi-centre research conducted in publicly funded health services has been operating for a number of years. However, radiation risk assessments in accordance with the Code of Practice [1] have not been similarly streamlined. Furthermore, a lack of uniformity in the implementation/interpretation of the Code in different jurisdictions is impacting the approval of research involving ionising radiation exposure. A Working Group was established to review medical physics work practices within Australia when providing radiation risk assessments in accordance with the Code.
Method An online survey was distributed to the ACPSEM membership during April 2019. Survey questions covered topics including (i) standard of care, (ii) calculation of dose, (iii) consent form risk statements, and (iv) governance. Answers were thematically analysed by coding to common categories and reviewed for consensus.
Results There were 27 survey responses from six jurisdictions. Victoria and NSW contributed 60% of the responses. Respondents provided risk assessments in Radiology (81%), Nuclear Medicine (89%) and Radiotherapy (11%). For most respondents (89%) the researcher decides if imaging using ionising radiation is standard of care or additional to it. However, a large percentage (70%) also acknowledged that a discussion between multiple parties often contributes to the decision. Almost all respondents confirmed calculating an effective dose specific to the facility, however, about 20% indicated using published values for low dose procedures. Additionally, there was an evident state-based variation in radiation risk models used.
Conclusion The survey demonstrated an inconsistent approach to implementation of the Code. State-based variations in the use of risk models will lead to significant differences between calculated risk. The survey results were used in a submission to the Radiation Health Committee who subsequently issued a statement in relation to multi-centre trials [2].
References/Acknowledgements

1. Australian Radiation Protection and Nuclear Safety Agency (2005) Code of Practice for the Exposure of Humans to Ionizing Radiation for Research Purposes, Radiation Protection Series (RPS) No. 8.
2. Radiation Health Committee (2020) Statement on ethical review for multi-centre trials.

P010 Dosimetric Evaluation of Dual Energy Computer Tomography with Iterative Metal Artefact Reduction for Radiotherapy Planning with Bilateral Pelvic Hip Prosthesis

Athreya Buddhavarapu[1], Sarah Elliott[2]

[1]Ballarat Austin Radiation Oncology Centre, Ballarat, Australia. Athreya.Buddhavarapu@austin.org.au; [2]Olivia Newton-John Cancer Wellness & Research Centre, Heidelberg, Australia. Sarah.Elliott@austin.org.au

Introduction Metal artefacts in computer tomography (CT) create contouring challenges in radiotherapy planning and potential dosimetric errors [1]. For patients with metal hip prosthesis implants, dual

energy CT combined with the iterative metal artefact reduction algorithm (DE iMAR) has been shown to reduce artefacts surrounding the prosthesis more than iMAR alone [2–5]. The aim of this work is to evaluate the dosimetry on DE iMAR datasets in a phantom simulation of a bilateral hip prosthesis.

Method A Gammex CT phantom was scanned using single (SE) and dual energy protocols on a Siemens AS Definition CT. The DE iMAR dataset was reconstructed to a virtual monochromatic energy of 120 keV, optimising image quality and matching that used for SE iMAR. The phantom contained titanium and stainless steel inserts, positioned to simulate a bilateral hip prosthesis. A ground truth (GT) scan was also acquired with bone replacing the metal inserts. In the planning system (Monaco v5.1), a single field (size 11.5 cm × 11.5 cm, energy 10 MV) was calculated on all image sets, using the corresponding CT to electron density conversion curves. An uncorrected scan (no iMAR) was included in the dosimetric evaluation for further context.

Results SE iMAR and DE iMAR images are shown in Fig. 1, with reduced artefacts surrounding the metal inserts in the latter. There was insignificant difference between image sets in uniformity (mean Hounsfield units) over regions of interest close to the metal, however noise (standard deviation in Hounsfield units) was lower in DE iMAR and comparable to GT. The cross axis dose profiles (Fig. 2) in the region of streak artefact show DE iMAR and SE iMAR within 1.7% of GT.

Conclusion Initial results of a simple phantom plan indicate that DE iMAR reduces metal artefacts more than SE iMAR, whilst providing similar dosimetry. Further work will extend to a phantom with actual hip prosthesis and evaluating dosimetric differences on complex plans.

Acknowledgements The authors would like to thank Nikki Caswell and Saju Sherly, for their assistance with this work.

References

1. Giantsoudi D, De Man B, Verburg J, et al. (2017) Metal artifacts in computed tomography for radiation therapy planning: Dosimetric effects and impact of metal artifact reduction. Phys Med Biol 62:R49–R80. https://doi.org/10.1088/1361-6560/aa5293
2. Higashigaito K, Angst F, Runge VM, et al. (2015) Metal Artifact Reduction in Pelvic Computed Tomography With Hip Prostheses. Invest Radiol 50:828–834. https://doi.org/10.1097/RLI.0000000000000191
3. Pawałowski B, Panek R, Szweda H, Piotrowski T (2020) Combination of dual-energy computed tomography and iterative metal artefact reduction to increase general quality of imaging for radiotherapy patients with high dense materials. Phantom study. Phys Medica 77:92–99. https://doi.org/10.1016/j.ejmp.2020.08.009
4. Lim P, Barber J, Sykes J (2019) Evaluation of dual energy CT and iterative metal artefact reduction (iMAR) for artefact reduction in radiation therapy. Australas Phys Eng Sci Med 42:1025–1032. https://doi.org/10.1007/s13246-019-00801-1
5. Bongers MN, Schabel C, Thomas C, et al. (2015) Comparison and combination of dual-energy- and iterative-based metal artefact reduction on hip prosthesis and dental implants. PLoS One 10:1–12. https://doi.org/10.1371/journal.pone.0143584

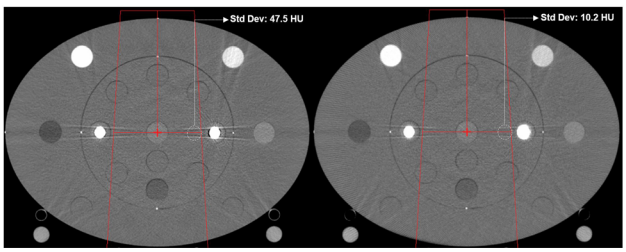

Fig. 1 Images of phantom with SE iMAR (left) and DE iMAR (right) scans, with beam orientation indicated. The titanium insert is on the left and stainless steel insert is on the right for both phantoms

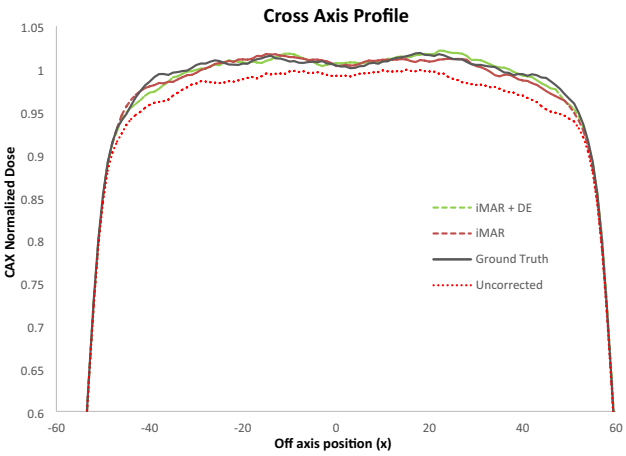

Fig. 2 Cross axis dose profiles within region of streak artefact (0.5 cm above centre of phantom) for all image sets

P011 Lung ventilation imaging from low-dose 4DCBCT for daily function adaptation: a proof of concept study

H. L. Byrne[1], O. Dillon[1], S. Blake[1], J. Kipritidis[2], R. O'Brien[1], P. Keall[1]

[1]ACRF Image X Institute, School of Health Sciences, The University of Sydney, Australia. hilary.byrne@sydney.edu.au (Presenting author); owen.dillon@sydney.edu.au; samuel.blake@sydney.edu.au; [2]Northern Sydney Cancer Centre, Royal North Shore Hospital, Australia; john.kipritidis@health.nsw.gov.au; ricky.obrien@sydney.edu.au; paul.keall@sydney.edu.au

Introduction CT ventilation imaging [1, 2] extracts lung function from 4DCT for informing radiotherapy planning. Radiation pneumonitis, a side effect of lung radiotherapy, is predicted more accurately by functionally-weighted dose-volume metrics (V20 for functional lung: AUC 0.70) than metrics that treat the lung as a homogeneous organ (V20 for total lung: AUC 0.52) [3]. However, lung function changes across the treatment course in response to radiotherapy itself [4, 5], so availability of ventilation images throughout treatment is desirable. The ability to generate CT ventilation images from standard 4D cone beam CT (4DCBCT) has been demonstrated [5], but current 4DCBCT requires 4-min scan times. The ADAPT clinical trial (NCT04070586) has demonstrated high quality 4DCBCT with 1-min scans and 3DCBCT-equivalent dose, making 4D imaging throughout treatment viable within current standard treatment workflows. In this study we compare ventilation images derived from the ADAPT scans to ventilation derived from 4DCT.

Method In the ADAPT clinical trial, 4DCT scans and two ADAPT 4DCBCT scans were acquired for 30 patients. The 'ADAPT' technique changed gantry rotation speed in response to patient breathing to acquire 4DCBCTs with only 200 projections and equivalent dose to 3DCBCT. In this study, for one patient the 4DCBCT was processed

using a deformable image registration and Jacobian-determinant based method to produce a ventilation map [6]. This was compared to ventilation derived from the 4DCT using the same method.

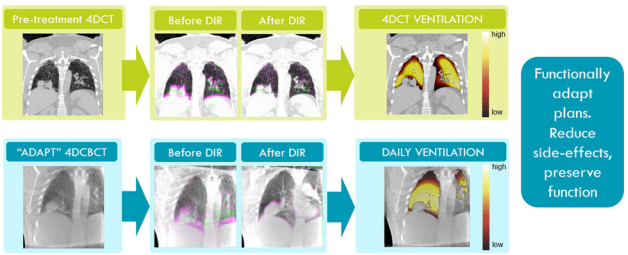

Fig. 1 Ventilation imaging for daily functional adaptive radiotherapy

Results Visually, the deformable image registration performed well and superior-inferior ventilation gradients were comparable. Quantitative single-lung comparison between 4DCT ventilation and "ADAPT" 4DCBCT ventilation yielded a Spearman correlation of 0.65.

Conclusion This study shows for the first time that ventilation can be derived from 1-min, 200-projection 4DCBCT acquired with standard clinical hardware showing daily monitoring of lung function across the course of treatment is viable.

References

1. Kipritidis J, Tahir BA, Cazoulat G, et al. (2019) The VAMPIRE challenge: A multi-institutional validation study of CT ventilation imaging. Medical Physics 46:1198–1217. https://doi.org/10.1002/mp.13346
2. Hegi-Johnson F, de Ruysscher D, Keall P, et al. (2019) Imaging of regional ventilation: Is CT ventilation imaging the answer? A systematic review of the validation data. Radiotherapy and Oncology 137:175–185. https://doi.org/10.1016/j.radonc.2019.03.010
3. Faught AM, Yamamoto T, Castillo R, et al. (2017) Evaluating Which Dose-Function Metrics Are Most Critical for Functional-Guided Radiation Therapy. International Journal of Radiation Oncology*Biology*Physics 99:202–209. https://doi.org/10.1016/j.ijrobp.2017.03.051
4. Siva S, Hardcastle N, Kron T, et al. (2015) Ventilation/Perfusion Positron Emission Tomography—Based Assessment of Radiation Injury to Lung. International Journal of Radiation Oncology*Biology*Physics 93:408–417. https://doi.org/10.1016/j.ijrobp.2015.06.005
5. Kipritidis J, Hugo G, Weiss E, et al. (2015) Measuring interfraction and intrafraction lung function changes during radiation therapy using four-dimensional cone beam CT ventilation imaging. Medical Physics 42:1255–1267. https://doi.org/10.1118/1.4907991
6. Kipritidis J, Woodruff HC, Eslick EM, et al. (2016) New pathways for end-to-end validation of CT ventilation imaging (CTVI) using deformable image registration. In: 2016 IEEE 13th International Symposium on Biomedical Imaging (ISBI). pp 939–942

P012 Conformance of a 3T MRI Scanner to the QIBA Diffusion Profile

M. E. Carr[1,2,3], K. E. Keenan[4], M. A. Boss[5], P. Metcalfe[1,2], A. Walker[1,2,3,6], L. C. Holloway[1,2,3,6,7]

[1]Centre for Medical Radiation Physics, University of Wollongong, Wollongong, Australia; [2]Ingham Institute for Applied Medical Research, Liverpool, Australia; [3]Department of Medical Physics, Liverpool and Macarthur Cancer Therapy Centre Liverpool, Australia. mec640@uowmail.edu.au (Presenting author); [4]National Institute of Standards and Technology, Colorado, United States. kathryn.keenan@nist.gov; [5]American College of Radiology, Philadelphia, United States. mboss@acr.org; metcalfe@uow.edu.au; [6]South Western Sydney Clinical School, University of New South Wales, Liverpool, Australia. amy.walker3@health.nsw.gov.au; [7]Institute of Medical Physics, University of Sydney, Camperdown, Australia. lois.holloway@health.nsw.gov.au

Introduction The Apparent Diffusion Coefficient (ADC) is an imaging biomarker derived from diffusion-weighted MR-images. The biomarker has potential in characterising disease [1] and monitoring treatment responses [2–3]. The 2019 Quantitative Imaging Biomarker Alliance (QIBA) Diffusion Profile outlines conformance limits for phantom imaging for evaluating an MR-scanners ability to measure ADC bias and reproducibly (https://qibawiki.rsna.org/index.php/Profiles). This study aimed to evaluate the QIBA Profile on a dedicated 3 T radiotherapy MRI-scanner. Additionally, investigations into longitudinal trends in scanner performance and phantom orientation dependency were completed.

Method A QIBA/NIST/NCI isotropic diffusion phantom was scanned monthly over one year on a 3T Siemens Magnetron Skyra scanner. The phantom contained 13 aqueous vials with varying concentrations of PVP (0% to 50% by mass fraction). These were surrounded by an ice-bath for thermal control and had known reference 0 °C ADC values [4]. Recommended Single-Shot EPI (SS-EPI) sequences were used to generate in-line ADC maps of the central slices of the phantom. Acquisitions were repeated four times, then the phantom was rotated before replicating imaging in each orthogonal plane. ADC maps were analysed by an in-house developed python script and aspects of the Profile were assessed: bias, linearity (R^2) and short/long term repeatability/reproducibility coefficient of variation (CV).

Results Median bias in the phantom's isocentre vial in transverse orientation was − 1.3%, with short- and long-term CV's of 0.1% and 0.9%, respectively. Linearity was calculated using all vials and found $R^2 = 0.9997$ with Slope = 1.0. Similar findings were observed for coronal and sagittal orientations (Fig. 2). In general, higher concentrated PVP vials (lower reference ADC's) had less reproducibility.

Figure 1: Variability in measured ADC observed over one year for transverse phantom orientation. Note: ■,● and + = isocentre, inner-ring and outer-ring phantom vials respectively.

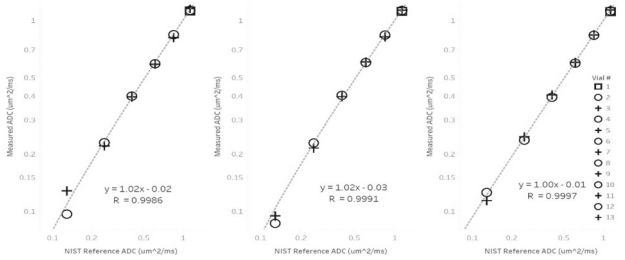

Figure 2: A strong linear correlation was found in all phantom orientations: coronal (left), sagittal (middle) and transverse (right).

Conclusion All scanner measurements conformed to the QIBA Profile limits. *b*-value dependence, SNR and random error analysis is ongoing for complete Profile assessment. Directional imaging was found to have a minor impact on the measurement variability whilst no long-term variability trends were observed.

Acknowledgements Access to the 3T MRI scanner at Liverpool Hospital was enabled by staff at the Cancer Therapy Centre in collaboration with Ingham Institute for Applied Medical Research (Physics). Further, this research was in part funded by the South Western Sydney Local Health District (SWSLHD) Top-Up Scholarship (2021- Madeline Carr).

References

1. Provenzale JM, Mukundan S, Barboriak DP (2006) Diffusion-weighted and perfusion MR imaging for brain tumor characterization and assessment of treatment response. Radiology 239:632–649. https://doi.org/10.1148/radiol.2393042031
2. Chenevert TL, Ross BD (2009) Diffusion imaging for therapy response assessment of brain tumor. Neuroimag Clin N Am 19:559–571. https://doi.org/10.1016/j.nic.2009.08.009
3. Thoeny HC, Ross BD (2010) Predicting and monitoring cancer treatment response with diffusion-weighted MRI. J Magn Reson Imaging 32:2–16. https://doi.org/10.1002/jmri.22167
4. Keenan KE, Carnika S, Gottlieb SC, Boss MA, Stupic KF (2017) Assessing changes in MRI measurands incurred in a scanner upgrade: Is my study compromised? In: Program #3992, 25th Annual Meeting ISMRM, Honolulu

P013 An unexpected change in the density of 3D printed PLA: on the importance of e-step calibration and QA to the clinical workflow

P. H. Charles[1,2,3], T. Kairn[2,3,4], S. B. Crowe[2,3,4,5]

[1]Herston Biofabrication Institute, Brisbane, Australia; [2]School of Information Technology and Electrical Engineering, University of Queensland, Australia; [3]Science and Engineering Faculty, Queensland University of Technology, Australia. Paul.Charles@health.qld.gov.au (Presenting author); [4]Radiation Oncology, Royal Brisbane and Women's Hospital, Australia. Tanya.Kairn@health.qld.gov.au; [5]Herston Biofabrication Institute, Brisbane, Australia. Scott.Crowe@health.qld.gov.au

Introduction 3D printers are increasingly utilised in radiotherapy departments. Common uses are printing of treatment bolus and dosimetry equipment, including phantoms. In most cases it is vital to accurately control the density of the 3D printed device. A thorax dosimetry phantom was printed in two distinct phases, several months apart, due to a project pause. It was observed that the density of the phantom was distinctly different between the two phases. This observation had important ramifications for all 3D printed devices in the department, so was investigated.

Method From a CT scan of the thorax phantom, the HU value of the of the "bone" (StoneFil, Formfutura), "tissue" (PLA, Raise; infill density = 98%) and "lung" (PLA, Raise; infill density = 19%) was calculated. The observed difference between phase 1 and phase 2 was quantified. Using the above material, cubes (side length 2 cm) with infill densities between 20 and 100% were printed using the same 3D printer (Raise3D Pro 2). The HU value of these cubes were compared to similar cubes printed around the time of phase 1 of the phantom. An investigation into the discrepancies was performed.

Results Fig. 1 displays the clearly observed density differences between the phase 1 (right side) and phase 2 (left side) of the thorax phantom.

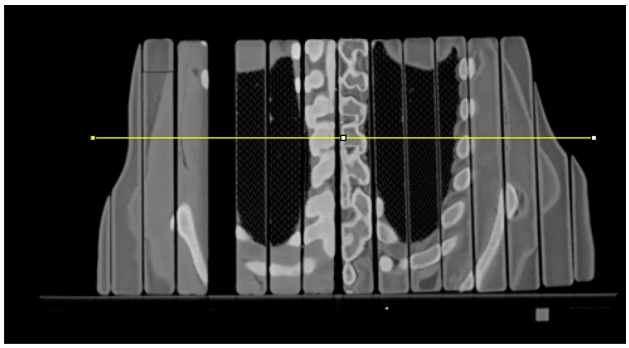

The HU value of 100% infill PLA was 10 HU during phase 1 and 200 HU during phase 2. The StoneFil HU value similarly increased from 630 to 850 HU.

Between phase 1 and phase 2 the 3D printer firmware (RaiseTouch) was upgraded (from 1.1.0.1021 to 1.4.2.715). The density increase was observed for all filaments, therefore an e-step calibration change may have occurred where it was unintentionally set to a value before the firmware upgrade (phase 1) and reset to a default value (phase 2).

Conclusion This work demonstrates two important points:

1. *All* individual 3D printed devices used in the clinic should be subject to rigorous quality assurance in case there are unexpected errors
1. *All* technical aspects of a 3D printer (including flow rate and e-step value) should be tested, quantified and documented at commissioning and after any upgrade

Acknowledgements This work was made possible by the Herston Biofabrication Institute Cancer Care Services programs, supported by the Metro North Hospital and Health Service.

P014 Listing of patient-matched 3D-printed radiotherapy bolus on the Australian Register of Therapeutic Goods

S. B. Crowe[1,2,3,4], B Murray[2,5], T. Poroa[1], J. Luscombe[1], D. Vincent[1], A. Livingstone[1], R. Wilks[1,2,3], T. Kairn[1,2,3,4]

[1]Cancer Care Services, Royal Brisbane and Women's Hospital, Brisbane, Queensland, Australia; [2]Herston Biofabrication Institute, Metro North Hospital and Health Service, Brisbane, Queensland, Australia; [3]School of Information Technology and Electrical Engineering, University of Queensland, Brisbane, Qld, Australia; [4]School of Chemistry and Physics, Queensland University of Technology, Brisbane, Queensland, Australia.

sb.crowe@gmail.com (Presenting author); [5]Australian Institute for Bioengineering and Nanotechnology, University of Queensland, Brisbane, Queensland, Australia. becca.murray@health.qld.gov.au; tania.poroa@health.qld.gov.au; jenna.luscombe@health.qld.gov.au; debra.vincent@health.qld.gov.au; alexander.livingstone@health.qld.gov.au; rachael.wilks@health.qld.gov.au; tanya.kairn@health.qld.gov.au

Introduction 3D-printed radiotherapy bolus meets the Australian Therapeutic Goods Administration (TGA) definition of a patient-matched medical device and is therefore subject to regulatory provisions. Specifically, a manufacturer must have the device listed on the Australian Register of Therapeutic Goods (ARTG) as a class I non-measuring, non-sterile device before it can be supplied. This study details how the requirements for an application for inclusion on the ARTG were addressed by the Royal Brisbane & Women's Hospital and Herston Biofabrication Institute.
Method Compliance with the medical device essential principles was achieved through the development of processes and a documentation framework based on ISO 13485 medical device quality management system principles. This included peer-reviewed risk assessments; documented design, manufacturing, quality and case plans; a process for tracking of requests, quality assessment, and feedback using our departmental oncology information system (see Fig. 1); and establishment of staff responsibilities and clinical workflows (including quality assurance testing processes and instructions for use).
Results Once the compliance to essential principles, risk assessment and associated documentation was completed, a declaration of conformity was submitted to the TGA with details of the device, signed versions of select supporting documentation, and a registration payment of $550 AUD. The device was listed on the ARTG for manufacture and supply by Metro North Hospital and Health Service (see Fig. 2), making the Royal Brisbane & Women's Hospital the first clinical department to be listed for patient-matched bolus.
Conclusion The supply of in-house manufactured radiotherapy bolus was made possible with the ARTG listing. The document templates and processes will facilitate efficient future ARTG applications for listing of class I 3D printed medical devices to be manufactured within the department.
Acknowledgements This work was made possible by the Herston Biofabrication Institute's Cancer Care Services and Urology programs who are supported by the Metro North Hospital and Health Service.

Task
3D Device Structure Approved
3D STL Exported for Production
3D Print Preparation
3D Print and Post Processing Complete
3D Device Wax/Pb Production
3D Device Visual and Manual Inspection
3D Device Physics QA
3D Device labelled and Packaged
3D Device Delivered
3D Pre-Treatment Fitting Required
3D Device Code Capture

Fig. 1 Quality check list items within Mosaiq oncology information system

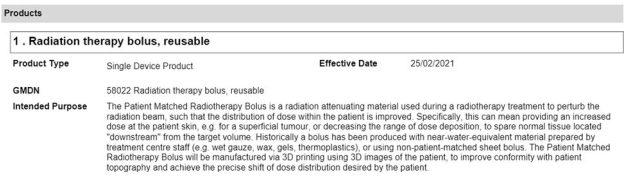
Products

1 . Radiation therapy bolus, reusable

Product Type	Single Device Product	Effective Date	25/02/2021
GMDN	58022 Radiation therapy bolus, reusable		
Intended Purpose	The Patient Matched Radiotherapy Bolus is a radiation attenuating material used during a radiotherapy treatment to perturb the radiation beam, such that the distribution of dose within the patient is improved. Specifically, this can mean providing an increased dose at the patient skin, e.g. for a superficial tumour, or decreasing the range of dose deposition, to spare normal tissue located "downstream" from the target volume. Historically a bolus has been produced with near-water-equivalent material prepared by treatment centre staff (e.g. wet gauze, wax, gels, thermoplastics), or using non-patient-matched sheet bolus. The Patient Matched Radiotherapy Bolus will be manufactured via 3D printing using 3D images of the patient, to improve conformity with patient topography and achieve the precise shift of dose distribution desired by the patient.		

Fig. 2 Public summary of ARTG Entry 355606

P015 Superficial mould brachytherapy device design and treatment planning using 3D scanning data

S. B. Crowe[1,2,3,4], E. Simpson-Page[1], J. Luscombe[1], R. Wilks[1,2,3], T. Kairn[1,2,3,4]

[1]Cancer Care Services, Royal Brisbane and Women's Hospital, Brisbane, Queensland, Australia; [2]Herston Biofabrication Institute, Metro North Hospital and Health Service, Brisbane, Queensland, Australia; [3]School of Information Technology and Electrical Engineering, University of Queensland, Brisbane, Qld, Australia; [4]School of Chemistry and Physics, Queensland University of Technology, Brisbane, Queensland, Australia. sb.crowe@gmail.com (Presenting author); emily.simpson-page@health.qld.gov.au; jenna.luscombe@health.qld.gov.au; rachael.wilks@health.qld.gov.au; tanya.kairn@health.qld.gov.au

Introduction The design of simple 3D printable patient-matched devices (e.g. uniform thickness bolus) can be achieved using models acquired from 3D scanning systems. However, the design of complex devices may require the use of a treatment planning system and dose calculation algorithm, to allow optimisation of device dimensions (including, for example, catheter channels). The use of 3D model files (e.g. STLs) is however not supported by most treatment planning systems.
Method An Artec Leo device was used to scan 5 volunteers with a total of 16 treatment areas marked with red pen (HREC approval QRBW/66064). Autodesk Meshmixer was used to create a treatment volume and preliminary mould design from the reconstructed 3D model, by selection of the visible treatment area and applicator area and extrusion of these surfaces to a user defined prescription depths and mould thicknesses. 3D slicer was used to convert the 3D models of the body, treatment volume and mould to a CT image dataset (conversion to a binary labelmap) and RTSTRUCT volumes. The rescale intercept and slope attributes within the CT image were modified to produce air- and water-equivalent HU. This data was imported into Varian Eclipse, where dwell positions and times were optimised for dose coverage.
Results An example treatment plan is shown in Fig. 1. Since brachytherapy dose calculations are performed clinically using a TG-43 algorithm, the lack of internal anatomy data did not impact dose calculation during treatment optimisation. For a clinical workflow, the mould could be 3D printed and included in a patient simulation CT for TG-186 model-based dose calculations.
Conclusion This study established a workflow to produce pseudo-CT datasets with segmented treatment volumes based on skin markings to allow complex superficial brachytherapy mould design and dose calculation.
Acknowledgements The investigators acknowledge the Royal Brisbane and Women's Hospital staff members who volunteered to be scanned by the investigators.

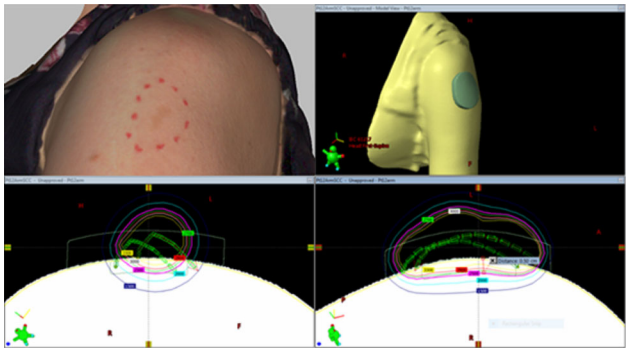

Fig. 32 Example superficial scan, segmentation and mould design

P016 Imaging for Radiotherapy in Australia: a Survey in Support of an ICRP Task Group

M. Djukelic, C. J. Martin[2], T. Kron[3]

[1]Sir Charles Gairdner Hospital, Perth, Australia. Mario.Djukelic@health.wa.gov.au; [2]University of Glasgow, Glasgow, UK and ICRP Task Group 116 chair. colin.j.martin@ntlworld.com; [3]Peter MacCallum Cancer Centre, Melbourne and University of Wollongong, Australia and ICRP Task Group 116 member. Tomas.Kron@petermac.org (presenting author)

Introduction In 2019 the International Commission on Radiological Protection set up a task group (TG116) to report on the use of imaging in radiotherapy. At about the same time ICRP initiated a mentorship program that should allow mentees to participate in ICRP activities. One of the activities for the mentees associated with TG116 was to support a survey on imaging in radiotherapy. We report on the patterns of practice found in the survey in Australia and New Zealand.
Method A survey with 130 items ranging from general information to imaging in planning and treatment delivery was designed by members of TG116. With the support of ACPSEM the survey was distributed to all chief physicists in radiotherapy departments in Australasia.
Results Twelve surveys were returned which is a reply rate of just over 10% of the number of centres in Australasia (111 as per IAEA Dirac database). Two thirds of the replies were from public centres and the survey covered a total of 55 linacs treating just under 2000 patients per month. All centres use CT based planning with one centre having a MRI scanner and a second a PET scanner dedicated to radiotherapy. The vast majority of linacs (53) was equipped with kV imaging and 90% of centres offered image guidance to more than 75% of patients. No centre formally recorded imaging dose or included it in the planning procedure. Only four centres reported having access to a diagnostic physicist (DIMP) for optimisation with three of the four centres that offered paediatric radiotherapy working with DIMPs to optimise dose.
Conclusion While the response rate of the survey was small it provides a glimpse of imaging practice in radiotherapy in Australasia. While equipment in particular for IGRT is excellent there appears to be room for more involvement of imaging physicists.
Acknowledgements ACPSEM office for distributing the surve

P017 A scripting solution in RayStation to account for patient immobilisation

Anthony Espinoza[1], S. Deshpande[1]

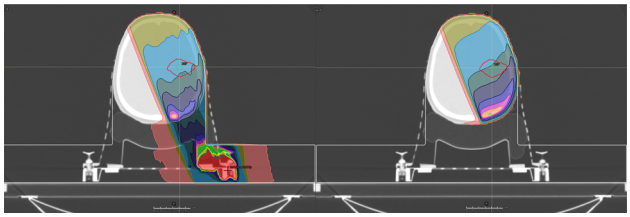

Fig. 29 Distribution for a 6X field when accounting for and ignoring immobilisation in H&N

[1]Liverpool and Macarthur Cancer Therapy Centres. Anthony.Espinoza@health.nsw.gov.au; Shrikant.Deshpande@health.nsw.gov.au

Introduction Dose computation in RayStation treatment planning system is bounded by the dose grid and a structure that represents the patient outline, referred to as the "External". Everything in the CT image that lies outside of the External and dose grid is regarded as vacuum and has no impact on the dose calculation. Fixation structures may exist outside of the External, but must have a material assigned to be included in calculations. RayStation offers the ability to create structure templates for couches and ancillary devices, but requires accurate representation of the devices and knowledge of material composition. This may be inefficient or impractical for sites with variable patient geometry and set up of immobilisation. A solution is extending the External volume using the scripting interface to generate a pseudo contour to include devices accurately and reproducibly for various patient setups.
Method A script was developed to generate the pseudo contour. Open fields and clinical VMAT Brains plans were calculated and compared to ignoring the immobilisation. Variations in doses between target coverage, OAR sparing and DVHs were assessed.
Results Initial results have found variations in dose using the expansion compared to ignoring the immobilisation. For a single field through H&N immobilisation, differences in dose can be seen due to high density materials (Fig. 1). In a VMAT plan, maximum local differences of up to 5% were observed.
Conclusion The impact of not accounting for the immobilisation devices has been found to be non-negligible and for VMAT plans may result in differences in PTV coverage. This script based solution allows for adaptable, accurate and efficient consideration to immobilisation in patient dose calculations that can be easily expanded to other treatment sites.

P018 A Novel Hybrid Approach to Automatic Cardiac Segmentation

R. N. Finnegan[1,2,3], P. Chlap[2,3,4], V. Chin[2,3,4], J. Dowling[1,4,5], A. Haidar[2,3,4], D. Thwaites[1], G. Delaney[2,4], J. Otton[4], L. Holloway[1,2,3,4]

[1]Institute of Medical Physics, University of Sydney, NSW; [2]Liverpool Cancer Therapy Centre, SWSLHD, NSW; [3]Ingham Institute for Applied Medical Research, NSW. robert.finnegan@sydney.edu.au (Presenting author); [4]South Western Sydney Clinical School, University of New South Wales, NSW. phillip.chlap@unsw.edu.au; vicky.chin@health.nsw.gov.au; [5]Australian e-Health Research Centre- CSIRO, Royal Brisbane Hospital, QLD. jason.dowling@csiro.au; a.haidar@unsw.edu.au; david.thwaites@sydney.edu.au; geoff.delaney@health.nsw.gov.au; j.otton@gmail.com; lois.holloway@health.nsw.gov.au

Introduction Incidental exposure of the heart during radiotherapy is associated with an increased risk of heart disease, however, this relationship is poorly understood. Increasing evidence suggests that cardiac substructure doses may be more predictive of cardiotoxicity risks, and thus more appropriate for establishing planning dose constraints. Analysis of large retrospective patient cohorts is necessary for risk modelling, which necessitates automatic segmentation. Our aim was to develop a method that could delineate the heart and cardiac substructures accurately, consistently, and with minimal errors.
Method Our approach combined a deep-learning (DL) model (nnU-Net [1]) for whole heart delineation with a novel anatomically-guided deformable image registration (DIR) process for mapping substructure contours from an atlas set (Fig. 1). We trained our DL model with clinical data (N = 300, Liverpool Cancer Therapy Centre), and used six atlases contoured by three observers for defining 15 cardiac substructures: four cardiac chambers, four coronary arteries, four cardiac valves, superior vena cava, ascending aorta, pulmonary artery. We tested our method on contoured CT data from 10 lung cancer patients, reporting measures of geometric similarity (Dice similarity coefficient, DSC and mean distance to agreement, MDA) and dose consistency (differences in mean and maximum dose) between automatic and manual delineations.
Results Our method produced substructure segmentations with good agreement with manual contours (Fig. 2). DSC and MDA values were close to the level of inter-observer contouring variability [2]. There were minimal systematic differences in dose metrics, although reducing variability at the patient level may require optimisation.
Conclusion Our hybrid approach derives benefits from both DL and atlas-based methods and will be used in future data-mining studies.
References/Acknowledgements
R N Finnegan acknowledges the support of Liverpool Cancer Therapy Centre, SWSLHD, and the support of the AusCAT team, in particular D Al Mouiee, X Huang, S Pang, and M Field.

1. Isensee, F., et al. (2021) nnU-Net: a self-configuring method for deep learning-based biomedical image segmentation. Nat Methods 18.2: 203–211. https://doi.org/10.1038/s41592-020-01008-z
2. Finnegan, R. et al. (2019) Feasibility of multi-atlas cardiac segmentation from thoracic planning CT in a probabilistic framework. Phys Med Biol 64:085006. https://doi.org/10.1088/1361-6560/ab0ea6

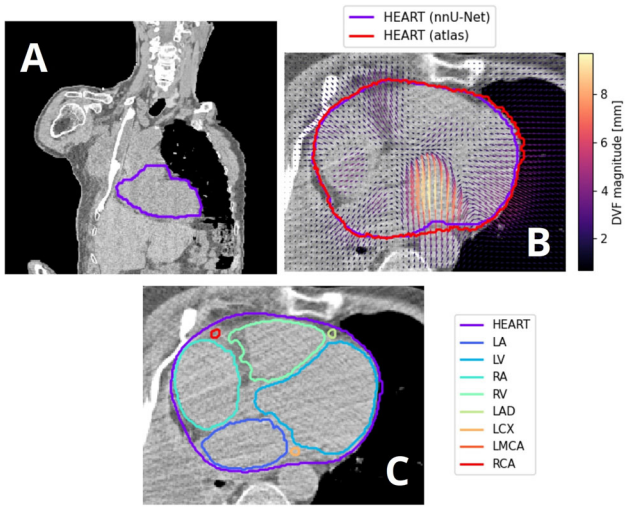

Fig. 1 **A** DL-based whole heart segmentation, **B** the novel DIR process, **C** resulting automatic segmentation

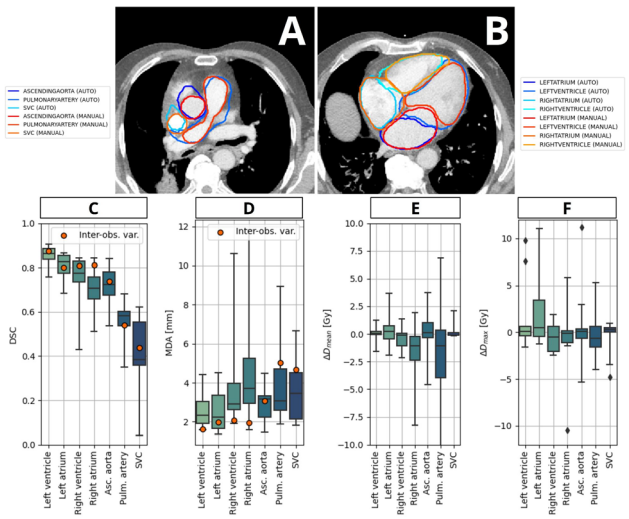

Fig. 2 **A**, **B** results for a representative patient. **C**, **D** Geometric similarity. **E**, **F** dose consistency

P019 Development of a Cross-Institutional Centralised Database to Leverage Radiotherapy Clinical Trial Data for Deep Learning Applications

Indrajit Ghosh[1], Chandrima Sengupta[1], Adam Mylonas[1], Paul Keall[1], Doan Trang Nguyen[2]

[1]ACRF Image X Institute, Faculty of Medicine and Health, University of Sydney, Sydney, NSW, Australia. indrajit.ghosh@sydney.edu.au; chandrima.sengupta@sydney.edu.au; adam.mylonas@sydney.edu.au; paul.keall@sydney.edu.au; [2]School of Biomedical Engineering, University of Technology Sydney, NSW, Australia. DoanTrang.Nguyen@uts.edu.au

Introduction Radiation therapy clinical trials [1] generate data such as pre-treatment series, image acquisitions from the linac, treatment plans, accumulated doses and log files. This data can be utilised to find useful patterns using statistical techniques and machine learning algorithms to create future image guided radiation therapy (IGRT) technology. This abstract documents the implementation of an imaging database, which extracts useful features from the files produced during two real-time IGRT Australian clinical trials and store them in a well organised, secure, and readily usable database. Its uses tried and tested database backends with cloud based RESTful API[5] technique to provide a useful toolkit for researchers and clinicians to utilise the data effectively.
Method The clinical data is stored in a secure, enterprise grade storage with strict access controls implemented, [1], which contains patient level data (CTs, structure sets, treatment plans) and fraction level data (pre-treatment CBCTs, intrafraction kV and MV images, machine log files, reconstructed delivered dose). Access to this data is controlled through role-based authentication through tokens such that access outside of the local server network can be provided, subject to each clinical trial protocol. The database solution provides client libraries for various software platforms with a secure role-based authentication system granting on-site access to this on-premises data utilising cloud VPN [2] technology, described in the following figures.

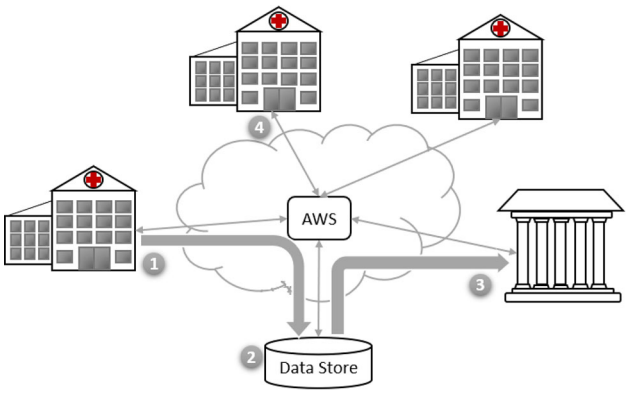

Figure 1: 1 Acquisition of deidentified imaging data and related artefacts from treatment centres and securely transferring them to an on premises data store. 2 Storage of access controlled data, which can be queried by researchers 3 and treatment planning and tumour tracking systems 4 via a cloud based interface.

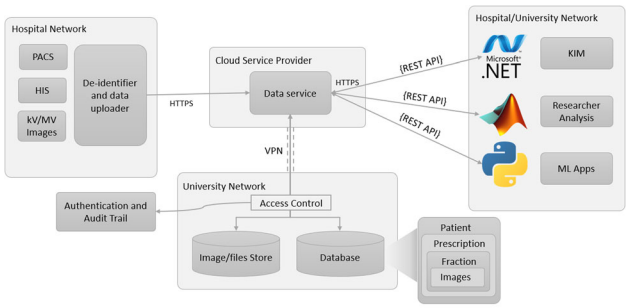

Figure 2: The high level architecture of the clinical trial database solution providing easy to integrate client libraries and RESTful APIs and data access via secure cloud based interfaces.

Results The database enables easy integration with existing tumour tracking applications deployed on site[3] and newer deep learning efforts. It allows collection of deidentified patient data from the treatment sites without involving third part data sharing platforms. Currently, the database contains clinical trial data from the TROG 15.01 SPARK and TROG 17.03 LARK trials.

Conclusion Implementation of the database provides a flexible platform to utilise existing clinical trial data for machine learning, quality assurance and enables a secure interface to add new data.

References

1. Keall, P., Nguyen, D.T., O'Brien, R., Hewson, E., Ball, H., Poulsen, P., Booth, J., Greer, P., Hunter, P., Wilton, L. and Bromley, R. (2020) Real-time image guided ablative prostate cancer radiation therapy: results from the TROG 15.01 SPARK Trial. International Journal of Radiation Oncology* Biology* Physics, 107(3), pp.530–538. https://doi.org/10.1016/j.ijrobp.2020.03.014
2. What is the Research Data Store (RDS)? https://sydneyuni.service-now.com/sm?id=kb_article_view&sysparm_article=KB0010833&sys_kb_id=1756239fdb26a010303d96888a96192c&spa=1 Accessed 04 June 2021
3. What is AWS Site-to-Site VPN? https://docs.aws.amazon.com/vpn/latest/s2svpn/VPC_VPN.html Accessed 04 June 2021
4. Hewson, E.A., Nguyen, D.T., O'Brien, R., Kim, J.H., Montanaro, T., Moodie, T., Greer, P.B., Hardcastle, N., Eade, T., Kneebone, A. and Hruby, G. (2019) The accuracy and precision of the KIM motion monitoring system used in the multi-institutional TROG 15.01 Stereotactic Prostate Ablative Radiotherapy with KIM (SPARK) trial. Medical physics, 46(11), pp.4725–4737. https://doi.org/10.1002/mp.13784
5. Lee, Y.Y.D., Nguyen, D.T., Moodie, T., O'Brien, R., McMaster, A., Hickey, A., Pritchard, N., Poulsen, P., Tabaksblat, E.M., Weber, B. and Worm, E. (2021) Study protocol of the LARK (TROG 17.03) clinical trial: a phase II trial investigating the dosimetric impact of Liver Ablative Radiotherapy using Kilovoltage intrafraction monitoring. BMC cancer, 21(1), pp.1–9. https://doi.org/10.1186/s12885-021-08184-x
6. Thomas Roy Fielding (2000) Architectural Styles and the Design of Network-based Software Architectures. Dissertation, University of California Irvine

P020 Recommended dose voxel size and statistical uncertainty parameters for precision of Monte Carlo dose calculation in stereotactic radiotherapy

Simon K. Goodall[1](Genesis Care WA), Martin A. Ebert[1,2,3]

[1]School of Physics, Mathematics, and Computing, Faculty of Engineering and Mathematical Sciences, University of Western Australia, Crawley, WA, Australia. simon.goodall@genesiscare.com (Presenting Author); Martin.Ebert@health.wa.gov.au

This work is recently published in JACMP https://doi.org/10.1002/acm2.13077

Introduction Monte Carlo (MC)-based treatment planning requires a choice of dose voxel size (DVS) and statistical uncertainty (SU). These parameters effect the precision of displayed dose distribution and time taken to complete a calculation.

Method In this investigation, 30 volumetric modulated arc therapy stereotactic radiotherapy treatment plans, 10 brain, 10 lung, and 10 spine were calculated in the Monaco 5.11.02 treatment planning system. Each plan was calculated with a DVS of 0.1 and 0.2 cm using SU values of 0.50%, 0.75%, 1.00%, 1.50%, and 2.00%, along with a ground truth calculation using a DVS of 0.1 cm and SU of 0.15%. The variance at each relative dose level was calculated for all SU settings to assess their relationship. The variation from the ground truth as applicable for each DVS and SU combination was determined for a range of DVH metrics and plan quality indices along with the time taken to complete the calculations. Finally, the effect of defining the maximum dose using a volume of 0.035 cc was compared to 0.100 cc when considering DVS and SU settings calculation.

Results Changes in the DVS produced greater variations from the ground truth calculation than changes in SU across the values tested. Plan quality metrics and mean dose values showed less sensitivity to changes in SU than DVH metrics.

Conclusion While maintaining an average calculation time of < 10 min, 75% of plans could be calculated with variations of $< 2.0\%$ from their ground truth values when using an SU setting of 1.50% and a DVS of 0.1 cm in the case of brain or spine plans, and a 0.2 cm DVS in the case of lung plans.

References/Acknowledgements

1. Chetty IJ, Curran B, Cygler JE, et al. Report of the AAPM Task Group No. 105: issues associated with clinical implementation of Monte Carlo-based photon and electron external beam treatment planning. Med Phys. 2007;34:4818–4853.
2. Chetty IJ, Rosu M, Kessler ML, et al. Reporting and analyzing statistical uncertainties in Monte Carlo–based treatment planning. Int J Radiat Oncol Biol Phys. 2006;65:1249–1259.
3. Ma CM, Li JS, Jiang SB, et al. Effect of statistical uncertainties on Monte Carlo treatment planning. Phys Med Biol. 2005;50:891–907.

4. Elekta. Monaco Dose Calculation Technical Reference; 2019 (LRMMON0001).
5. Jeraj R, Keall P. The effect of statistical uncertainty on inverse treatment planning based on Monte Carlo dose calculation. Phys Med Biol. 2000;45:3601–3613.
6. Keall PJ, Siebers JV, Jeraj R, Mohan R. The effect of dose calculation uncertainty on the evaluation of radiotherapy plans. Med Phys. 2000;27:478–484.
7. Buffa FM, Nahum AE. Monte Carlo dose calculations and radiobiological modelling: analysis of the effect of the statistical noise of the dose distribution on the probability of tumour control. Phys Med Biol. 2000;45:3009–3023.

P021 Towards Automating the Process of Standardizing Nomenclatures in Organs at Risk and Target Volumes: A Deep Learning based Approach

A. Haidar[1,2], M. Field[1,2], V. Batumalai[1,2], K. Cloak[1,2], D. Al Mouiee[1,2], P. Chlap[1,2], X Huang[2,3,4], V. Chin[1,4], M. Carolan[5,6], J. Sykes[7,8,9], S. K. Vinod[1,10], G. Delaney[1,10], L Holloway[1,2]

[1]South Western Sydney Clinical School, University of New South Wales & Ingham Institute for Applied Medical Research, NSW, Australia; [2]Department of Medical Physics, Liverpool and Macarthur Cancer Therapy Centre, Australia. a.haidar@unsw.edu.au; Matthew.field@unsw.edu.au; vikneswary.batumalai@health.nsw.gov.au; k.cloak@unsw.edu.au; d.almouiee@unsw.edu.au; phillip.chlap@unsw.edu.au; [3]Image-X Institute, University of Sydney, NSW, Australia; [4]Ingham Institute for Applied Medical Research. xiaoshui.huang@sydney.edu.au; vicky.chin@unsw.edu.au; [5]University of Wollongong, NSW, Australia; [6]Illawarra Cancer Care Center, NSW, Australia. Martin.Carolan@health.nsw.gov.au; [7]University of Sydney, NSW, Australia; [8]Westmead Hospital, Westmead, NSW, Australia; [9]Blacktown Hospital, Blacktown, NSW, Australia. Jonathan.Sykes@health.nsw.gov.au; [10]Liverpool and Macarthur Cancer Therapy Centres, NSW, Australia. Shalini.Vinod@health.nsw.gov.au; Geoff.Delaney@health.nsw.gov.au; lois.holloway@health.nsw.gov.au

Introduction In progressing the use of big data in health systems, standardised nomenclatures are required to enable data pooling and analyses. In many radiotherapy planning systems and retrospective datasets, target volume and organ-at-risk (OAR) nomenclature has not been standardised. Currently, researchers collect, process, and standardise identification of target and OAR volumes through rule-based approaches based on discussions with the clinicians, which is an expensive and time-consuming process. Several methods have been proposed to standardise volume identification using machine learning (ML) [1, 2]. However, these studies utilised one or no target volumes, which does not represent real-world scenarios. We aimed to analyse the applicability of ML algorithms in identifying volumes in a clinical dataset of patients treated with radiotherapy.

Method A dataset consisting of ~ 1260 breast cancer patients (2014–2018) was collected from Liverpool & Macarthur Cancer Therapy Centres. The target and OAR volumes were initially identified based on discussions with the clinicians. Three types of input features were generated to represent each target and OAR volume: textual features, positional and volumetric features, and central slices (slices with the highest number of contoured tumour pixels). The dataset was divided into training, validation, and test datasets. A multi-input deep neural network, that is capable of learning from multiple data modalities, was utilized for training (Fig. 1). For comparison purposes, three other networks were developed separately using one of three characteristics (text, positional and volumetric, images).

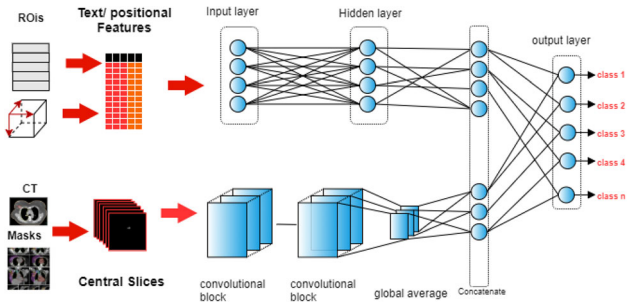

Fig. 34 Overview of the proposed multimodal deep neural network

Table 4 Classification accuracy of the developed models

Model	Classification accuracy (%)
Text features	86.849
Positional-volumetric features	80.174
Central slices	85.047
All features combined (multi-modal network)	99.800

Results Preliminary analyses showed that the developed multimodal network was capable of distinguishing the volumes with higher accuracy on the test dataset, as opposed to three other networks as shown in Table 1.

Conclusion ML based automation methods can be beneficial for the standardisation of volume nomenclature when considering the inclusion of multiple volume characteristics. This is an ongoing project, where further experiments are underway to further analyse the robustness of the approach.

References

1. Yang, Q., Chao, H., Nguyen, D., & Jiang, S. (2020). Mining Domain Knowledge: Improved Framework Towards Automatically Standardizing Anatomical Structure Nomenclature in Radiotherapy. IEEE Access, 8, 105286–105300.
2. Sleeman IV, W. C., Nalluri, J., Syed, K., Ghosh, P., Krawczyk, B., Hagan, M., … & Kapoor, R. (2020). A Machine Learning method for relabeling arbitrary DICOM structure sets to TG-263 defined labels. Journal of Biomedical Informatics, 109, 103527.

P022 The dose to fingers from PET radiopharmaceuticals: a Monte Carlo evaluation

Y. V. Matyagin[1], K. Hickson[1], P. J. Collins[2]

[1]Medical Physics and Radiation Safety, SA Medical Imaging, Adelaide, Australia. Yuri.Matyagin@sa.gov.au; Kevin.Hickson@sa.gov.au (Presenting author); The University of Adelaide, Adelaide, Australia. Peter.Collins@adelaide.edu.au

Introduction Dispensing/administering radiopharmaceuticals can result in a high radiation dose to staff fingers, and syringe shields must be used to reduce exposure. In the present study, Monte Carlo simulations were used to estimate finger doses from handling diagnostic Positron-Emission-Tomography (PET) radiopharmaceuticals in half-filled unshielded/shielded syringes. Finger doses from fully filled syringes were studied in our previous work [1].
Method DOSRZnrc/EGSnrc software was used to determine the 'skin' absorbed dose (60-s exposure) in a tissue-equivalent 'finger' phantom positioned (A) directly over the radioactivity, and (B) at the rear of a 5-ml-syringe. Aqueous solutions (2.5 ml) of F-18, Cu-64, Ga-68, Zr-89 and I-124 were simulated with activities of 320, 74, 120, 74 and 74 MBq, respectively. Simulations were performed with and without an 8.05-mm-thick tungsten syringe-shield. 'Skin' doses at 0.07-mm depth (ICRU [2]) and 0.25-mm depth (typical depth of the skin basal layer [3]) were calculated.
Results 'Finger' doses are shown in the table.

Radionuclide			F-18	Cu-64	Ga-68	Zr-89	I-124
Activity (MBq)			310	74	120	74	74
0.07-mm-depth dose	(mGy)						
	Unshielded	A*	18	1.2	72	6.4	13
	B*		0.37	0.017	0.15	0.10	0.096
	Shielded	A	0.72	0.033	0.27	0.27	0.23
		B	0.0068	0.00037	0.0031	0.0082	0.0072
0.25-mm-depth dose	(mGy)						
	Unshielded	A	14	0.80	62	5.4	11
	B		0.37	0.016	0.15	0.099	0.095
	Shielded	A	0.66	0.030	0.25	0.27	0.22
		B	0.0059	0.00033	0.0028	0.0081	0.0071

* *A* and *B*: 'finger' positions

Conclusion Syringe shields are highly effective and should be used whenever possible. Finger exposure is also reduced by more than 1 order of magnitude if the syringe is held at the end, instead of over the radioactivity. The annual extremities dose limit (500 mGy) will be exceeded after 27 (F-18), 430 (Cu-64), 6 (Ga-68), 77 (Zr-89), or 37 (I-124) studies with 60-s-exposure and poor technique (unshielded syringe and fingers over radioactivity).

References

1. Matyagin YV, Collins PJ, Hickson K (2020) Monte Carlo evaluation of dose to fingers from handling PET radiopharmaceuticals. EPSM 2019, Engineering and Physical Sciences in Medicine. Phys Eng Sci Med 43(1):354–355, O092. https://doi.org/10.1007/s13246-019-00826-6
2. International Commission on Radiation Units and Measurements (ICRU) (1993) Quantities and Units in Radiation Protection Dosimetry. ICRU Report 51, ICRU Publications, Bethesda, 1993b
3. Pattison JE, Bachmann DJ, Beddoe AH (1996) Gamma dosimetry at surfaces of cylindrical containers. J Radiol Prot 16(4):249–261

P023 Comparison of 4D-MRI and 4D-CT for lung cancer volume and motion assessment

S. Higuchi[1,2], J. Ludbrook[1], L. OConnor[1], A. L. Zerafa[1], P. Greer[1,3], J. Simpson[1], J. Goodwin[1,3]

[1]Radiation Oncology Department, Calvary Mater Newcastle, Newcastle, NSW, Australia;
[2]Satomi.HiguchiGoodwin@calvarymater.org.au (Presenting author). Jane.Ludbrook@calvarymater.org.au; Laura.OConnor@calvarymater.org.au; Amy.Zerafa@calvarymater.org.au; [3]School of Mathematical and Physical Sciences, University of Newcastle, NSW, Australia. Peter.Greer@newcastle.edu.au; John.Simpson@calvarymater.org.au; Jonathan.Goodwin@calvarymater.org.au

Introduction 4D-CT is the current gold standard for lung tumour motion assessment for radiation treatment planning. However, these images can be unreliable in cases of irregular breathing and are susceptible to image artefact in regions close to the diaphragm. 4D-MRI has superior soft tissue contrast and is a non-ionising technique, which may offer supplemental information for radiation treatment planning in some patients. In this study we evaulated 4D-MRI measured lung tumour motion range, tumour volume, and self navigation respiratory traces, with respective 4D-CT image and respiratory data.
Method 17 patients underwent standard treatment CT as well as an MRI session. For 4D-MRI, transverse averaged and coronal images with self-navigation were acquired. For respiratory phase binning, 5 bins were reconstructed for 4D-MRI and 10 bins for 4D-CT. A 3D slicer tool[1] was used to segment tumour to quantify superior–inferior tumour motion.
Results Significantly smaller volumes were observed in 4D-MRI (Fig. 1). Breathing frequency analysis of 16 patient respiratory traces acquired during 4D-CT and 4D-MRI showed: good agreement (10/16); slower in 4D-MRI (4/16) and slower in 4D-CT (2/16), suggesting potential tmour motion differences in these 6 patients.The Inferior portion of the movement was found to be better covered with 4D-CT image data, whereas the superior portion of the movement covered better with 4D-MRI (Fig. 2). This pattern was apparent in all lower tumour cases except one, which showed no movement.
Conclusion MRI measured tumour volumes were typically smaller than CT, due in part to improved tumour delineation. Discrepancies in

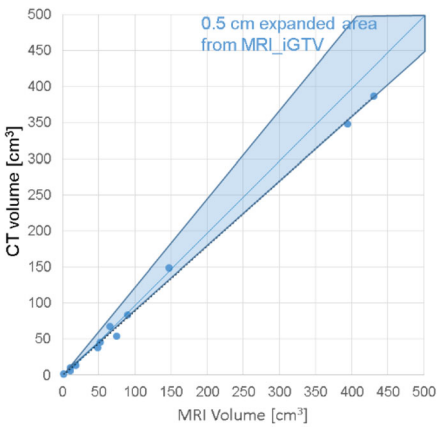

Fig. 1 Volume size for 4DCT and 4DMRI. (Pearson's $r = 0.99$, $p < 0.0001$, AverageCT_inhale + exhale volume = 98.7[cm3], averageMR_inhale + exhale volume = 88.9[cm3], Paired ttest $p < 0.02$ showed significantly smaller volume in MRI, but within the 0.5 cm expansion margin for PTV.)

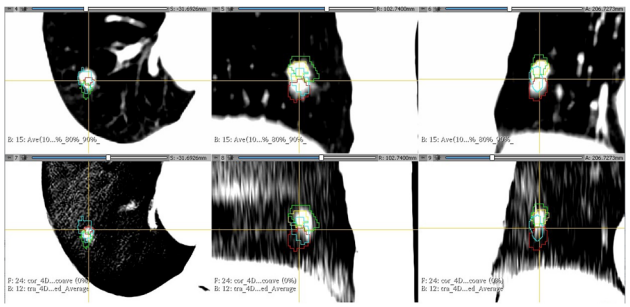

Fig. 2 Coloured contours show the tumour position at end-inhale (red) and end-exhale (yellow) of 4DCT, and end-inhale (cyan) and end-exhale (green) of MRI. Average intensity image of 4DCT (top row) and transverse average image of 4DMRI (bottom row) with axial (left column), sagittal (middle column) and coronal (right column) sections

extent of tumour motion were observed in patients with lower lobe tumour, where tumour motion is greater. We are currently investigating 4D-CBCT and respiratory data in the same patient cohort to evaluate discrepancies between the three modalities, as well as the dosimetric impact of using 4D-MRI derived contours for the existing patient treatment plan.

Acknowledgements This work was supported by Calvary Mater Newcastle Calvary Mater Newcastle CCRR grant.
Jianing Pang, Siemens Healthineers, for radial vibe with motion correction MRI prototype sequence development.

Ethical statement The involvement of patients in this works has been reviewed and approved by the Hunter New England Human Research Ethics Committee, Australia (2020/STE04342)

References

1. Velazquez ER, Parmar C, Jermoumi M, Mak RH, van Baardwijk A, Fennessy FM, Lewis JH, De Ruysscher D, Kikinis R, Lambin P, Aerts HJWL (2013) Volumetric CT-based segmentation of NSCLC using 3D-Slicer Sci Rep 18;3:3529: 1–7. https://doi.org/10.1038/srep03529

P024 Hazard analysis in radiation therapy: Applying System-Theoretic Process Analysis to MLC tracking

J. Hindmarsh[1], J. Booth[2], S. Dieterich[3], P. Keall[1]

[1]ACRF Image X Institute, Faculty of Medicine and Health, University of Sydney, Australia. jonathan.hindmarsh@sydney.edu.au (Presenting author); [2]Northern Sydney Cancer Centre, Royal North Shore Hospital, Sydney, Australia. Jeremy.Booth@health.nsw.gov.au; [3]Department of Radiation Oncology, UC Davis Medical Center, Sacramento, USA. sdieterich@ucdavis.edu; Paul.Keall@sydney.edu.au

Introduction The ability to dynamically track a target during treatment with the MLC is a technique that has been promised for many years [1]. With the improving ability to track an internal target, [2] clinical MLC tracking prostate [3] and lung cancer treatments [4] and pre-clinical implementations of MLC tracking on multiple vendor systems, MLC tracking may soon be a widely available radiation therapy technology. With the introduction of MLC tracking comes the need to rethink and revise our current treatment QA and safety processes. AAPM has recommended the use of failure mode and effects analysis (FMEA) and process mapping to assist in this process [5]. However, FMEA is a time consuming and involved process [6]. Comparatively, System-Theoretic Process Analysis (STPA) was designed specifically for the complex modern world [7]. STPA differs from FMEA in that it works backward from what you want to prevent and can include multiple failure and interaction hazards and inherently incorporates software, design, and human factors. The aim of this study was to investigate applying STPA to MLC tracking.

Method STPA was applied to MLC tracking as defined by AAPM TG 264 [8] using the STPA Handbook [9] as a guide. The STPA process generates scenarios that can lead to undesirable outcomes (referred to as losses in STPA). These scenarios were then used to formulate tests and system requirements to prevent them.

Results STPA losses, events that can lead to losses (hazards), and controls to prevent these hazards (constraints) were defined for MLC tracking and the system control structure was modelled (Fig. 35). Unsafe control actions (UCAs) were determined for each of the control actions and following this, loss scenarios were created.

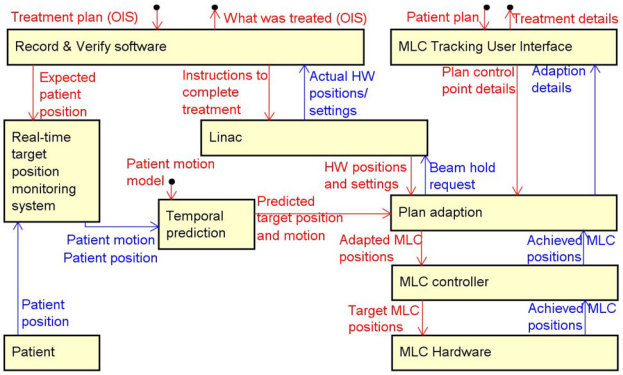

Figure 35: STPA System Control Structure for MLC Tracking

Conclusion The loss scenarios and system constraints can be used to develop QA and system requirements for future implementations of MLC tracking.

References

1. D'Souza WD, Naqvi SA, Yu CX (2005) Real-time intra-fraction-motion tracking using the treatment couch: a feasibility study. Phys Med Biol 50:4021–4033. https://doi.org/10.1088/0031-9155/50/17/007
2. Keall PJ, Nguyen DT, O'Brien R, et al. (2018) Review of Real-Time 3-Dimensional Image Guided Radiation Therapy on Standard-Equipped Cancer Radiation Therapy Systems: Are We at the Tipping Point for the Era of Real-Time Radiation Therapy? Int J Radiat Oncol 102:922–931. https://doi.org/10.1016/j.ijrobp.2018.04.016
3. Huq MS, Fraass BA, Dunscombe PB, et al. (2016) The report of Task Group 100 of the AAPM: Application of risk analysis methods to radiation therapy quality management. Med Phys 43:4209–4262. https://doi.org/10.1118/1.4947547
4. Silvis-Cividjian N, Verbakel W, Admiraal M (2020) Using a systems-theoretic approach to analyze safety in radiation therapy-first steps and lessons learned. Saf Sci 122:104519. https://doi.org/10.1016/j.ssci.2019.104519
5. Leveson NG (2012) Engineering a Safer World: Systems Thinking Applied to Safety. MIT Press, Cambridge, UNITED STATES
6. Keall PJ, Sawant A, Berbeco RI, et al. (2020) AAPM Task Group 264: The safe clinical implementation of MLC tracking in radiotherapy. Med Phys. https://doi.org/10.1002/mp.14625
7. Leveson NG, Thomas JP (2018) STPA Handbook

P025 Performances of Varian TrueBeam IGRT and IGRT-6DOF couch under maximum load

Hossain M. Deloar[1], J. Mathew[1], W. Glenn[1], V. Peng[1], P. Narayanan[1], T. Kron[1]

[1]Department of Physical Sciences, Peter MacCallum Cancer Centre, Bendigo, Australia. Deloar.Hossain@petermac.org (Presenting author); Joby.Mathew@petermac.org; Glenn.Williams@petermac.org; Valery.Peng@petermac.org; Pradush.Narayanan@petermac.org; Tomas.Kron@petermac.org

Introduction Maximum load of the TrueBeam-IGRT and IGRT-6DOF couch recommended by Varian are 228 kg and 200 kg, respectively. To treat bariatric patients on these couches, we tested couch deflection/operation under max load.

Method Water filled containers were placed on the couch for two different scenarios of treatments: (i) headfirst-scan and (ii) feet-first-scan. For first scenario, the superior part of the TrueBeam-IGRT and IGRT-6DOF couch were loaded with 158 kg and 140 kg respectively, to simulate patient's upper body; and the inferior part of the True-Beam-IGRT-couch and IGRT-6DOF couch with 70 kg and 60 kg, respectively to simulate the lower body (Fig. 1). For second scenario, the load distribution was exchanged.

Figure1: Load distributions, 158 kg to superior part and 70 kg to the inferior part of the couch

Couch sag were recorded at various index positions. All measurements were done at isocentre position and at individual index positions for the maximum couch extent by recording the differences of the couch VRT with and without load. Variation of couch driver current for different couch parameters VRT, LAT, LNG and ROT, etc. were recorded. IGRT under max load was also verified.

Results The couch sag at isocentre for various index positions were ranging from 5 mm-10 mm for IGRT-couch and 2 mm-6 mm for 6DOF-couch. Differences of couch sag between the two treatment scenarios were approximately 1 mm for index positions F1, 0, H1 and H2, and for H3 position was 2 mm. Couch sag at the extended index positions were approximately 2 mm more than that measured at isocentre. Average currents for the Couch LNG and VRT with load were 1.6 and 1.3 times higher than without load. IGRT tests under the maximum load was also successful.

Conclusion Couch sag for the treatment scenario "head first scan" is approximate 2 mm larger than the scenario "foot first scan". To treat obese patient for lower abdomen treatment and pelvic area "foot first scan" is recommended.

References

1. Patrick Towns, Blair Free, George Cernica, et al. Practical issues in treating heavy patients on a LINAC treatment couch. J Appl Clin Med Phy. Winter 2005:6(1):135–42.
2. Varian TrueBeam Technical Reference Guide Volume 1, 2014.

P026 In vitro assays to assess safety of targeted radionuclide therapy of pancreatic cancer

A. Hull[1,2], Y. Li[1], W Hsieh[2,3], D. Bartholomeusz[2,4], W. Tieu[5], E. Bezak[1,6]

[1]Cancer Research Institute & Allied Health and Human Performance Academic Unit, University of South Australia, Australia; [2]Department of PET, Nuclear Medicine & Bone Mineral Densitometry, Royal Adelaide Hospital, SA Medical Imaging, Australia. ashleigh.hull@mymail.unisa.edu.au (Presenting author); judy.li@unisa.edu.au; [3]AHHP, University of South Australia, Australia. william.hsieh@sa.gov.au; [4]Adelaide Medical School, The University of Adelaide, Australia. dylan.bartholoemeusz@sa.gov.au; [5]Molecular Imaging and Therapeutic Research Unit, SAHMRI, Australia. william.tieu@sahmri.com; [6]School of Physical Sciences, The University of Adelaide, Australia. eva.bezak@unisa.edu.au

Introduction Pancreatic cancer continues to be a leading cause of cancer-related death and urgently needs better diagnostic and therapeutic interventions to improve survival. Targeted radionuclide therapy (TRT) is a promising cancer therapy and may be beneficial in the treatment of pancreatic cancer. The development of radioimmunoconjugates for TRT relies on preclinical testing to assess binding specificity and cellular internalisation, providing insights into the potential safety and feasibility of these agents. The aim of this study was to develop a therapeutic radioimmunoconjugate for TRT of pancreatic cancer and perform in vitro assays to predict the safety of the radioimmunoconjugate. In this study, the radioimmunoconjugate was formed using lutetium-177 (^{177}Lu) and the C595 antibody which targets cancer-specific mucin 1 epitopes (MUC1-CE) overexpressed in pancreatic cancer [1].

Method The C595 antibody was conjugated to the bifunctional chelator p-SCN-Bn-DOTA. The resulting DOTA-C595 conjugate was radiolabelled to [^{177}Lu]$LuCl_2$ using standard methods. The immunoreactivity of [^{177}Lu]Lu-DOTA-C595 was assessed using a cell binding assay and Lindmo assay [2]. Cellular internalisation of [^{177}Lu]Lu-DOTA-C595 was evaluated at t = 1, 5, 24, 30 and 48 h. The pancreatic cancer cell lines PANC-1 (strong MUC1-CE expression) and AsPC-1 (low MUC1-CE expression) were used in all assays.

Results In the cell binding studies [^{177}Lu]Lu-DOTA-C595 demonstrated significantly greater binding to the MUC1-CE positive cell line at concentrations of 100 nM and greater (Fig. 1). The Lindmo assay further confirmed the strong immunoreactivity of [^{177}Lu]Lu-DOTA-C595 to MUC1-CE. Rapid and high internalisation of [^{177}Lu]Lu-DOTA-C595 was observed with the percentage of internalised activity exceeding 40% at 1 h and further increasing to over 70% at 30 h.

Conclusion The strong immunoreactivity to MUC1-CE and high internalisation in cell lines highlight the feasibility of applying [^{177}Lu]Lu-DOTA-C595 TRT to pancreatic cancer.

1142365107950

References

1. Hull A, Li Y, Bartholomeusz D, Hsieh W, Escarbe S, Ruszkiewicz A, Bezak E (2020) The expression profile and

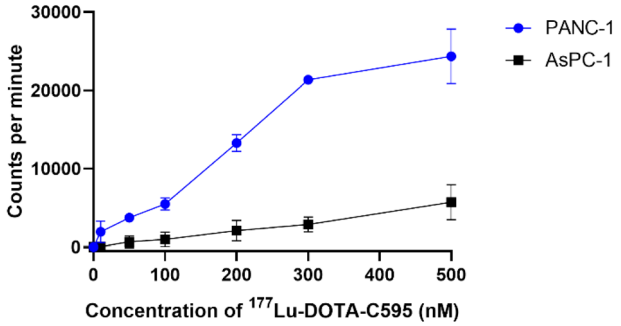

Fig. 1 Cell binding assay of [^{177}Lu]Lu-DOTA-C595 to PANC-1 and AsPC-1 cell lines

textural characteristics of C595-reactive MUC1 in pancreatic ductal adenocarcinoma for targeted radionuclide therapy. Cancers (Basel) 13(1):61. https://doi.org/10.3390/cancers13010061

2. Lindmo T, Boven E, Cuttitta F, Fedorko J, Bunn PA (1984) Determination of the immunoreactive function of radiolabeled monoclonal antibodies by linear extrapolation to binding at infinite antigen excess. J Immunol Methods 72:77–89. https://doi.org/10.1016/0022-1759(84)90435-6

P027 Dosimetric effect of cryostat characterization on clinical treatment plans for MR linac

U. Jelen[1], Z. Moutrie[1], C. Pagulayan[1], N. Dunkerley[1], M. G. Jameson[1]

[1]GenesisCare, The Mill, 41–43 Bourke Road, Alexandria, NSW, Australia. Urszula.Jelen@genesiscare.com (Presenting author); Zoe.Moutrie@genesiscare.com; Claire.Pagulayan@genesiscare.com; Nicolle.Dunkerley@genesiscare.com; Michael.Jameson@genesiscare.com

Introduction In the Elekta Unity MR linac (Elekta, Crawley, UK), the radiation beam traverses the helium cryostat and the body coil. While they are designed to be as homogeneous as possible, their transmission as a function of gantry angle must be accounted for in the TPS [1]. The aim of this work was to investigate the impact of the change of this characterization curve, due to the helium level variation, on clinical treatment plan dosimetry.
Method The initial curve was acquired during the commissioning and has been built into the beam model in the Monaco TPS (Elekta, Crawley, UK). Following a helium top-up, the curve was re-acquired and a new beam model was generated. Next, 10 SBRT prostate and 10 SBRT oligo metastases commissioning plans were re-calculated using the modified model and relevant dosimetric indices were compared.
Results Maximum differences in the measured transmission curves were around 1% for limited gantry angles. For the SBRT prostate plans, the CTV mean dose was reduced by − 0.6% (− 0.7% to − 0.5%) and PTV $D_{95\%}$ by − 0.6% (− 0.7% to − 0.5%). The maximum doses ($D_{0.1ccm}$) to the OARs were also reduced, for example by − 0.6% (− 0.7% to − 0.2%) for rectum and by − 0.6% (− 0.8% to − 0.3%) for bladder. For the oligo metastases plans, the GTV mean dose was reduced by − 0.5% (− 1% to − 0.2%) and the PTV $D_{95\%}$ by − 0.2% (− 0.9% to 0.3%). Similarly to the prostate cases, the reduction of the $D_{0.1ccm}$ was observed for the OARs, however due to variable location the average values are not available.
Conclusion A discrepancy between the modelled and the actual cryostat transmission leads to systematic dose calculation inaccuracies. While their magnitude was shown to be small in our case, it should be checked and considered in the context of the overall treatment chain accuracy requirements.
Acknowledgements The authors acknowledge Jason Arts, Armia George and Elekta for providing the beam model for testing.
References
1. Woodings S, Bluemink JJ, de Vries JFW, Niatsetski Y, van Veelen B, Schillings J, Kok JGM, Wolthaus JWH, Hackett SL, van Asselen B (2018) Beam characterization of the 1.5T MRI-Linac. Phys Med Biol 63:085015. https://doi.org/10.1088/1361-6560/aab566

P028 Validation of secondary dose calculation software for the Elekta Unity MR Linac

U. Jelen[1], Z. Moutrie[1], M. G. Jameson[1]

[1]GenesisCare, The Mill, 41–43 Bourke Road, Alexandria, NSW, Australia. Urszula.Jelen@genesiscare.com (Presenting author); Zoe.Moutrie@genesiscare.com; Michael.Jameson@genesiscare.com

Introduction In the MR linac (MRL) treatment workflow, the QA for online adapted plans relies on an independent MU check, as dose measurement is possible only after the treatment. For this purpose, during commissioning of our MRL, a beam model was created in Radcalc v6.4 (Lifeline Software Inc, USA), available in our department at that time. The model, based on published work [1], involved some compromises, as the profile asymmetry due to the magnetic field was not modelled. More recently, a new version of Radcalc, accounting for this effect, had been released (v7.1). The aim of this work was to commission a beam model using Radcalc v7.1 and to investigate its agreement with the TPS calculation.
Method The new model was created in Radcalc v7.1 using the same input data the previous one. The agreement of the point dose calculations with the TPS was compared for the two models for a set of validation plans, which included: square fields, irregular fields, commissioning treatment plans (10 60/20 prostate, 10 SBRT prostate and 10 SBRT oligo metastases) and 15 clinical plans that failed MU verification using the current model.
Results The overall point dose deviation between the TPS and the Radcalc calculations improved by 0.3% for square and by 2.6% for irregular fields. For commissioning plans the average improvement was 0.5% for prostate and 0.7% for oligo metastases plans. In both cases, the maximum deviation for individual beams also improved on average by 1% (-6.4% to 4.5%). Finally, only 1 clinical plan failed with the new model.
Conclusion The MRL beam model accounting for magnetic field effects performed better in all cases. While the accuracy of the previous model was acceptable in most of the scenarios (calculations agreed with the TPS within tolerance), the new model reduced the number of MU verification fails.
Acknowledgements The authors would like to acknowledge the University of Iowa for sharing the Radcalc beam model and Lifeline Software Inc and Michael Grace for facilitating the access to the Radcalc software.
References
1. Graves SA, Snyder JE, Boczkowski A, St-Aubin J, Wang D, Yaddanapudi S, Hyer DE (2019) Commissioning and performance evaluation of RadCalc for the Elekta unity MRI-linac. J Appl Clin Med Phys 20:54–62. https://doi.org/10.1002/acm2.12760

P029 ExacTrac intrafractional uncertainty analysis for prostate stereotactic body radiotherapy using cone beam CT for pre-treatment localisation

B. R. Jordan[1], C J Colyer[1]

[1]Medical Physics, GenesisCare Oncology (South Australia), Australia. barry.jordan@genesiscare.com (Presenting author); christopher.colyer@genesiscare.com

Introduction The objective of this study was to evaluate intrafractional auto-matching uncertainties using the Exactrac (BrainLab, Feldkirchen, Germany) X-ray stereoscopic system for prostate stereotactic body radiotherapy (SBRT) with implanted fiducial markers by initial pre-treatment localisation with cone beam CT (CBCT, Elekta XVI).

Method A customised prostate phantom with 3 implanted gold seeds was positioned to isocentre by CBCT prior to intrafractional imaging. Using the Hexapod 6D couch, known offsets were applied separately to the phantom in 6 directions (3 translational, 3 rotational) of 0 mm, 1 mm, 2 mm, 0°, 1° and 2°, and the ability of ExacTrac's image-matching functions to detect and correct these offsets were recorded.

Results Auto-matching statistics using the implanted marker (seeds) matching function were found to be more precise than the bony anatomy function. The total standard deviations (SD) for the translational shifts using the implanted marker and bony anatomy functions were 0.1 mm and 0.3 mm vertically, 0.1 mm and 0.3 mm longitudinally, and 0.1 mm and 0.4 mm laterally, respectively. The standard deviations for the rotational shifts using the implanted marker and bony anatomy matching functions were 0.2° and 1.2° for the yaw (angle vert), 0.3° and 1.1° for the pitch (angle long), and 0.2° and 1.2° for the roll (angle lat) directions, respectively.

Conclusion The reduced uncertainties from introducing a CBCT into the workflow for initial localisation resulted in a decreased probability of inhibits due to false positives during treatment and the potential for reducing planning target volume (PTV) margins around the prostate without compromising dose coverage. The reported ExacTrac auto-matching uncertainties in this study on an Elekta linear accelerator are comparable to that on integrated motion monitoring systems on Varian linear accelerators despite ExacTrac's relatively limited intrafractional imaging range and frequency.

References

1. Rijken J, Sidhom M (2020) An assessment of the ExacTrac intrafraction imaging capabilities for flattening filter free prostate stereotactic body radiotherapy. Physical and Engineering Sciences in Medicine 43:849–855
2. Shi C, Tazi A, Fang DX, Iannuzzi C (2012) Study of Exactrac X-ray 6D IGRT setup uncertainty for marker-based prostate IMRT treatment. J Appl Clin Med Phys 13(3):35–42
3. Badakhshi H, Wust P, Budach V, Graf R (2013) Image-guided radiotherapy with implanted markers and kilovoltage imaging and 6-dimensional position corrections for intrafractional motion of the prostate. Anticancer Res 33(9):4117–4121
4. Satoshi T, Satoru U, Eisuke A, Hiraku S, Atsushi O, Hironori S, Takumi Y, Motoki K, Hidefumi A (2019) The impact of the three degrees-of-freedom fiducial marker-based setup compared to soft tissue-based setup in hypofractionated intensity-modulated radiotherapy for prostate cancer. J Appl Clin Med Phys 20:53–59

P030 HyperArc commissioning and clinical implementation

K. Kandasamy[1], A. Cullen[1], E. Seymour[1], S. Docherty[1], B. Zwan[1], R. Poldy[1], R. David[1], P. Christensen[1], C. Lee[1]

[1]Radiation Oncology, Central Coast Cancer Centre. kankean.kandasamy@health.nsw.gov.au; ashley.cullen@health.nsw.gov.au; erin.seymour@health.nsw.gov.au; kankean.kandasamy@health.nsw.gov.au; benjamin.zswan@health.nsw.gov.au; rachel.poldy@health.nsw.gov.au; rajasekar.david@health.nsw.gov.au; paul.christensen@health.nsw.gov.au; christopher.lee@health.nsw.gov.au

Introduction HyperArc [1] is the automated Varian platform for multi-target, single isocentre (MTSI) intercranial radiotherapy. Verification of HyperArc is challenging due to the need for geometric accuracy [2], uncertainties in small field dosimetry [3], and limitations in commercial phantom solutions for non-coplanar VMAT dosimetry and hidden target tests (HTT) [4, 5]. Our experience with commissioning and clinical implementation is described.

Method The project consisted of; (1) a plan quality study comparing HyperArc and cone-based deliveries for five patient datasets using RTOG metrics, (2) characterisation of dosimetric accuracy versus off-axis distance (OAD) using Gafchromic film in a locally developed phantom, (3) assessment of geometric accuracy using a novel HTT approach, and 4) assessment of intra-fraction motion from pre- and post- treatment CBCTs.

Results (1) The conformity index (CI) of both plan types were comparable with HyperArc (1.34 ± 0.21) and cone plans (1.43 ± 0.21). When considering Brain V12Gy, HyperArc outperformed cones the number of lesions was > 5. For Brain V2Gy, cones were preferable with the results correlated to number of lesions. (2) Dose agreement was within AAPM recommended tolerances, however variation in dose increased for small field targets at OAD > 10 cm. (3) HTT results showed geometric error increased with OAD. The maximum error was 1.5 mm at 10 cm OAD. (4) The intra-faction motion (Table 1) was found to be directionally dependent with the worse-case being translation in and rotations about the z-axis.

Based on these validation results, OAD-dependent PTV margins have been developed. Due to limitations in dosimetric and geometric accuracy single-isocentre treatments have been limited to cases where with OAD < 7 cm.

Table 1 Intra-fraction translations and rotations

Axis (IEC60121)	Translation (mm) Mean ± SD	Rotation (mm) Mean ± SD
x-axis	0.55 ± 0.41	0.69 ± 0.77
y-axis	0.63 ± 0.55	0.76 ± 0.68
z-axis	0.80 ± 1.42	1.34 ± 1.56

Conclusion HyperArc has been successfully implemented and has replaced the use of cone treatments at our centre. The methodologies in this work can be utilised by other centres to safely implement MTSI radiotherapy.

References

1. Alongi, F., et al., *First experience and clinical results using a new non-coplanar mono-isocenter technique (HyperArc^{TM}) for Linac-based VMAT radiosurgery in brain metastases*. Journal of cancer research and clinical oncology, 2019. **145**(1): p. 193–200.
2. Prentou, G., et al., *Dosimetric impact of rotational errors on the quality of VMAT-SRS for multiple brain metastases: Comparison between single-and two-isocenter treatment planning techniques*. Journal of applied clinical medical physics, 2020. **21**(3): p. 32–44.
3. Das, I.J., J. Morales, and P. Francescon. *Small field dosimetry: What have we learnt? in AIP Conference Proceedings*. 2016. AIP Publishing LLC.
4. Capaldi, D.P., et al., *An integrated quality assurance phantom for frameless single-isocenter multitarget stereotactic radiosurgery*. Physics in Medicine & Biology, 2020. **65**(11): p. 115006.
5. Poder, J., et al., *Development of a dedicated phantom for multi-target single-isocentre stereotactic radiosurgery end to end testing*. Journal of applied clinical medical physics, 2018. **19**(6): p. 99–108.

P031 Development and Commissioning of a Multi-Target-Single-Isocentric SRS Verification Phantom with Novel Dynamic VMAT Winston-Lutz Capability

K. Kandasamy[1], P. Christensen[1], B. Zwan[1], A. Cullen[1], R. Poldy[1], E. Seymour[1], R. David[1], C. Lee[1]

[1]Radiation Oncology, Central Coast Cancer Centre.
kankean.kandasamy@health.nsw.gov.au;
paul.christensen@health.nsw.gov.au;
benjamin.zwan@health.nsw.gov.au;
ashley.cullen@health.nsw.gov.au; rachel.poldy@health.nsw.gov.au;
erin.seymour@health.nsw.gov.au;
rajasekar.david@health.nsw.gov.au;
christopher.lee@health.nsw.gov.au

Introduction The multi-target, single-isocentric Stereotactic Radiosurgery (MTSI-SRS) approach to treating metastatic brain cancer [1, 2] has spurred demand in fit for purpose verification options[3, 4]. This work expands upon a recently developed phantom stack solution[5] by introducing 3D printed Polylactic Acid (PLA) stacks, multi-planar film modules, and a novel hidden target testing (HTT) solution that allows for geometric Winston-Lutz (WL) verification of dynamic deliveries for multiple off-axis targets.

Method Film modules and spacers were manufactured using PLA filament and verified accurate positioning. Simultaneous dosimetric verification of clinical targets was conducted by aligning the clinical plans to the phantom geometry and aligning the film holder using appropriate stack arrangement.

WL target modules were manufactured with steel ball bearings embedded in PLA blocks. Dynamic MLC defined plans were created with apertures conforming around the off-axis ball bearing targets. The phantom was then irradiated using the HyperArc on a Varian TrueBeam. Gantry angle resolved MV images were acquired using the CDog Frame Grabber (Calvary Mater Hospital, Newcastle). Software was developed to generate DRRs of the VMAT arcs and to calculate deviations between planned and delivered relative positions of the ball and apertures over the non-coplanar plan.

The sensitivity of the verification process was characterised by introducing known translational and rotational errors to phantom setup. Characterisation of film dosimetry in PLA material is described elsewhere.

Results The HTT verification process was able to detect translational discrepancies greater than 1 mm in all directions for all targets and resolve rotational discrepancies of greater than 0.5 degrees.

The average gamma pass rates γ(3%, 2 mm, 10%) for film measurements was 98.5% (σ = 2.5%) and sensitive to clinically significant errors in dose.

Conclusion The phantom, including the novel dynamic HTT process, was successfully tested for use in the commissioning and verification of MTSI SRS treatments.

References/Acknowledgements

1. Palmer, J.D., et al., Single-isocenter multitarget stereotactic radiosurgery is safe and effective in the treatment of multiple brain metastases. Advances in radiation oncology, 2020. **5**(1): p. 70–76.
2. Alongi, F., et al., Long-term disease outcome and volume-based decision strategy in a large cohort of multiple brain metastases treated with a mono-isocentric linac-based Stereotactic Radiosurgery technique. Clinical and Translational Oncology, 2021: p. 1–10.
3. Prentou, G., et al., Dosimetric impact of rotational errors on the quality of VMAT-SRS for multiple brain metastases: Comparison between single-and two-isocenter treatment planning techniques. Journal of applied clinical medical physics, 2020. **21**(3): p. 32–44.
4. McKenna, J.T., The development and testing of a novel spherical radiotherapy phantom system for the commissioning and patient-specific quality assurance of mono-isocentric multiple mets SRS plans. Medical Physics, 2021. **48**(1): p. 105–113.
5. Poder, J., et al., Development of a dedicated phantom for multi-target single-isocentre stereotactic radiosurgery end to end testing. Journal of applied clinical medical physics, 2018. **19**(6): p. 99–108.

P032 Radiation Dose Perturbations caused by titanium reconstruction frames in head and neck surgery

Georgio Andrew Katsifis[1,2], David R. McKenzie[1,2], Natalka Suchowerska[1,2]

[1]University of Sydney, School of Physics, Australia; [2]VectorLAB, Chris O'Brien Lifehouse, Australia. gkat2146@uni.sydney.edu.au

Introduction Stability and design convenience are key contributions in the selection of a surgical reconstruction frame in head and neck surgery. Despite titanium causing perturbation in a radiation field, such as artefacts in CT images and hot and cold spots at the implant tissue interface, titanium remains popular due to its strength, rigidity and biocompatibility. For radiotherapy patients, osteoradionecrosis and implant failure correlate with high radiation doses [1, 2] near the implant tissue interface. While the irradiation is necessary for cancer patients, the geometry may be customised to reduce pockets of high dose. The regions of interest are where the regenerating tissue is proliferating, such as the exterior of the reconstruction frame and the cavities intended to encourage bone ingrowth. A solution to this problem may be to replace titanium with a material such as Polyether-ether-ketone (PEEK) with radiation scattering properties close to that of water.

Method The MC simulation is carried out on GATE utilising Geant4, with all the post-processing performed in Python and MATLAB. A 6MV photon Varian Truebeam field is incident on the reconstruction frame, made of titanium, PEEK or bulk water (Fig. 1). The circular image masks are created to evaluate the doses to the cavity in the reconstruction frames of different radii.

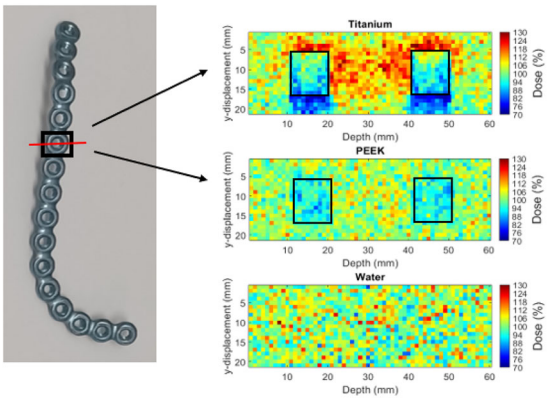

Figure 1. a) Titanium reconstruction frame commonly used in orthopaedic surgery. b) Dose distribution taken in the x-z plane of one titanium ring, where the incident beam approaches from the top of the page along the z-axis. The black box indicates the interface of implant and surrounding tissue.

Results The dose distributions are calculated for each ring as a function of cavity radius, both along the beam axis and in the lateral direction. Figure 1b shows the dose distribution in the cross section of one of the rings of the reconstruction frame. The dose in the cavity is significantly higher for titanium implants and is a function of cavity diameter and volume fraction.

Conclusion As reconstruction frames sequentially include cavities in their design, consideration needs to be given to minimising high dose gradients, which compromise osseointegration, severely weakening the bone-implant interface.

Acknowledgements

Dr Brad Oborn for useful discussions

NHMRC Ideas Grant funding

References

1. Walker, M.P., et al., Impact of Radiotherapy Dose on Dentition Breakdown in Head and Neck Cancer Patients. Practical radiation oncology, 2011. **1**(3): p. 142–148.
2. Hansen, H.J., et al., Dosimetric distribution to the tooth-bearing regions of the mandible following intensity-modulated radiation therapy for base of tongue cancer. Oral Surgery, Oral Medicine, Oral Pathology and Oral Radiology, 2012. **114**(2): p. e50-e54.

P033 A study on the impact of metal artefacts in radiotherapy

Young Woo Kim[1], Dr. Robin Hill[1,2], Dr. Samara Alzaidi[2]

[1]Institute of Medical Physics, School of Physics, University of Sydney, Australia. ykim7170@uni.sydney.edu.au; [2]Department of Radiation Oncology, Chris O'Brien Lifehouse, Sydney, Australia. Robin.Hill@lh.org.au; Samara.Alzaidi@lh.org.au

Introduction High density materials can cause significant artefacts in reconstructed CT images. Metal artefacts reduction (MAR) algorithms can reduce these but do not necessarily correct for all artefacts. In this work, the impact of the MAR and resultant dosimetric changes has been studied in the radiotherapy setting.

Method A CT phantom with metals rods (aluminium, brass, stainless steel and titanium) with sizes ranging from 3 – 27 mm were scanned using a Toshiba LB Aquilion CT scanner. CT images were reconstructed with and without the single energy metal artefact reduction (SEMAR) algorithm. The reconstructed size of the rods was compared to their physical size and the variations in CT number recorded [1]. The Eclipse treatment planning system was used to evaluate doses between the AXB and AAA algorithms with 6 and 10 MV x-ray beams (WFF and FFF).

Results SEMAR was able to correct most of streak artefacts in CT images in all metals but created more severe with the titanium and aluminium rods. The reconstructed diameter of each metal rod was larger than their physical size by up to 2.2 mm. The CT number of reconstructed rods decreased as the diameter of rod increased. In Eclipse, the dose reduction at points below the metal rods increased as the density and diameter of rods increases. AAA overestimated dose by up to 1.5%, 4.4% and 8.9% than AXB in presence of aluminium, titanium and stainless steel respectively.

Conclusion SEMAR showed good performance in reducing metal artefacts but seems to be optimized for higher density materials. The dosimetric impact of high density rods were found that as the density and size of material increases the degree of dose reduction increases.

References/Acknowledgements

1. Jeong, S., Kim, S. H., Hwang, E. J., Shin, C. I., Han, J. K., & Choi, B. I. (2015). Usefulness of a metal artifact reduction algorithm for orthopedic implants in abdominal CT: phantom and clinical study results. *AJR. American journal of roentgenology*, *204*(2), 307–317.

P034 Assessment of the Shimadzu Scatter Correction Algorithm in Portable Chest Radiographs

M. Lawson[1], L. Qian[1], K. Lau[1], T. Lau[2], M. Badawy[1]

[1]Monash Health Imaging, Monash Health, VIC, Australia. Michael.Lawson@monashhealth.org (Presenting author); Lijun.Qian@monashhealth.org; Ken.Lau@monashhealth.org; [2]QScan Radiology Clinics, QLD, Australia. lau.theo@gmail.com; Mohamed.Badawy@monashhealth.org

Introduction Portable chest radiographs (CXRs) play a crucial role in radiology. Most portable CXRs are performed without anti-scatter grids due to practical constraints. In 2017, Shimadzu released a scatter correction post-processing algorithm (SCA) which aimed to reduce the presence of scatter in portable CXRs acquired without a grid. The SCA protocol acquires images using the same parameters as standard CXRs, therefore not impacting patient dose. This study assesses the SCA's impact on image quality (IQ) in portable CXRs.

Method For objective IQ assessment, a modified ANSI chest phantom embedded with a PIX-13 phantom was imaged under standard CXR conditions. Images were generated with different SCA strengths and with a physical grid. Contrast-to-noise ratios (CNRs) in three low-contrast disks were determined within each of the images. For subjective IQ assessment, 30 clinical CXRs acquired with the SCA were retrospectively retrieved from Shimadzu Mobile-DaRt-MX8 units. Additional copies of the same CXRs were created with the SCA retrospectively turned off. Two blinded radiologists independently rated anatomical regions within the CXRs for clarity on a 5-point-Likert-scale. Cohen's-kappa statistics and Mann–Whitney-U-tests determined the inter-observer agreement and whether a statistical difference in IQ existed between the SC and non-SC images for each anatomical region.

Results It was shown the CNR improved with higher algorithm strengths for the two highest contrast disks (Fig. 1). The algorithm negatively impacted the CNR of the lowest contrast disk due to a higher noise level. Subjectively, a substantial level of inter-observer agreement existed for each anatomical region. Overall, observers recorded the SCA significantly improved IQ in clinical CXRs in all anatomical regions.

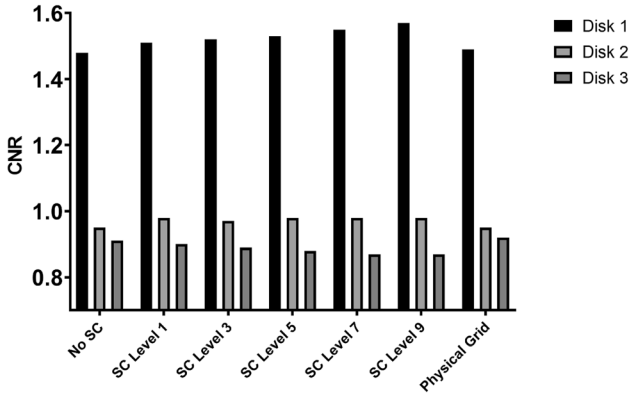

Fig. 36 Contrast to noise ratio of three contrast disks for different algorithm strengths

Conclusion The use of the Shimadzu SCA improved CNR for areas of large contrast. The increase in noise reduced CNR in lower contrast regions. Subjectively, the use of SCA significantly improved IQ for all anatomical regions within the chest.

References

Brady Z, Scoullar H, Grinsted B, Ewert K, Kavnoudias H, Jarema A, Crocker J, Wills R, Houston G, Law M, Varma D. Technique, radiation safety and image quality for chest X-ray imaging through glass and in mobile settings during the COVID-19 pandemic. Physical and engineering sciences in medicine. 2020 Sep;43(3):765–79.

Landis JR, Koch GG. The measurement of observer agreement for categorical data. biometrics. 1977 Mar 1:159–74.

P035 Thermal drift in Surface Guided Radiation Therapy

J. Lehmann[1,2,3], T. Standen[1], G. Kaur[1], J. Wolf[1], A. Wilfert[1]

[1]Department of Radiation Oncology, Calvary Mater Newcastle, Newcastle, Australia; [2]Institute of Medical Physics, University of Sydney, Sydney, Australia; [3]School of Mathematical and Physical Sciences, University of Newcastle, Newcastle, Australia.
Joerg.Lehmann@calvarymater.org.au (Presenting author);
Therese.Pedersen@calvarymater.org.au;
Guneet.Kaur@calvarymater.org.au;
Joshua.Wolf@calvarymater.org.au;
Alex.Wilfert@calvarymater.org.au

Introduction Thermal drift of optical systems employed for surface guided radiation therapy (SGRT) adds uncertainty to patient setup and monitoring. Drift is assessed as part of system commissioning [1]. This work looks at drift at system warmup and due to cooling down in between uses and it estimates its clinical impact.

Method Drift has been assessed for four clinical C-Rad Catalyst + HD systems. Measurements were performed via repeated execution of the DailyCheck procedure over 90 min. This provided position and thereby drift information for each of the three camera pods individually. For the combined performance of the system, which is most relevant for the clinical impact, measurements were performed in patient monitoring mode (cMotion) using a stationary anthropomorphic phantom. Measurements were repeated with a new (beta) version of the C-Rad control software which has a feature to manage drift by keeping the system in a warm state.

Results Different camera pods behave differently in terms of drift direction and magnitude. Individual axes showed drifts of 0–1.2 mm. A 30 min break cooled down cameras causing drifts of up to 0.8 mm. Rotations drifted $< 0.2°$. In patient monitoring mode the drifts varied between the four systems in direction and magnitude with 0.7- 1 mm (vectors) from cold and 0.6–0.8 mm after a 30 min break. For a typical patient treatment with SGRT assisted setup and the SGRT based position monitoring, this translated to uncertainties of 0.5–0.7 mm for setup and for monitoring. With the beta software, drifts after breaks were found to be below 0.1 mm.

Conclusion Thermal drift of optical systems employed for SGRT should be considered. This includes drift at warmup of the system as well as drift due to cooling down in between uses. As systems differ, the impact of drifts on patient positioning and monitoring should be quantified by each user individually.

References

1. Willoughby T, Lehmann J, Bencomo JA, Jani SK, Santanam L, Sethi A, Solberg TD, Tome WA, Waldron TJ (2012) Quality assurance for nonradiographic radiotherapy localization and positioning systems: report of Task Group 147. Med Phys 39:1728–47. https://doi.org/10.1118/1.3681967

P036 Obtaining Optimal Couch Angle and Auto-planning For Multiple Cranial Lesions Through Scripting

Ronnie Wing Kin Leung[1]

[1]Auckland Radiation Oncology, Auckland, New Zealand.
ronnie.leung@aro.co.nz (Presenting author)

Introduction Traditionally, couch-kick is normally required when planning on multiple cranial lesions to sharpen the dose fall-off. However, the couch angle selection depends on planner's experience and sometimes it is challenging to minimize the dose contribution to surrounding targets. This study aims to find the optimal couch angle and auto-plan using script.

Method In each case, the script firstly checks if the targets overlap by using Dice Similarity Coefficient and their centre-of-mass's distances are less than 3 cm. A range of beam sets with different couch and gantry angles combinations depending on the lesion's location will be added. An optimal couch angle is suggested at the end such that the average brain dose and the dose maximum of surrounding targets are the least using this equation:

$$min\left(\frac{BrainDose_i}{\sum_i^n BrainDose_i} \times \frac{PTV1_i}{\sum_i^n PTV1_i} \times \frac{PTV2_i}{\sum_i^n PTV2_i} \cdots\right)$$

where i is the ith couch combination and n is total number of combination

Three cases with 11 lesions in total were used in this study and compared to manual planning. Average brain dose (ABD), conformity index (CI) and gradient index (GI) were compared.

Results The ABD, CI and GI were 117.7 cGy, 0.756 and 5.02 respectively in scripted plans, while 119.3 cGy, 0.749 and 4.82 in manual plans.

Conclusion Optimal couch angle and treatment planning standardization for multiple brain metastases can be achieved through scripting which is independent of planner's experience.

P037 A novel real-time IGRT method to track the prostate without fiducial markers

Zeyao Li[1], Adam Mylonas[2], Ryan Brown[3], Jeremy Booth[1,3], Doan Trang Nguyen[2,3,4]

[1]Institute of Medical Physics, School of Physics, The University of Sydney, Sydney, AU. zeli4213@uni.sydney.edu.au; [2]ACRF Image X Institute, Faculty of Medicine and Health, The University of Sydney, Sydney, AU. adam.mylonas@sydney.edu.au; [3]Northern Sydney Cancer Centre, Royal North Shore Hospital, Sydney, AU. ryan.brown@health.nsw.gov.au; jeremy.booth@health.nsw.gov.au; [4]School of Biomedical Engineering, University of Technology Sydney, Sydney, AU. Doan.Nguyen1@health.nsw.gov.au

Introduction Intrafraction motion of the prostate deteriorates the dose delivery [1]. On a standard linac, existing solutions to intrafraction motion rely on implanted fiducial markers for low contrast organs such as the prostate. Accurate markerless prostate tracking would avoid invasive/expensive surgery for implantation and increase accessibility. In this study, we develop and evaluate the feasibility of a markerless prostate tracking framework using deep learning.

Method A Generative Adversarial Network (GAN) framework was developed to perform semantic segmentation of the prostate on kV images during treatment, assuming a rotating gantry geometry. The GAN model was pre-trained on 17 prostate cancer patient kV projections (200 degrees) and evaluated on 5 patients with kV images acquired from 2 treatment fractions each. The training set contained images of patients with fiducial markers that were filtered out digitally. The test set contained images of patients without implanted fiducial markers. To personalise the model for each patient, the planning CT and the prostate CTV contour were used to generate digitally reconstructed radiographs (DRRs) at 0.1-degree angular intervals. The predicted contour on each tested image was subsequently compared with the ground-truth projection of the planned CTV contour corrected for daily manual 3D-3D match by two therapists. The accuracy of the method was evaluated using Dice similarity coefficient (DSC), geometric centroid difference and Hausdorff distance.

Results Fig. 1 shows the predicted and planned contours at cardinal angles. The GAN predictions achieved a population DSC of 0.92 ± 0.06, a mean centroid difference in the Medial–Lateral/Anterior–Posterior direction of -0.3 ± 2.6 mm and the Superior-Inferior direction of 1.0 ± 1.4 mm. Hausdorff distance on average was 2.7 ± 1.7 mm.

Conclusion A novel framework for markerless prostate real-time IGRT was proposed and evaluated on patient images. For the first time, real-time IGRT of the prostate without fiducial markers was shown to be feasible.

References/Acknowledgements

1. Paul Keall, Doan Trang Nguyen, Ricky O'Brien, Emily Hewson, Helen Ball, Per Poulsen, Jeremy Booth, Peter Greer, Perry Hunter, Lee Wilton, Regina Bromley, John Kipritidis, Thomas Eade, Andrew Kneebone, George Hruby, Trevor Moodie, Amy Hayden, Sandra Turner, Sankar Arumugam, Mark Sidhom, Nicholas Hardcastle, Shankar Siva, Keen-Hun Tai, Val Gebski, Jarad Martin, "Real-time image guided ablative prostate cancer radiation therapy: results from the TROG 15.01 SPARK Trial" International Journal of Radiation Oncology* Biology* Physics,107(3):530–8, 2020.

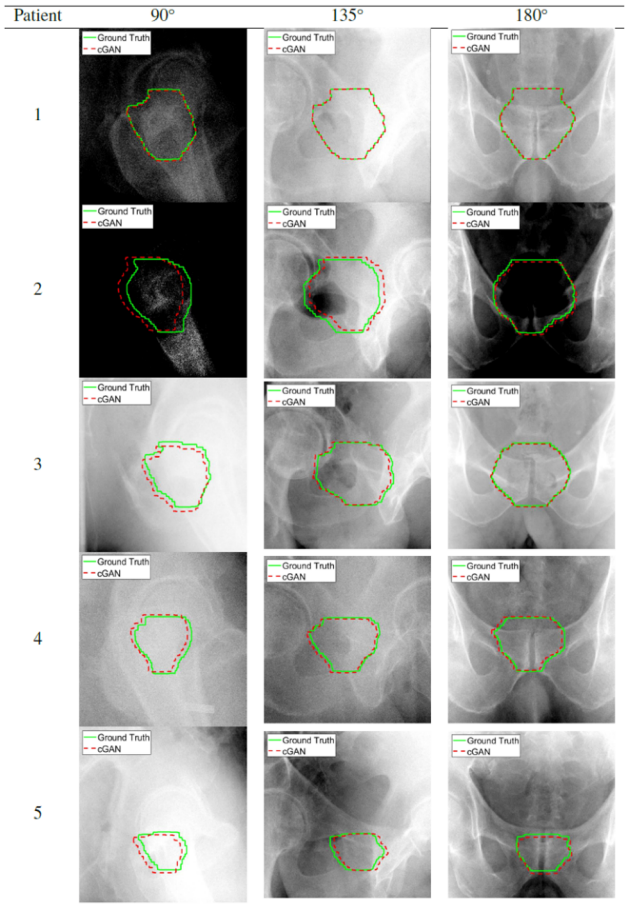

Fig. 33 Example segmentation results on patient images using our deep-learning method

P038 Application of Machine Learning in Head and Neck Cancer Recurrence Prediction

S. F. Liu[1], H. Liu[1], P. Ramachandran[1], T. Bui[1], V. Seshadri[1], S. Porceddu[1]

[1]Radiation Oncology, Princess Alexandra Hospital, Ipswich Road, Australia. SauFan.Liu@health.qld.gov.au (Presenting author); Howard.Liu@health.qld.gov.au; Prabhakar.Ramachandran@health.qld.gov.au; Thanh.Bui@health.qld.gov.au; Venkatakrishnan.Seshadri@health.qld.gov.au; Sandro.Porceddu@health.qld.gov.au

Introduction Artificial intelligence or machine learning is the latest computing technology that can be used to predict the treatment outcome. ^{18}F-FDG PET images were acquired for head and neck cancer patients before and after radiotherapy. The absolute value of Standardized Uptake Value (SUV) is not recommended to be used alone to determine individual treatment outcome. In this study, four machine learning algorithms using two training methods were employed to predict the treatment outcome.

Method There were two cohorts for PET datasets, the PAH scanned and external scanned, resulting in 98 contoured lesions with 5 mm margin. Radiomics features of all the contoured were extracted using an in house developed software. Prediction models were generated using four different machine learning algorithms that included the Support Vector Classifier (SVC), Decision Tree (DT), Logistic

Regression (LR), and Random Forest (RF) models. Two training methods was explored: 1) leave-one-out cross-validation, and 2) 70% of the data and 30% of data for training and testing models.
Results Overall the prediction accuracy of all four prediction models was higher than 70%. However, the RF prediction model achieved the best performance among the four prediction models. The accuracy, sensitivity, specificity, positive predictive value, negative predictive value, for the RF model were 86.7%, 91.7%, 66.7%, 91.7%, 66.7%, respectively.
Conclusion Due to very limited number of lesions, leave-one-out cross-validation was found to be more reliable to train the prediction models in this study. The RF prediction model can utilise the imaging characteristics of the tumour on the pre-/post-treatment PET scans to predict which patients are likely to respond to radiotherapy and subsequently do not require additional neck surgery after treatment. The study has shown promise and further research is being conducted to validate the findings in a larger cohort of patients.

P039 Correction of Dosimetry Bias in Extreme Asymmetric Field VMAT plans in Pinnacle

S. F. Liu[1], C. E. Jones[1], B. Perrett[1], A. Kazi[1], V. Seshadri[1], J. Ukath[1], P. Ramachandran[1]

[1]Radiation Oncology, Princess Alexandra Hospital, Ipswich Road, Australia. SauFan.Liu@health.qld.gov.au (Presenting author); Catherine.Jones3@health.qld.gov.au; Ben.Perrett@health.qld.gov.au; Aleksandra.Kazi@health.qld.gov.au; Venkatakrishnan.Seshadri@health.qld.gov.au; Jaysree.Ukath@health.qld.gov.au; Prabhakar.Ramachandran@health.qld.gov.au

Introduction A control point spacing of 4 degrees is routinely used for most VMAT optimisations in Pinnacle due to limited computing resources. One of the issues with this approach is the dosimetry bias observed for some extreme asymmetric field VMAT plans. The aim of this work was to minimize this bias by optimizing Pinnacle machine models and investigating the impact of degree per control point setting in VMAT plans.
Method Firstly, the MLC offset table was optimized based on measurements from three linear accelerators, however the dosimetry bias remained. Therefore, in the next step, modelling parameters such as depth dose energy, buildup, flattening field modelling, source, and MLC transmission parameters were tuned. Extensive testing was performed prior to releasing the model for clinical use.

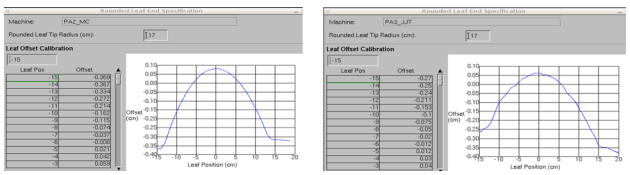

Fig. 38 Pinnacle suggested MLC offset table (left); Current MLC offset table (right)
Results The new Pinnacle machine models were validated using gamma analysis of PDDs and profiles, as well as verification of output factors and point doses. Asymmetric field VMAT plans were also recalculated using the new models. The MLC transmission was tuned over several iterations as it was found to have large impact on the agreement between point dose measurements and Octavius measurements. The new models were used to develop VMAT plans for various treatment sites. Patient specific QA was performed with independent QA equipment including EPID, Octavius array, point dose, and film measurements in a thorax phantom. All results were well within QA tolerances.
Conclusion The new models were found to improve the dosimetry for asymmetric VMAT fields employed 4° per control point spacing, and QA-analyses were within tolerance. However, a 2° per control point optimization may be required to provide improved results for high dose gradient stereotactic VMAT plans (such as spine SABR) and for VMAT plans with simultaneous integrated boost to targets smaller than 1 cm diameter.

P040 Unexpected Ring Artefact On CBCT Images

S. F. Liu[1], C. E. Jones[1], B. Perrett[1], H. Wang[2], S. Kumar[2]

[1]Radiation Oncology, Princess Alexandra Hospital, Ipswich Road, Australia. SauFan.Liu@health.qld.gov.au (Presenting author); Catherine.Jones3@health.qld.gov.au; Ben.Perrett@health.qld.gov.au; [2]Elekta. Hui.Wang@elekta.com; Sanjay.Kumar@elekta.com

Introduction Cone Beam Computed Tomography (CBCT) is used daily for patient setup before radiotherapy treatment. CBCT images at the Princess Alexandra Hospital are generated using Elekta's X-ray Volume Imaging (XVI). Routine CBCT QA is performed during morning runup. However, during a patient's set-up imaging, an unexpected ring artefact was observed on the clinical patient's CBCT images. This artefact was not detected during the morning routine CBCT QA due to the usage of a different combination of filters and imaging presets.

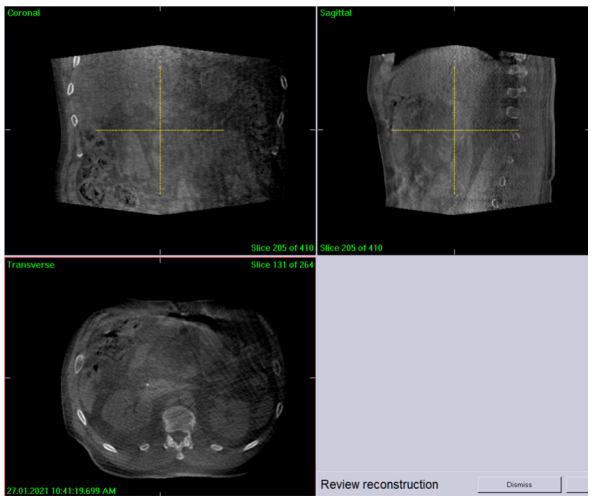

Fig. 39 Unexpected ring artefact on the patient CBCT images
Method The Catphan® 500 phantom was initially used to investigate the unexpected ring artefact with the F1 and M20 filters. However, the ring artefact did not appear clearly within the uniformity module. Therefore, a wider and longer uniform 32 cm diameter CTDI phantom was used.
Results The ring artefact on the CTDI phantom was reproducible with the F1 and M20 filters. Elekta engineers' initially attempted to eliminate the ring artefact by removing the dead pixels and recalibrating the KV panel. However, the ring artefact persisted. Next, the KV panel was recalibrated with all covers of the KV tube and panel removed, and the ring artefact disappeared. To confirm that the cover

of KV tube was the cause of the ring artefact, the engineers repeated the recalibration with the cover of KV panel removed. This confirmed the cover of KV tube was the cause of the ring artefact.

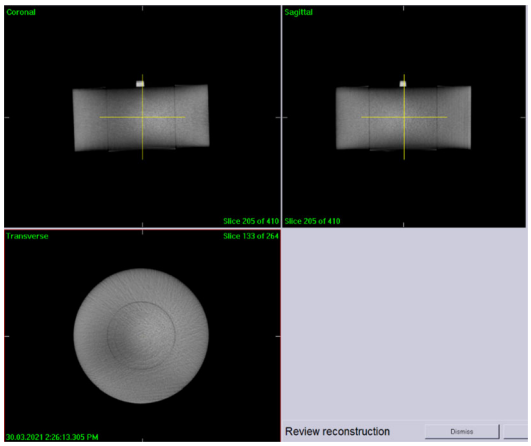

Fig. 40 The ring artefact was reproducible on the CTDI phantom

The cover of the KV tube was replaced, and a calibration was performed with the new cover in place. However, a smaller ring artefact still appeared. Calibration was then performed with the new cover removed, with the absence of the ring artefact.

Conclusion CBCT calibration with KV tube covers with rough surfaces may result in artefacts in subsequent CBCT images. In these cases, calibration should be performed with the tube cover removed.

P041 Tumour Motion-inclusive Dose Reconstruction in Pinnacle Treatment Planning System (TPS)

Jianjie Luo, Author[1], Chandrima Sengupta[2], Daniel Mason[1], Doan Nguyen[3]

Nepean Cancer Care Centre, NSW, Australia. jianjie.luo@health.nsw.gov.au (Presenting author); University of Sydney, Australia. chandrima.sengupta@sydney.edu.au; Daniel.mason@health.nsw.gov.au; [3]University of Technology Sydney. DoanTrang.Nguyen@uts.edu.au

Introduction Tumour motion may result in differences in planned and delivered doses. The actual distribution of radiation dose over the complete course of radiation therapy is often, in general, poorly quantified [1]. With the use of the motion information provided by a real-time tracking system used for the Liver Ablative Radiotherapy [2,3] (LARK) Clinical Trial (TROG 17.03), we have successfully quantified the dose delivered to a patient.

Method This study uses the Pinnacle[3] TPS for dose reconstruction and an Elekta Versa HD LINAC for patient treatment. A real-time tracking system (KIM) was used to track the fiducial markers implanted in the liver target during the treatment. A tracking file containing the fiducial marker positions and corresponding gantry angles was generated. A program was developed using the Pinnacle Scripting language and Python codes, to convert a Dynamic Arc beam (VMAT) into multiple Static beams at two degree gantry increments. The VMAT beam was compared to a Static beam plan to ensure the accuracy of the script. For patient dose calculation each Static beam was assigned its own isocentre corresponding to the target position and gantry angle in the tracking file.

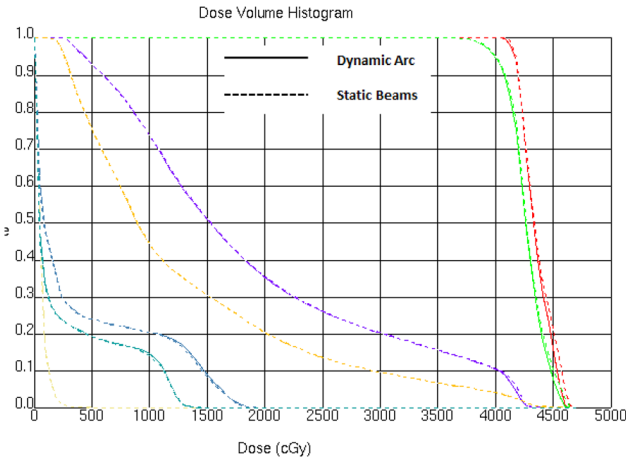

Fig. 1 DVHs difference between VMAT and Static beams calculation with no isocentre shift

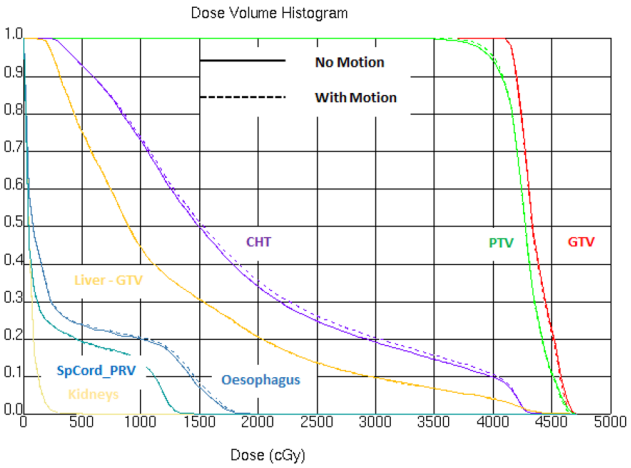

Fig. 2 DVHs difference using Static beams calculation with and without patient motion

Results Pinnacle uses different dose algorithms when calculating a VMAT beam compared to Static beam. The difference in calculated dose is demonstrated in Fig. 1. The Static beam plan was then used as a reference to compare to LARK plans with simulated patient motion. Differences in planned versus delivered DVH for a patient under real-time fiducial marker monitoring are shown in Fig. 2.

Conclusion With the use of a real time tracking system, the dose delivered to the patient in motion can be reconstructed using the Pinnacle TPS.

References/Acknowledgements

1. Jaffray DA, Lindsay PE, Brock KK, Deasy JO, Tomé WA. Accurate accumulation of dose for improved understanding of radiation effects in normal tissue. International Journal of Radiation Oncology* Biology* Physics. 2010 Mar 1;76(3):S135-9.
2. Ng, Jin Aun, et al. "Kilovoltage intrafraction monitoring for prostate intensity modulated arc therapy: first clinical results." International Journal of Radiation Oncology* Biology* Physics 84.5 (2012): e655-e661.
3. Currently, the system can only be used under specific conditions in approved clinical trials. Permission from Elekta was sought prior to integration of KIM with the Elekta system.

P042 Investigating the image quality of Short Thorax Cone Beam Computed Tomography protocols on a Varian TrueBeam linac.

Tim Markwell[1], Julie-Anne Miller[1]

[1]Radiation Oncology Princess Alexandra Hospital Raymond Terrace (ROPART), Brisbane, Australia. tim.markwell@health.qld.gov.au; Julie-Anne.Miller@health.qld.gov.au

Introduction The Varian TrueBeam 2.7 platform includes advanced imaging functions that may useful for specific clinical situations e.g. Breath Hold CBCT. This work investigates Short Thorax CBCT imaging protocols, which utilise very short imaging arcs, to reduce the imaging acquisition time. As the arcs are less than 200 degrees (120 to 150 degrees [1]), the reconstruction quality can be affected by significant artifacts.
Method Using the Short Thorax protocol for a range of arc lengths, image quality was investigated using a Catphan 604 [2], and a SBRT Thorax phantom. CT Number, uniformity, spatial resolution and geometrical accuracy were assessed, as well as 3D geometrical accuracy using the Thorax phantom.

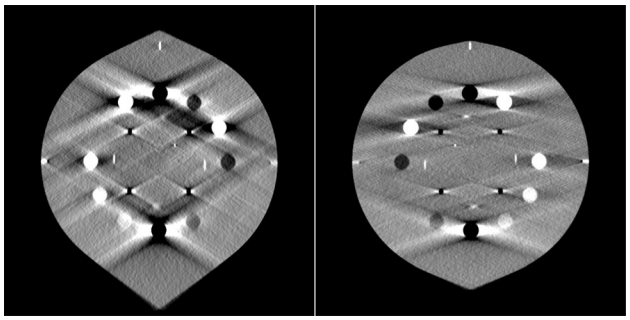

Fig. 41 CT Number slice from the Catphan for the 120 arc length (left) and 150 degree arc length (Right)

Results

Most of the imaging metrics showed a acceptable quality when compared to full CBCT protocols. However significant reconstruction artifacts were present, as well as shape distortion of features due to the limited gantry range. There is an increased uncertainty in the accuracy of using these particular CBCT protocols for patient setup, but under certain clinical situations may provide additional useful information where a very short imaging acquisition time (20 s to 30 s) is important.
Conclusion The image quality of the new Short Thorax CBCT protocols were investigated, showing possible clinical benefit under certain situations, however significant artifacts are present.
References

1. TrueBeam Technical Reference Guide—Volume 2: Imaging (2018)
2. The Phantom Laboratory Catphan 604 manual (2015)

P043 Automated plan generation: Initial experience as a Monaco 6.0 scripting pilot site

P. Mc Loone[1], L. Muñoz[2], J. Morton[3], A. Mazurek[4], M. Price[4]

[1]GenesisCare, Sydney, Australia. peter.mcloone@genesiscare.com.au (Presenting author); [2]GenesisCare, Flinders Private Hospital, South Australia, Australia; [3]GenesisCare, South Australia, Australia; [4]GenesisCare, Western Australia, Australia

Introduction Autonomation of a patient plan creation within the treatment planning system (TPS) allows for consistency and efficiency while reducing the risk of error in a resource intensive process. This work focuses on the initial use of Monaco 6.0 (Elekta, Sweden) scripting, MIM 6.8.9 (MIM Software Inc., USA) and in-house software to automate plan generation post contour creation with no or minimal planner interaction.
Method The Radiation Oncologist generates of patient specific Care Plan in an inhouse software system, *RO Portal*. This provides the Monaco Automated Planning Interface, which is based on C# with the prescribed dose, fractionation, and patient specific tumour stream. Workflows within MIM were used to check data integrity of contours for export where DICOM data is subsequently handled by the automation engine. Upon reaching the TPS import folder, generalised class solutions templated for individual tumour streams were applied and altered based on the information parsed from RO Portal. Both stages of optimisation were then applied and upon completion, the system saved the plan and exited. Plan quality was then assessed via script using site specific dosimetric criteria. Automated export of patient plans and reports were also transferred to Mosaiq 2.81 (Elekta Inc, USA) record and verify after plan approval by the Radiation Oncologist. Patients sites that lack templates were imported, had a couch and generic template applied before the system exited, optimizing the planning workflow. The foundational blocks have been built to automate any other treatment site once a template is developed.

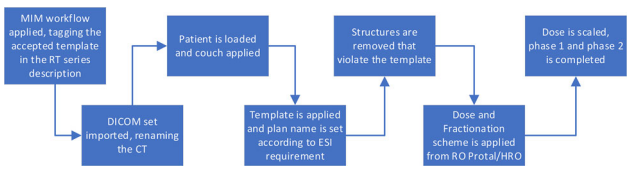

Fig. 42 Planning automation workflow

Results To date 40% Intact prostate cases have been automated without the need for user intervention. Overall, 30% of our cases in two of our states have been fully automated.
Conclusion A scalable automated plan generation system has been designed using the Monaco API, with the ability to remove the user from the process beyond contour generation until plan checking is required.
References/Acknowledgements

Monaco API Manual, Elekta.

GenesisCare Australia have an Alpha agreement with Elekta and are part of the pilot program for Monaco 6.0.

P044 Can artificial intelligence be used to predict future brain metastases?

P. Ramachandran (Presenting Author) [1], A. Mehta[1], V. Seshadri[1], M. Foote[1], J. Trapp[2], M Pinkham[1]

[1]Radiation Oncology, Princess Alexandra Hospital, Ipswich Road, Australia. Prabhakar.Ramachandran@health.qld.gov.au; Akash.Mehta@health.qld.gov.au; Venkatakrishnan.Seshadri@health.qld.gov.au; Matthew.Foote@health.qld.gov.au; [2]Queensland University of Technology, Brisbane, Australia. Jamie.trapp@qut.edu.au; Mark.Pinkham@health.qld.gov.au

Aim The aim of this study is to test the potential for using deep learning algorithms to prospectively predict for the emergence of new brain metastases on future imaging using only the MR images acquired for treatment planning.

Methods and Materials A cohort of 25 patients with brain metastases treated on the Leksell Gamma Knife (GK) and with serial post-radiotherapy imaging were selected for this study. For each patient, high resolution T1W + Gd was acquired on the day of GK treatment then every 3 months after for at least 2 years. The U-Net model was employed to predict future brain metastases from the initial treatment MR datasets. Treatment MR datasets were extracted from the GammaPlan treatment planning system including datasets used for initial treatment, follow-up and datasets used for the treatment of newly formed brain metastases. The deformable registration algorithm in Velocity was used to register the MR datasets. The leave-one-out cross validation method was employed to train the model which ensures each patient dataset gets tested exactly once and n-1 patient datasets are used to train the model. The predicted contours were then compared against the ground truth contours.

Results Our preliminary results show that the model has the potential to predict tumours in a few cases in datasets with lowest time gap between the initial treatment and follow-up scans.

Conclusion Deep learning may provide some insights into the prediction of new brain metastases appearing down the line but needs more data to provide a substantiative response. There are a lot of factors that influence the prediction of new metastases including the primary cancer type and the time that has passed between datasets with new brain metastases and the initial treatment datasets.

P045 Gamma Knife Icon: machine commissioning, treatment planning system validation and quality assurance

Atousa Montaseri[1], Elena Ungureanu[1], James Korte[1], Tomas Kron[1]

[1]Physical Sciences, Peter MacCallum Cancer Centre. Atousa.Montaseri@petermac.org (Presenting author); Elena.Ungureanu@petermac.org; James.Korte@petermac.org; Tomas.Kron@petermac.org

Introduction Gamma Knife Icon was installed at Peter MacCallum Cancer Centre in late 2020. Icon includes 192 Cobalt sources and is used for intracranial stereotactic radiosurgery. Icon is also equipped with cone beam CT (CBCT) and a high definition infra-red motion management (HDMM) system, allowing for non-invasive mask treatments in addition to frame-based traditional technique.

Methods Gamma Knife commissioning involved testing of the treatment unit, the imaging system, HDMM and the treatment planning system, Leksell Gamma Plan (LGP). Machine output and collimator output factors were measured following IAEA TRS483 protocol. EBT3 film was used for beam profile measurements. CBCT was evaluated for geometric accuracy, image quality and dose. The accuracy of the dose calculation algorithms was validated by measurements in solid water and in an anthropomorphic phantom. Validation of MRI scanning sequences for GK treatment planning was performed. On-going quality assurance (QA) processes, baselines and tolerance levels were established during the commissioning process.

Results The measured absolute dose rate was 3.388 ± 0.004 Gy/min. Collimator output factors agreed within 0.5% with the Monte Carlo derived factors used by LGP. Measured dose profiles match the LGP model within 0.5 mm. The coincidence between the radiological focus point and CBCT centre was within 0.2 mm. Accuracy of HDMM camera in detecting motions as small as 0.1 mm was confirmed and the gating feature proven reliable. GK specific MRI sequences showed mean geometrical distortions less than 1 mm. Good agreement between the calculated and measured dose distributions was shown, with the gamma pass rates greater than 90% for all plans, when using 3%/1 mm criteria for the spherical solid water phantom and 5%/1 mm for the anthropomorphic phantom.

Conclusion All machine parameters were investigated beyond scope of manufacturer acceptance testing and proven to be reliable. Routine QA processes have been developed and successfully implemented.

References

1. Dosimetry of Small Static Fields Used in External Beam Radiotherapy (TRS 483): An International code of Practice for Reference and Relative Dose Determination, IAEA 2017
2. I AlDahlawi, D Prasad, M B Podgorsak (2017) Evaluation of stability of sterotactic space defined by cone-beam CT for the Leksell Gamma Knife Icon. J Appl Clin Med Phys 18 (3), 67–72
3. B Maraghechi, T Kim, T Mitchel, S M Goddu, J Dise, et.al. (2021) Filmless quality assurance of a Leksell Gamma Knife Icon. J Appl Clin Med Phys 22 (1), 59–67
4. W N Duggar, B Morris, A Fatemi, J Bonds, R He, et.al (2019) Gamma Knife Icon CBCT offers improved localization workflow for frame-based treatment. J Appl Clin Med Phys 20 (11), 95–103
5. M Zeverino, M Jaccard, D Patin, N Ryckx, M Marguet, et al. (20017) Commissioning of the Leksell Gamma Knife Icon Med. Phys. 44 (2), 355–363
6. A Fatemi, S Taghizadeh, C Yang, M Kanakamedala, B Morris, S Vijaayakumar (2017) Machine-specific magnetic resonance imaging quality control procedures for stereotactic radiosurgery treatment planning. Cureus 9(12): e1957

P046 First Australasian experiences of the Integral Quality Monitor (IQM) and the impact of the COVID-19 pandemic on installation

A. Gray[1], A. Xing[1,2], G. Goozee[1,2,3], V. Moutrie[1,2], K Michel[4]

[1]Liverpool and Macarthur Cancer Therapy Centres, Sydney, NSW Australia; [2]Ingham Institute for Applied Medical Research, Liverpool, NSW Australia; [3]South Western Sydney Clinical School, University of NSW, Liverpool, NSW Australia. Alison.Gray@health.nsw.gov.au; Aitang.Xing@health.nsw.gov.au; Gary.Goozee@health.nsw.gov.au; Vaughan.Moutrie@health.nsw.gov.au (Presenting author); [4]iRT Systems GmbH, Koblenz, Germany. kmichel@i-rt.de

Introduction The Integral Quality Monitor (IQM) is a large ionisation chamber, developed by iRT Systems (Germany), which attaches to the linear accelerator head. It can be used for patient specific-

quality assurance (PSQA) (pre-treatment), during-treatment QA and machine QA. Two units and a multi-room kit were purchased for two cancer therapy centres with matched treatment units. The units were the first of their kind to be installed in Australasia. Typically, installation, acceptance, modelling and training is performed onsite with iRT, however due to the COVID-19 pandemic, alternative installation arrangements were required.

Method Discussions were held with iRT to determine an alternative installation schedule and options for remote access. The IT setup and in-room setup was performed by local Physics, IT and Elekta staff online with iRT. Acceptance of the units was conducted by Physics staff at both sites concurrently over 4 evenings, with iRT online. iRT conducted modelling and test patient calculations overnight. Training was conducted on a 5th evening. Current PSQA procedures were continued for two months in parallel with IQM measurements and results compared.

Results The main issues which needed to be overcome related to time differences and remote network access restrictions. While some delays occurred, e.g. due to loss of the remote connection by iRT overnight, the installation was completed in the scheduled time frame. The initial PSQA results indicate that the IQM will be suitable for PSQA for standard IMRT and VMAT treatments. The time to perform PSQA is also reduced to due part of the preparation and reporting processes being automated.

Conclusion The IQM installation was successfully completed with iRT staff remotely accessing the database from Germany. Initial PSQA results indicate suitability for ongoing use.

Acknowledgements Thanks to the local physics team who assisted with after-hours measurements during the installation process.

P047 A method for routine validation of ArcCheck array calibration

V. Moutrie[1]

[1]Liverpool and Macarthur Cancer Therapy Centres, Sydney, Australia. vaughan.moutrie@health.nsw.gov.au (Presenting author)

Introduction ArcCheck array calibration can be performed by the user within the SNC Patient software. A process to validate the calibration, both when it is first created and periodically to monitor change in diode response, was desired.

Method A number of large rectangular test fields, designed to evaluate the consistency of displayed dose across the detectors, were delivered to the phantom. The longitudinal response was assessed using the gamma analysis tools within SNC Patient to compare 10 cm × 20 cm fields delivered first to one end of the detector area and then to the opposite end. This was performed at the cardinal gantry angles. Circumferential response was evaluated by comparing the diode readings in the centre of eight 10 cm × 10 cm fields at 45° gantry intervals. An ion chamber reading was used to correct for couch transmission and angular dependence of dose output. A new array calibration was collected and retrospectively applied to the same test fields in order to devise analysis criteria that was suitable for differentiating a poor calibration from a good one.

Results For ongoing routine use, analysis settings of "AD", "TH%" = 90 and "Diff%" = 1 and a required pass rate of 95% were identified as suitable settings to identify a suboptimal calibration. The new calibration demonstrated much better performance than the existing for the longitudinal array response, with the range of pass rates increasing from 70.8–81.0% to 95.5–100%. The circumferential response was evaluated by comparing normalised values to the mean. The spread of results tightened from − 1.6–1.2% to − 1.0–1.3%, with absolute mean difference reducing from 0.76% to 0.53%.

Conclusion An efficient and sensitive technique for validating ArcCheck array calibration was established. The process was successful in identifying flaws in an existing calibration before a significant decline in clinical results was observed and can be easily implemented at any institution.

References/Acknowledgements Thank you to Dr Amy Walker for assisting with the presentation of these results.

P048 Clinical experience of offline patient-specific QA of treatment delivery on an Elekta Unity MR-Linac

Nicolle Dunkerley[1], **Z. Moutrie**[1], **C. Pagulayan**[1], **Urszula Jelen**[1], **M. G. Jameson**[2]

[1]GenesisCare, St Vincent's Clinic, Darlinghurst, NSW. nicolle.dunkerly@genesiscare.com; Zoe.Moutrie@genesiscare.com (presenting author); claire.pagulayan@genesiscare.com; Urszula.jelen@genesiscare.com; [2]GenesisCare, The Mill, 41–43 Bourke Road, Alexandria, NSW, Australia. Michael.Jameson@genesiscare.com

Introduction Patient specific quality assurance (PSQA) is performed by physicists to provide a level of confidence in the deliverability inverse planned radiation therapy treatment. [1]. For linear accelerators that utilise MRI, the available tools considered safe and appropriate are limited. We will present the first twelve months experience offline patient specific quality assurance.

Method All patients receiving treatment on the MRL at our centre had their reference plan and at least one adapted plan measured using an ArcCheck-MR® (AC) (Sun Nuclear Corporation, FL, US) Fig. 1 and a SemiFlex (PTW, Freiburg, Germany) ionisation chamber (IC). Over 70 patients and over 185 plans were evaluated using gamma analysis with the criteria of 3%,3 mm or 3%,2 mm and over 95% passing. Ion chamber measurements at the centre of a high dose with low gradient was recorded for all possible plans with criteria of within 3% considered a pass.

Results All patient plans achieved better than 95% agreement, on average 97.1 ± 3.2 the ArcCheck measurements based on their clinical criteria, with dose per fraction, treatment site and type of plan (reference or adapted) playing no significant role in the pass rate. When considering set-up uncertainty this number became 98.7 ± 1.9. For the ion chamber results the + 0.48% ± 1.6 dose homogeneity and set-up uncertainty did influencethe number of plans passing the ion chamber criteria.

Conclusion Our patient-specific QA program using ArcCHECK-MR and ionization chamber was employed for 12 months and our data

Fig. 1 ArcCheck MR on Elekta QA cradle on the Unity couch before an PSQA measurement

demonstrates good deliverability for our single MR-Linac and compares well to other centres. [2].

References/Acknowledgements

1. Miften M, Olch A, Mihailidis D, et al. (2018) Tolerance limits and methodologies for IMRT measurement-based verification QA: Recommendations of AAPM Task Group No. 218. Medical Physics 45:e53–e83. https://doi.org/10.1002/mp.12810
2. Yang B, Wong Y, Lam W, et al. (2021) Initial clinical experience of patient-specific QA of treatment delivery in online adaptive radiotherapy using a 1.5 T MR-Linac. Biomedical Physics & Engineering Express 7:035022

P049 Will a black tablet really make my RO go faster?: Comparing user input devices for online contouring

Z. Moutrie[1], J. de Leon[1], Monique Heinke[1], Sandy Sampaio[1], Ian Baxter[2], David Crawford[1], Louise Hogan[1], Conrad Loo[1], Maddison Picton[1], C Pagulayan[1], Urszula Jelen[1], Nicolle Dunkerley[1], M. G. Jameson[2], Tania Twentyman[2]

[1]GenesisCare, St Vincent's Clinic, Darlinghurst, NSW. Zoe.Moutrie@genesiscare.com (presenting author); Jeremy.DeLeon@genesiscare.com; monique.heinke@genesiscare.com; sandy.sampaio@genesiscare.com; [2]GenesisCare, The Mill, 41–43 Bourke Road, Alexandria, NSW, Australia. ian.baxter@genesiscare.com; david.crawford@genesiscare.com; lousie.hogan@genesiscare.com; conrad.loo@genesiscare.com; Maddison.picton@genesiscare.com; claire.pagulayan@genesiscare.com; Urszula.jelen@genesiscare.com; nicolle.dunkerly@genesiscare.com; Michael.Jameson@genesiscare.com; tania.twentyman@genesiscare.com

Introduction The advantage of fully adaptive treatments is the ability to completely customise the treatment for the anatomy of the day. The disadvantage is that contouring deformable ROIs can be time consuming for the radiation oncologist or radiation therapist. One way to reduce intra-fraction uncertainty/motion is by shortening the patient on-bed time, therefore efficient methods for imaging, contouring, planning and QA are advantageous. In this study we examine what tools can be used to reduce the contouring time.

Method Online contouring times were recorded over a period for clinical staff delineating key ROIs for patients receiving fully adaptive treatments on our MRL (using an adapt to shape workflow) using: (1) using a mouse/keyboard and (2)a cintiq 22 WACOM tablet.

Results For all anatomical sites, targets and clinical staff there was an average reduction in contouring times of 20% for the Radiation Oncologist. The most significant decrease in contouring times were in the left-handed staff. Even for staff members who had not used a WACOM terminal before, the contouring times reduced.

Conclusion A graphics tablet can be used to reduce contouring time and reduce on-bed time for fully adaptive MRL treatments.

P050 Feasibility of normal lung sparing in single-dose biology-guided radiotherapy treatments of lung cancer

Oluwaseyi M. Oderinde[1], Thomas Cornwell[1], Sibo Tian[2], Xiaofeng Yang[2], Kristin A Higgins[2], Angela Da Silva[1], Shervin M. Shirvani[1]

[1]RefleXion Medical, Hayward, CA, USA. ooderinde@reflexion.com (Presenting author); tcornwell@reflexion.com; [2]Radiation Oncology, Winship Cancer Institute of Emory University, Atlanta, USA. sibo.tian@emory.edu; xyang43@emory.edu; kristin.higgins@emory.edu; adasilva@reflexion.com; sean@reflexion.com

Introduction In biology-guided radiotherapy (BgRT), outgoing emissions after administration of an injected radiotracer like FDG are used to dynamically guide radiation treatment delivery to the PET-avid target in real-time, resulting in a tracked dose distribution. This study evaluated the feasibility of lung-sparing in ultra-high dose single-fraction BgRT for lung cancer.

Method This retrospective study selected two lung cancer patients (P1 and P2) for ultra-high single-dose BgRT (sdBgRT) planning and free-breathing single-dose radiotherapy (fbSDRT) planning with an internal tumor volume technique. The planning objective was to deliver 28 Gy to the planning target volume (PTV) in a single treatment session. Treatment planning was performed using the RefleXion^{TM} X1 treatment planning system. For BgRT planning, a tracked BgRT-PTV (5 mm expansion of GTV) was contoured using the mid-ventilation phase. Percentage of normal lung volume receiving at least 5 Gy in increments of 5 Gy (V5—V20) and mean lung dose (MLD) were analyzed from the dose-volume histogram of sdBgRT and SDRT plans.

Results Both lung cases met dosimetric objectives and normal constraints. PTVs of sdBgRT plans were smaller by 22.66% and 53.64% (for P1 and P2, respectively) as compared to fbSDRT PTVs. The average achieved mean GTV doses were 36.32 $\pm$ 1.67 and 33.38 $\pm$ 1.25 Gy for sdBgRT and fbSDRT, respectively. Comparing sdBgRT plans with fbSDRT plans, the percentage of lung volume that received V20, V15, V10, and MLD were reduced in all cases, by an average of 35%, 23%, 18%, and 8%, respectively. However, V5 was increased by 10.23% in P1 and a reduced by 7.19% in P2 in sdBgRT plans.

Conclusion Compared to fbSDRT, sdBgRT plans reduced target volumes and improved normal lung sparing across multiple parameters. This investigation highlights the potential of BgRT for combining a dynamic, tracked dose distribution with ultra-high single-fraction doses. Further study is needed on clinical outcomes.

P051 Investigating the correlation between imaging and surface-guidance for a variety of patient cohorts

S. W. Sam[1], M. Wanklyn[2], T. Gorjiara[2]

[1]School of Physics, Faculty of Science, University of Sydney, Camperdown, NSW, Australia. ssam3887@uni.sydney.edu.au (Presenting author); [2]GenesisCare, Department of Radiation Oncology, The Mater Hospital, Crows Nest, NSW, Australia. Mark.Wanklyn@genesiscare.com; Tina.Gorjiara@genesiscare.com

Introduction AlignRT® is the SGRT system used for patient positioning and intrafraction monitoring based on a 3D surface. The correlation between the skin surface (AlignRT) and tumour (imaging) especially deep-seated tumours, is still questionable. This retrospective study investigates the impact of tumour depth on the correlation between the imaging shift and AlignRT post-imaging shift for different patient cohorts.

Method Four patient cohorts (Breast VMAT and IMRT, Prostate SBRT, Lung SBRT, and Cranial SRS) with shallow- and deep-seated tumours were included in this study. The imaging shifts applied to align the patients back to the planned position were compared to the post-imaging shifts recorded by the AlignRT system. Regression and Bland–Altman analysis were then used to study the correlation between imaging and AlignRT shifts, in longitudinal, lateral and

vertical coordinates. The coefficient of determination (R^2) and Limits of Agreement (LOA) were calculated from these two analyses.
Results Excellent correlations ($R^2 \approx 1$) and agreements (LOA within 2 mm tolerance level and 5 mm PTV margin) between AlignRT and different imaging modalities for all patient cohorts were achieved. kV-CBCT had a good correlation with AlignRT for both bolus and non-bolus breast patients in all directions. Results showed larger disagreements between kV-CBCT and AlignRT in longitudinal directions compared to the other coordinates for prostate SBRT, lung SBRT, and Cranial SRS patients.
Conclusion AlignRT is reliable for patient positioning and intrafraction monitoring regardless of the tumour depth. However, the accuracy is limited by tumour motion during the treatment and requires further investigation. Imaging is considered the gold standard for position verification.

P052 Modeling and dosimetric performance of a Collapsed Cone Convolution and a Monte Carlo based dose calculation algorithm for the clinical use of Aktina Stereotactic Cones with RayStation Treatment Planning System

A. Schofield[1], M. Newall[1], D. Inwood[1], S. Downes[1], S. Corde[1]

[1]Nelune Comprehensive Cancer Centre (NCCC), Prince of Wales Hospital, Randwick NSW. Andrew.Schofield@health.nsw.gov.au; Matthew.Newall@health.nsw.gov.au; Dean.Inwood@health.nsw.gov.au; Simon.Downes@health.nsw.gov.au; Stephanie.CordeTehei@health.nsw.gov.au

Introduction The NCCC recently purchased Aktina small field collimators to be used with an Elekta Versa linear accelerator for stereotactic treatments. In this work, a Collapsed Cone Convolution (CCC) and a Monte Carlo (MC) 6MV photon beam was modelled in Raystation 9B and validated for clinical treatment planning.
Method All beam data for cones of diameter 5 mm-39 mm was measured in accordance with the IAEA code of practice (TRS 483) [1]. Two flattened 6MV beam models were created within RayPhysics (CCC and MC). PDDs, profiles, and OFs were calculated within RayStation's planning module and compared to measurement. Point doses for arcs within a water tank and heterogeneous slab geometries containing bone and air were verified. End-to-end testing (including an independent audit) was conducted via measurements using EBT3 films and a SRS MapCheck diode array, housed inside a StereoPhan. CBCT image guidance was used to align the phantom in which non-coplanar patient plans were delivered. Gamma comparisons were made between the measured and calculated datasets. Finally, an assessment of calculation time was made as a function of cone size and statistical uncertainty.
Results Acceptable agreement was achieved across all profiles and PDDs to within 2% beyond d_{max}, with the largest discrepancy found in the build-up region (34% and 27% for CCC and MC respectively). All dose measurements were acceptable with the largest differences found for arcs traversing an air cavity (1.7% and 3.7% for CCC and MC respectively). All composite measurements of patient plans passed the gamma criteria of 4%/1 mm and a majority at 1%/1 mm (5/16 measurements below 95%). For a 10 arc plan, calculation time was around 30 s (CCC) and 22-136 s for a 5 mm-39 mm cone, 0.3% uncertainty (MC).
Conclusion The performance of both models was deemed acceptable. The MC model recommended for final dose calculations for continuity of our clinical practice.
References/Acknowledgements

1. IAEA and AAPM, TRS-483. Dosimetry of Small Static Fields Used in External Beam Radiotherapy. 2017

P053 Automated patient data retrievals: A technical note

Warwick L.J Smith[1], Dane Lynch[1]

[1]Department of Radiation Oncology, Sir Charlies Gairdner Hospital, Western Australia. Warwick.Smith2@health.wa.gov.au (Presenting author); dane.lynch@outlook.com (Presenting author)

Introduction There is a growing problem many radiation oncology centres are facing with returning patients, which were previously treated with now outdated treatment planning systems (TPS) such as Xio and Monaco. Efficiently restoring previous treatments into correctly formatted DICOM files for modern TPS's has proven to be difficult, time consuming, and costly, as many centres will often continue to pay for licenses to retrieve dated patient plans from Xio or Monaco. The use of programming and automation offers a way for thousands of previous patient CTs, plans, structure sets, and doses to be restored for clinical use in a timely manner. The goal of this project being the complete end to end data retrieval from patient server databases through Xio and Monaco, and into the Eclipse TPS.
Method Python is an object orientated programming language which when coupled with Java, provides a powerful tool which can perform many functions autonomously through scripting without requiring the backend access for a given TPS. Sir Charles Gairdner Hospital, Perth, Western Australia utilises an open-source program called SikuliX, which enables the unique custom manipulation of Xio and Monaco to autonomously retrieve and convert previous treatment plans in Xio and Monaco to the required DICOM format which is used in Eclipse. The SikuliX software uses a combination of Jython, Googles optical character referencing (OCR) and image recognition software powered by OpenCV.
Results Using SikuliX, a scripting pipeline was written to automatically import/ export previous treatment plans in Xio, Monaco and Eclipse with minimal required input. An inhouse plan validation checklist created by experienced Senior Medical Physicist was used to verify each plan had successfully been exported and imported into Eclipse.
Conclusion The successful implementation of autonomous software for patient data retrieval was accomplished using open source software. Hundreds of patients a day were able to be restored to Eclipse with confidence that each plan was restored correctly and without fault.

P054 Calculation of CTV-PTV margins for patients with brain tumors using XVI imaging systems

E. Spelleken[1], M. Murray[2], D. Papworth[2]

[1]GenesisCare, Rockhampton Base Hospital. Emma.spelleken@genesiscare.com (Presenting Author);
[2]GenesisCare, Chermside Medical Centre, Brisbane

Introduction ESTRO-ACROP guidelines state that a PTV margin should take into account set up and planning uncertainties (1). A 3–5 mm margin is recommended however each department should undergo an audit of set up uncertainties too determine what margin is suitable. Currently the CTV to PTV margin in GenesisCare QLD is set at 5 mm for brain tumors. This study aims to assess the patient set up errors that occur for radical brain tumour cases for centres at

GenesisCare QLD utilising the Elekta platform. Studies have been performed on Varian platforms however little information could be found for Elekta platforms (2,3).
Method 10 patients were selected who were treated with VMAT using daily CBCTs obtained on the XVI imaging system. These patients were treated across 6 Elekta Versa HDs. The radiotherapy was fractionated into 28–30 treatments. The systematic and random errors were calculated for the translational dimensions. The optimal PTV margin was the calculated using van Herk et al.'s formula (4):
Results The systematic errors ($\sum$) were calculated to be 0.124 mm, 0.156 mm and 0.122 mm in the vertical, lateral and longitudinal directions respectively. The random errors (σ) were calculated to be 0.187 mm, 0.141 mm and 1.53 mm, respectively. The calculated margin was 4.409 mm, 4.887 mm and 4.121mmin the vertical, lateral and longitudinal directions respectively.
Conclusion Therefore, it was recommended that the PTV margin for radical brain treatments remain at 5 mm when using the Elekta platforms. This study also showed that it is important to do a departmental audit to ensure that the chosen PTV margin is accurate for the machine being used.
References

1. Niyazi M et al.2016. ESTRO-ACROP guideline 'target delineation of glioblastomas'. *Radiotherapy and Oncology* 118: 35–42
2. Oh YK et al.2014. Assessment of setup uncertainties for various tumour sites when using daily CBCT for more than 2200 VMAT treatments. *J Int Radiation Oncology Biol Phys* 15(2): 85–99
3. Oh SA et al.2016. Analysis of the setup uncertainty and margin of the daily ExacTracc 6D image guided system for patients with brain tumors. *PLoS One* 11(3). https://doi.org/10.1371/journal.pone.0151709
4. Van Herk et al.2002. Inclusion of geometric uncertainties in treatment plan evaluation. *J Int Radiation Oncology Biol Phys* 52(5):1407–1422

P055 UNSCEAR Global Evaluation of Medical Exposure

P. D. Thomas[1], F. Shannoun[2]

[1]Medical Imaging Section, ARPANSA. peter.thomas@arpansa.gov.au (Presenting author); [2]United Nations Scientific Committee on the Effects of Atomic Radiation, Austria

Introduction The United Nations Scientific Committee on the Effects of Atomic Radiation (UNSCEAR) was established by the United Nations General Assembly in 1955. Its mandate is to assess and report on the levels and effects of exposure to ionizing radiation. UNSCEAR makes periodic assessments of the global level of medical exposures. The most recent evaluation was approved in November 2020.
Method Data on annual frequency of examinations and associated radiation dose were derived from the UNSCEAR Global Survey on Medical Exposure and from the peer-reviewed scientific literature. Mathematical models of procedure frequencies within seven broad classifications were developed to generate projections for those countries that did not provide data for the survey. The procedure categories used were: conventional radiology (excluding dental radiology), dental radiology, computed tomography, interventional radiology, diagnostic nuclear medicine, radionuclide therapy and radiation therapy.
Results An estimated 4.2 billion examinations are performed annually. The annual collective effective dose was estimated at 4.2 million man Sv giving an annual effective dose per caput of 0.57 mSv (excluding exposures from radiation therapy). In addition, an estimated 6.2 million courses of radiation therapy treatment and 1.4 million radionuclide therapy treatments are performed each year. Uncertainties in the overall number of examinations and in the collective effective dose are estimated at ± 30%. Computed tomography makes the largest contribution (62%) to the collective dose, followed by conventional radiology 23%, interventional radiology 8%, and nuclear medicine 7%. Dental radiology only contributes 0.2% of the collective dose, despite making up 26% of all examinations.
Conclusion Medical exposure remains the largest human-made source of ionizing radiation exposure. Annual effective dose per caput has reduced to 0.57 mSv compared to 0.65 mSv in the previous assessment [1], however the difference is within the estimated uncertainty. This trend contrasts with the notable increases seen in the previous two UNSCEAR assessments.
References

1. UNSCEAR. Sources and Effects of Ionizing Radiation. Volume I: Sources: Report to the General Assembly, Scientific Annexes A and B. UNSCEAR 2008 Report. United Nations Scientific Committee on the Effects of Atomic Radiation. United Nations sales publication E.10.XI.3. United Nations, New York, 2010.

P056 Commissioning Brainlab's Exactrac Dynamic X-ray & 4D thermal-surface imaging system

Emma K. Horgan (Presenting author)[1], Luke K. Webb[1], Chris Noble[1], Prabhakar Ramachandran[1]

[1]Radiation Oncology, Princess Alexandra Hospital, Ipswich Rd, Brisbane, Australia. Emma.Horgan@health.qld.gov.au; Luke.Webb@health.qld.gov.au; Chris.Noble@health.qld.gov.au; Prabhakar.Ramachandran@health.qld.gov.au

Introduction The Princess Alexandra Hospital installed Brainlab's Exactrac Dynamic in September 2020. This system is designed for precision patient monitoring and has the ability to merge surface, thermal and stereoscopic x-ray imaging to enable accurate patient setup and intra-fraction monitoring. In this study we propose a methodology to validate the x-ray, thermal and surface imaging systems.
Method A Quasar motion platform and 1-D water tank arm were retrofitted to enable dual-axis positioning of an anthropomorphic pelvis phantom. A surface error tolerance was set to 1 mm with a 1 s duration. During the treatment beam, the phantom was made to move remotely past this tolerance and the results were recorded. This was repeated for different tolerance settings. The same setup and tolerances were used to assess the x-ray error detection capabilities by increasing the surface tracking tolerances to their maximum value. To test the impact of the thermal camera on the surface detection, a stepped plastic water phantom was positioned on the dual-axis platform. This produced a positionally symmetric plane that could be shifted laterally with no discernible difference to the surface ROI. A thermal (reptile heating) cable was sandwiched between the plastic water in a coil-like arrangement. The platform was moved laterally, and it was noted whether a beam hold/surface error was detected as a result of thermal gradient changes.
Results The Exactrac Dynamic system was found to perform as specified by the manufacturer; it could accurately track patient surfaces and initiate beam holds when discrepancies were detected.
Figure 1 shows the results of the thermal imaging camera which successfully enabled a beam hold when the camera detected a lateral shift in the phantom. This shift wasn't detected without thermal monitoring.

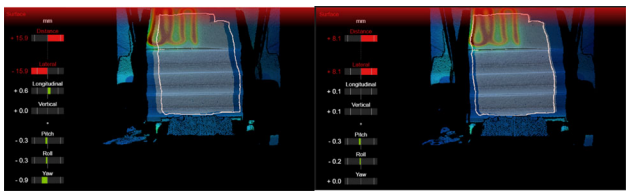

Fig. 43 Images obtained from the surface camera showing a detected shift due to the changes in thermal gradient

Conclusion Our proposed methodology was able to validate the x-ray, thermal and surface systems and detect translational shifts, resulting in beam gating when thresholds were exceeded. The x-ray, surface and thermal imaging cameras were found to be reliable tools in verifying patient position.

P057 Australian requirements for 3D printed medical devices used in brachytherapy

R. Wilks[1,2,3], S. B. Crowe[1,2,3,4], B. Murray[2,5], S. Pleschka[1,2]

[1]Cancer Care Services, Royal Brisbane and Women's Hospital, Brisbane, Queensland, Australia; [2]Herston Biofabrication Institute, Metro North Hospital and Health Service, Brisbane, Queensland, Australia; School of Information Technology and Electrical Engineering, University of Queensland, Brisbane, [3]Queensland, Australia. rachael.wilks@health.qld.gov.au (Presenting author); [4]School of Chemistry and Physics, Queensland University of Technology, Brisbane, Queensland, Australia. sb.crowe@gmail.com; [5]Australian Institute for Bioengineering and Nanotechnology, University of Queensland, Brisbane, Queensland, Australia. becca.murray@health.qld.gov.au; shaun.pleschka@health.qld.gov.au

Introduction The Australian Therapeutic Goods Administration (TGA) requires a medical device to be listed on the Australian Register of Therapeutic Goods (ARTG). The TGA regulates these medical devices using a risk based approach, where a device is assessed based on their intended purpose. The classification of a device will determine the extent of the assessment procedures required to comply with the Essential Principles, ensuring the device is safe and fit for purpose. For reusable 3D printed treatment devices in radiation oncology that may be used inside the body, such as brachytherapy applicators, this needs consideration of material choice and processing requirements. This study summarises the conformity assessment procedures required for 3D printed brachytherapy applicators to comply with the Essential Principles in Australia.

Method Risk and conformity assessments for devices produced at the Royal Brisbane and Women's Hospital (RBWH) were performed and reviewed by experienced staff. Classifications of different brachytherapy applicators were determined using the TGA classification system. The Australian Standards [1] was consulted to determine the Spaulding Classification and therefore the required level of reprocessing between fractions.

Results For 3D printed brachytherapy applicators manufactured at the RBWH, instructions for use incorporating appropriate reprocessing requirements were developed for distribution with devices. Cleaning instructions were validated to ensure contaminants were removed and bioburden wasbeen reduced to a suitable level as specified by international standards. Table 1 provides a summary of the reprocessing requirements for brachytherapy devices for different sites. Examples of common 3D printable materials that support these processes, with the appropriate level of biocompatibility, are also suggested.

Conclusion The required level of reprocessing of a medical device is based in its purpose and the associated risks of use. Brachytherapy centres need to consider the reprocessing capabilities offered by their central sterilising department when introducing patient-matched or customised 3D printed brachytherapy applicators.

Acknowledgements Rachael Wilks' contribution to this work was supported by a RBWH and RBWH Foundation Post Graduate Scholarship.

Table 5 Summary of brachytherapy applicator classifications and reprocessing requirements

Brachytherapy site	TGA Classification	Spaulding Classification	Reprocessing requirements	Example 3D printing materials
Skin	Class I	Non critical	Clean as necessary with detergent solution May be followed by low-intermediate grade disinfection	PLA, ABS, TPU
Mucous Membrane: Intracavitary vaginal Intrauterine, intraluminal	Class I Class IIa	Semi-critical	In order of preference: Moist heat sterilisation Low temperature sterilisation Thermal disinfection High level chemical disinfection	Nylon, Polycarbonate (PC), photopolymer resin
Interstitial (e.g. as a template/ guide)	Class IIa	Critical	In order of preference: Moist heat sterilisation Low temperature sterilisation	PC-ISO, Nylon, Photopolymer resin

References

1. Standards Australia/Standards New Zealand, "Australian/New Zealand Standard: Reprocessing of reusable medical devices in health service organizations," AS/NZS 4187:2014.